11th EFRC CONFERENCE

September 13 – 14, 2018
Madrid, Spain

EFRC
EUROPEAN FORUM
for RECIPROCATING
COMPRESSORS

WWW.RECIP.ORG

11th EFRC CONFERENCE

CONFERENCE SPONSORS

11th EFRC CONFERENCE
September 13 – 14, 2018, Madrid

WWW.RECIP.ORG

11th EFRC CONFERENCE
September 13 – 14, 2018, Madrid

AVAILABILITY AND RELIABILITY

PULSATIONS AND VIBRATION

COMPRESSOR AND COMPONENT DESIGN

PULSATIONS AND VIBRATIONS

CONTENTS

11th EFRC CONFERENCE
September 13 – 14, 2018, Madrid

ENGINEERING OF COMPRESSOR PLANTS

MEASURING AND MODELLING

PULSATIONS AND VIBRATIONS

CONTENTS

11th EFRC CONFERENCE
September 13 – 14, 2018, Madrid

EFRC

TRIBOLOGY AND WEAR

DIGITALISATION

CONTENTS

11th EFRC CONFERENCE
September 13 – 14, 2018, Madrid

CONTENTS BY CONTRIBUTOR

11th EFRC CONFERENCE
September 13 – 14, 2018, Madrid

CONTENTS BY CONTRIBUTOR

11th EFRC CONFERENCE
September 13 – 14, 2018, Madrid

CONTENTS BY CONTRIBUTOR

11th EFRC CONFERENCE
September 13 – 14, 2018, Madrid

CONTENTS BY CONTRIBUTOR

11th EFRC CONFERENCE
September 13 – 14, 2018, Madrid

STASSKOL

TECHNISCHE UNIVERSITÄT DRESDEN

TNO

TOTAL REFINING & CHEMICALS

CONTENTS BY CONTRIBUTOR

11th EFRC CONFERENCE
September 13 – 14, 2018, Madrid

WOOD

WROCŁAW UNIVERSITY

CONTENTS BY CONTRIBUTOR

HYDROGEN COMPRESSION FOR MULTIPLE NEEDS

THE NEA 360° PORTFOLIO TO BOOST HYDROCRACKERS

Hydrocrackers comprise the heart of the refinery. Inside the giant reactors, heavy waxy feedstock is converted into lighter products such as jet fuel, kerosene and diesel fuel. Today's crackers need large quantities of hydrogen to convert high-sulfur material into low-sulfur fuels for vehicles and airplanes under high temperatures of up to 800°C/1,500°F.

As hydrocrackers require major invests, reliable equipment such as reciprocating compressor packages are mandatory. The **NEA heavy-duty hydrogen compressor** is named as the best-in-class solution for hydrocrackers due to its tailor-made design and flexibility in driving high volume flows of up to 100,000 Nm³/h at some hundred bar discharge pressure and up to 30 MW power. As reliability counts, no single installation is left unattended. From start-up to maintenance and professional diagnostics, the service provider **NEAC Compressor Service** keeps the compressor running. Worldwide, with full life-time support.

Authorized OEM supplier for reciprocating compressor lines:

Chicago Pneumatic · KSB · Linde · HALBERG · Demag · Hofer · Borsig (recos built in Berlin up to the end of 1995) · PENN Process Compressors

HOFER manufactures diaphragm and hydraulically driven piston compressors, and offers high-pressure piping systems with threaded connections. Perfectly tight even under vibrations from hydrocrackers.

STASSKOL supplies sealing elements such as intermediate packings as well as guide and piston rings based on in-house materials for lubricated and non-lube hydrogen piston compressors. PEEK materials are ideally suited for high gas pressures and thus high mechanical loads during the hydrocracking process.

NEA X connects engineering and digital technology. Its solution provides Condition Management with OEM expertise, transferring intelligent service and diagnostics to tangible values: optimized assets availability, more time to plan right actions, and improving profitability.

NEUMAN & ESSER GROUP

www.neuman-esser.com

Troubleshooting of recurrent cylinder head stud bolt failures on Natural Gas compressors

by:

Guillaume GIEN
Rotating Machinery Engineer
TOTAL Refining & Chemicals
Harfleur, France
guillaume.gien@total.com

Jean-Christophe COURCOL
Expert & Head of Rotating Dpt
TOTAL Refining & Chemicals
Harfleur, France
jean-christophe.courcol@total.com

Wolfgang VOITICEK
Director Bare Block
Leobersdorfer Maschinenfabrik GmbH
Leobersdorf, Austria
Wolfgang.Voiticek@lmf.at

11th EFRC CONFERENCE
September 13 – 14, 2018, Madrid

Abstract:
This paper is presenting the historical record of two Natural Gas reciprocating compressors (1-stage, 2-throw), feeding a Steam Methane reformer Unit, since start-up in 2006. These compressors have suffered numerous stud fractures on all four heads, went through various stud upgrades implemented without success. Finally, an FEA analysis revealed the root cause of the failure, the failure mechanism, and the final design upgrade to solve the problem will be presented.
The compressors have been running without further stud fracture since June ’16.

by: Guillaume Gien, Jean-Christophe Courcol – TOTAL; Wolfgang Voiticek – LMF

1 Introduction

Those 2 API 618 reciprocating compressors (1-stage, 2-throw) have been commissioned and started-up in 2006. They feed natural gas to a Steam Methane Reformer unit producing pure hydrogen for a Hydrocracker Unit. Both compressors are running parallel from 28barg to 44barg. Soon after start-up, the first cylinder head stud bold started to fail.

Numerous fractures have followed:

- July 2008: 1 Bolt fracture on cylinder west of compressor B
- February 2009: 2 Bolt fractures on cylinder west compressor B
- April 2010: 1 Bolt fracture on cylinder west of compressor A
- April 2010: 2nd Bolt fracture on cylinder west of compressor A
- August 2015: 1 Bolt fracture on cylinder east of compressor B
- February 2016: 2 Bolt fractures on cylinder west of compressor B

At first, a trial and error approach has been taken including preventive replacement of complete bolt sets during opportunity stops (catalyst change). A number of combinations of stud materials and thread executions (machined or rolled) at various torques have been tested without success.

There was a real safety issue on top of the availability issue. Up to 2 studs out of 12 had already been simultaneously found broken.
The risk of cylinder head projection was real.

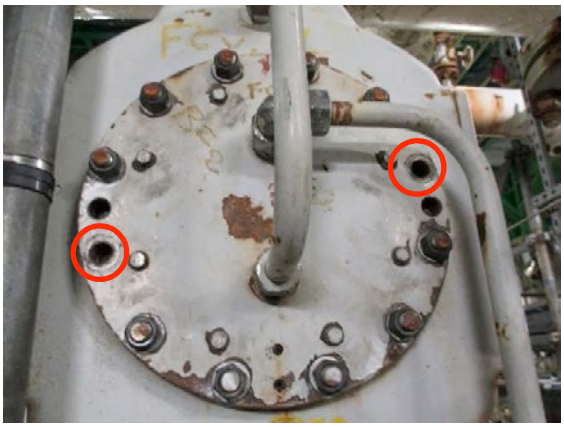

Picture 1: front view of cylinder head with the location of broken studs

The studs were always breaking on the last thread screwed in the cylinder, at the contact surface between cylinder and head.

Picture 2: broken studs

Fracture face analysis revealed fatigue failure of the studs with crack initiation in the root of the thread.

When the problem was raised to the attention of the central troubleshooting team of the USER, after the February 2016 fracture, the decision was made to involve the OEM in a proper root cause analysis in order to solve this reoccurring problem.

2 Root cause analysis process

2.1 Problem Statement

Under normal assembly behaviour, the bolts only withstand the axial preload applied during the initial tightening. This preload must be higher than the forces applied to the assembly in service. The faced fatigue failure means that additional alternating stresses were applied to the bolts in service. The following study explains were they came from.

2.2 Finite Element Analysis

Cylinder head has been newly drafted in 3D since the original drawing was 2D. A Finite Element Analysis of the cylinder head assembly has been performed to better understand the behaviour of the assembly in service.

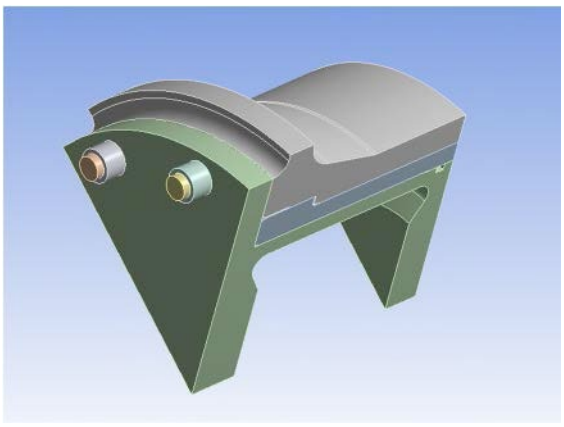

Figure 1: 3D model

by: Guillaume Gien, Jean-Christophe Courcol – TOTAL; Wolfgang Voiticek – LMF

2.3 Results

This analysis, based on a simplified model, has revealed that the cylinder head was too flexible and its flange was bending through the pressure efforts. As a result of this bending, the nut was pivoting with the head surface and introducing bending moment on the studs on top of the tensile stresses. This bending was alternating at the same frequency as the pressure variation in the cylinder.

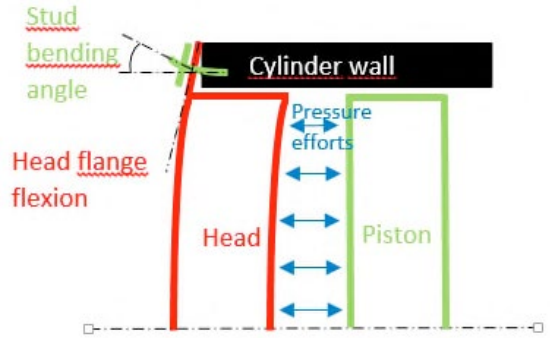

Figure 2: Sketch of cylinder head flange bending

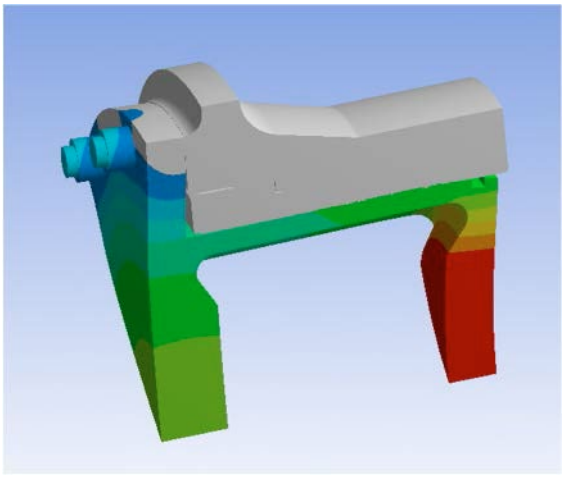

Figure 3: Cylinder head deformation

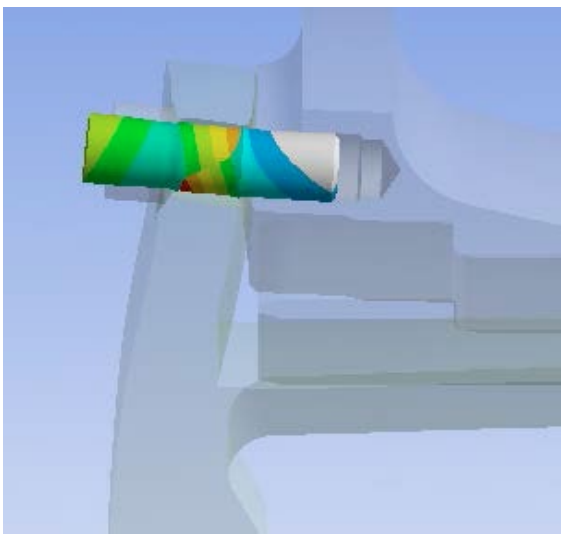

Figure 4: Bolt bending

As a result, the stress level in the stud section was not evenly distributed and variation up to 25% was noticed across the section.

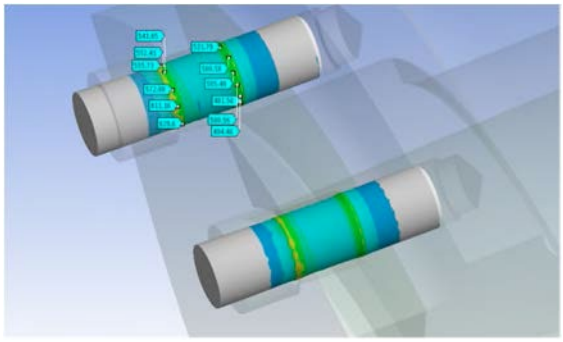

Figure 5: Uneven stress distribution in bolt sections

These alternative bending stresses on the stud initiated fatigue cracks on the thread root that were propagating and eventually leading to studs fracture.

The head flexibility had been underestimated and the additional bending stresses in the studs had not been considered.

Fatigue endurance had not been checked and only the static safety factor of 2.4 of the studs was calculated based on maximum gas load.

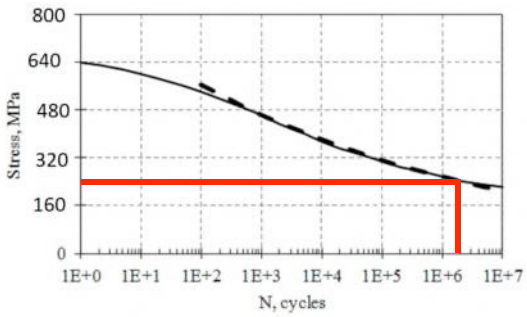

Figure 6: Wöhler S/N curve for class 8.8 stud showing finite life cycles

After more in-depth calculation, the existing design was meant to break.

3 Design modification

3.1 Stud modification

Considering the problem, the decision was taken to increase the stud length to increase pre-stretch and improve tolerance to bending. A design with reduced shank according to DIN 2510 with rolled threads was considered.

by: Guillaume Gien, Jean-Christophe Courcol – TOTAL; Wolfgang Voiticek – LMF

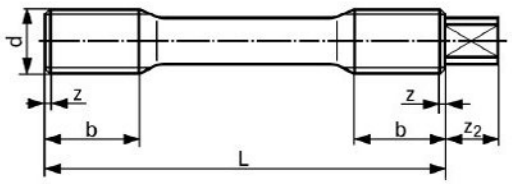

Figure 7: DIN 2510 stud with reduced shank

The material grade was changed from 8.8 to 12.9 and the torque has been increased from 180Nm to 210Nm

This was providing an increase in safety factor considering gas load from 2.4 to 3.5.

A set of cylindrical spacers was added under the nut of the assembly.

The head deflexion was checked with this new assembly, but although some improvement was there, we could still note up to 0.025mm deflexion of the head flange at the nut location and 13% in stress difference across stud section.

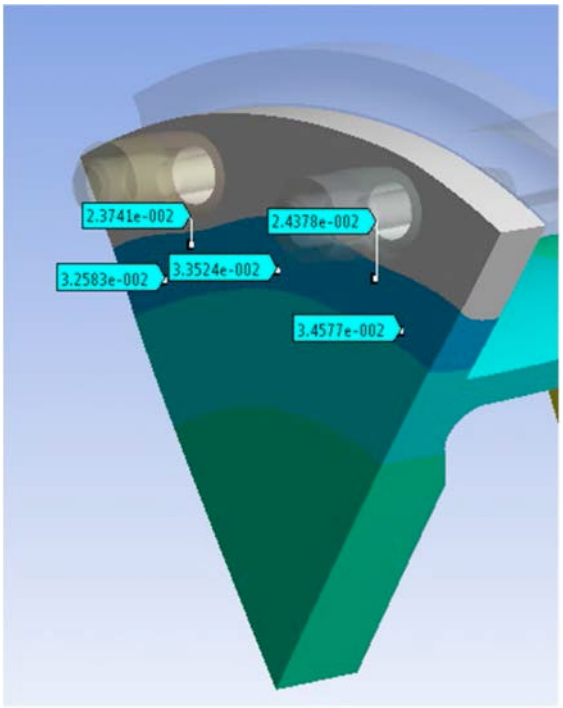

Figure 8: Cylinder head deflexion with extension sleeves

Modification of the cylinder head was also required to limit the deflection.

3.2 Cylinder head modification

Since the root cause was the head flange flexibility, the modification of the head appeared necessary.

Two options were possible:

1 Manufacture new heads with thicker flanges
2 Stiffen the existing heads by introducing reinforcement ring in place of the cylindrical spacers

Option 2 was selected since it was quicker and cheaper to implement.

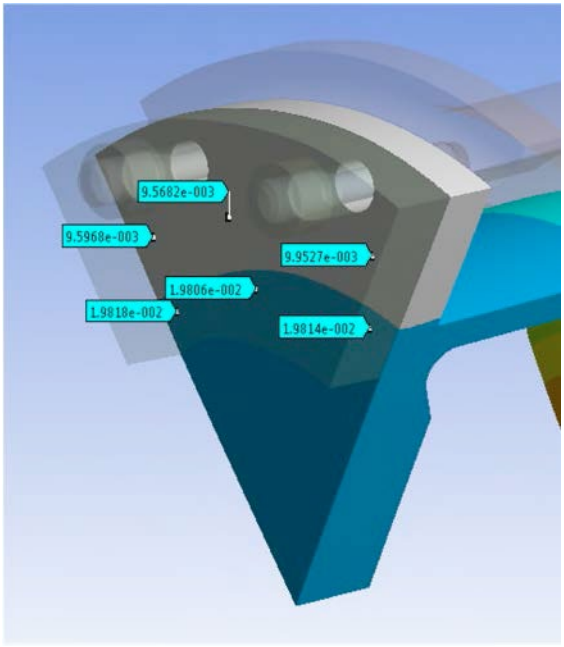

Figure 9: Cylinder head deflexion with the reinforcement ring

With the reinforcement ring in place, the deflexion of the head flange at the nut location was limited to 0.009mm and the difference in stress across the stud section limited to 2N/mm^2.

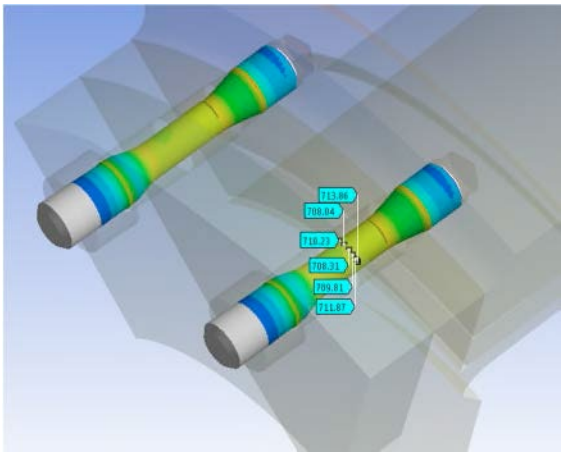

Figure 10: Even stress distribution on bolt sections

The below fatigue calculation using Modified Goodman Curves are showing the improvement provided by the new design.

by: Guillaume Gien, Jean-Christophe Courcol – TOTAL; Wolfgang Voiticek – LMF

- Reduction in alternating stress provided by reinforcement ring and higher stud preload (torque).
- Increased Modified Endurance Limit provided by higher material grade.

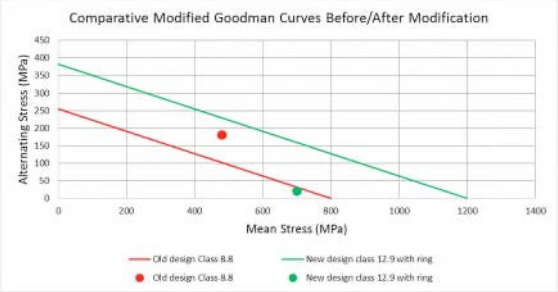

Figure 11: Fatigue calculation comparison before/after modification

3.3 Final design modification

Based on above simulation and calculations the design was modified as per below table.

	Old design	New design
Studs	DIN 939	DIN 2510
Length	M16 x 60	M16 x 100
Grade	8.8	12.9
Torque	180 Nm	210 Nm
Ring	None	25 mm thick * 75 mm wide
Bolt thread	machined	rolled
Yield Stress	640 MPa	1080 MPa

Table 1: design comparison

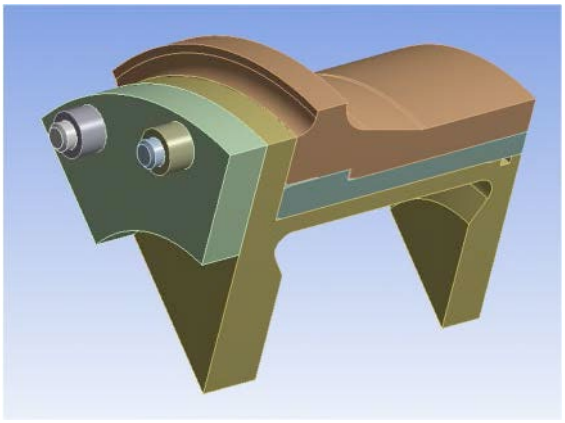

Figure 12: Final head assembly design with reinforcement ring, extended studs of higher material grade

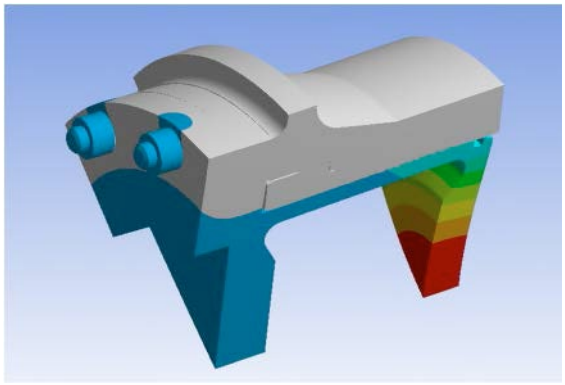

Figure 13: Cylinder head deformation after modification

3.4 Implementation of modification at site

Parts have been manufactured in due time by the OEM in order to install them on all 4 cylinders during an opportunity stop in May 2016. For easier assembly at site considering cooling water piping connected to the head, the reinforcement ring was cut in 2 identical sectors.

Picture 3: New reinforcement ring and studs

by: Guillaume Gien, Jean-Christophe Courcol – TOTAL; Wolfgang Voiticek – LMF

Picture 4: Front view of new reinforcement ring and studs after installation on the head

Picture 5: Side view of new reinforcement ring and studs after installation on the head

Since the modification was implemented in May 2016, the compressors have been put back into service and no further stud fracture has been faced. Daily operator visual inspections of the heads and studs are carried out and preventive non-destructive examination of all sets of studs is scheduled for the next major overhaul.

4 Conclusion

Design issues can sometimes be encountered in the early stage of a newly commissioned compressor. Operators shall always make aware the OEM of those problems and a joined effort often leads to a successful design modification. A reliable machine is mandatory for safety and availability point of view.

Stud fractures on reciprocating compressors are not uncommon due to the alternating forces applied to them. Great care should be taken to apply the right lubricant and torque during the assembly in order to get the correct pre-stretch of the stud and avoid the alternating stress.

As a consequence of these findings, OEM have improved the design process of the cylinder unit. An additional calculation step has been added to the calculation process, on top of the common pressure calculation of the cylinder head (and valve covers).

It is now mandatory to calculate the bending deflexion of each cylinder head and valve cover. The acceptance criteria is defined as 0,01mm maximum deflexion for the cylinder head and valve cover.

Following above design process improvement, all tailor made compressors delivered between 2005 and 2015 have been scanned and recalculated to check compliance with new acceptance criteria. In two cases, the cylinder head had to be modified due to non-compliance.

Since the implementation of this additional calculation step, no further failure of the cylinder head stud bolts was reported.

ADVANCING PERFORMANCE | + RELIABILITY + EFFICIENCY

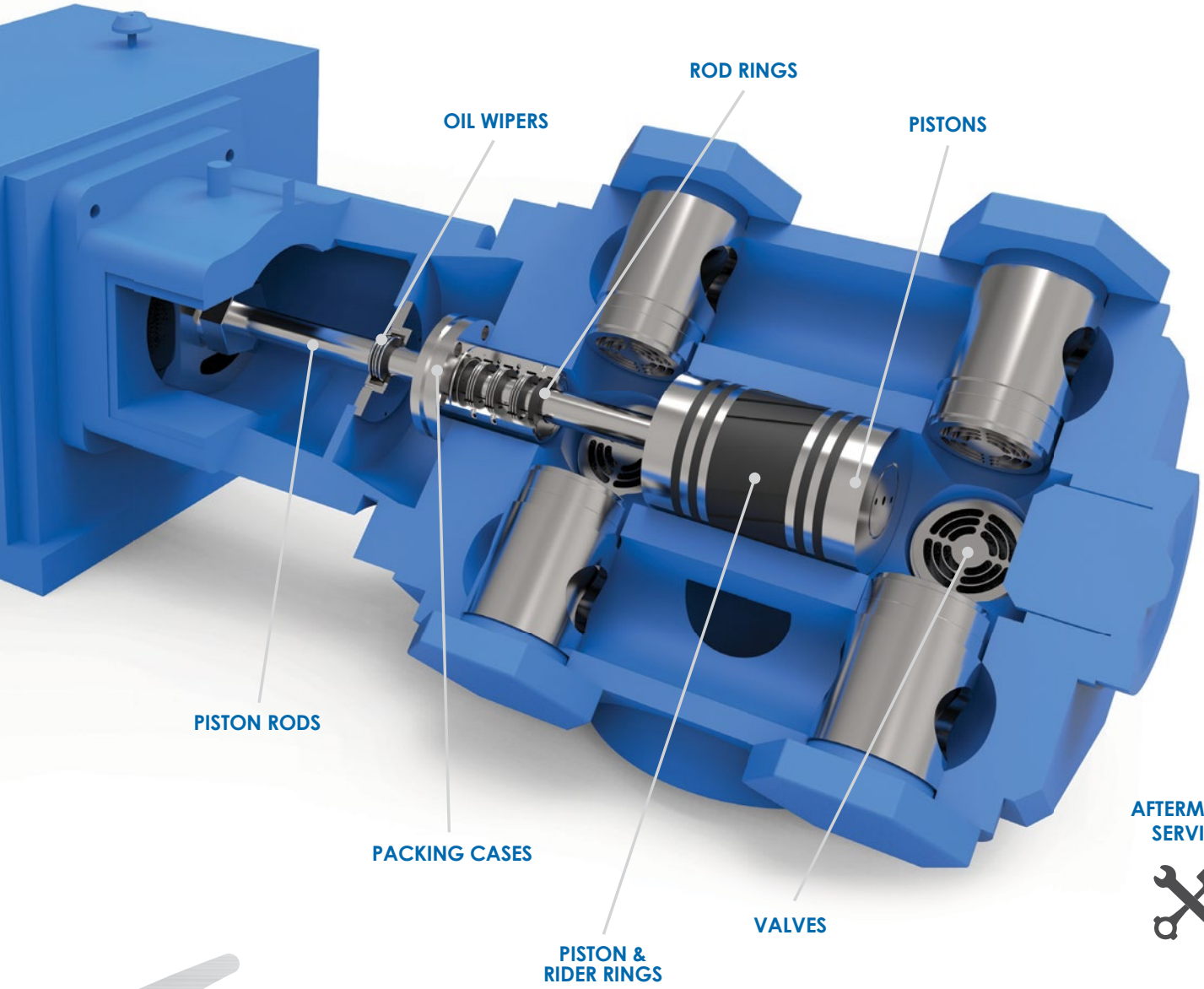

Cook Compression offers custom-engineered components, repair and reconditioning services and technical support for reciprocating compressors around the world. Our solutions extend run times, increase efficiency, address emissions, reduce operating costs, eliminate unplanned downtime and resolve chronic problems—delivering quantifiable advances in performance.

COOK® COMPRESSION
A DOVER COMPANY

+44 151 355 5937
cookcompression.com

Influences on Torsional Vibration Analysis of Electromagnetic Effects of an Induction Motor driving a rigidly flanged Reciprocating Compressor

by:

Baldussu, Alessandro
Oil & Gas Turbomachinery Process Solutions – Engineering
Baker Hughes, a GE company
Florence, Italy
alessandro.baldussu@bhge.com

Fernández Valdés, César Luis
Central Engineering Office
REPSOL
Madrid, Spain
cfernandezv@repsol.com

11th EFRC CONFERENCE
September 13 – 14, 2018, Madrid

Abstract:
In literature, the *Electromagnetic Spring (EM)* effect on induction motors driving Reciprocating Compressors is well known. This influence has been studied on trains with torsionally-soft couplings that led to the shift of the 1st *Torsional Natural Frequency (TNF)* and the growth of a new rigid mode, i.e. TNF-0, with a very low frequency value. Usually, in rigidly coupled trains, the latter effect is considered negligible.
This paper is aimed at presenting a practical example where the rigid mode growth, due to EM effects, generates electro-mechanical resonance that implied unacceptable current pulsation fluctuations.
The train had been originally designed according to API 618 criteria using a purely mechanical lumped masses model. To understand the impact of the rigid mode, i.e. TNF-0, a new model, which includes the Electromagnetic Spring effect influence, has been developed. To validate the study two sets of Torsional Natural Frequencies measurements have been recorded, i.e. before and after the corrective actions had been implemented.
On rigidly flanged single bearing induction motors the EM effects can be neglected if the driver and driven *Inertia ratio (Ir)* is high. The field data collected on a refinery application driving a *Reciprocating Compressor (RC)* have shown that the influence of EM effects is affected by the accuracy of driver's mechanical parameters. To properly design a new unit or develop adequate corrective actions, the mode shapes and their variations, according to Inertia ratio, must be considered fitly. Moreover, the position of the 1st TNF node influences the dynamic response of the train if in correspondence of the driver's spider shaft section.
The aim of this paper is to provide guidelines for additional checks, required during *Torsional Vibration Analysis (TVA)* when dealing with the above-mentioned configurations particularly when the driven equipment inertia is much lower than the driver inertia.

by: Alessandro Baldussu – Baker Hughes GE; César Luis Fernández Valdés – REPSOL

1 Introduction

In Murray, Howes & Zacharias[1] one of the first system approaches to torsional analysis has been presented. In this archetypal work, the primary focus was to consider the total effect of the interaction of the train components, from a purely mechanical standpoint, in order to avoid the delays caused by the temptation of designing a compressor based on rules of thumbs. Late after, Knop[2] have analysed the importance of motor dynamics in reciprocating compressor. This study concludes that the analysis of motor air gap torque should be included into the purely mechanical model. The EM effect has been modelled using a stiffness parameter and a viscous damping parameter connected between the driver rotor core and the ground. The former parameters imply that the shift of the 1st TNF, and the latter connection introduces a TNF-0 or so-called rigid mode that has typically a very low frequency. Holopainen et Al.[3] have completed the study considering the modelling, the analysis and the design of electric drives as a part of torsional systems. The subject has been reviewed from a broad perspective aimed at helping rotor-dynamic professionals without a background on electric drives. Finally, analysis and design guidelines were proposed throughout the paper.

Unfortunately, even nowadays the above-mentioned holistic approach that integrates electric drivers, frequency converters -if present-, and electric network -including transformers- it is extremely time consuming. Moreover, the required cross-functional design is not yet ready to be addressed by actual organizations. These are the reasons why simplified electro-mechanical approaches are still used in the industry.

Hauptmann, Eckert & Howes[4] - Brunelli et Al.[5] widely presented the theoretical background of the influence of torsional vibrations of EM effects across induction motors air gap. These fluctuating electro-magnetic torques at the rotor turn into current pulsations in the stator winding. Hauptmann, Eckert & Howes[6] proposed an approximated method for calculating this dangerous phenomenon. Feese & Kokot[7] used the above-mentioned simplified approach driving their attention to the recommendations for reciprocating trains using flexible couplings.

Upon the completion of the analysis of the existing literature on this topic, it was found out that no specific studies had been developed to address the impact of the EM effect for rigidly coupled RC trains.

This paper focuses the attention on the growth of the rigid mode, and the consequences of electro-mechanical resonances for rigidly flanged reciprocating compressor trains driven by induction motors.

2 Torsional Design

According to API 618, TNFs of the complete driver-compressor system shall not coincide or be too close to any frequency of a periodic forcing phenomenon (excitation) applied to the rotor system. The intersection of a TNF with a periodic excitation may hinder the operation of the complete unit creating excessive vibrations. In the next paragraphs the process used to perform the torsional design of the train will be presented.

2.1 Mass Elastic Modelling

Due to the high complexity of the reciprocating compressor train, an equivalent model is composed by a series of flywheels representing both the crankshaft and the connected parts. A crankshaft mass-elastic model is typically created by lumping the inertia at each throw and calculating the equivalent torsional stiffness between throws. The flywheel, always present from a torsional point of view, can be represented by a single concentrated mass with mass polar moment of inertia.

Double-bearing electric motor drivers are always connected to the RC via a flexible coupling, whereas single-bearing motors are rigidly coupled to the compressor. If a flexible coupling is present the most appropriately way of modelling is by means of a single torsional spring. The coupling vendor provides the torsional stiffness and the correspondent inertias of the relevant coupling halves at each end. In case of double row rubber coupling, the model is composed of 3 masses and 2 torsional springs. It is important to note that the stiffness of elastomeric couplings is 1 to 2 orders of magnitude smaller than that of the other shaft intervals.

The drivers are usually modelled with a single lumped mass and with an equivalent torsional stiffness of the shaft interval i.e. from the rotor windings centre to the drive end flange. Internal motor fans –if present- are modelled as single lumped masses

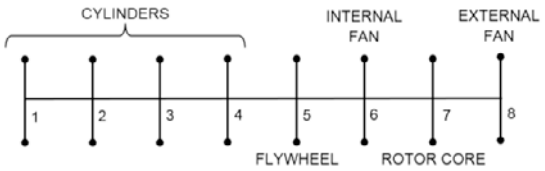

Figure 1: Lumped mass Reciprocating Compressor Train Model

Figure 1 represents the lumped mass model of the BHGE Nuovo Pignone Reciprocating Compressor system installed in a REPSOL refinery.

The compression train under study is composed of a 4-cylinder compressor, a flywheel (i.e. mass No. 5)

by: Alessandro Baldussu – Baker Hughes GE; César Luis Fernández Valdés – REPSOL

which is directly flanged on drive end side, and a single bearing electric motor driver (i.e. masses 6 to 8).

The single bearing driver, manufactured by ABB, has two fans respectively internal and external which are shrunk to the shaft. The drive end side is rigidly flanged with the RC flange and the flywheel with calibrated tie rods. In this case, a dedicated lumped masses and relative torsional interval stiffness have been developed to properly determine the torsional response of the train.

After the determination of the lumped masses model a Torsional Vibration Analysis of a fixed speed reciprocating system can be generally described as a seven-step procedure (Murray, Howes & Zacharias[1])

i. determine the system's Torsional Natural Frequencies (TNFs)

ii. determine the compressor torque effort

iii. predict the amount of interference between torque effort and TNFs

iv. evaluate the torsional forced response, including damping

v. modify the system until stress is acceptable

vi. evaluate electrical current pulsations, and remodify the model if necessary

vii. confirm results over the range of operating conditions.

In the process described above there is a single parameter that can be largely modified in order to define the final torsional design i.e. the flywheel inertia.

In the next section the flywheel selection, and the consequences on the train dynamic response of its modification, will be presented.

2.2 Flywheel Selection – Torsional Design

Once the reciprocating compressor has been configured, i.e. cylinder diameters, ballasts masses, phase delay, cylinder disposition, etc. the inertia of the first section of the compression train is defined and no further modifications are possible.

After the evaluation of the necessary power to execute the compression work and according to the electrical net characteristics, the driver frame is selected and the correspondent rotor core inertia value and torsional stiffness are mostly defined.

In accordance with the point *v.* from the process described in the previous section a *Flywheel (FW)* mass is usually inserted between the compressor drive end side and the driver. In fact, the FW allows to adjust the whole train inertia. A proper selection is necessary to prevent running in a state of resonance. In addition, the flywheel inertia is selected to limit the train irregularity degree to acceptable values, preventing excessive current variations in the electric motor windings, and thus in the electrical network which may affect other equipment connected to the same electrical system.

Finally, in a directly flanged reciprocating compressor train, which uses a single bearing driver configuration, the flywheel results the simplest single component to be replaced if a problem of resonance occurs in the field.

The next sub-sections will present the design steps followed during the torsional design of the compression train developed by BHGE for REPSOL.

2.2.1 SMALL Flywheel Design

During the first torsional design it was selected a flywheel with a small inertia value compared to the driver inertia. Equation No. 1 defines the inertia ratio between the driver and the driven components:

$$Ir = \frac{Driver\ Inertia}{RC + FW\ Inertia} \qquad Formula\ (1)$$

For the SMALL-FW configuration, the **Ir = 9.35**, which implies a big prevalence of the driver inertia respect to the driven one.

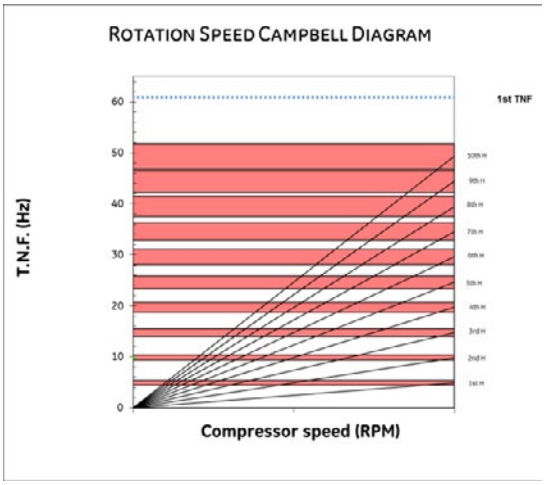

Figure 2: Campbell Diagram – SMALL Flywheel

In this case the TNFs are positioned outside the API range (i.e. up to and including the 10th harmonics). The selection allowed to reduce the torques on the driver's shaft due to a reduced harmonic contribution of the higher frequencies.

The Campbell diagram is represented in Figure 2 with the API bands highlighted in red. The 1st TNF is indicated with a blue dotted line.

by: Alessandro Baldussu – Baker Hughes GE; César Luis Fernández Valdés – REPSOL

In accordance with the mass numbers presented in Figure 1, the following graph shows the first three mode shapes of the SMALL-FW train design.

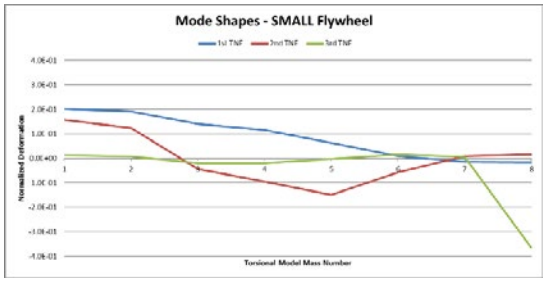

Figure 3: Mode Shapes – SMALL Flywheel

2.3 Current Pulsation Phenomena

In the presented design, i.e. SMALL FW, all the API requirements and BHGE internal criteria and design standards had been applied, including:

1. TNFs separation margins
2. Torques limitations for fatigue life
3. Irregularity degree

In spite of having achieved acceptable values for all the above-mentioned design parameters, the when the compressor train was commissioned in the refinery it suffered extremely high current variations. In fact, the pulsations reached values higher than 80% versus the 40% allowed for this type of motor design, and the absorbed current pulsation stopped the commissioning activity until the identification of the necessary corrective actions.

In order to exclude a wrong estimation of the torsional natural frequencies of the train, a set of field measurements have been performed. The 1st TNF presented a Δ = 0.3 [Hz] i.e. 0.5% accuracy between the predicted value and the measured one. This finding allowed to conclude that none uncertainty in the mass-elastic system, concerning the real train properties, have been introduced.

Feese & Kokot[7] deeply analysed the electromagnetic effects on TNFs for induction motors driving reciprocating compressors with a soft coupling.

Description	Variable
Number of stator poles	N_1
Breakdown motor torque	T_B
Rated full load torque	T_R
Freq. of superimposed torsional vibration	ω
Electrical supply frequency	Ω_s
Slip at rated speed	S_r

Table 1: Data from Electric Motor Manufacturer

It is important to note that in the relevant literature this effect was not considered relevant for direct flanged connections.

Due to the elevated level of current pulsation reached by the SMALL-FW configuration on field it has been decided to apply the simplified formulation presented by Feese & Kokot[7] reported in Table 1 and formulas 2, 3 and 4 in order to verify the influence of EM effect.

The electrical time constant is:

$$T_L = \left(\frac{1}{\Omega_S}\right) \cdot \left(\frac{1}{2S_r}\right) \cdot \left(\frac{T_R}{T_B}\right) \qquad Formula\ (2)$$

The EM Stiffness is defined as:

$$K_{em} = N_1 \cdot T_B \frac{(\omega \cdot T_L)^2}{(1 + (\omega \cdot T_L)^2)} \qquad Formula\ (3)$$

The EM Damping is calculated per:

$$C_{em} = K_{em} \cdot \frac{T_L}{(\omega \cdot T_L)^2} \qquad Formula\ (4)$$

Applying this simplified formula on the SMALL-FW configuration, there is the growth of a TNF-0 with an extremely low value i.e. 4.39 [Hz] that has a separation of c.a. 11% with respect to the RC rated speed.

Figure 4 shows the Campbell Diagram, including the Rigid Mode i.e. TNF-0.

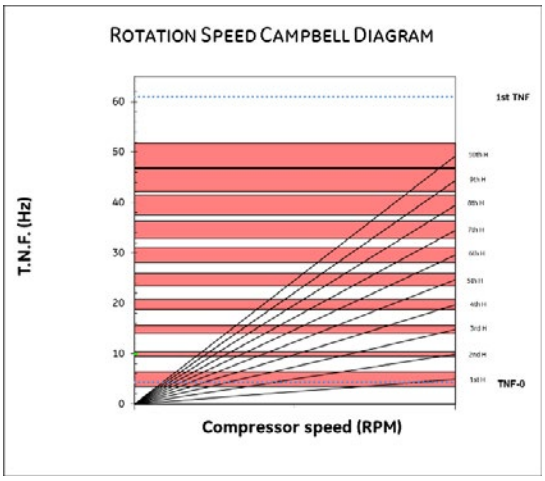

Figure 4: Campbell Diagram – SMALL-FW Considering Rigid Mode i.e. TNF-0

On the other hand, the shift of 1st TNF, on direct coupling connections, is extremely limited (<2%)

by: Alessandro Baldussu – Baker Hughes GE; César Luis Fernández Valdés – REPSOL

which can be considered acceptable respect to the actual calculation tools tolerances.

In order to draw a correct conclusion, a key aspect have to be taken into account, the formulation used to calculate the EM effects is an approach derived by an approximate electro-mechanical approach. This is the reason why the API separation margin for 1st TNF i.e. +/-10% is not sufficient to guarantee the absence of electromechanical resonances.

Based on the field experience, in order to avoid any possible resonances, in absence of other design practice or indications, for TNF-0 it has been decided to consider for the new designs a separation margin of +/-30% respect RC rated speed.

3 Design Optimization

Starting from the assumption about the correctness of the mass-elastic model used to predict the TNFs it has been developed an optimization that considers only the mechanical parameters. This calculation model has been used to reach the correct separation margins and respect the minimum inertia required by the driver to limit the current pulsation.

3.1 FW Selection – Corrective Action

The next sub-sections will present the design steps followed during the corrective actions development for the compression train installed by BHGE for REPSOL after the current pulsation issues.

3.1.1 BIG FW Design

To solve the current pulsation issue, it has been selected a second flywheel i.e. BIG-FW, with an inertia value similar respect the driver inertia. The Inertia ratio for this configuration is **Ir = 1.198** which implies an equilibrated ratio between the driver inertia and the driven one.

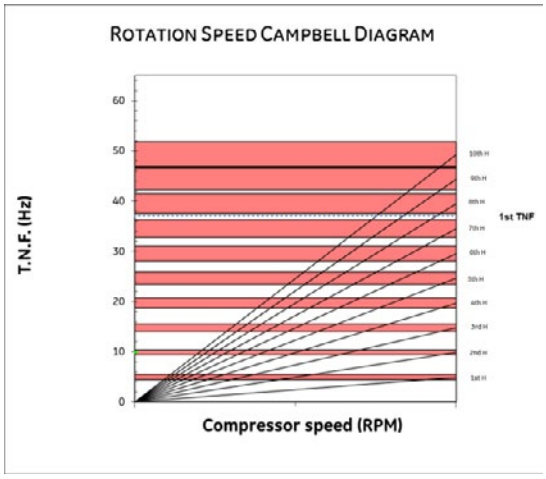

Figure 5: Campbell Diagram – BIG Flywheel

The TNFs of BIG-FW design are positioned inside the API range i.e. between the 7th and 8th harmonic with an adequate separation margin as per API recommendation in order to properly avoid uncertainties in the system mass-elastic properties.

The Campbell diagram is represented in Figure 5 with the API bands highlighted in red. The 1st TNF is indicated with a blue dotted line.

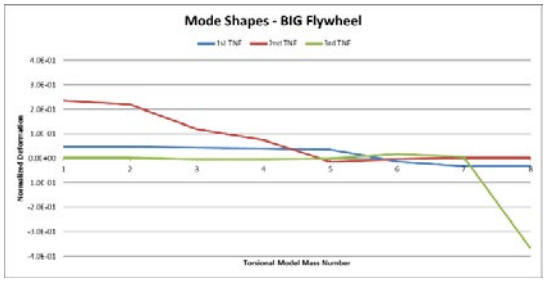

Figure 6: Mode Shapes – BIG Flywheel

In accordance with the mass numbers presented in Figure 1, Figure 6 represents the first three mode shapes of the BIG-FW train design.

Finally, the FW selection allowed to remain within the allowable alternating torques limits on driver shaft as per driver manufacturer indications.

3.2 Mechanical Resonance Phenomena

For the BIG-FW design configuration all the requirements according to API criteria and internal design standards have been applied:

1. TNFs separation margins
2. Torques limitations for fatigue life
3. Irregularity degree

Moreover, two new requirements have been implemented:

a. Minimum driven inertia i.e. RC plus FW

b. Maximum allowable FW weight

The requirement (a). has been introduced to reach the minimum value of inertia required to limit the current pulsation according to driver manufacturer calculations i.e. < 40%

On the other hand, requirement (b). allowed to use the available driver without modification on bearing supports.

As per the previous design, none of the above-mentioned design checks had unacceptable values, but the train, after the corrective action i.e. the installation of the BIG-FW, suffered by extremely high alternating torque fluctuation problems.

So much so, that the torque pulsation on driver shaft reached values higher than the fatigue life values allowed for this driver's design and to guarantee the shaft line life it had to be defined a non-fly zone for partial loads.

by: Alessandro Baldussu – Baker Hughes GE; César Luis Fernández Valdés – REPSOL

In order to understand the reasons behind this unexpected behaviour of the compression train a second field measurements campaign was performed.

The 1st TNF presented a Δ = 1.9 [Hz] i.e. 4.8% this allowed to deduce that important uncertainties in the system mass-elastic train properties have been introduced.

3.3 Sensitivity of mass-elastic parameters

According to Murray et Al.[8] the shaft torque and the corresponding stresses in a drive direct coupled reciprocating compressor system are significantly influenced by the system's mass-elastic properties. In this case the fully match during the first field data versus the predicted TNF led to exclude the uncertainties.

In order to study the reasons why the second field data surprisingly presented a big error in the TNF prediction a *Design Of Experiment* (DOE) with the variation of all the parameters of the train has been conducted. A set of three torsional models have been tested:

A. FW variation (SMALL/BIG FW)

B. Driver's parameters variation

C. RC's parameters variation

Model A, FW variation, has been primary used to define the corrective action but due to the discrepancy encountered in the second field data set respect to the predicted TNFs values no predictivity can be assigned to this set of values. The DOE results are reported in Table 2.

	Variations			OPTIM	1st TNF			
					CALCULATED	MEASURED		
MODEL	RC	FW	DRIVER	RUNS	HZ	HZ	ΔHZ	ΔTNF1
A	=	SMALL	=	159	60.87	60.57	-0.3	0.50%
		BIG		73	37.12	39.00	1.9	-4.82%

Table 2: Model A – SMALL/BIG Flywheel DOE

In Murray et Al.[8] a set of uncertainties bands have been identified and specifically with the Rotor Spiders/Bars/Lamination design a stiffening effect and an underestimation of the inertia have been recognized. In order to validate this assumption, a set of values combinations i.e. driver shaft stiffness and rotor core inertia have been studied. In Table 3 the results of the best set of values considered in the plausible values space have been presented.

	Variations			OPTIM	1st TNF			
					CALCULATED	MEASURED		
MODEL	RC	FW	DRIVER	RUNS	HZ	HZ	ΔHZ	ΔTNF1
B	=	SMALL	VARY	140	61.30	60.59	-0.7	1.17%
		BIG		140	38.85	39.00	0.1	-0.38%

Table 3: Model B – Driver's parameters DOE

Finally, to verify the parameters used for the compressor modelling a set of values combinations have been studied. In Table 4 the DOE results show that none of the combinations of values considered has been able to properly predict the TNF measured at site.

	Variations			OPTIM	1st TNF			
					CALCULATED	MEASURED		
MODEL	RC	FW	DRIVER	RUNS	HZ	HZ	ΔHZ	ΔTNF1
C	VARY	SMALL	=	162	60.87/69.26	60.57	-0.3/-8.7	0.50%/14.35%
		BIG		162	36.6/37.5	39.00	2.4/1.5	-6.10%/-3.85%

Table 4: Model C – RC's parameters DOE

3.4 Mode Shapes Analysis

The DOE of Model B allowed to identify, in the mechanical driver's parameters, the presence of uncertainty in the values used during the calculations carried out to define the corrective action as per the BIG FW design.

Wang, Feese and Pettinato[9] defined a comprehensive list of uncertainties in modelling that can be divided into errors and variations.

In their list some errors have been identified in the mechanical's driver parameters but none of them allowed to understand why using the same torsional model A, a set of field data has been in accordance with the predicted values i.e. SMALL-FW Design and the other is not i.e. BIG-FW Design.

A deep analysis of the mode shape variations, allowed to understand that the position of the 1st TNF node is a function of the Inertia ratio presented in formula 1. In fact, the 1st TNF node moves along the shaft line depending on the value assumed for Ir. The relative position influences the dynamic response of the train especially if the node is in the proximity of the flexible elements such as the driver's shaft spiders. Therefore, especially in the case of direct coupled induction motor, this ratio can have different weights in the uncertainty influence of the driver's mechanical parameters.

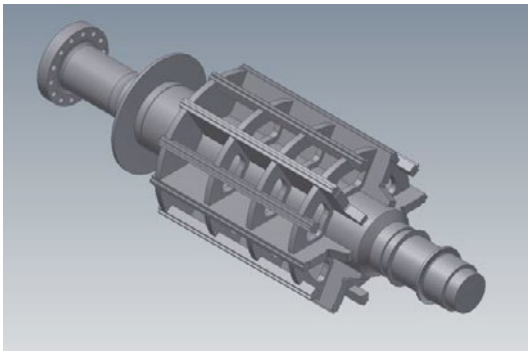

Figure 7: 3D Model of driver shaft

by: Alessandro Baldussu – Baker Hughes GE; César Luis Fernández Valdés – REPSOL

In Figure 7 a 3D driver's shaft model is presented with a schematic representation of the internal fan i.e. the thin disc on the left side between the drive end flange and the rotor spiders.

The rotor spider design has a stiffness between the flange and the rotor core, i.e. section 6-7 according the mass numbers used in the model represented in Figure 1, that is c.a. 200% respect to the stiffness of the section between the flange and the internal fan i.e. section 5-6. The latter is comparable with the compressor shaft section that led the rotor core to have a stiffness predominant respect to the other sections.

Moreover, in the SMALL-FW design the rotor core has an inertia that is c.a. 10 times respect to the load inertia i.e. RC + FW.

Analysing the mode shape presented in Figure 3 it is possible to identify that the rotor core features are predominant in the deformation. In fact, the rotor core reacts "like a wall" that is absorbing all the deformation accumulated by the compressor during its operation. In the SMALL-FW configuration, the flywheel inertia is not able to absorb the energy given by the inherent irregularity of the reciprocating machine. The result is an absence of rotor core deformations that oscillates with the same irregularity of the RC flange leading high current pulsation levels.

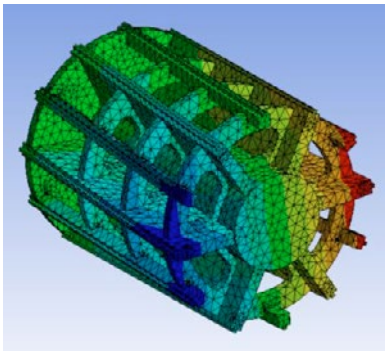

Figure 8: FEM Analysis of driver shaft

On the other hand, analysing the mode shape presented in Figure 6 i.e. BIG-FW design it is possible to identify a complete different behaviour. In this case the driver has an inertia that is comparable to the to the load inertia i.e. **Ir ≈ 1**.

The deformation of the 1st TNF is mostly concentrated in the section between the FW and the drive end side of the motor shaft. In fact, the higher FW inertia is able to absorb the energy given by the inherent irregularity of the reciprocating machine limiting the level of oscillation on the rotor core.

It can be noted that, on the 1st mode shape the RC side deformations are practically constant. In fact, only the deformation of the rotor spiders section introduces a significant contribution in the dynamic behaviour of the train.

The BIG-FW design, compared to the SMALL-FW one, shows that the rotor core stiffness influences the dynamic behaviour of the entire train. In fact, due to the comparable inertia of the driven and the driver loads, this results in a higher deformation of the rotor core section, and the latter aspect results fundamental in the dynamic behaviour of the train.

According to the fact that the rotor core section with the spiders has a stiffness, which is roughly. double in respect to the other sections, a small uncertainty causes big impacts on the predictivity of the model.

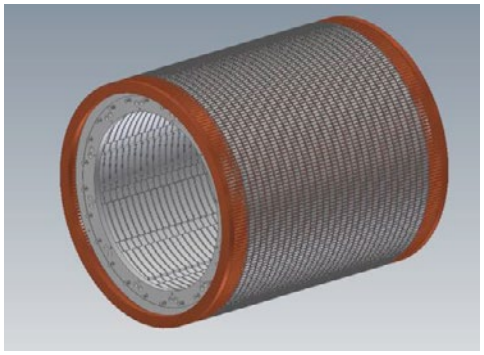

Figure 9: Rotor Core 3D model fully featured

To take into account properly this aspect and avoid mistakes in the prediction a detailed FEM analysis of the spider shaft section has been developed (Fig. 8). The results showed a discrepancy on the rotor stiffness approximatively of 13.5% compared to the values used during the design phase.

Finally, a 3D rotor core model, fully featured, has been developed (Fig. 9) and a discrepancy on the relative inertia of -9%, has been identified.

4 Field Data – Model D Validation

In order to validate the hypotheses, the calculations and all the considerations done during the development of this project a new set of field data measures has been carried out.

A new Model D, which uses the revised driver mechanical parameters has been developed. These values have been obtained using a FEM analysis to calculate the stiffness and, a fully featured 3D model to evaluate the rotor inertia.

The model D differs from model A only for the updated driver mechanical parameters. In fact, none variations have been introduced on the RC parameters, which have been originally obtained by means of FEM analysis and 3D CAD modelling.

With this new set of values, the 1st TNF is exactly positioned in between 7th and 8th harmonic in compliance with API margins.

by: Alessandro Baldussu – Baker Hughes GE; César Luis Fernández Valdés – REPSOL

In Table 5 the comparison between the expected 1st TNF value and the measured one is presented.

1st TNF [Hz] – TVA ANALYSIS	1st TNF [Hz] – MEASURED
36.91	36.90

Table 5: Model D – expected vs measured 1st TNF

Furthermore, in Figure 10 the results of the strain gage field data with the indication of the 1st and 2nd TNF during the shutdown are reported.

Theoretical torsional Model D provides a full match of the measured 1st TNF with an accuracy of 0.03 % (difference = 0.01Hz).

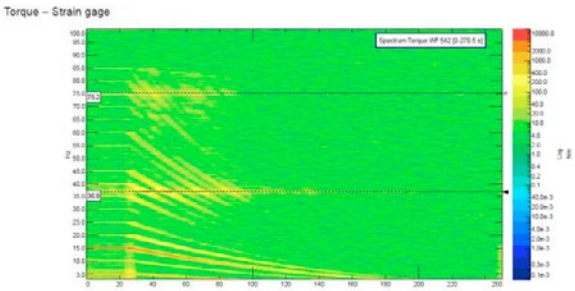

Figure 10: Torque – Strain gage measurements

5 Conclusions and Recommendation

In case of reciprocating compressors trains driven by directly flanged induction motors, the uncertainties on the mechanical driver parameters is a function of the Inertia Ratio defined in *Formula (1)*.

This error is characterized by a different influence as a function of the selected configuration. In fact, with the *Ir* variations – driven vs driver inertias – and the relative position of the 1st TNF node, the dynamic response of the train varies.

When *Ir* is close to 1, the uncertainties on stiffness and inertia of the driver can lead to wrong estimations of the Torsional Natural Frequencies.

On the other hand, if the driver inertia is much higher than the RC + Flywheel inertia, the uncertainties on driver shaft stiffness do not introduce errors higher than the acceptable calculation tolerances in the estimation of the Torsional Natural Frequencies.

In the former case (i.e. *Ir* close to 1) it is necessary to perform an evaluation of the motor dynamics effect due to the Electro-Magnetic Field Effect. This analysis, for synchronous motors, can be also performed according to the simplified formulations. For example, in Feese & Kokot[7] is present the most suitable one to foresee and avoid any possible electrical resonance in respect to the rotating compressor speed.

5.1 TVA Design Procedure

In order to properly execute a torsional design of a fixed speed reciprocating system, after the determination of the lumped masses model, preferably using FEM analyses and the 3D modelling of all the components, the Torsional Vibration Analysis generally described as a seven-step procedure by Murray, Howes & Zacharias[1] can be improved adding the following verifications steps:

i. determine the system TNFs

ii. determine the compressor torque effort

iii. predict the amount of interference between torque effort and TNFs

iv. evaluate the torsional forced response, including damping

v. verify the Ir = driver/RC+FW ratio

   a. Driver Inertia c.a. equal to RC+FW inertia: verify the uncertainties on the mechanical properties of the driver shaft

   b. Driver Inertia >> RC+FW Inertia: apply the simplified formulation of electromagnetic effects to verify:

      i. Electrical resonances

      ii. Angular oscillation level

vi. verify the mode shapes variations and the position of 1st TNF node according to the Ir = driver/RC+FW inertia ratio variation

vii. confirm results over the range of operating conditions

In case of trains configured as follows:

- direct flanged
- rigidly coupled
- induction motors

the separation margin between the TNF-0 i.e. rigid mode, calculated by means of electromagnetic effect simplified formulas, must be bigger than +/-30% respect the rotating compressor speed.

The above-mentioned separation margin has been decided after the analysis, with the simplified formulation of the EM effect, of more than 30 BH-GE Nuovo Pignone Reciprocating Compressor Trains installed on the fleet, rigidly coupled and driven by induction motors provided by different manufacturers.

In fact, the only train which encountered the pulsation current problem phenomena has been the one with the value of separation margin lower than 30% of the TNF-0 respect to RC the rated speed.

by: Alessandro Baldussu – Baker Hughes GE; César Luis Fernández Valdés – REPSOL

5.2 Recommendations

During the torsional design phase, it should be considered the electromagnetic effects on TNFs also for motors driving reciprocating compressors with direct flanged.

Special attention must be paid to the correct calculation of the torsional stiffness since the spider shaft core stiffening contribution is difficult to predict.

The motor manufacturer must provide the shaft detailed drawing including the inertia and stiffness parameters calculated considering a tolerance lower than ±5% in order not to affect the predictability of the torsional model.

6 Acknowledgements

The authors would like to thank ABB S.p.A. Vittuone – Italy, especially Eng. Daniele Cinque for the calculations performed, and Eng. Giuseppe Murru for the support and the excellent collaboration attitude shown during the study of the possible root causes and the driver's mechanical parameters influences on the encountered design challenges.

References

[1] Murray, Howes & Zacharias (1995): A System Approach to Torsional Analysis, Canadian Machinery Vibration Association National Conference, Halifix.

[2] Knop (2012): The Importance of motor Dynamics in Reciprocating Compressor Drives, 8th Conference of the EFRC, Dusseldorf.

[3] Holopainen, & Alt. (2013): Electric motors and Drivers in Torsional Vibration Analysis and Design, Proceedings of the Forty-Second Turbomachinery Symposium, Houston.

[4] Hauptmann, Eckert & Howes (2013): The Influence on Torsional Vibration Analysis of Electromagnetic Effects Across an Induction Motor, Gas Machinery Conference, Albuquerque.

[5] Brunelli & Alt. (2015): Torsional Vibration Analysis of Reciprocating Compressor Trains Driven by Induction Motors, 9th International Conference on Compressors and their Systems, IOP Publishing.

[6] Hauptmann, Eckert & Howes (2014): Approximate Method for Calculating Current Pulsations Caused by Induction Motors Driving Reciprocating Compressors, Gas Machinery Research Council, Dallas.

[7] Feese & Kokot (2016): Electromagnetic Effects on the Torsional Natural Frequencies of an Induction Motor Driven Reciprocating Compressor with a Soft Coupling, 45th Turbomachinery & 32nd Pump Symposia, Huston.

[8] Murray & Alt. (1996): Sensitivity of Torsional Analysis to Uncertainty in System Mass-Elastic Properties, International Pipeline Conferences – volume 2, ASME.

[9] Wang, Feese & Pettinato (2012): Torsional Natural Frequencies Measurements vs. Prediction, Proceeding of the Forty-First Turbomachinery Symposium, Huston.

EUROPEAN FORUM
for RECIPROCATING
COMPRESSORS

COMPRESSOR AND COMPONENT DESIGN

STASSKOL

Calculation of Transient Flow in Sealing Elements

by:

Dr. Ing. Georg Flade
STASSKOL GmbH
Stassfurt, Germany
georg.flade@stasskol.de

11th EFRC CONFERENCE
September 13 – 14, 2018, Madrid

Abstract:
The consideration of transient flow behavior in reciprocating compressors is getting more and more important. This applies to piston rod packings and piston rings as well as to other design elements of the compressor system. The numerical calculation of dynamic pressure effects at the compressor sealing elements was already presented in numerous papers. The main focus had been on unsteady flow behavior in labyrinth packings or on leakage rates over labyrinth pistons. By using measurement results of the compressor testbed, the theoretical model can be adjusted to calculate the non-steady behavior of standard contacting packing rings as well as to calculate the flow through contacting piston rings. The calculation results are used to define design criteria for rings and packings such as:

- Use of pressure breaker rings depending on application parameters
- Pressure breaker ring design depending on application parameters
- Number and design of pressure relief grooves for rider rings

In addition to the utilization during the design phase, the calculation method can be used for failure diagnostics of sealing elements in reciprocating compressors.

by: Dr. Georg Flade – STASSKOL

1 Introduction

Sealing elements in reciprocating compressors are exposed to transient boundary conditions. Obviously, the cylinder pressure varies between suction pressure and discharge pressure. But, beside this, there are other influences like external pressure pulsations or valve fluttering, which lead to high pressure dynamics inside the compressor cylinder.

Due to fluctuating pressures inside the cylinder, the forces acting on some of the sealing elements permanently change their direction. There are several ways to design the sealing elements that can resist the fluctuating forces. Other sealing element designs are able to minimize the pressure fluctuations. Nevertheless, dynamic forces play an important role as potential root cause for failures of sealing elements.

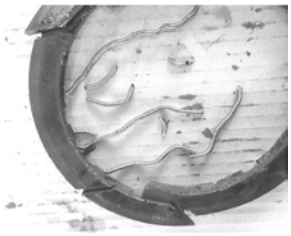

Figure 1: Damaged sealing ring caused by broken spring

Figure 2: Damaged spring eye leading to spring failure

Figure1 above shows a damaged sealing ring. The damage was caused by a broken spring. A typical failure mode of sealing ring springs is shown in figure 2. The spring wire in the eye is worn off by the dynamical movement of the spring. In order to diminish the fluctuation of the pressure leading to those dynamical movements, pressure breaker rings that have different design styles are installed in one or more packing cups at the cylinder end of the packing. The main purpose of the investigation is to get a better understanding of the flow dynamics inside packing chambers. This is to evaluate the sealing efficiency of different pressure breaker ring styles and to develop design criteria for piston rod packings depending on different pressures and different gases. Apart from the transient flow in piston rod packings, other questions can be investigated by using the same method, e.g. the leakage flow through a passage of piston and guide rings allowing to define design criteria for rider bands.

2. Calculation Model

The two figures below show the calculation models for the flow through a piston rod packing and the flow over a cascade of piston rings and rider bands.

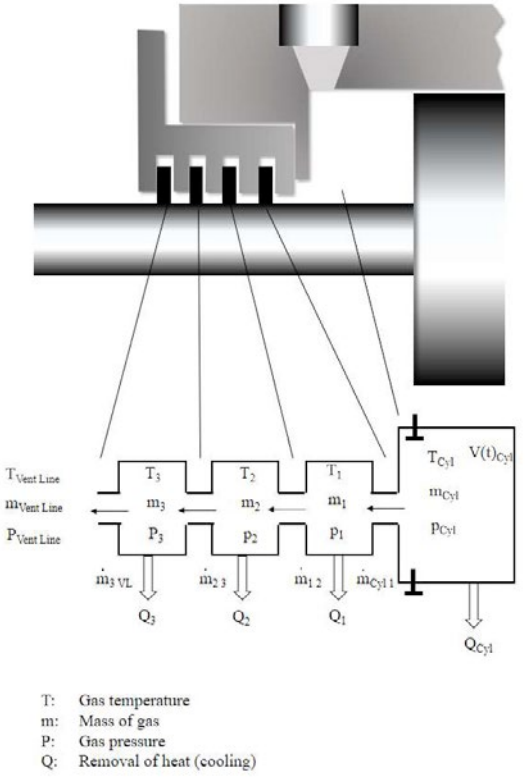

Figure 3: Calculation model for the flow through a piston rod packing

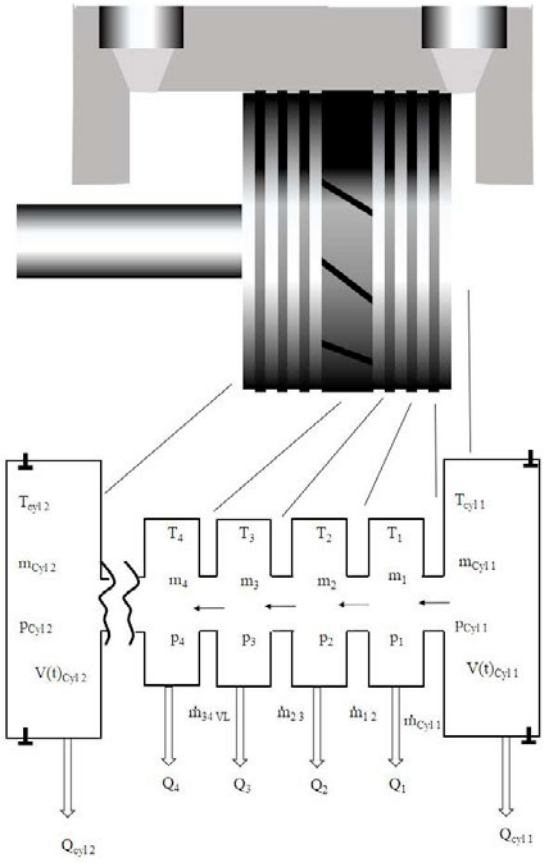

Figure 4: Calculation model for the flow through a piston ring passage

by: Dr. Georg Flade – STASSKOL

The mass balance and the energy balance are calculated for every chamber of the system including the cylinders.

The following equations (1) and (2) describe the thermodynamic condition in each element in the model above. The heat flux e.g. due to cooling systems and the gas mass flows between the different chambers are considered.

$$\frac{dp_C}{dt} = p_C \left(\frac{1}{T_C}\frac{dT_C}{dt} - \frac{1}{V_C}\frac{dV_C}{dt} + \frac{1}{m_C}(\dot{m}_{in} - \dot{m}_{out}) \right) \quad (1)$$

The term $\frac{dp_C}{dt}$ is the pressure transient in the chamber. The temperature transient of each chamber is $\frac{dT_C}{dt}$, and $\frac{dV_C}{dt}$ stands for the volume transient, which is zero for all chambers having a constant volume. For cylinder rooms, this value is to be determined considering the piston dynamics. All mass flows coming into the chamber are described by $\dot{m}_{in}$, the mass flow coming out is $\dot{m}_{out}$.

$$\frac{dT_C}{dt} = T_C \left(\frac{\kappa-1}{\kappa}\frac{1}{p_C}\frac{dp_C}{dt} - \frac{1}{V_C}\frac{dV_C}{dt} + \frac{1}{m_C}\dot{m}_{out} \right) + \sum_{i=1}^{n} T_{i_{Gas,in}} \frac{\dot{m}_{in,i}}{m_C} + \frac{1}{m_C\, c_p}\dot{Q}_{wall} \quad (2)$$

The isentropic coefficient is κ. The term $T_{i_{Gas,in}} \frac{\dot{m}_{in,i}}{m_C}$ stands for every mass flow with the index i, coming into the chamber multiplied by its temperature $T_{i_{Gas,in}}$. The heat flux over the wall is considered by the term $\dot{Q}_{wall}$. It is a negative value in most cases, since packing chambers and compressor cylinders are cooled in most cases. This means that heat then is removed from the chambers of the model. The term m_c represents the mass of the gas inside the chamber.

The calculation of the mass flow between two chambers depends of the type of the sealing element. Some elements, such as solid pressure breakers, solid labyrinth elements or sealing elements with relief grooves do not significantly change their cross-sectional area when the pressure difference over the sealing element is changing. For those items the mass flow between two chambers with index 1 and 2 is calculated using the following equation that describes the isentropic orifice mass flow.

$$\dot{m}_{1,2} = A\,\alpha \frac{p_1}{RT_1}\left(\frac{p_2}{p_1}\right)^{\frac{1}{\kappa}} \sqrt{\frac{2\kappa}{\kappa-1} RT_1 \left(1 - \left(\frac{p_2}{p_1}\right)^{\frac{\kappa-1}{\kappa}}\right)} \quad (3)$$

The factor A represents the cross-sectional area of a connecting element between two chambers. The gas behaviour is considered by the gas constant R. The real mass flow can be lower than theoretically expected due to viscous friction. In case of a supercritical pressure ratio:

$$\frac{p_2}{p_1} < \left(\frac{2}{\kappa+1}\right)^{\frac{\kappa}{\kappa-1}} \quad (4)$$

the pressure p_2 in equation (3) is replaced by the critical pressure p_{crit}:

$$p_{crit} = p_1 \left(\frac{2}{\kappa+1}\right)^{\frac{\kappa}{\kappa-1}} \quad (5)$$

On the other hand, the gas mass flow can be higher as well due to gap-bridging, when pressure is built up using the speed of the gas after passing the critical section. Both can be considered by the flow coefficient α.

Other sealing elements such as contacting packing rings cannot be handled as orifices. Due to very small gaps, the Reynolds number is low and the flow is dominated by the viscosity.

$$\dot{m}_{1,2} = \beta \frac{A\ h^2}{24\,\eta\,R\,T_1 L}\left({p_1}^2 - {p_2}^2\right) \quad (6)$$

The dynamic viscosity is η, the gap length is represented by L and h stands for the gap width. As the contact rings are pressed onto the sealing surfaces by the differential pressure of the gas, the gap width depends on the differential pressure of the sealing element. The principle is discussed in [3] were diagrams for certain ring configurations are displayed. According to [3], here the following correlation between pressure difference and gap width is used:

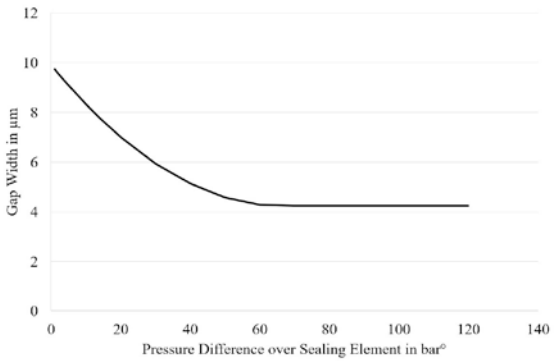

Figure 5: Sealing gap depending on pressure difference over sealing element

The mass flow calculated using the gap width taken from the correlation shown in figure 5 is scaled using the factor β in (6) to meet the measured values for the leakages. The Reynolds number

$Re = \frac{2\,\dot{m}\,h}{A\,\eta}$ has to be checked to verify whether the flow is laminar (Re < 2000)

The third group of sealing elements are represented by a combination of an orifice having a constant cross-sectional area and a pressure dependent contact area. This refers e.g. to piston rings especially in a partly worn condition, were the open gap is simulated as an orifice and the contact areas between liner and ring and between piston and piston ring are considered using equation (6).

by: Dr. Georg Flade – STASSKOL

3. Measurement Equipment and Adjustment of the Model

STASSKOL has a unique testbed compressor which allows the test of sealing elements under very realistic conditions. [4]

Figure 6: Compressor testbed

The compressor testbed is designed to handle real process gases like bone dry Hydrogen, Nitrogen or customer specific gas compositions. The gas is compressed in two cylinder sides per axis and every compressor axis is equipped with two packings for material and design tests. As there are no discharge valves, only the gas leakage over the packings has to be refilled via the inlet valves.

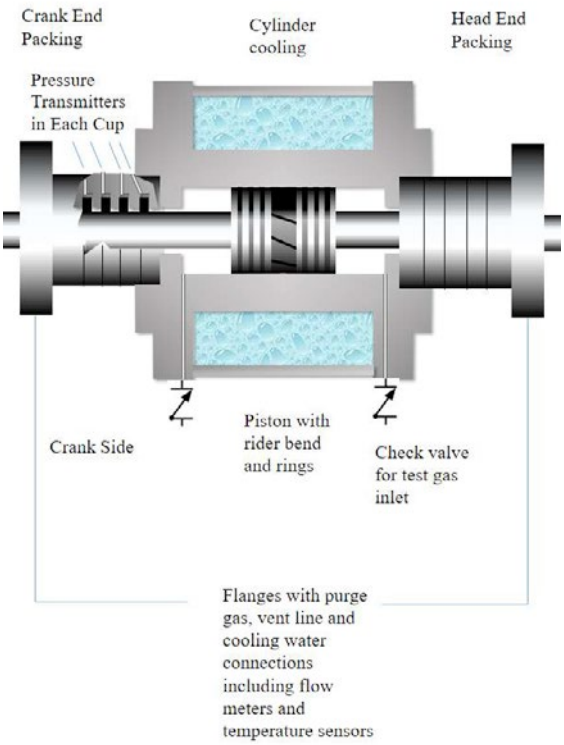

Figure 7: Scheme of testbed cylinder

Every packing is equipped with measurement equipment such as flow meters for leakage gas and buffer gas and temperature sensors. The figure below shows the scheme of a testbed cylinder. The pressure and the temperature can be measured in every packing cup.

In the first step, a testbed packing is modelled using the calculation tool. The direct comparison of measurement results and calculated values allows the reverse determination of several influencing factors which are not accessible easily otherwise. This refers to cylinder heat transfer coefficients, which can be estimated considering the total heat removal. This also applies to effective flow areas $A\,\alpha$ and the factor β in equation (6) for modelling packing ring pairs when the measured leakage rate over the packing is set as an input value to the program.

4. Comparison between Measurement Results and Calculated Results

The pressure drop over the different contacting packing rings is not constant over whole service life of the packing internals. See e.g. [6]. It depends on wear condition of every single sealing ring. Thus, any correlation factors determined for equation (3) or (6) represent a “snapshot” of the packing condition. However, those snapshots are very usefull to answer several questions.

In order to find out the damping efficiency of different pressure breaker ring styles, measurements of several designs were made on the compressor testbed described above. As the compressor testbed does not have discharge valves, the p-t chart of the testbed cylinder looks different from the p-t chart of a typical reciprocating compressor. Instead of having a suction phase and a discharge phase, we see a curve looking like a modified sinus-curve. However, by considering the special testbed conditions in the calculation model, the measured cylinder pressure curve can be simulated with the program. As a result the above mentioned correlation factors can be determined. .

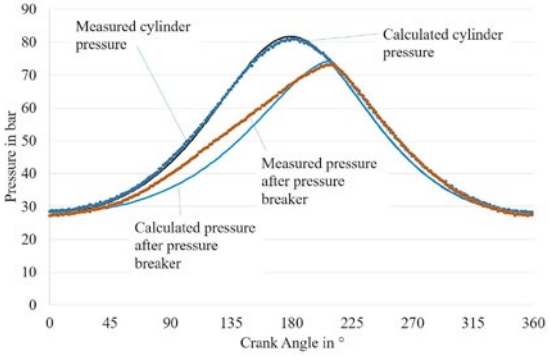

Figure 8: Measured values of cylinder pressure and pressure of 1st cup vs. calculated values (example)

by: Dr. Georg Flade – STASSKOL

5. "Virtual" Testbed

The measurement results of the test compressor have to be transferred to the specific operational conditions of rings and packings. Considering the parameters, which are proven by measurements, the sealing elements can be put on a "virtual testbed".

Using the software, the real compressor operation including the valves and their throttling, the real compressor speed and the real compressor dimension can be considered easily.

It is also possible to set gas pulsations on suction side and discharge side as boundary conditions.

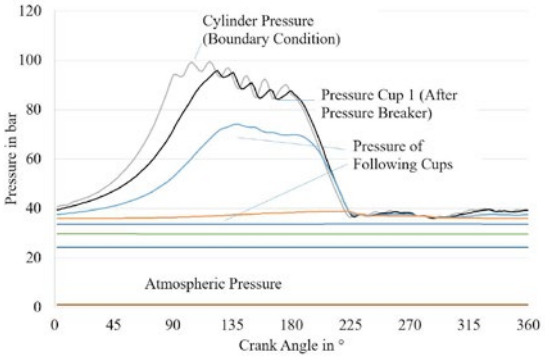

Figure 9: Cylinder pressure (boundary condition) and calculated pressures in the packing cups

Using the calculation results, the acting forces on the packing rings and pressure breaker can be analysed. This is used to define selection criteria for pressure breaker ring styles and sealing ring styles. The software can also be used for root cause investigations in case of packing failures.

6. Calculation of Flow over Piston Rings

In addition to the analysis of pressure distribution inside piston rod packings, it is also possible to do calculations of pressures and mass flows over a cascade of piston rings and rider bands. A typical question is the necessary relief groove area to keep the pressure difference of rider bands as low as possible. Amongst other factors like oil distribution, this is one of the design criteria that determines the number and shape of pressure relief grooves.

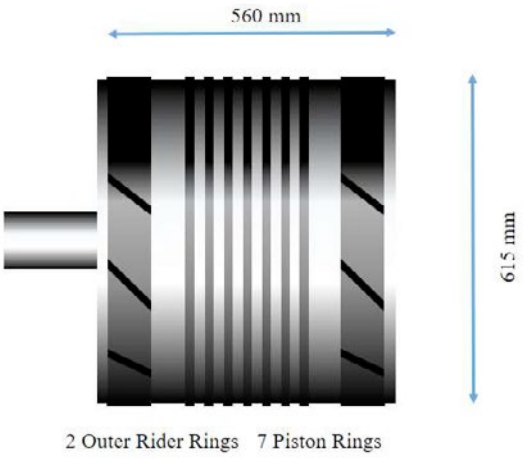

Figure 10: Piston with ring arrangement

The calculation was made for the piston shown in figure 10. The compressor data are the following:

Piston Diameter:	615 mm
Stroke:	360 mm
Gas:	Nitrogen
Speed:	700 rpm

The calculation results show the pressure in every piston chamber. The pressure difference over the rider rings is plotted separately on the 2nd y axis on the right side. The diagram shows that the pressure difference over both rider rings is showing values up to 4 bars. This is not resulting in immediate failure of the rider ring, but the rider ring is designed for supporting and guiding the piston. As the API 618 [7] requires not to exceed a bearing load of 0,035 N/mm² for non-lube service and 0,07 N/mm² for lube service, one can see, that the calculated pressure differences are not negligible. Any additional load to the above mentioned values should be kept to a minimum, as the wear reserve of rider rings is lower than the wear reserve of piston rings that are designed to withstand pressure differences.

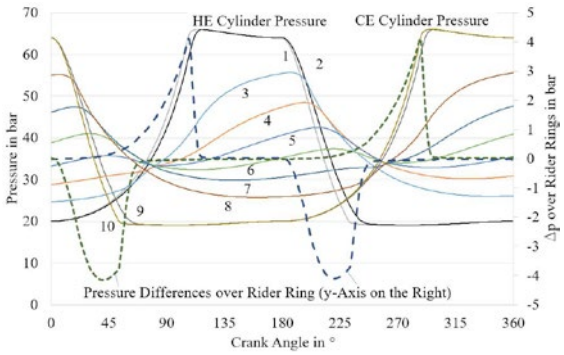

Fig. 11: Pressure distribution over the piston shown in picture 9. 1: HE cylinder pressure, 2: pressure after HE rider ring, 3…8: pressures between piston rings, 9: pressure before CE rider ring, 10: CE cylinder pressure

by: Dr. Georg Flade – STASSKOL

The calculation was also done considering a doubled number of relief grooves.

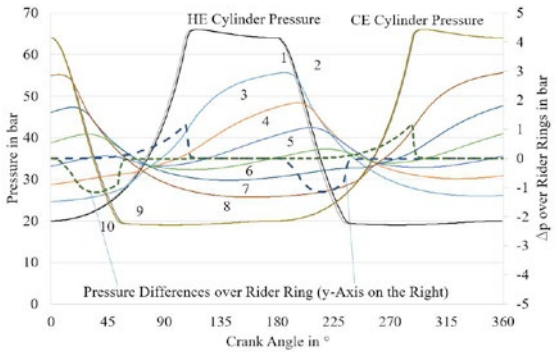

Fig. 12: Pressure distribiution over the piston shown in picture 9. Number of relief grooves was doubled. Numbers are described in figure 11.

When the number of relief grooves is doubled, the pressure differences over the rider rings are reduced roughly by factor of 4. This corresponds to the Bernoulli equation in which is saying, that the pressure difference depend on the second power of the speed.

7. Summary and Outlook

A calculation model was developed to calculate the transient behaviour of pressures and temperatures inside piston rod packings and inside cascades of piston and rider rings. Results of testbed measurements allow to find out necessary input parameters as well as an evaluation of the calculation results. Pulsations in the gas passage and valve behaviour can be considered within the calculation. The results are used to define design criteria for rings and packings and also to analyse potential root causes in case of ring or packing failures.

References

[1] Graunke,.K.: Labyrinthspaltströmung eines Labyrinthkolben-Kompressors, aus Handbuch Verdichter, Vulkan Verlag Essen (1990)

[2] Müller, H.K.: Abdichtung bewegter Maschinenteile, Medienverlag Ursula Müller Waiblingen (1990)

[3] Aboazma, I.: Beitrag zum Verschleiss- und Abdichtverhalten von Hochdruckkolbenstangedichtungen in Kolben-verdichtern, Dissertation TU Berlin (2000)

[4] Langela, M.: Novel Oil Wiper System, 10th EFRC Conference Düsseldorf 2016

[5] Kleinert, H.-J.: Taschenbuch Maschinenbau Band 5 Kolbenmaschinen Strömungsmaschinen, Verlag Technik Berlin 1989

[6] Feistel, N.: Performance Improvement of Dry-Running Sealing Systems by Optimazation of Wear Compensation, 9th EFRC Conference Vienna 2014

[7] American Petroleum Institute: Reciprocating Compressors for Petroleum, Chemical, and Gas Industry Services, API Standard 618, 5th edition 2007

Burckhardt Compression

A Novel Poppet Valve Design – The Arrowpoppet

by:

Reiner Schulz
Research and Development
Burckhardt Compression AG
CH-8404 Winterthur, Switzerland
reiner.schulz@burckhardtcompression.com

11th EFRC CONFERENCE
September 13 – 14, 2018, Madrid

Abstract:
This paper presents a novel poppet valve design for reciprocating compressors. In comparison to other valve types, poppet valves offer advantages due to their easy reconditioning. In order to extend the area of application of poppet valves, a new poppet valve type, the Arrowpoppet, will be introduced. After illustrating the main conceptual design considerations and providing a comparison with the existing design, this paper traces the project development from the conceptual design stage through preliminary assessment procedures to the selection of a prototype design. CFD has been used to provide a detailed insights into the flow and forces acting on the poppets. Details of the design, initial operating experiences with the prototype under laboratory conditions as well as results from field tests are cited. The paper concludes with a comparison of the potential performance differences by comparing the equivalent flow area of different valve types.

by: Reiner Schulz – Burckhardt Compression

1 Introduction

In many installations, a reciprocating compressor can be regarded as the heart of an installation. The reliability of the compressor affects overall system availability as well as an entire plant's financial performance. The performance and reliability of the compressor itself are highly dependent on the valves.

Valve failures are responsible for a high percentage of unscheduled shutdowns. The most common causes of valve failures are wear and fatigue, often caused by high impact velocities as well as application conditions with dirt or debris, resulting in accelerated wear, restricted opening and closing or even blocked valves. It is obvious that effects such as rebound or stiction – which are themselves affected by e.g. pulsations – are important for valve dynamics and thus the performance and reliability of a compressor.

The most widely-used valve types in API 618 compressors are plate, ring and poppet valves in their various embodiments [1]. Poppet valves offer customer benefits as they offer the easiest and most economical reconditioning. Furthermore, their modular design results in a limited spare part variety. The production of these valve components is economical due to the large number of identical components.

The ratio of equivalent area – i.e. area of an ideal orifice causing the same pressure loss as the valve – to the valve pocket area at maximum lift (valve efficiency) is an important performance indicator. Needless to say, the better the valve efficiency, the lower the pressure losses; however, due to the unsteady flow in a compressor, not only the effective flow area of the valve is a relevant parameter, but also pulsations and proper valve timing are important for compressor efficiency. Valve designs with low inertia improve valve dynamics and result in a greater time averaged effective flow area of the valve. The effective valve flow area is not strictly proportional to lift since the jet in the valve gap fills less of the reference curtain area as it transforms from an attached wall jet to a separated free jet. Within this paper, we limit ourselves to steady state flow under idealised conditions.

The valve design also affects the volumetric efficiency of a compression cylinder through the clearance volume. However, the contribution of the valve to overall clearance volume is usually small and for common compression ratios, the effect may be insignificant. Regardless, new designs aim at reduced clearance volume because the higher the clearance, the poorer the volumetric efficiency.

Why a new design? Because considerations as described below suggest that the concept of the poppet valve – with its undisputable customer benefits – can be further improved both in terms of performance and reliability.

2 Design concept

2.1 General design considerations

The basic concept of the Arrowpoppet is similar to that of standard poppet valves: several individually-sprung plastic valve bodies are combined with a metallic valve seat, which may comprise replaceable parts for easy overhaul by the customer, and a metallic valve guard. However, in contrast to poppet valves of conventional design [2-7] – which use bores in the valve guard to form a linear guide – the Arrowpoppet uses an axle and has the linear guide inside.

This design change is motivated by the following limitations of the conventional design:

Due to the location of the centre of attack of the lateral forces outside the linear guide, the poppet tilts, resulting in edge pressures (figure 2.1). The edge pressure leads to increased wear and after a longer period of operation, the outer surface of the poppet forming the linear guide usually becomes barrel-shaped. In any case, this is a limiting factor of poppet life.

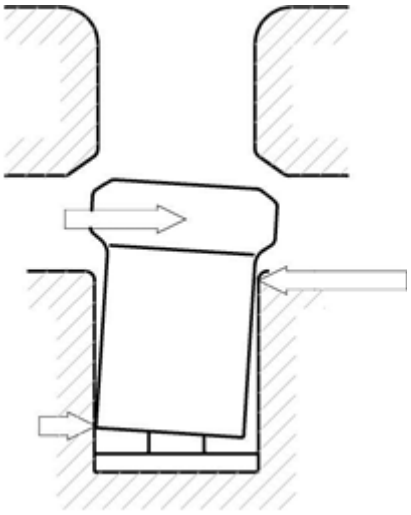

Figure 2.1: Sketch illustrating forces acting on partially-opened poppet

by: Reiner Schulz – Burckhardt Compression

If the gas carries impurities as particulate matter, this debris very easily enters into the linear guide. In some designs, particles flow directly into the guide, while in others the mushroom-shaped head of the poppet offers some protection. Nonetheless, in any case, there is a flow through the linear guide, because at the end of the bore a vent hole is provided to allow the gas to communicate with the chamber behind the poppet and to prevent dirt from accumulating and limiting the stroke. In the fully open position of the poppet, the flow is restricted but generally not completely shut off due to the tilted position of the poppet (figure 2.2).

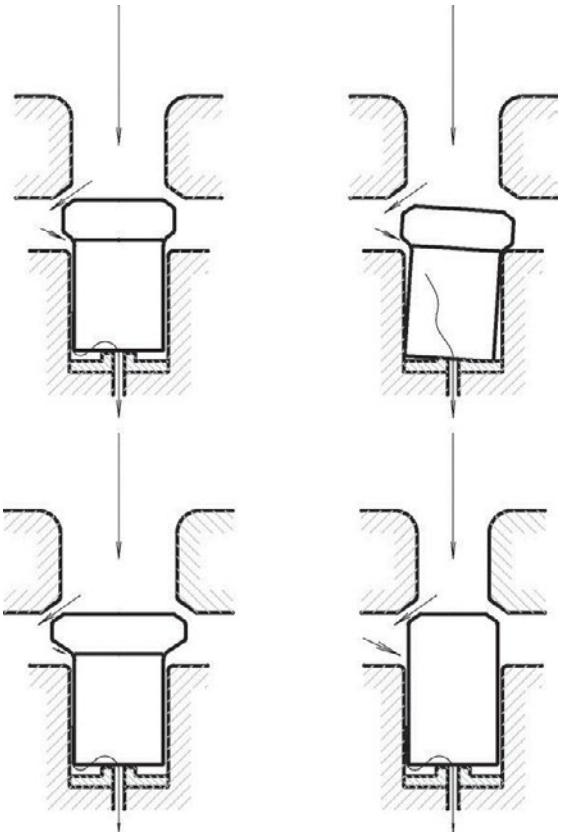

Figure 2.2: Sketch illustrating potential path of impurities into linear guide, different types of poppets

The space for the spring is rather limited and if not designed carefully, buckling and wall contact of the spring may occur. This may not be a problem as long as the valves are new; however, if the poppet is worn, the increased tilting angle allowed by a barrel-shaped shaft gives rise to additional stress in the spring. Contact and hence wear between the spring wire and poppet may occur, and if the spring wire is worn sufficiently the spring breaks due to the locally-reduced cross-sectional area (figure 2.3).

In order to keep stress levels in the spring within limits, a sufficient number of windings are required, and for a given spring rate the wire diameter increases also with the number of turns. The space between the windings is limited, whereby they may hit on each other due to natural vibrations of the spring, which are caused by the impacts of the poppet, resulting in additional wear.

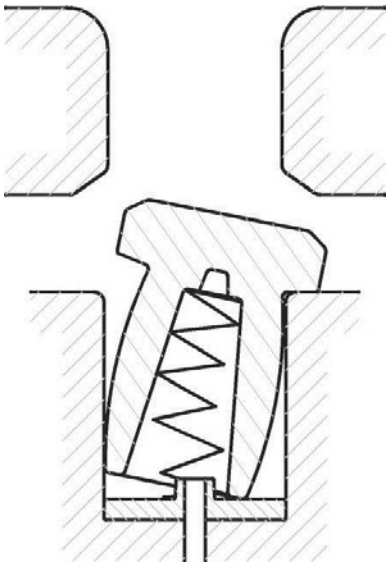

Figure 2.3: Sketch explaining spring wire – poppet wall contact (worn poppet)

The forces acting in radial direction as well as all moments acting on the poppets during opening and closing should be minimised. The fluid enters through the valve seat, flows through the annular gap between poppet and seat, enters the volume between valve seat and (in the conventional design) leaves through holes in the valve guard. Even under ideal conditions – i.e. steady flow, evenly distributed as in wind tunnel tests – there is an asymmetrical pressure distribution around the poppets (except the potential one located centrally), causing lateral forces.

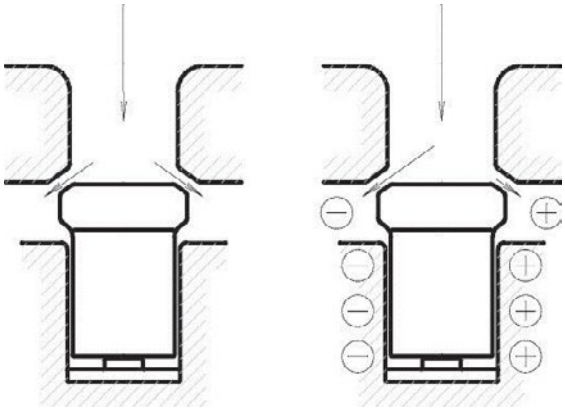

Figure 2.4: Sketch showing the effect of pressure gradients continuing into the guide

by: Reiner Schulz – Burckhardt Compression

In a compressor, this effect is much more pronounced due to the uneven flow distribution caused by the valve pocket and unsteady flow phenomena. The gradients of the pressures acting on the poppets continue into the linear guide, and the large diameter of the linear guide of the conventional poppets results in higher lateral forces, i.e. an enlargement of the guide diameter does not reduce the specific bearing load (figure 2.4).

The clearance volume of the suction valve is determined by the height of the poppets, whereby the longer the poppets, the higher the clearance volume (figure 2.5). A shorter poppet design results in reduced clearance volume.

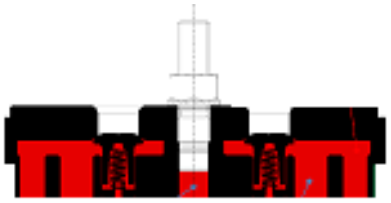

Figure 2.5: Clearance volume of conventional suction poppet valve

2.2 Arrowpoppet design

2.2.1 Poppet

In contrast to the conventional design, the Arrowpoppet uses a central pin as a linear guide. The end of this pin can be placed further in the direction of the valve seat, whereby the linear guide is significantly improved because of a lateral force almost always attacking between the ends of the linear guide, resulting in a cylinder – cylinder line contact instead of edge pressure (figure 2.6). Hence, wear is significantly reduced.

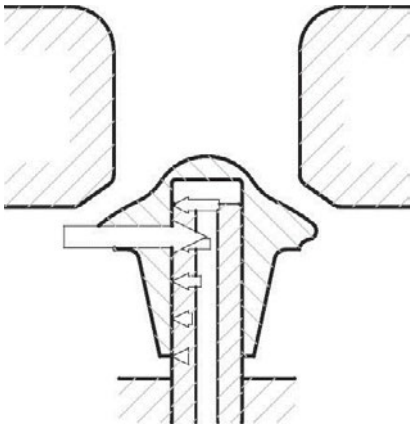

Figure 2.6: Sketch of a lateral force attacking Arrowpoppet and resulting distributed load

The location of the pin top results in the sombrero-like contour of the poppet on the side facing the inflow. The effect of this shape on flow is negligible, because otherwise the stagnant zone would be larger.

There are no significant pressure gradients in the linear guide itself and therefore no significant lateral forces from the linear guide.

There is also no significant flow through the linear guide, because due to the open design of the valve guard, the pressure difference between the end of the vent hole in the pin and the bore in the poppet is small. Therefore, even small dust particles following the flow are hardly carried into the guide, while larger dust particles pass by anyway.

The spring is located outside (figure 2.7) and has a much larger diameter than the one in conventional poppets. This results in a much lower stress level (less than 40%) for the same spring rate when compared based on the same number of windings. However, aiming at stress levels much lower than the fatigue limit determined under consideration of all safety factors, dynamics, and local stress spikes, is pointless. Therefore the number of turns is reduced, resulting in much larger distances between the windings, whereby contact and associated wear is avoided.

Figure 2.7: Typical Arrowpoppets with open spring, different plastic materials

A comparison of poppets of the same nominal size (20 mm) shows the much smaller height of the Arrowpoppet (figure 2.8), resulting in reduced clearance volume of the suction valve. The clearance volume of the discharge valve is not dependent on the height of the poppet. The higher poppet material stress due to the higher impact speeds of the discharge valve may be mitigated by a longer and more compressible shaft, i.e. two different types of poppets may be used for the

by: Reiner Schulz – Burckhardt Compression

suction and discharge valve, without negative effects on the clearance volume.

Figure 2.8: Comparison of a standard to an Arrowpoppet of nominal size (i.e. the diameter of the bore in valve seat) = 20 mm

2.2.2 Valve guard

Two different designs of valve guards are used. For smaller valves, the valve guard is milled from billet material, whereas for larger valves it is cut from sheet metal and bolted to the seat (figure 2.9). In both cases, the pins are individual parts mounted by either pressing in or riveting (orbital riveting). The individual pins are manufactured from suitable material and different designs may be used.

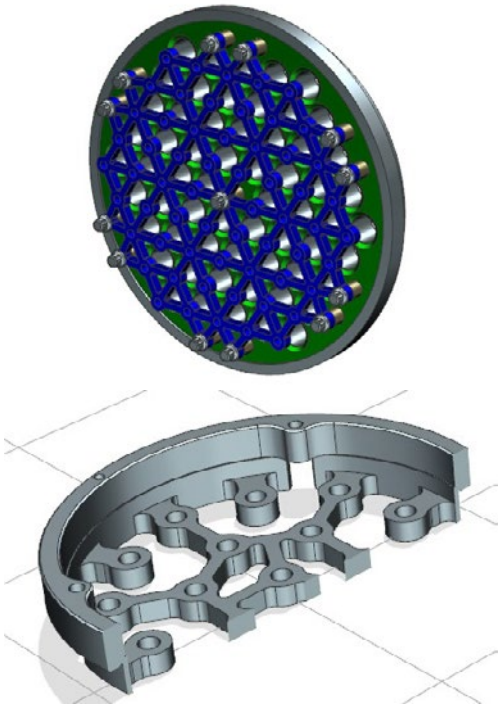

Figure 2.9: The two different types of Arrow-poppet valve guards in use thus far

2.2.3 Valve seat

The valve seat uses the replaceable seat plate that is well known from standard poppets [8], whereby reconditioning is simplified.

Versions with hardened valve seats are being tested.

A third version uses replaceable seat inserts. The spare part inventory is simplified, as the same inserts are used for several valve sizes.

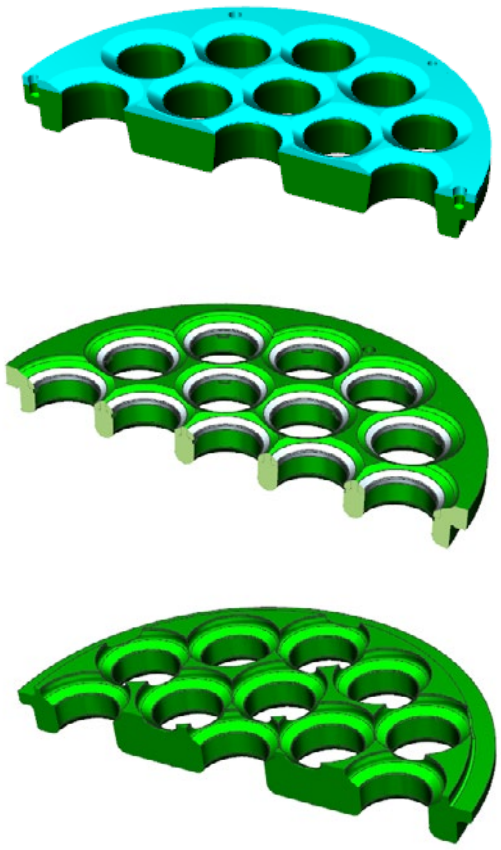

Figure 2.10: Different types of Arrowpoppet valve seats (replaceable seat plate, replaceable inserts, hardened valve seats, from top to bottom)

2.3 Future developments

Closed Design Variant

The Arrowpoppet can be realized with an open or enclosed spring. Although the Arrowpoppet design reduces stress in the spring wire and increases the distance between wall and wire significantly, making spring failures very unlikely, a closed design may be preferred in some applications.

by: Reiner Schulz – Burckhardt Compression

Bumpers

In order to reduce stresses on the poppets caused by the opening impact, several designs aiming at cushioning are possible. In the simplest embodiment, a cushioning insert in the axle body is used. Other simple possibilities are a flexible poppet shaft and plastic parts. The working principle of a damping plate (impact is divided into smaller impacts) as used in plate valves may also be applied.

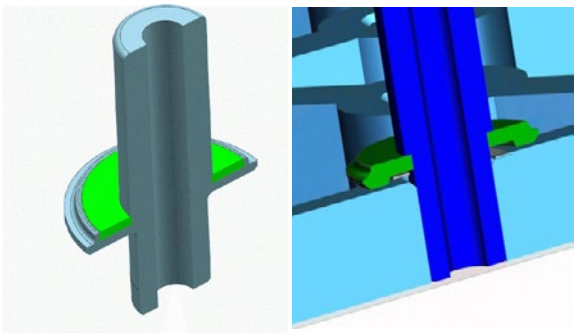

Figure 2.11: Bumper concepts for Arrowpoppets

Unloader

Arrowpoppets may use a central bolt for mounting a conventional finger unloader. An example of a finger unloader mounted to the valve without a central bolt is shown in figure 2.12. The fingers are individually sprung, which ensures that even if the unloader is worn out, no unduly large forces are acting on the poppets.

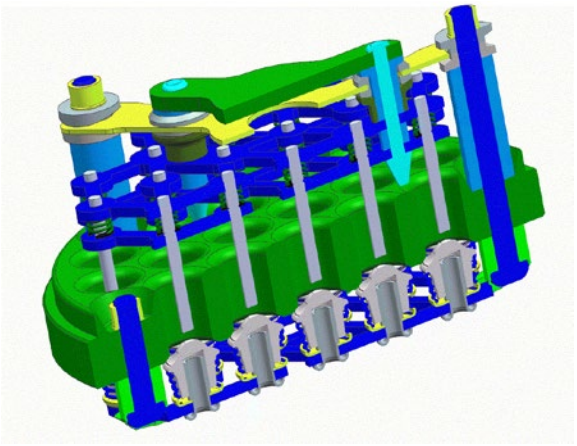

Figure 2.12: Finger unloader for Arrowpoppet valves without central bolt

Valve Cartridge with Unloader

A finger unloader for a valve without central bolt is preferably mounted to the valve cage, which may be bolted to the valve, thus resulting in minimum flow restriction and maximum strength and durability. An anti-rotation device may be integrated via a leaf spring.

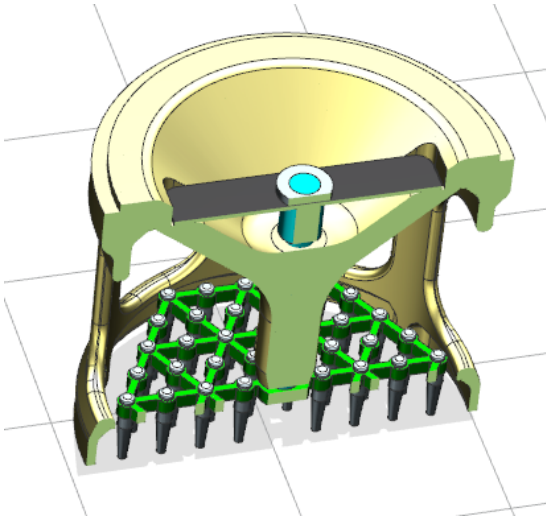

Figure 2.13: Finger unloader for Arrowpoppet valves mounted to valve cage

Valve Cartridge with Support

Deflections of the valve seat may give rise to wear, this may be a problem for large valves. A valve seat of high stiffness requires high thickness, leading to increased clearance volume of the discharge valve. By bolting the valve seat to the valve cage, a much thinner discharge valve seat resulting in lower clearance volume is possible (figure 2.14).

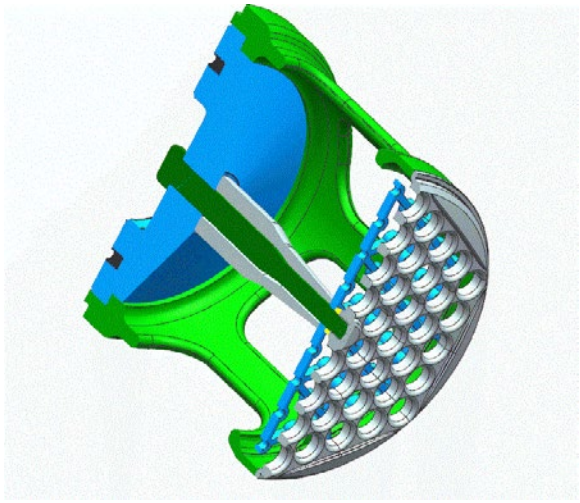

Figure 2.14: Valve seat bolted to valve cage resulting in higher stiffness of discharge valve seat

by: Reiner Schulz – Burckhardt Compression

3 Dimensioning and CFD

In a first step, the proportions of a single poppet element were investigated under ideal conditions. The question is what basic arrangement of poppets should be used in a valve of (in comparison to the poppets) large dimensions. From a certain size upwards, the identical arrangement of poppets is used to achieve a simple scalable and modular construction.

In principle, the poppets can be placed at the corners of any polygon, although only equilateral triangles or squares are meaningful.

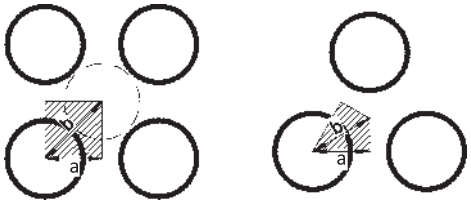

Figure. 3.1: Basic arrangement of poppets

In conventional poppet valves – i.e. guided on the outside – drillings are used in both the valve seat and the valve guard, and it is obvious to use holes of about the same diameter in both of them for good spatial utilization. For the square arrangement the same averaged velocity results from the continuity equation (figure 3.1).

In the Arrowpoppet design, the obstruction from the valve guard is negligible and the openings in the valve guard are not necessarily cylindrical or drilled. For this reason, a triangular form is more appropriate, as the differences of the meridional sections and therefore flow cross sections are significantly smaller, as can be seen from the ratio of lengths a / b in Figure 3.1 (1.15 instead of 1.42). The more even distribution over the circumference results in optimised flow.

The pressure loss depending on flow conditions and the forces acting on a single valve element have been investigated for different designs by CFD, depending on lift and pitch, i.e. the distance of the poppets among each other.

Sector models of Arrowpoppet elements, sector models of valves as well as complete models of valves have been investigated (figure 3.2).

As an example of CFD analysis of stationary flow through sector models, the effective flow area of an Arrowpoppet segment dependent on lift is shown in Figure 3.3 for four different spacings of the poppets. Mach and Reynolds number were varied.

The Arrowpoppet reaches 80% of the maximum flow at a stroke of 2/3 of the maximum lift.

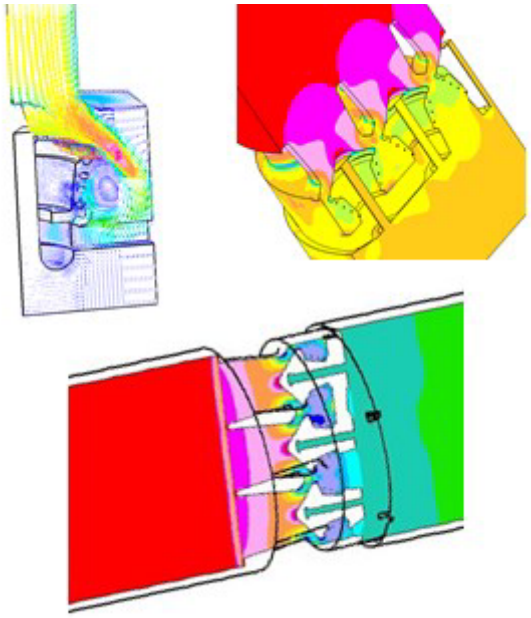

Figure. 3.2: Models for steady-state CFD investigations: sector model of Arrowpoppet element (velocity plot, top left), sector and complete models of valves (pressure plots, top right and bottom)

Maximum lift is defined as 25% of the nominal poppet diameter (note that the slope of the curve is still increasing, i.e. with higher lift higher flow could be reached, especially for the spacing of the poppets resulting in high flow).

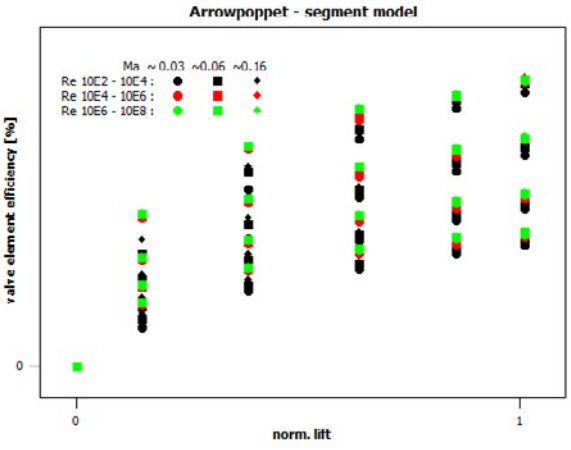

Figure. 3.3: Example of eff. flow coefficient chart (dependent on lift, pitch, Mach number and Reynolds number range)

by: Reiner Schulz – Burckhardt Compression

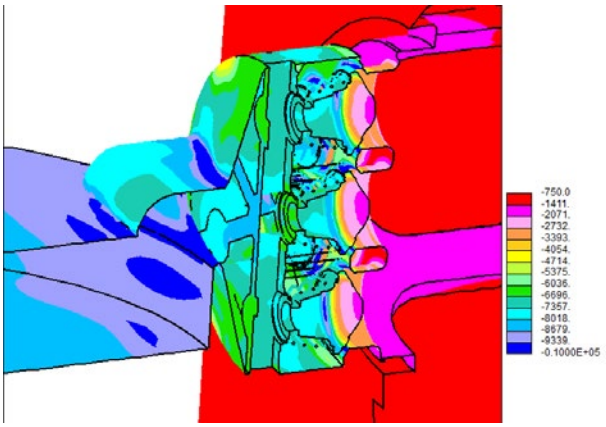

Figure. 3.4: *Snapshot of pressure distribution [Pa], suction valve, moving mesh (fluid-stucture interaction) CFD simulation of compressor stage equipped with Arrowpoppets*

As already mentioned, it would go beyond the scope of this paper to address the effects caused by the valve pocket, valve movement, and pulsations, nevertheless simulations of transient flow with fluid structure interaction have been performed. Figure 3.4 shows a snapshot of the transient flow in an Arrowpoppet suction valve.

3.2 Comparison with other valve types

An illustrative comparison of the flow efficiency of different valve types has been published in [3] and [4]. According to these publications, poppet valves appear at the right and lower end of the graph.

However, with any valve type, there are valve sizes that are favourable for the dimensions of given internal parts like springs and poppets etc. and valve sizes that result in unfavourable conditions. For this reason, scatter bands were supplemented for the Burckhard Poppets (diagram 3.3, bottom).

In contrast to the diagrams taken from [3] and [4], lift is normalised with maximum stroke. As a more objective and relevant parameter, total travel resulting in maximum tolerable wear for the respective valve type should be used for normalising, which is currently not possible due to a lack of data.

A reduction in valve pressure losses cannot result in a one-to-one improvement of compressor efficiency due to the effects of the valve pocket on flow and pressure losses as well as the effect of pulsations and valve dynamics; nevertheless, a valve with low pressure loss is essential for efficient compressor operation.

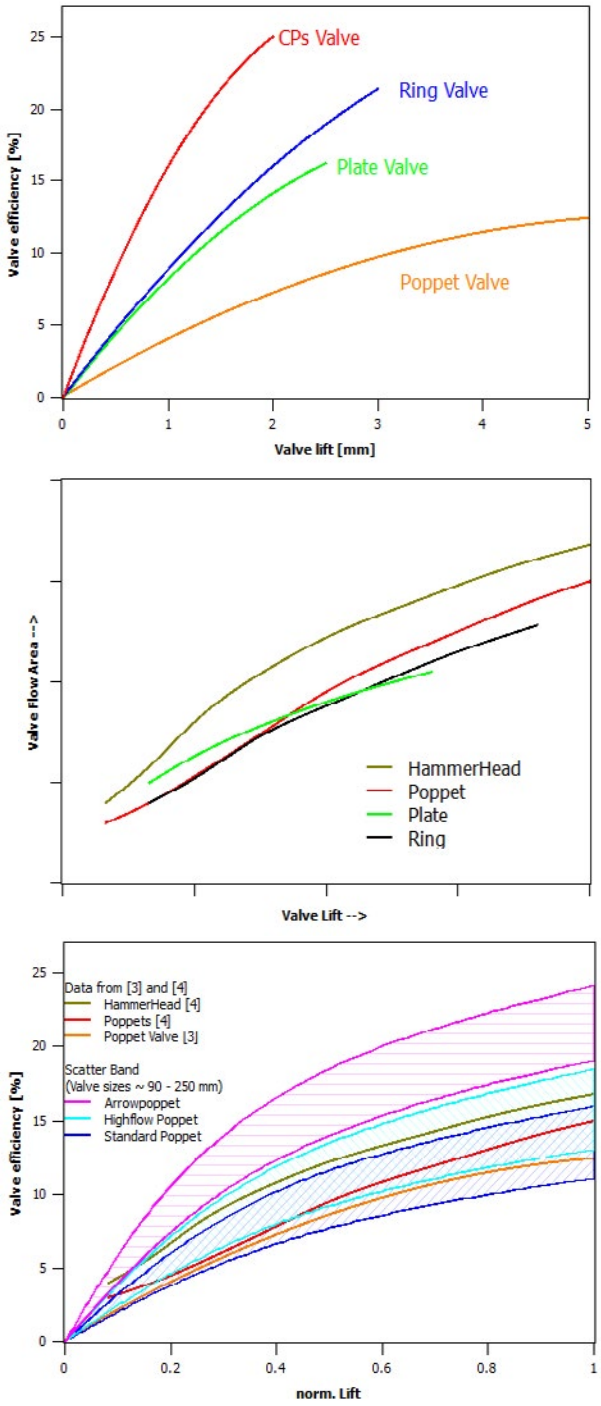

Diagram 3.3: *Comparison of efficiency of valve types, taken from [3] (top) and [4] (middle), comparison of different poppet valve types including Arrowpoppet (bottom)*

The efficiency of the Arrowpoppet is in the range of optimised plate valves with rounded edges (large poppets reach even higher efficiencies) and therefore the field of application of poppet valves is extended in direction of high efficiency valves.

by: Reiner Schulz – Burckhardt Compression

4 Examples and test results

4.1 Compressor tests

Different sizes of Arrowpoppet valves have been built and tested for up to several hundred hours, in different in-house test compressors as well as a compressor operated by the FHNW (University of Applied Sciences, Brugg-Windisch, Switzerland).

Figure 4.1: Valves used for testing

The four different sizes (from approximately 95 to 180 mm) use a valve guard machined from billet material. Two different poppet sizes suitable for different pressure levels have been investigated (figure 4.1). The tests confirmed slightly reduced specific power consumption of the Arrowpoppet in comparison to plate valves under identical operating conditions. Due to the high pressure losses of the valve pocket the optimisation potential is rather limited in this specific compressor.

4.2 Field tests

Tests are being conducted in an industrial air separation plant in bonedry nitrogen. The valves are in the 250 mm diameter size range, and the design uses valve guards cut from sheet metal (figure 4.2).

Figure 4.2: One of the valves as used in a field test after 7000 h operation

The photos were taken after 7000 h, the test is still ongoing. Experience thus far shows that the time between overhaul is increased by a factor of 3.5 in comparison to the standard poppet for the discharge valve. The suction valve is still installed and has exceeded 8000 h while the test remains in progress; therefore, no final assessment is possible. However, the life expectancy in comparison to the standard design for this specific application will certainly be increased by a factor of 5 or even more. It is clear from the test how small design modifications can extend the life of the discharge valve beyond the 7000 h reached in the first attempt. The application in bonedry nitrogen is known to be demanding for poppet valve wear. Further improvements are possible by using e.g. other materials.

by: Reiner Schulz – Burckhardt Compression

5 Conclusion

In this paper, a new poppet valve design –the Arrowpoppet– characterised by improved effective flow area and longer life has been described. Like standard poppets, which are offered in more or less similar form by different manufacturers, the concept is based on poppets made of plastic, which are mounted on a linear guide. As with conventional poppet valves, the poppets are easily replaceable by the customer, whereby maintenance is considerably simplified.

In contrast to conventional poppet valves, the linear guide makes use of a centrally-located axle. Due to the associated more favourable position of the ends of the linear guide relative to the lateral forces and torques acting on a poppet, line contact is predominant during motion. Accordingly, edge pressures and thus wear are minimised. In addition, the linear guides are better protected against the ingress of particulate matter, and therefore greater insensitivity to dusty fluids is expected. The lateral forces acting on the poppets are lower because pressure differentials in the space between the valve seat and guard do not affect the pressure distribution in the guide. A much longer life (several times longer in comparison to standard poppets) has been confirmed in a bonedry nitrogen application.

The valve efficiency is significantly improved, not only in comparison to standard poppets, because the pressure losses caused by the valve guard are eliminated. The losses of the Arrowpoppet are in the same range as radiused disc valves.

Concepts for matching accessories (e.g. unloaders) are currently under development or in a testing phase. Field tests have confirmed the concept being sufficiently mature for launch.

6 Acknowledgments

As already mentioned, field tests have been performed. The author would like to thank especially our industrial partners as well as all other contributors for their co-operation.

References

1 Raimund Arztmann: Operation and Maintenance of different valve types, 6. Workshop reciprocating compressors, Rheine, Germany, October 2002

Sales brochures

2 Dresser_Rand:
Magnum Valves, Form 6033-15

3 Dresser_Rand:
Magnum HammerHead Valve, Form 6045-15

4 Hoerbiger:
cp_high_speed_small_pocket_en.pdf

5 CPI:
POPPET.ENG.1608.LTR

6 CECO:
eMAX POPPET VALVES Form 2115 9/11

7 GE:
Compressor Poppet Valves, Ajax Product, Brochure (4416) (01/2016)

8 Burckhardt_Compression:
Compressor Valves, Brochure 23.24.14.40 (10/2016)

A LIFETIME EXPERIENCE IN RECIPROCATING COMPRESSORS

Since 1977 we have been repairing foundations, installing new machinery, aligning, and regrouting all kinds of **Reciprocating** and **Rotating Machinery**.
Noise and **vibration** indicate issues that can affect a machine's reliability, such as imbalanced parts, and can even cause machines to fail through their own damaging effects.
As the only epoxy grout manufacturer with its own engineering and contracting arm, **Alphatec Engineering** is uniquely placed to give you the best combination of products and services, together with our commitment to quality reflected with our ISO 9001

ALPHATEC grouting specialists
www.alphatec-engineering.com

Contact Us
Spain +34-961-451-599
info@alphatec-engineering.com

GROUTING SPECIALISTS

In **Alphatec Engineering** we have different procedure of repairing critical machinery foundations, and the best technique of application of our polymer products.
Our main products are epoxy resin based grouts with inert fillers for stiffness and heat resistance, which we use to repair cracked or damaged foundations and to install new machinery following the **OEM** and **API RP**

PROJECTS

End-User	Location	Equipment type (No) - Output	Condition	Job Description
Asahi Chemical	Japan	Ingersoll-Rand HHE compressor - 7.7 MW	Existing	Partial regrout & pressure injection repair
BayernOil GmbH	Germany	Worthington BDC gas compressor - 410 kW	1967	Full regrout & foundation repair
Caltex Petrochem Corp	New Zealand	Cooper V-275 GWMK - 3.8 MW	82/06	Engine & compressor regrout & foundation repair
EP Petroecuador	Ecuador	Recip compressors	New	Alphatec Epoxy Grout AT-800 supply
ExxonMobil Chemicals	Belgium	Ingersoll-Rand primary compressor - 3.25 MW	1975	Foundation repair and anchor bolt repairs
Gujarat State Fertiliser	India	Kobe LM-6 recip-compressor - 5.6 MW	Existing	Regrout & pressure injection foundation repair
Incitec Pivot Fertilisers	Australia	Dresser-Rand HHE recip compressor - 4.0 MW	Existing	Foundation repair, re-alignment, & regrout
JGC Corporation	Nigeria	Rotating machinery	New	Alphatec Epoxy Grout AT-800 supply
KNPC	Kuwait	All rotating machinery (300+) - Various	New	Alphatec Epoxy Grout AT-800 supply & supervision
Marubeni/MOGE	Myanmar	Waukesha/Ariel compressors (3)	New	Align machines, supply & install epoxy grouts
MOL Nyrt. Group	Hungary	Halberstadt compressors (3) - 1.4 MW	1983	Pressure injection foundation repair & regrout
Petkim Izmir	Turkey	Nuovo Pignone pr & hyper compressor - 2.65 MW	1985	Foundation repair, realignment & regrout
Petrochemical Industries	Kuwait	I-R HHE compressors (3)	Existing	Regrout & pressure injection foundation repair
Petromin Mobil Yanbu	Saudi Arabia	Compressors (10) - Various	New	Alphatec Epoxy Grout AT-800 supply
Petronas Melaka	Malaysia	Dresser-Rand HHE gas compressors (3) - 3.8 MW	1998	Regrout & realignment of 3 HHE compressors
Petroplus Cressier	France	Thomassen 1MC1 gas compressor - 480 kW	1964	Foundation repair & encapsulation, full regrout
Repsol Puertollano	Spain	Nuovo-Pignone 6PH/2 hyper compressor - 4.5 MW	1974	Regrout & pressure injection foundation repair
Santa Fe Energy	Indonesia	Waukesha/Ariel compressors (5)	New	Align machines, supply & install epoxy grouts
Shell Refinery	Singapore	Thomassen recip compressor - 3.0 MW	1981	Pressure injection foundation repair
Total La Mede	France	Ingersoll-Rand recip compressor - 1.69 MW	1992	Regrout and pressure injection foundation repair
Yong Nam Chemical	Korea	GE compressor motor drive - 5.3 MW	Existing	Regrout & pressure injection foundation repair

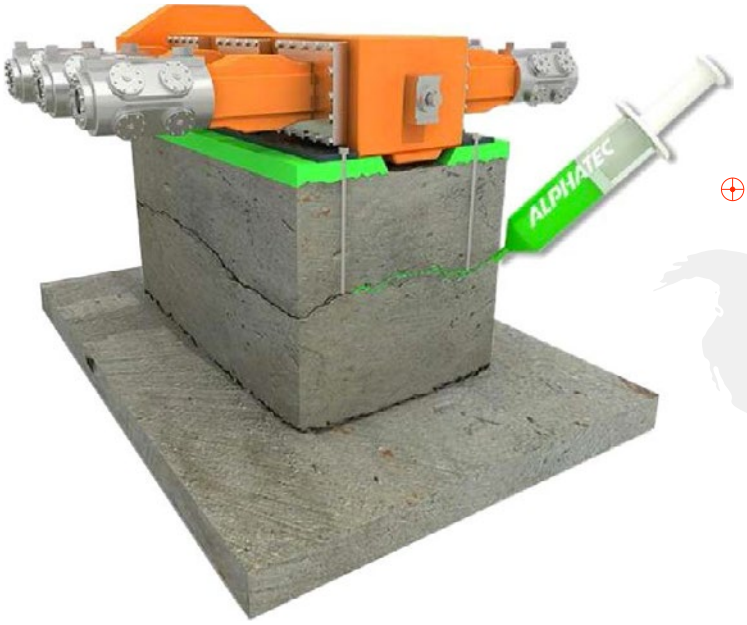

"We offer both products and services to the industries we serve, but primarily, we offer solutions to problems"
- Giles Goldsbro
Founder & Managing Director

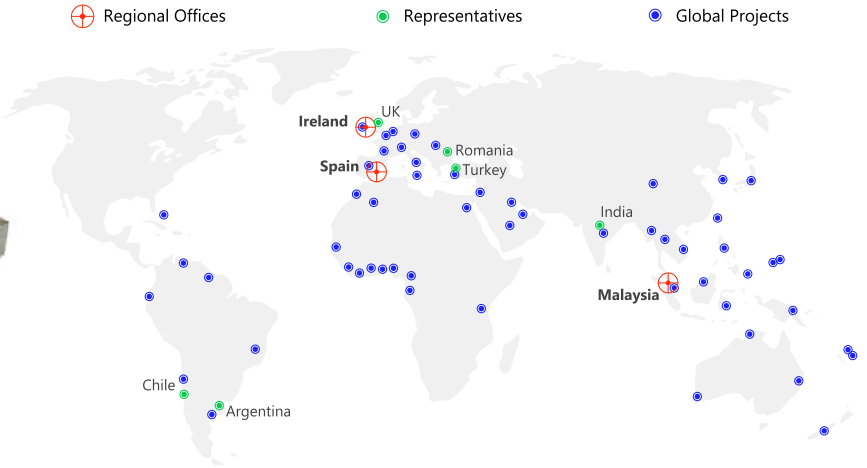

Alphatec® global services with more than 4,000 contracts in 57 countries

HOERBIGER

Non-Lube operation: Do it right if necessary – a practical guideline and examples

by:

Dipl. Ing. Ralf Krich
Engineering
Hoerbiger Service GmbH
Hamburg / Maxdorf, Germany
ralf.krich@hoerbiger.com

11th EFRC CONFERENCE
September 13 – 14, 2018, Madrid

Abstract:
Most reciprocating compressors in the process industry are horizontal units and have drop lubrication into the cylinder. Some processes require oil-free compression. Since this is challenging with respect to tribology, sometimes this is done with limited success only.. In contrast to vertical units, horizontal cylinders require rider bands and sealing rings in various arrangements to perform, while still maintaining low friction and a long service life. In addition to different piston, ring, and running surface designs, factors that have an effect are the material pairings, geometry, fixed speed, stroke and liner contact length, as well as temperature and pressure levels. Non-lube operation requires not only wear elements, but also counter-faces to withstand operation, while operators are still seeking to achieve similar lifetimes in continuous operation.
What does a design have to look like, not only to save short term costs, but also to ensure long lasting operation? This should be possible with the right combination of all parameters and following a few basic rules. If that is not already adequately considered in the design of the compressor, it is often possible to achieve significant improvement by making modifications.
Still, operators should know that there is no simple solution, if oil lubrication is to be entirely eliminated. Short strokes, high speed, high pressures and wrong friction partners lead to dissatisfied operators.
After installation, a significant improvement can often not be achieved by material changes only. The piston design may have a big influence, not only on the lifetime but also on temperatures, as the examples in this presentation will show. This paper shall give hands-on best practices and examples on potential modification to achieve better non-lube operation.

by: Ralf Krich – HOERBIGER

1 Introduction

This paper shows experiences of projects of the last years with relation to non-lube operation of reciprocating compressors. This kind of operation is also known as “dry running”. Examples describe modifications and upgrades to demonstrate what is necessary to achieve satisfying results with non-lube operation.

Most reciprocating compressors in the process industry and compressed natural gas are horizontal units and have drop lubrication in the areas of the piston rings and packings. Under some circumstances the process requires to eliminate this lubrication oil. This has showed varying levels of success.

In contrast to vertical units, cylinders with horizontal pistons require relatively large rider bands or segments to carry not only the sealing rings performing the compression work, but also the relatively heavy metal piston, while still maintaining low friction and a long service life.

In addition to a different piston, ring, and running surface designs, parameters that have an effect are the material pairings, geometry, speed, stroke, and running length. Temperature and pressure levels are also of importance. Non-lube operation requires not only wear elements, but also counter surfaces to be able to withstand operation without lubrication, while operators are still seeking to achieve similar lifetimes in continuous operation compared to lube operation.

2 Basic theory and parameters of non-lube operation

What are reasons to support non-lube operation, and what are the reasons against it? What does design have to look like to not only save costs on the short run, but to ensure long lasting operation as well?

Successful operation should be possible with the right combination of all parameters and following a few basic rules. If that is not already adequately considered in the design of the compressor, it is often possible to achieve significant improvement by making a few modifications.

Still, operators should be aware, in terms of their expectations, that there is no simple solution if oil lubrication is to be entirely eliminated. Short strokes, high speeds, high pressures and incompatible friction surfaces lead to poor operating results.

The entire problem usually starts with rated speed available from the compressor motor. An electric motor generally provides the direct driving force with fixed speeds depending on available power grid (Table 1).

		synchronous speed	
no of poles	no of pole pairs	n *sync* 50 Hz	n *synch* 60 Hz
		RPM	RPM
2	1	3000,0	3600,0
4	2	1500,0	1800,0
6	3	1000,0	1200,0
8	4	750,0	900,0
10	5	600,0	720,0
12	6	500,0	600,0
14	7	428,6	514,3
16	8	375,0	450,0
18	9	333,3	400,0
20	10	300,0	360,0
22	11	272,7	327,3
24	12	250,0	300,0
26	13	230,8	276,9

(Table 1) Synchronous speed based on poles and frequency

by: Ralf Krich – HOERBIGER

Since primarily asynchronous motors with speeds between approximately 296 and 725 rpm (Table 2) are used in Europe, in non-lube applications, pairing options of stroke and compressor speed (table 3) are limited, depending on manufacturer.

	Speed	
no of poles	n *sync* 50 Hz	n *asynch* 50 Hz
	RPM	RPM
4	1500,0	1450,0
6	1000,0	970,0
8	750,0	725,0
10	600,0	580,0
12	500,0	485,0
14	428,6	418,0
16	375,0	367,0
18	333,3	327,0
20	300,0	296,0
22	272,7	270,0

(Table 2) Common speeds for reciprocating compressors in Europe

There are no clear rules with respect to speed when it comes to reciprocating compressors, which are often designed based on API 618 (Section 6.4). As a result, neither manufacturers nor operators are required to follow rules for stroke and ring arrangement, and design and production are done according to their own standards. Often agreement only exists with respect to the piston speed, but no provisions are in place as to how – primarily, in what combination – this is achieved.

API 618 (Figure 1) provides no indications whatsoever as to how a dry-running cylinder or compressor should be designed in detail. Consequently, a wide range of units exist that have piston speeds ranging from below 3 m/s to more than 4 m/s.

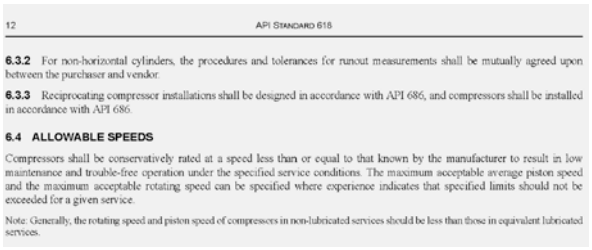

12 API STANDARD 618

6.3.2 For non-horizontal cylinders, the procedures and tolerances for runout measurements shall be mutually agreed upon between the purchaser and vendor.

6.3.3 Reciprocating compressor installations shall be designed in accordance with API 686, and compressors shall be installed in accordance with API 686.

6.4 ALLOWABLE SPEEDS

Compressors shall be conservatively rated at a speed less than or equal to that known by the manufacturer to result in low maintenance and trouble-free operation under the specified service conditions. The maximum acceptable average piston speed and the maximum acceptable rotating speed can be specified where experience indicates that specified limits should not be exceeded for a given service.

Note: Generally, the rotating speed and piston speed of compressors in non-lubricated services should be less than those in equivalent lubricated services.

(Fig.1) Section about allowable speeds in API 618

The assumption that low piston speed automatically results in a long service life is unfortunately not correct. While a unit with a high speed and short stroke may have a lower piston speed than a unit with a long stroke and a low speed, experiences have shown that compressors with larger strokes will generally achieve better operating results based on the running length or ring length. A few speeds and strokes combinations in Table 3 demonstrate how almost identical piston speeds can be achieved.

Speed	Stroke	Stroke	Pistonspeed
RPM	mm	inch	m/s
270	350,0	13,78	3,15
296	320,0	12,60	3,16
327	304,8	12,00	3,32
370	270,0	10,63	3,33
420	254,0	10,00	3,56
490	220,0	8,66	3,59
270	450,0	17,72	4,05
580	203,2	8,00	3,93

(Table 3) Combinations stroke and speed to realize similar piston speed

While API 618 does not provide any indications as to the piston speed and number of piston rings necessary for compression, Section 6.10.3.2 (Figure 2) precisely limits the permissible specific load of the rider rings or segments to 0.035 N/mm2. Once again, it is left up to operators and manufacturers how to design the piston and which material is used. While vertical compressors are generally equipped with a narrow guide ring, and V-type compressors due to their practically horizontal orientation of their weight require one wide guide ring, horizontal units often require at least two wide rings/segments. The combination of piston and rider rings then results in significant total ring length, which is often smaller than the stroke of the compressor.

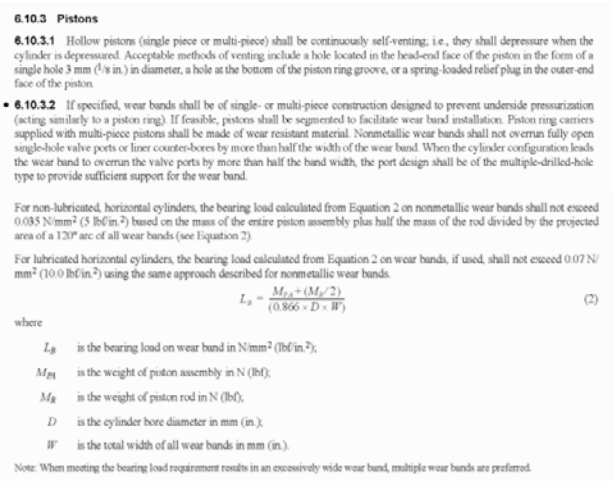

6.10.3 Pistons

6.10.3.1 Hollow pistons (single piece or multi-piece) shall be continuously self-venting, i.e., they shall depressure when the cylinder is depressured. Acceptable methods of venting include a hole located in the head-end face of the piston in the form of a single hole 3 mm (1/8 in.) in diameter, a hole at the bottom of the piston ring groove, or a spring-loaded relief plug in the outer-end face of the piston.

6.10.3.2 If specified, wear bands shall be of single- or multi-piece construction designed to prevent underside pressurization (acting similarly to a piston ring). If feasible, pistons shall be segmented to facilitate wear band installation. Piston ring carriers supplied with multi-piece pistons shall be made of wear resistant material. Nonmetallic wear bands shall not overrun fully open single-hole valve ports or liner counter-bores by more than half the width of the wear band. When the cylinder configuration leads the wear band to overrun the valve ports by more than half the band width, the port design shall be of the multiple-drilled-hole type to provide sufficient support for the wear band.

For non-lubricated, horizontal cylinders, the bearing load calculated from Equation 2 on nonmetallic wear bands shall not exceed 0.035 N/mm² (5 lbf/in.²) based on the mass of the entire piston assembly plus half the mass of the rod divided by the projected area of a 120° arc of all wear bands (see Equation 2).

For lubricated horizontal cylinders, the bearing load calculated from Equation 2 on wear bands, if used, shall not exceed 0.07 N/mm² (10.0 lbf/in.²) using the same approach described for nonmetallic wear bands.

$$L_B = \frac{M_{PA} + (M_R/2)}{(0.866 \times D \times W)} \quad (2)$$

where

L_B is the bearing load on wear band in N/mm² (lbf/in.²);

M_{PA} is the weight of piston assembly in N (lbf);

M_R is the weight of piston rod in N (lbf);

D is the cylinder bore diameter in mm (in.);

W is the total width of all wear bands in mm (in.).

Note: When meeting the bearing load requirement results in an excessively wide wear band, multiple wear bands are preferred.

(Fig.2) Section piston & ring design in API 618

Manufacturers and operators frequently select greatly varying numbers of piston rings based on the gas pressure and other parameters. Table 4 below shows different company standards, and additionally the width of the particular ring grooves and lands may vary as well.

by: Ralf Krich – HOERBIGER

Spec 1						
Differential Pressure (bar)	double acting-lubricated		single acting-lubricated double acting dry running		single acting - dry running	
	MW< 10	MW>=10	MW< 10	MW>=10	MW< 10	MW>=10
0 - 6	3	2	3	2	4	3
7 - 16	4	3	5	4	6	5
17 - 30	4	3	6	5	7	6
31 - 50	5	4	8	6	10	8
51 - 75	6	5	9	7	13	10
76 - 100	8	6	10	8	14	11
100 - 150	9	7	13	10	not used	not used
150 - 200	10	8	14	11		

Spec 2			
Differential Pressure (bar)	double acting-lubricated	double acting-dry running	
		MW<15	MW>=15
0 - 6	3	5	3
7 - 16	4	6	4
17 - 30	5	7	5
31 - 50	6	6+ 2	0+ 6
51 - 75	8	6+ 4	0+ 8
76 - 100	10	10+ 4	0+ 13

Spec 3			
pressure (bar)	double acting-lubricated		double acting-dry running
	MW<10	MW>=10	
0 - 21	3	2	3
21 - 41	4	3	4
41 - 69	5	4	5
69 - 110	6	5	6
110 - 207	7	6	7

Spec 4			
pressure (bar)	double acting-lubricated	double acting-dry running	
		MW<10 and bone dry	MW>=10 and wet
0 - 5	2	3	2
5 - 10	2	4	3
10 - 15	3	5	4
15 - 25	4	6	5
25 - 30	5	7	6
30 - 50	6	8	7
50 - 100	7	9	8
100 - 200	8	NA	NA
200 - 320	9	NA	NA
320 - 400	10	NA	NA

(Table 4) 4 Specifications about number of piston rings in relation to pressure

In general, smaller piston rings are used with high pressure and/or small diameters.

Depending on piston weight, a minimum width may be required for rider rings or segments, which must then be distributed among multiple rings. Rings wider than ~90 mm are problematic to manufacture. Because of thermal expansion these require high axial clearances. Starting at low temperatures can cause the rings "hammering" in the grooves.

As explained above, the piston speed, selected for dry running, is not very meaningful. A random sample of 185 horizontal, dry running reciprocating compressors installed between 1980 and 2000 showed the majority running with a piston speed below 3.4 m/s (Figure 3)

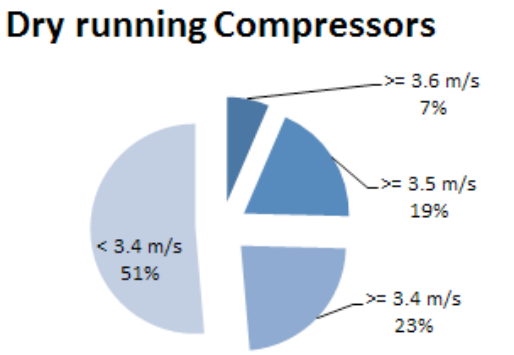

(Fig. 3) Proportional distribution in a random sample of dry running compressors installed before the millennium change

The following examples include not only the piston speeds, but the rotational speed, stroke and ring lengths as well. The running length is the sum derived from the stroke and ring length. In addition, however, the ring length from the first to the last piston ring is mentioned, which is referred to as the critical ring length. In my, and a number of experts', opinion, it is extremely important to review that in comparison to the stroke. While guide rings between the piston rings are shielded against dirt, those outside the piston rings run on fresh gas cooled surfaces. All other rings must dissipate their frictional heat to the running surface, and consequently to the cylinder.
The example (Figure 4) is showing that rider rings within the piston rings could heat transfer if the stroke is relatively short.

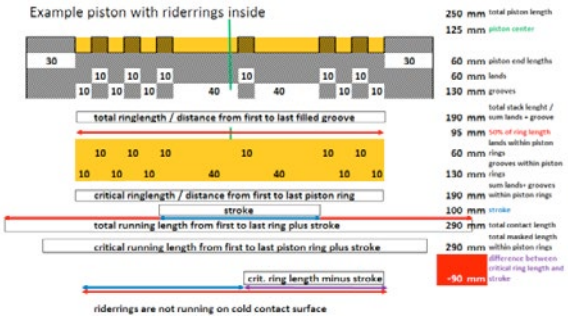

(Fig. 4) Length relation for a piston with rider rings inside piston rings. The difference between critical ring length and stroke is negative; therefore we have bad cooling effects.

The other example (Figure 5) is showing the example with riderrings outside, with the positive effect of these rings running on cold surface outside the masking piston rings.

by: Ralf Krich – HOERBIGER

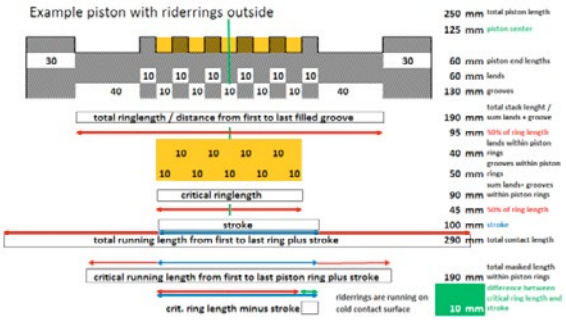

(Fig. 5) Example about lengths relation for a piston with rider rings outside piston rings. The difference between critical ring length and stroke is positive; therefore we have good cooling effects.

Often slip fit liner are installed, as a popular non-lube choice, made for ease of replacement, or if cylinder cooling is non-existent or inadequate, than temperatures far exceeding the gas discharge temperature may develop on the running surface, and thus on the rings.

More often, the rider rings undergo greater axial expansion than calculated, resulting in bulging in the middle. Rod drop analyses even reveal increasing gap values. Depending on the radial clearance, the rider ring exhibits disproportionate wear in the middle and, in some cases, may even make contact across the entire circumference, which again increases wear. Figure 6 shows such a piston with rings.

(Fig. 6) Piston with extensive wear one middle sections of the rider rings

3 Conversion of two fresh and recycle gas compressors from non-lube to lube operation to ensure 2 years continuous operation service

The operator, a German refinery, had been experiencing problems with the compressors since they were commissioned. A high number of unforeseen failures after start-up and various running time problems with the components used motivated the operator to discuss the options of an upgrade. The high risk of additional failures and the related loss of production, as well as enormous costs for spare parts and service formed the foundation for the analysis. These compressors are designed with 4 different cylinders. The observations below are limited to the most critical instance of the highest pressure stage with the largest ring length. Figure 7 shows a cross sectional image of the cylinder prior to the revamp.

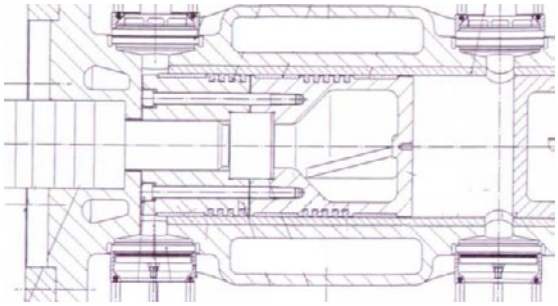

(Fig. 7) view on a cylinder with piston having one rider-ring within the piston rings

The operating data included hydrogen compression from 41 to 80 bara, and temperatures from approximately 45ºC to 125ºC.
The unit is equipped with an electro-hydraulic stepless valve unloading system, which potentially increases the discharge temperatures. The design temperature was therefore established at 180ºC. This unit, which had a rod load of 300 kN, was built for this purpose with an extremely short stroke of only 190 mm. Combined with a motor speed of 595 rpm, the piston speed was close to 3.8 m/s.

The impressive 90 mm piston rod and the two-piece cast piston necessitated 3 guide rings at 80 mm each for non-lube operation, and the design engineer selected 9 piston rings for the delta pressure of about 40 bar. The stack ring length of 450 mm includes the two guide rings on the head end. The liner running length is 640 mm. With a guide ring interposed between the piston rings, the critical ring length as masked length is 270 mm, or 80 mm larger than the stroke, which is the length between the outer piston rings (Figure 8).

by: Ralf Krich – HOERBIGER

Even after the ring materials had been modified, unsatisfactory running times of less than 2000 hours were obtained.

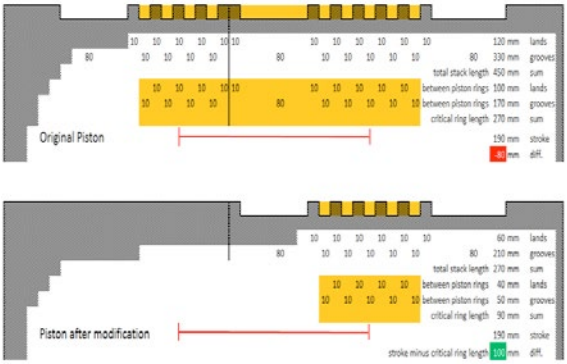

(Fig. 8) Layout of piston before and after modification

In connection with the described operating parameters, it was apparent that only an upgrade to lubricated cylinders would allow successful operating time. The priorities before the modification were a reduction of the high wear, conversion to lubricated operation (Figures 9, 10 and 11), and modification of necessary components. The structural layout would be maintained, requiring no additional space.

(Fig. 9) drilling of lube connections

(Fig. 10) new lubricator

Existing dampers are equipped with simple separators. The operator converted the hand exfiltration to automatic. The bottom of Figure 8 and Figure 12 show piston after the modifications, featuring only 2 guide rings and 5 piston rings.

(Fig. 11) new lube connections

(Fig. 12) modified piston

The new stack ring length is a total of 270 mm. The critical masked ring length between the piston rings is only 90 mm, which is now 100 mm shorter than the stroke; however, this is less relevant in what is now a lubricated design. As independent service provider the implementation of the entire project, including on-site activities, the modifications to the cylinders and components, delivery of new parts, installation and start-up was handled in a turn-key project. The customer has a more reliable solution at significantly lower costs for spare parts and service operating more than 16.000 hours with one set of rings.

4 Capacity increase as a result of changed bore diameters and clearance volumes in dry running boxer compressors

Because of rising production requirements, the operator was seeking an increase in capacity of approximately 10% from the reciprocating compressors that were upgraded in this example (Figure 13), which was anticipated to be possible utilizing the power of the electric motor and utilizing the maximum allowed rod load.

(Fig. 13) 1 of 3 compressors to be modified

The reciprocating compressors upgraded (Figure 13) were 3 nearly identical units with a stroke of 305 mm at a speed of 371 rpm, resulting in a piston speed of almost 3.8 m/s. The H2 mixed gas is compressed from 23 to 48 bara. The main task was to increase capacity by about 8%. For this purpose, the diameters of the cylinders were bored from 300 mm to 315 mm. Additionally, the clearance volumes were significantly reduced.

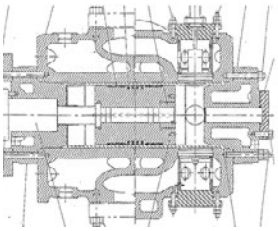

(Fig. 14) original cylinder)

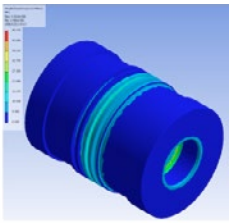

(Fig.15) piston FEA

As independent service provider 2-piece pistons (Figures 15 and 16) using the multi stud nut assembly method were designed, and at 279 mm, the entire ring length is already approximately 26 mm larger than the stroke. The running length is approximately 584 mm. The critical ring length between the outer piston rings is only 81 mm. The specific load on the guide rings is considerably less than 0.035 N/mm2. The team of technicians removed the cylinders and took them into the Service Center for the upgrade (Figure 17), where the liners were removed and the cylinders were bored. New liners and piston (Figure 16) were installed, and new clearance volume dummies were prepared.

by: Ralf Krich – HOERBIGER

The desired increase in capacity was achieved. Due to dynamic electro-hydraulic stepless flow control, the electric motor is never overloaded.
The leak tests were successfully concluded, and assembly in the plant and at the refinery was carried out on schedule. All three units have since been upgraded, and the higher capacity has been verified.

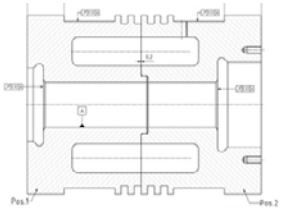

(Fig. 16) new piston

(Fig. 17) cylinder honing

The compressor was additionally equipped with new valve designs and pulsation calculations were performed for verification. The unit was put into operation including complete documentation and CE marking. The service life of the piston rings exceeds 14,000 hours.

5 Longer service life of guide rings due to modified piston and moved oscillating masses from cylinder into motion work

The operator of a 2-stage refinery compressor in Germany was no longer satisfied with the short lifetimes of the piston rings. Engineering analyzed the root cause and developed suggestions for modifications. It was found that the 245 mm piston (Figure 18), with 8 piston- and 4 rider rings had a weight of 163 kg, generated extensive friction. At a speed of 420 rpm it had a stroke of 250 mm.

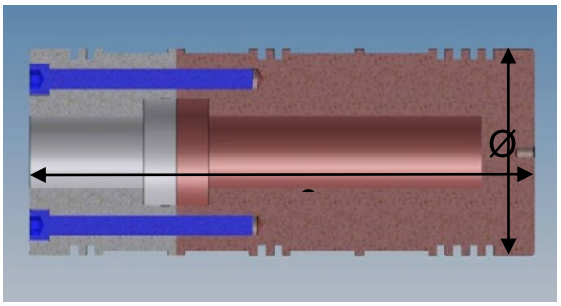

(Fig. 18) original piston design with distributed rings

At 3.5 m/s, the piston speed is moderate. The entire stack ring length is almost 320 mm, and the liner contact length is about 570 mm. What was particularly striking was that the critical ring length was also 320 mm, since all 4 guide rings were installed between the piston rings. The logical objective was to bring the critical ring length down being smaller than the stroke. The target dimension was 240 mm.

The developed solution provides for a modification of the single-acting piston (Figure 19). To begin with, measurements were conducted, the weight was recorded, and the original design was closely examined and recalculated. FEA was employed to determine the loads the new piston would have to withstand. The goal was to reduce the ring length and significantly lower the weight of the piston. In addition to the gas forces, pre-stressing forces and tightening torque were determined for the calculation.

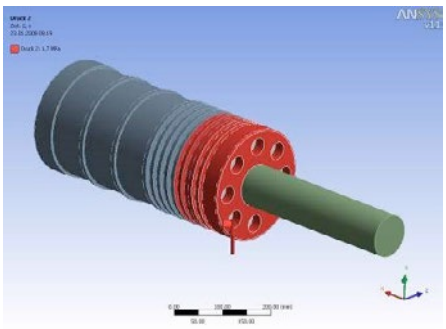

(Fig. 19) new piston with piston rings on one end

A variety of designs were investigated, such as cast and welded designs and machining from solid material, as were different materials. The newly designed piston has a critical ring length of only 160 mm and weights 112 kg. Ultimately, it was possible to create the contour for the cavity (Figures 20 and 21) out of solid material.

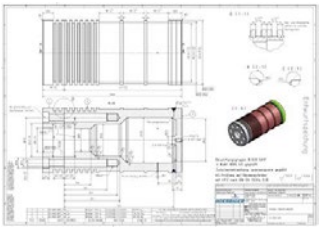

(Fig. 20) drawing of welded piston version

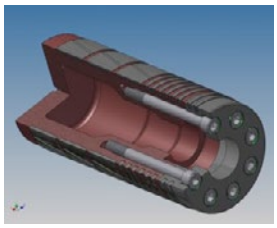

(Fig. 21) piston from solid bar machined

This eliminated both the need for an expensive casting pattern and a critical welded design.

To realize exact identical inertia forces the weight of the crosshead (Figure 22) was increased.

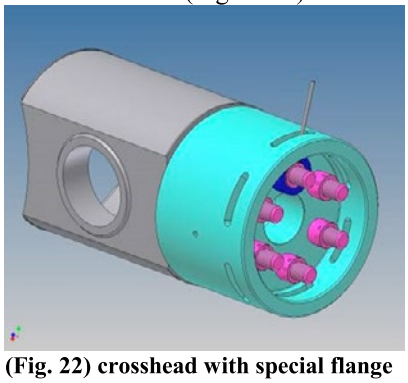

(Fig. 22) crosshead with special flange

by: Ralf Krich – HOERBIGER

None of the modifications requires more than three rider rings, yielding a shorter ring length. The strength is sufficient for all modifications.
The piston rod remained unchanged.

The operator has since confirmed lower ring wear as well as lower discharge temperatures, obviously because of lower frictional heat, along with slightly higher capacity.
Consequently this implemented successful upgrade was duplicated on the second compressor.

6 Reduced temperatures and increased capacity by conversion of cylinder/piston with labyrinth seal to conventional bore and piston with contact rings

Operators of certain labyrinth compressors (Figures 23+31) are increasingly recognizing the shortcomings of these units. The design is based on a lubricated piston rod guide between the crosshead and piston rod packing on the one hand, and a delicate labyrinth in the cylinder bore as well as the piston skirt on the other (Figure 24). The system, nominally a non-contact design, nonetheless exhibits wear over longer operating periods, and operators are forced to replace piston skirts, or even cylinders from time to time. Operators who do not want to replace these expensive components experience an increasing loss of capacity, combined with rising gas temperatures, which often surpass permissible alarm and shutoff values that manufacturers have set at relatively low levels because otherwise the piston rod sealing systems, cylinder bore and piston would wear even more quickly.

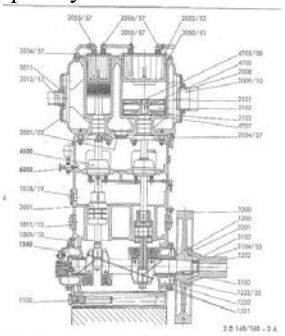

(Figure 23)
Assembly drawing of vertical 2 stage labyrinth compressor

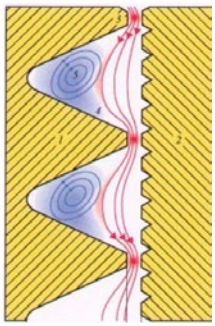

(Figure 24)
Design of non-contact labyrinth seal

This system offers major advantages when dealing with gases that have a high percentage of particles since these solids would result in greater wear of the rings and the running surface if conventional contact rings were used. Still, these compressors can be found in a fair number of applications that use clean gases such as CO_2, and the benefit of using them is questionable. In addition, it is safe to assume that leakage is considerably higher, even in a new compressor, than if the piston were regularly equipped with contact rings. If a lubricated piston was to be calculated at 100% leak tightness, it is typically customary to expect only 97% for non-lube operation. For labyrinth units, this base value could be estimated from our examples in a range from approximately 90% to 95%.

This has prompted us to upgrade a number of these labyrinth compressors in recent years to equip them with contact rings. Two examples in breweries are shown below.

In a Dutch brewery, the cylinders of both stages were bored, leaving the wall thickness in keeping with the groove base of the cylinder labyrinth. The bores were then honed for the use of rings for non-lube operation. The old labyrinth pistons (Figures 25-26) were replaced.

(Fig. 25) original 2nd stage piston

(Fig. 26) original 1st stage piston

A set of new 2-piece pistons (Figures 27 to 30) was designed in 3D using FEA and produced. Guide rings were not used, because rod guide bushings on top of crossheads are installed anyhow.

Only 2 and 3 piston rings were selected, respectively, for the operating parameters.
This made the ring length considerably shorter than the stroke, and as a result, lower wear is to be expected.

(Fig. 27+ 28) new 1st stage piston

(Fig. 29+ 30) new 2nd stage piston

by: Ralf Krich – HOERBIGER

Table 6 is showing an extract of the operating data before and after the modification. Whereas the unit couldn't be operated for longer periods before the modification, the brewery can now use the unit continuously.

Operating data with labyrinth piston		
Stage 1 discharge temperature	> 145	°C
Shut-off temperature according to OEM	130	°C
Stage 2 discharge temperature	>150	°C
Shut-off temperature according to OEM	135	°C
Capacity	1800	kg/h
No continuous operation is possible (compressor was shut off due to high temperature)		
Operating data with contact ring piston		
Stage 1 discharge temperature > 115ºC	>115	°C
Stage 2 discharge temperature > 120ºC	>120	°C
(shut-off temperatures as above)		
Capacity	2100	kg/h
Capacity 2100 Kg/h CO_2 (117%) Continuous operation is possible		

(Table 6) new 2nd stage piston

The electric motor temperature and load were within the allowable design limits.
A stroke of 100 mm and a speed of 506 rpm yield a very low piston speed of only 1.7 m/s. At 36 mm and 50 mm, respectively, the ring lengths are considerably shorter than the stroke in both instances.

(Fig. 31) The CO2 compressor operating after the modification of both pistons

A CO2 labyrinth compressor was also revamped in an Australian brewery. Problems were discovered on-site. Piston skirts (Figure 32) were being replaced at 1 to 3 month intervals. Nonetheless, elevated leakage was a constant.

The cylinder was modified by removing the labyrinth and installing new pistons (Figure 33) with piston rings and a respective guide ring made of special PTFE grade material.

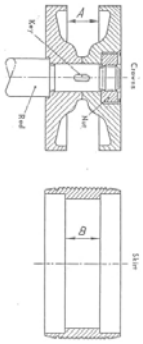

(Fig. 32) original piston with labyrinth

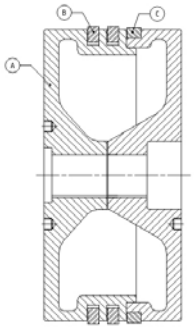

(Fig. 33) contact ring piston

The advantages for the customer are that the compressor is running more smoothly and more quietly.
Large cost savings are achieved by replacing less expensive wear parts annually instead of having to replace expensive components approximately 4 to 6 times a year.

The capacity is considerably increased and reliability is greater since the piston no longer has metal contact with the cylinder and the discharge temperature were lowered from 160ºC to about 106ºC.

7 Conclusion

The above projects are all showing the challenges of compressors when they are designed for dry running, none-lubricated, operation. Sometimes this is done to save operating costs for the lube oil units and separation of liquids. Anyhow there is a tendency to install short stroke with higher speed motors (lower number of poles) which also reduces costs at installation due to reduced foot-print.

The lifetime of the wear parts is often not considered in the required effort to reduce long-term operational costs. Wear part life of less than 8000 hours, is often accepted without need.

Often it is a discussion about ring material, but not as much, about piston design. This paper should open the eyes to make aware about issues to be obeyed when buying non lube compressors or eventually to upgrade piston and cylinders when possible and feasible.

by: Ralf Krich – HOERBIGER

8 References

[1] API Standard 618 "Reciprocating Compressors for Petroleum, Chemical and Gas Industry Services," 5th Edition American Petroleum Institute Dec 2007

[2] Kriegel, G. "Beitrag zur Berechnung des Radialverschleißes von Trockenlaufkolbenringen (Article on the Calculation of Radial Wear of Dry Running Piston Rings)", Dissertation, Dresden University of Technology 1978

[3] Feistel, N. "Beitrag zum Betriebsverhalten trocken laufender Dichtsysteme zur Abdichtung der Arbeitsräume von Kolbenkompressoren (Article on the Operating Behavior of Dry Running Sealing Systems Used to Seal the Working Chambers of Reciprocating Compressors)", Dissertation, Technical Faculty of the University of Erlangen Nuremberg 2001

[4] Tuma, S. "Taking the guesswork out of PTFE seals," 6th Conference of the EFRC, Düsseldorf 2008

[5] Langela, M. "Material Development transferability counts," 7th Conference of the EFRC, Florence 2010

[6] Krich, R./Reese, M. "Wie Umbauten von Kolbenverdichtern durch unabhängigen Technologiepartner den Gebrauchswert erhöhen (How Revamps of Reciprocating Compressors by an Independent Technology Partner Increase Practical Value)," 15th Kötter Workshop Reciprocating Compressors, Rheine 2011

[7] Williams,B.F. "Non-lubricated Moderate Speed Reciprocating Compressors in a Hydrogen Plant," 8th Conference of the EFRC, Düsseldorf 2012

EUROPEAN FORUM
for RECIPROCATING
COMPRESSORS

DIGITALISATION

STASSKOL

Smart Packing

by:

Dr. Marc Langela
STASSKOL GmbH
39418 Staßfurt, Germany
marc.langela@stasskol.de

11th EFRC CONFERENCE
September 13 – 14, 2018, Madrid

Abstract:
In compressor applications, the sealing elements of piston rod packings are mostly manufactured out of optimized PTFE and PEEK compounds with additives for reinforcement and self-lubrication. The lifetime of the sealing elements is sometimes the bottleneck towards a sufficient service time between two routine maintenances and choosing the right material is a crucial task for the reliability of compressor systems. In industrial process applications the wear behavior of sealing materials can be strongly influenced by the characteristics of the application.
Even the most suitable sealing materials are sometimes failing due to variations at the process parameters as well as due to impurities in the gas that might suddenly occur. In some field cases the compressor fails within short times while material & design of the sealing elements are the same that did run sufficiently for several years. Additionally, sometimes A and B machines that are compressing the same gas at the same conditions with the same material and design are showing a significantly different performance.
In summary, even the best combination of sealing material and sealing ring design can only reduce the risk of failure to a minimum but it never can ensure 100 % of reliability.
Very often, the packing condition is monitored by measuring either the leakage rate or the temperature of the leakage gas at the vent-line. A temperature increase or a leakage gas flow increase above a critical value gives an indication about the wear status of the internals of the piston rod packing. However, modern sealing ring designs are very tight and the leakage rate stays at a low level until the end of the lifetime of the sealing elements is reached. At this point the leakage rate dramatically increases and the compressor has to be immediately serviced which sometimes causes unexpected downtimes and high costs especially at non-redundant critical compressor applications.
STASSKOL has developed a “Smart Packing solution” that is able to online monitor the wear status of the sealing elements within a piston rod packing. The wear of each sealing ring can be visualized and so the wear behavior of the whole piston rod packing can be characterized. Most important, the maintenance of the compressor system can be scheduled according to the predicted remaining lifetime of the sealing elements.

by: Dr. Marc Langela – STASSKOL

1 Introduction

Reciprocating compressors are widely used to compress gaseous media for industrial applications, for example at chemical plants for hydrogenation reactions, polymerizations or Polysilicon productions. These are fully-integrated and automated industrial processes, which are running continuously and therefore a failure in compressor operation can cause unexpected and expensive down-time.

In consequence, the reliability is one of the most important properties of reciprocating compressor systems. The crucial items in respect to reliability are often the spare parts of the bare compressor. According to a study performed by Dresser-Rand, piston rod packing are at 2nd place of the failure reasons with 17.8 % (see Figure 1).

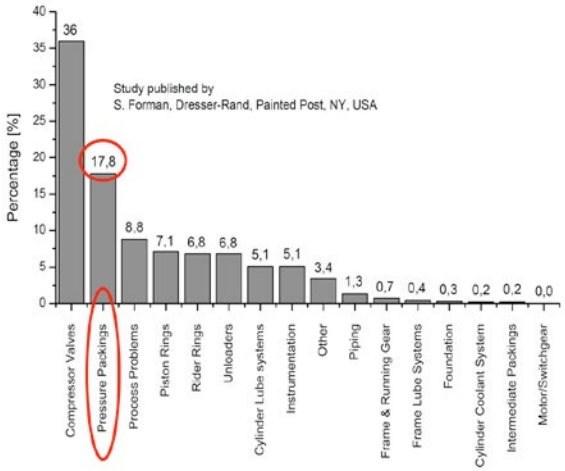

Figure 1: Reasons for compressor failure[1]

The materials of the sealing elements are tuned for maximum lifetime but also this optimization has its limits. Furthermore, negative influences like gas impurities, process variations, etc. can lead to increased wear and reduced reliability. Therefore, even the best material and design cannot guarantee sufficient operation to a level of 100 %.

In consequence, an online wear status of the sealing elements of a piston rod packing is needed to achieve the best reliability of the system and to utilize the maximum running hours of the sealing elements.

2 Up to date solutions

Already today, the industry tries to estimate the wear status of the piston rod packing internals by:
a) measuring the temperature at the vent line
b) measuring the leakage gas flow or
c) measuring the temperature within the pressure packing.

Background of all these methods is the assumption that the amount of leakage gas strongly corresponds to the wear status of the piston rod packing.

Compressor tests were performed to investigate this link. A fast wearing material (full wear after approx. 800 hours) was used in order to measure the leakage rate of the piston rod packing throughout the full operational duration of the internals. It was found that the leakage rate shows high fluctuations during the whole test duration (see Figure 2). The flow rate exceeded 30 m³/h shortly after 800 hrs (not shown at Figure 2) and the test was finished.

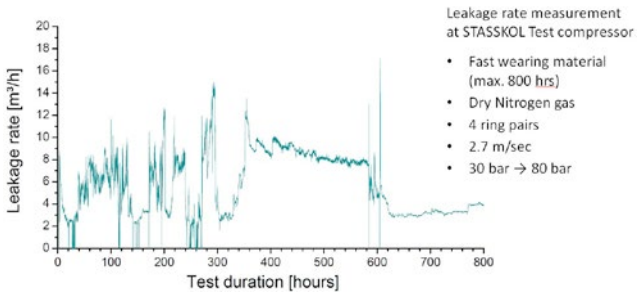

Figure 2: Leakage rate during compressor operation (measured by In-House compressor)

Therefore, the wear status of piston rod packing internals cannot be estimated by measuring the leakage rate at the vent line and a direct measurement of the packing internals is needed.

3 Direct wear measurement

The concept starts with the question about the dimensional changes of the sealing elements during wear. The wear takes place at the inner diameter of the sealing ring and the elements are moving towards the piston rod (see Figure 3).

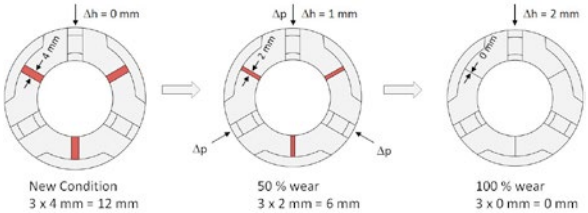

Figure 3: Wear behavior of the single sealing ring design

Thus, the outer diameter of the sealing ring decreases and this can be measured by using an adequate sensor arrangement. A symmetric sealing ring design has to be used in order to ensure an even wear throughout the whole circumference. The single sealing ring with its 120° segments is such a ring design. At a gap of 4 mm between every sealing element, the outer diameter will be reduced by 2 mm at full ring wear.

by: Dr. Marc Langela – STASSKOL

4 Sensor selection

The sensor for measuring the outer diameter of the sealing ring should be able to handle the following process conditions:

- Pressure up to 100 bar
- Temperature up to 150 °C
- Insensitive to impurities (debris, oil, etc.)
- Compact dimensions (low amount of space)
- Measurement range of minimum 2 mm

A direct comparison of different sensors shows, that an eddy current sensor might be the best choice for this application (see Figure 4).

Figure 4: Pro and cons of different sensor systems

Capacitive sensors are not resistant against impurities, ultrasonic sensors are not pressure resistant, and IR and mechanical sensors require too much space. Another option might be a confocal sensor system, but this is not resistant against the pressure within the piston rod packing.

5 Measurement setup

Eddy current sensors are available in small sizes, but even the smallest Eddy current sensors are barely fitting into the walls of the packing cups in radial direction. The installation in radial direction would be perfect for direct observation of the outer diameter of a sealing ring. The space within a chamber wall is limited and there is no access from the outer diameter of a piston rod packing as the packing is located within a bore at the cylinder block. Thus, the eddy current sensor has to be installed in axial direction and an indicator pin has to be used to transfer the positioning information of the sealing segment to the sensor (see Figure 5).

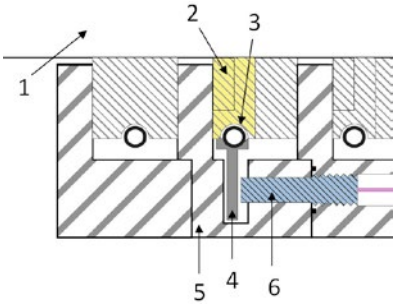

Figure 5: Sensor (6) arrangement with indicator pin (4)

The idea behind it was to transfer the movement of the sealing ring (2) towards the piston rod (1) by using an indicator pin (4). If the sealing ring moves toward the piston rod, the indicator pin will follow this movement and the Eddy current sensor will measure the movement of the indicator pin. This concept was successful, but the changes of the sensor signal were too small for a sufficient accuracy of the measurement.
In order to increase the sensitivity of the system we introduced a sloped surface at the indicator pin (see Figure 6).

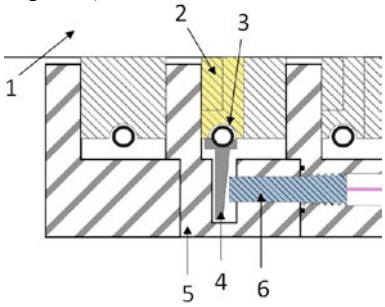

Figure 6: Sensor (6) arrangement by using an indicator rod (4) with sloped surface

Now, with a sloped surface, the signal of the Eddy current sensor changes constantly during the movement of the indicator pin. The segment of the sealing ring will move towards the piston rod if wear takes place. The indicator pin follows and due to the slope of the pin, the metallic surface moves away from the sensor, leading to an increase of the signal. The sensitivity of the sensor (dependence of the signal on the movement of the indicator pin) can be tuned by adjusting the slope (see Figure 7).

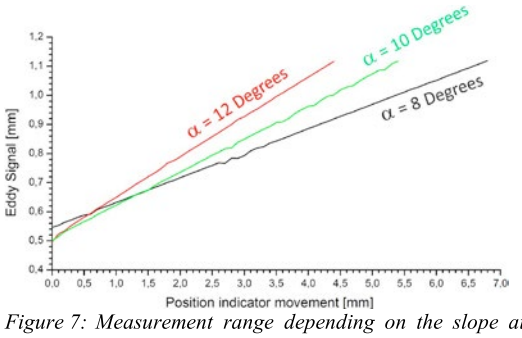

Figure 7: Measurement range depending on the slope at the indicator pin

Different rod sizes are requiring different gaps between the elements of a sealing ring and therefore the movement towards the rod during wear changes. This can be adjusted by changing the measurement range using different slopes. Additionally, we have to consider the rod drop, which also leads to a movement of the sealing rings.

The rod drop can add to the movement during wear or in other installation arrangements, it can work against this movement.

by: Dr. Marc Langela – STASSKOL

If we calculate with a sealing element movement of 2 mm due to wear (like illustrated at Figure 3) and we add an allowable maximum rod drop of 2 mm, then this will end up in a total movement of the sealing element of 4 mm. If the rod drop works in the opposite direction of the sealing ring wear, then the total movement of the sealing ring segment can be zero, even at full wear.
Thus, we have to adjust the measurement range and we have to measure the rod drop within the smart packing system for taking the movement of the rod into account when calculating the wear status of the sealing ring.

6 Compressor test

With this measurement setup, a series of 1st tests were performed at the compressor test bed (see Figure 8).

Figure 8: Compressor test bed

The following parameters were used during the compressor tests:
- Suction pressure: 30 bar(g)
- Discharge pressure: 80 bar(g)
- Piston rod diameter: 70 mm
- Piston rod velocity: 2.7 m/sec
- Temperature at sealing ring: 100 °C
- Gas: Nitrogen with low dew point (< -80 °C)
- Sealing material: PTFE + glass fiber (fast wear)

As listed above, a sealing material with fast wear at the given conditions was used to test the system within relatively short period of time. After installation of the sealing ring (only one ring at the piston rod packing), the test was started and the signal of the Eddy current sensor was recorded.
The single sealing ring design was chosen at a rod diameter of 70 mm and the gap between each of the three sealing segments was 2 mm. This gives a total gap of 6 mm throughout the whole circumference. At full wear, all three segments will be moved 2 mm towards the piston rod for wear compensation. Figure 9 shows the development of the signal of the Eddy current sensor during the compressor test.

At this test, the sensor was mounted within a horizontal packing on the top side, so the rod drop was substracted from the raw Eddy Signal by using the theorem of intersecting lines. However, the test duration was only about 95 hours and within this time the rod drop signal did not change significantly. The curve shows the corrected Eddy signal averaged over a period of 60 seconds. If the signal is recorded over the crank angle without averaging, then there would be more vibrations of the signal due to pressure pulsations and rod run-out.

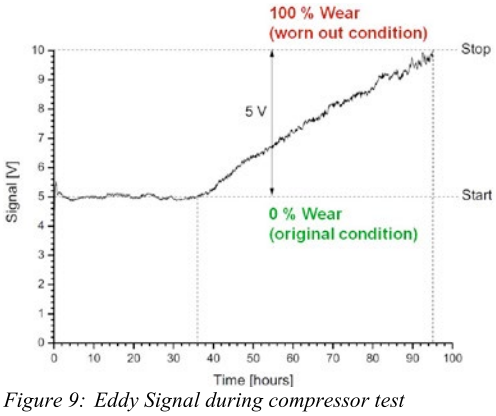

Figure 9: Eddy Signal during compressor test

The signal starts at 5 V (0% of wear) and after a run in phase of approximately 35 hours the wear starts and the signal constantly increases. After 95 hours, a value of 10 V was reached, which was the value for a ring wear of 100 %. The compressor was stopped after getting the 10 V signal and the piston rod packing was disassembled. A measurement did show that all gaps of the packing ring were used up, so, the sealing ring was fully worn out. This shows that the sensor arrangement works sufficiently.

7 Summary and Outlook

We emphasized the importance of online wear measurement of the sealing elements within a pressure packing for improving the compressor reliability and for a 100 % utilization of the performance of the sealing ring material.
A sensor was chosen and a measurement concept was developed for measuring the movement of a sealing ring segment towards the piston rod surface during wear. The measurement concept was optimized by introducing an indicator pin with a sloped surface. The sensitivity of the sensor concept can be varied by changing the slope at the indicator pin.
For verification of the system, first compressor tests were carried out and the signal was recorded from new condition to 100 % wear of the one sealing ring that was installed within the pressure packing.

by: Dr. Marc Langela – STASSKOL

In the near future additional tests will be carried out by using a piston rod packing with one sensor at each sealing ring (see Figure 10).

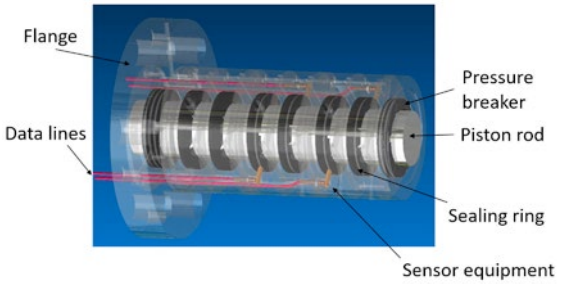

Figure 10:Piston rod packing with one sensor at each sealing ring (4 sealing rings in total)

The smart packing system will be very beneficial for critical applications where unscheduled downtime of the compressor system is very expensive. It is able to monitor the status of the internal parts within a piston rod packing and therefore to calculate the wear status of the packing system.

Therefore, it is possible to calculate residual running times and to produce new sealing elements just in time. The maintenance can be scheduled optimally to reduce downtime to a minimum. Additionally, the performance of the sealing material can be utilized to a 100% for achieving maximum service times between two maintenance stops.

---

[1] Forman, S. (2002): Compressor Valves and Unloaders for Reciprocating Compressors", technical report, Dresser-Rand, Painted Post, 19 pages, 2002

The challenge of Industry 4.0 applied to a stepless capacity regulation system

by:

M. Schiavone, A. Raggi, A. Giampà
Dott. Ing. Mario COZZANI S.r.l.
Arcola (SP), Italy
info@cozzani.com

11th EFRC CONFERENCE
September 13 – 14, 2018, Madrid

Abstract:
The digitalisation within the Industry 4.0 brings a new vision of the systems management and life cycle. In System Engineering applications such change is based on Internet of Things (IoT) and real time communication. Nowadays the continuous development of the communication technologies enables a disruptive improvement of the life cycle processes and its management. In particular, the technological development allows the outsourcing of processes and brings great advantages to the plant managers and suppliers, working in an integrated way. The article shows some cases of remote management applied to the electric capacity regulation systems for reciprocating compressors. This article describes the advantages of the major IoT applications for customers and end-users, throughout the entire product life cycle: from commissioning and start-up, management of warnings and deviations, predictive and planned maintenance; in addition to that, the article shows the benefits that users experience from these advanced technologies, energy saving at first.

by: M. Schiavone, A. Raggi, A. Giampà – COZZANI

1 Introduction

Nowadays Internet of Things (IoT) is changing the way companies create products, services as well as the customer experience. This is why IoT is the core area of investments and innovation.

In the recent years, the continuous improvements and extension of internet connections and the availability of specific hardware enable a constant growth of IoT.

The possibility of connecting and interacting with systems remotely offers at first the possibility to create new and innovative services and also allows improvements in performances, lifetime, and security.

In particular IT and data security is one of the main aspects of IoT to be managed: every connected system is potentially a system exposed to threats. This is why the development of IoT systems requires the implementation of more secure systems.

This paper describes how IoT can be applied to a stepless capacity control system and it shows the corresponding benefits throughout the product life-cycle, based on real applications.

2 Challenges of IoT applied to stepless capacity control systems

The increasing need of reducing the energy consumption of reciprocating compressors leads to new technologies that allow advanced capacity control systems.

The stepless capacity control can be managed by different methods such as: compressor variable speed, variable frequency, reverse-flow with valve opening time control [1]. These methods have been implemented also for heavy-duty applications.

2.1 The electromagnetic stepless capacity control system

This paper focuses on the first in the world electromagnetic capacity control system. The system manages the reverse flow, hence the capacity, by acting the suction valve closure at every compression cycle.

This system has been applied worldwide on a variety of reciprocating compressor types and applications.

The compressor capacity can be reduced allowing a reverse flow towards the suction plenum. In this circumstance the valve plunger is forced to maintain the valve sealing elements in the open position from the very first timestep of the suction cycle until a specific timestep defined by the control system. The force and the motion on the valve sealing elements are delivered by electromagnetic force acting on the valve plunger through the actuator rod (the actuators are shown in Figure 1).

Figure 1. Two actuators of an electromagnetic capacity control system.

One of the main advantages of this system is the suppression of any possible fluttering motion of the sealing element. This is achieved by imposing the sealing element displacement and its steady position. This allows a reduction of wear of springs and sealing elements (either plates or rings), ensuring higher reliability, longer valve life, and reduction of Mean Time Between Maintenance (MTBM).

The precision and the repeatability required to control the sealing element motion throughout the compressor cycle are ensured and managed by an advanced control system, which is interfaced with the compressor control room.

The required set point can be set in the control room by specifying the parameter to be maintained constant. The parameter can be the suction pressure, the discharge pressure, the inter-stage pressure or other parameters according to the control room requirements. This signal can either be generated automatically by a close-loop digital regulator implemented within the DCS, or it can be set manually in the DCS or in a local cabinet next to the compressor (in this way the capacity control is managed with an open loop). In the first case as the suction pressure drifts from a reference value, the controller (usually located in the control room) modifies the suction valve closure delay: this will

by: M. Schiavone, A. Raggi, A. Giampà – COZZANI

maintain the set point value constant and will control the compressor capacity.

Throughout the operations, the control system performs diagnosis routines on each actuator. In the unlikely event of actuator failure, the control system cuts-off the actuator and the system continues to operate. In addition to that, the control system adopts specific strategies based on the compressor configuration to keep delivering the capacity requested. This is achieved by shifting the load between the available actuators until the failed actuator will be replaced.

2.2 The remote connection system

The remote connection system links the capacity control system to the Data Centre with a VPN connection (a scheme of the network is shown in Figure 2).

This allows the Service Team to connect to customer cabinet and the Data Centre to receive data and emails from the control boards.

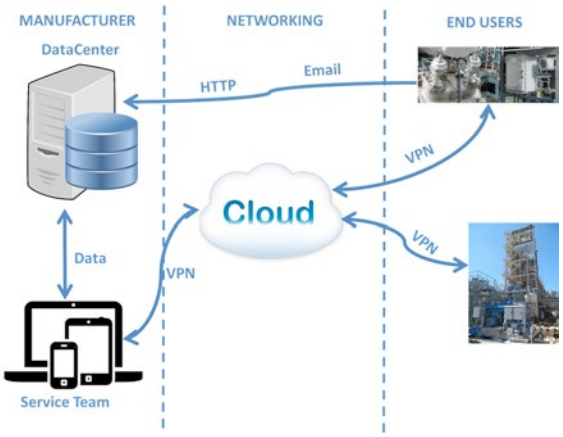

Figure 2. Architecture of a remote control module for stepless capacity control systems

The implementation of a remote connection system within a stepless capacity control system brings several advantages for the End-User. For instance, maintenance activities are targeted to the real needs and maximise efficiency and minimise the time and resources required for the maintenance operations. This capability is also the basis to deliver predictive maintenance on the operating systems.

In the event of an adjustment or modification of the compressor operating conditions, the control system also allows parameter changes. This allows having a system always tuned and highly efficient.

One of the key challenges with remote connections of the industrial control systems is the need to ensure network security, integrity and reliability. These requirements lead to the implementation of several features that must be considered to design the system. These are security protocols based on VPN connection, protected data storage, password with two-factor authentication for each operator, and so on. In addition to that, the selection of partners with internationally recognized security standard ensures the security management, continuous improvement on the long-term, and fully redundant network of distributed access and VPN servers. All these aspects help to keep pace with changes, identify vulnerabilities, predict security threats and, finally, limit business impacts in case of a security breach.

2.3 Functionalities of the remote connection system

The remote connected system is focused on data security, and allows the following activities:

2.3.1 Teleservice

Remote access allows either continuous or single monitoring and diagnosis. This possibility allows parameter adjustments, and also to support on field technicians during operations.

2.3.2 Remote data

Data from stepless capacity control systems can be collected and addressed to the Data Centre from any application or site. This set of data is accessible to the Service Team, via web service, to monitor the capacity control system health and usage. Such data is typically used to detect eventual deviations and to plan and support proactively maintenance operations.

The remote connection module records continuously data for each tag. Each tag is registered at fixed intervals, and data is recorded with timestamp in a database. This database can be examined for statistical analysis, history log, and trend analysis also in real time. Data files are transferred via secured protocols to the Data Centre.

2.3.3 Server web HMI

The remote connection module includes an integrated web server for monitoring usage. The remote connection module offers an effective HMI which can be easily accessed from any web browser.

by: M. Schiavone, A. Raggi, A. Giampà – COZZANI

2.3.4 Alarms management

The remote connection system includes several functionalities related to the alarm management. In particular it can track the full alarm cycle as alarm trigger (ALM), alarm acknowledgment (ACK), return to normal operating conditions (RTN), alarm end (END). Alarms can be notified via email or text messages.

The functionalities described can be extended to compressor variables, by integrating input/output signals (either analogic or digital), or by PLC connection through drivers for most common PLC.

2.4 Types of networking

The type of networking selected allow the separation between control system network and the End-User network. The network types are listed below. The selection of the network type varies and it is usually defined depending the End-User preferences and available network.

2.4.1 WAN

In this case the connection is established with a LAN cable. It can be used if the EU has an Ethernet cable network available by the compressor site.

2.4.2 PSTN

In this case the connection is established with a cable derived from a PSTN line. It can be used to connect directly the Capacity Control System without any relation with the EU network.

2.4.3 WIFI

In this case the connection is established on the End-User Wireless network. It can be used if the EU has a Wi-Fi network by the compressor site.

2.4.4 UMTS

In this case the connection is established on mobile network with a SIM card installed into the system. It can be used to connect directly the Capacity Control System without any relation with the EU network and without any EU installation job.

3 The manufacturer support for Customer needs

The growing complexity of capacity control systems requires the support of specialists –as the Producer- for the correct management of the typical operations.

These operations usually are: commissioning (in which parameters setup occur), compressor and system start-up (in which parameters are checked against the effective operating conditions), normal functioning (in which deviations with respect to the ideal trends are monitored), full system planned maintenance (during which on-field technicians together with in-office technicians, are able to ensure and check the system performs correctly).

The remote connection allows the capacity control systems to be constantly monitored and checked by the Service Team. This ensures the system performs correctly throughout the operations of its life cycle, with clear reliability and cost reductions experienced by the End-Users.

The integrated alarm functions inform the Service Team via email and/or text messages of deviations with respect to the nominal behaviour in real time. The in-office Service team can check and detect the causes of the anomaly with very limited costs, if compared with the traditional on-site service team operation.

Any operation that can be managed via software is available to the in-office Service Team, as if they were on-site.
In addition to that, the in-office team has access to the system history log. This allows the analysis of trends and deviations of key variables, such as board temperatures (as shown in Figure 3), velocities, 4-20 mA signals etc.

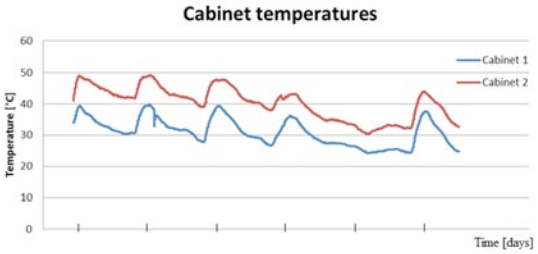

Figure 3. Temperature trend within the electric board of a stepless capacity control system.

4 Examples of service cases with remote connectivity

This section reports few examples of operations in which the remote connection system enabled fast responses and case resolutions, minimising the costs on-site ([2], [3]).

4.1 Functionality test (commissioning, normal operation, maintenance)

by: M. Schiavone, A. Raggi, A. Giampà – COZZANI

Compressor power:	355 kW
Number of stages:	1
Working gas:	H2+CH4+H2S
Country of installation:	Germany

Table 1. Compressor information.

During an operation carried out by the End-User on a compressor equipped with a capacity control system (see Table 1), it has been required to disassemble some components of it. As the operation was completed, and system was re-assembled, the End-User requested the Service Team to supervise remotely the capacity control system re-start.

The Service Team analysed remotely the operations carried out on the system by the End-User, and identified the tasks required to verify the setup was correct.

The activities that were carried out were standard procedures, which are usually performed during the system commissioning, or full system maintenance.

Service Team remotely coordinated the End-User team and all scheduled tests were completed with success. At this point both the compressor and the capacity control system were re-started correctly.

4.2 Start-up

Compressor power:	1400 kW
Number of stages:	2
Working gas:	CO2+CO+H2S
Country of installation:	China

Table 2. Compressor information.

Four capacity control systems have been installed on four new reciprocating compressor units (see Table 2), which would have worked under the same operating conditions. At the end of the systems installation the End-User asked the Service Team to supervise the start-up of one of the four compressors. During that supervision the capacity control has been monitored on-site and verified ensuring the correct behaviour under different degrees of capacity control. During the same occasion trends of compressor parameters have been recorded and analysed.

The start-up of the other three compressors were planned later: for each of these three start-ups the supervision has been carried out remotely, as scheduled by the End-User.

The capability of setting up a connection with the capacity control systems allowed a reliable verification of the correct functioning of the capacity controls for each of the remaining three compressors. The verification activity has been completed by comparing the data acquired during the first setup with the data recorded during the next three start-ups. In particular, data stored in the compressor control room have been compared with those initially recorded and stored in the Data Centre.

4.3 Root causes and resolution: incorrect flywheel sensor target installation

Compressor power:	350 kW
Number of stages:	3
Working gas:	C2H4+C6H14+Others
Country of installation:	Italy

Table 3. Compressor information.

During a non-scheduled maintenance operation on a compressor (see Table 3), an End-User had to dismount and reassemble the flywheel. In such occasion, the End-User has not notified the Service Team about the maintenance action in progress, by requesting any check on the correct functioning of the capacity control system. As the compressor and capacity control were restarted some anomalies have been noticed.

In particular, by setting the capacity control system to zero capacity, the compressor was effectively delivering what requested. However, if any other degree of regulation was imposed, the compressor delivered full capacity. In addition to that, the actuators were performing some non-synchronized actuation cycles.

In order to identify the root cause of the problem, a time slot has been selected with the End-User in which the compressor could be operated as requested (full capacity); next, data was analysed live (via the remote connectivity system). The operating condition selected was full capacity in order to mitigate any actuation cycles that may be harmful for the compressor.

During the observation of the system at full capacity, it was observed that the compressor was working constantly at 333RPM, while the capacity control system was recording random speeds (different to the effective speed).

Compressor rotational speed and piston position is determined by using a sensor, which reads the passing frequency of a target located on the flywheel (Top Dead Centre Sensor, shown in Figure 4). The Service Team observed -remotely- an anomaly on the speed measure and suggested to the End-User to verify that the positioning of both the sensors and target complied with the technical documentation of the stepless capacity control system.

The End-User verified the positioning was not correct, and fixed the positioning as specified. The system started again to perform correctly.

by: M. Schiavone, A. Raggi, A. Giampà – COZZANI

Figure 4. Flywheel Top Dead Centre Sensor TDC used in the capacity control system.

4.4 Alarm notifications during compressor functioning

Compressor power:	1730 kW
Number of stages:	4
Working gas:	N2+H2
Country of installation:	Switzerland

Table 4. Compressor information.

The plant by which the capacity control system was installed was down in order to carry out some planned maintenance activities. The capacity control system installed on the compressor (see Table 4) would have been subject to the planned maintenance, which was scheduled on the following days. The system, however, was still connected to the power supply, and it was still turned on in stand-by for the compressor start-up.

In that circumstance the control board detected an anomaly in the system and transmitted the warning to the Service Team via the remote connectivity system. As the warning was notified, the Service Team started to analyse the capacity control system status and proceeded to investigate the root cause. The root cause turned up to be a disconnection of the feedback cables that connect the actuators to the control board. The Service Team could promptly contact the End-User, giving the warning that some actuators and connection wires have been disconnected without turning off the power supply first –as indicated in the user procedures-.

The prompt communication of this warning –detected by the Service Team and notified to the End-User- led to the interruption of the maintenance operations until the electronic board power supply was turned off, avoiding any potential damage or health and safety implications.

4.5 Parameters modification on a working compressor

Compressor power:	355 kW
Number of stages:	1
Working gas:	H2+CH4+H2S
Country of installation:	Germany

Table 5. Compressor information.

A compressor equipped with the capacity control system was operating under nominal operating conditions (see Table 5). Suddenly the temperature in the suction plenum increased rapidly and exceeded the maximum limit, hence the compressor engaged an emergency stop. Before re-starting, the End-User requested a check of the functionalities of the capacity control system. The check showed that, despite the flow regulation degree was maintained constant, the mass flow was reduced drastically.

At this point the Service Team checked the history trends of the signals, by consulting the history log stored in the Data Centre. The analysis showed that as the mass flow changed –as described by the End-User-, no other signal coming from the control room had changed. Next, a connection has been setup with the control board and it was finally observed that the digital input to idle the compressor was not coherent with the value received by the control system. The anomaly was therefore addressed to a problem on the reading of a signal that manages the idle condition of the compressor, regardless the capacity degree requested, in fact it has been found that a wire terminal clip came loose. The Service Team was allowed by the End-User to modify remotely some parameters and bypass the status of that digital input. This operation has been possible without impacting on either the compressor or the capacity control. From that moment on, the capacity could have been regulated from the control room, from 0% to 100% flow, with no limitation to any of the End-User operations.

As the End-User allowed the Service Team to operate, the team could analyse, perform the root cause, identify the solution, and deliver the fix and a functioning system in very short period of time.

The signal terminal connection was restored at the next planned maintenance, avoiding any interruption of the production processes.

5 Customised maintenance

The capacity control system records several variables about the effective functioning of the devices and systems subject to planned maintenance. This information allows the End-User, OEM, and manufacturer Service teams to identify optimised maintenance plans.

by: M. Schiavone, A. Raggi, A. Giampà – COZZANI

Thanks to the remote connectivity, the capacity control systems can share data with the Data Centre, allowing continuous availability of data and information that help the End-User throughout the life-cycle. In particular more efficient maintenance plans can be offered, and MTBM being extended up to two years and more based on real condition of the components, performance analysis during service and the effective usage of the compressor.

6 Conclusions

The article shows real application of how IoT can be applied to a stepless control system, hence the generation of innovative benefits and services for the End-User.

The system analysed in the article is the first stepless capacity control system equipped with an electromagnetic actuator in the world. The system is patented and deployed on several reciprocating compressors installed worldwide.

The article described the characteristics and functionalities of the remote connectivity system: five real cases of utility of this system have been presented, and the advantages experienced by the End-Users have been described. In particular, the main advantages can be summarised as the optimisation of on-site service activities in terms of both minimisation of response time and minimisation of operations on field, resulting in cost savings.

The real cases presented in this article have been selected from the main life-cycle phases, starting from commissioning, to start-up, ordinary operations, and maintenance.

As regard as the commissioning and start-up after maintenance, several functional tests are possible with the compressor in a stop status. As far as the compressor start-up it is possible to monitor the behaviour of the capacity control system, in order to optimise the parameters and reach the maximum efficiency of the capacity control system. Regarding the ordinary use of the compressor, the diagnosis and problem fixes can be delivered via the remote connectivity. In particular, the mechanical deviations can be resolved by remote diagnosis and supply of instructions to the End-User; the electrical deviations can be managed with software-fix packages, and the generic anomalies with warnings sent via email and SMS.

In conclusion, the availability of a remote connectivity system integrated within the stepless capacity control system allows the most efficient supervision of the system behaviour, ensuring extremely short response times with respect to the traditional service action on-site. In addition to that, the remote connectivity system ensures an immediate diagnosis, therefore in the event that on-site service is required, it is possible to prepare, plan and deploy the service action in the most efficient way.

Thanks to the remote connectivity system, it is also possible to analyse the performances in service and issue customised maintenance plans based on compressor configuration, capacity regulation degree required, Customer needs and finally achieving the extension of the MTBM up to two years and more.

References

1 – Workshop “Compressor Control", 5th EFRC-Conference 2007 Prague
2 – A.Raggi, A.Giampà, M.Grassi “Capacity Control System Applications and developments”, 9th EFRC-Conference 2014, Hofburg, Vienna
3 – A.Raggi, A.Costanzelli, Wang Yong “Energy Savings Through Electromechanical Stepless Capacity Control” - COMPRESSORtech2 OCTOBER 2017
4 – API Standard 618 “Reciprocating Compressors for Petroleum, Chemical and Gas Industry Services”

Root-Cause Analysis with Digital Twins – Discussion and Application

by:

A. van't Wel
PitPoint BV
Nieuwegein, The Netherlands
Arthur.vantWel@pitpoint.nl

C. Tümer, P. Egberts
TNO
Delft, The Netherlands
Can.Tumer@tno.nl, Paul.Egberts@tno.nl

11th EFRC CONFERENCE
September 13 – 14, 2018, Madrid

Abstract:
Several root-cause analyses (RCA) are executed every year that target fluid-structure interaction problems in production and process installations. Within the workflow of these projects, field surveys go hand in hand with computer simulations where, a simulation model is calibrated with measurement results on which the effect of possible improvements can be explored digitally.
The success of RCA is dependent on every step of the workflow, with several open to discussion, e.g. the optimal quantity and position of sensors (observability), the selection of to-be calibrated simulation model parameters and their respective uncertainties. Current approaches are in general focused to an individual step (observability, or model calibration) and fall short in providing a complete workflow. Furthermore, the available methods are mostly deterministic and lack insight into the uncertain aspects of these systems.
Over the years, TNO has developed a cost effective RCA approach, which diligently covers the process from top to bottom and from both deterministic and uncertainty quantification perspectives. In this paper, the theoretical foundations of this approach are explained on a case study. PitPoint B.V. operates several compact, high-speed CNG compressor installations which supply grid gas to a variety of transportation vehicles. Some installations required unplanned maintenance due to vibration problems, e.g. failures in the piping and the supporting layout.

by: A. van't Wel – PITPOINT; C. Tümer, P. Egberts – TNO

1 Introduction

In order to gain deeper insight in physical systems, using simulation models have become commonplace in various disciplines of engineering. Numerical modelling has already been established as the standard during the design phase of systems, such as bridges, process and production systems etc., and the application areas of these numerical models (digital twins) have been growing in many directions; root-cause analysis[1], system health monitoring[2], damage identification[3] and many others.

This paper aims to highlight challenges in employing digital twins within fluid-structure interaction applications, presents and demonstrates subsequent techniques to solve these challenges in a root-cause analysis case study for a natural gas compression station. The paper addresses the following three main points;

- **O1**: Despite their wide acceptance and frequent use, results of numerical models (digital twins) do not necessarily match measured data on many occasions. In case numerical models are expected to be a part of root-cause analysis or health monitoring workflows, they need to satisfactorily represent the reality.
  Systems tend to get more complex over time which leads to increasing uncertainty of numerical models. To reflect the real-life behaviour of complicated systems, digital twins need to be calibrated in light of measurement data.
  Conducting these calibration tasks manually is either too cumbersome or simply impossible without a significant loss of accuracy, especially since physical problems are usually combinatorial and all uncertain parameters need to be handled *at once*. In this respect, automatic calibration (*model updating*) methods are needed.
- **O2**: The quality of model calibration techniques depend largely on the quality of measurements. Model calibration cannot be accurate if behaviours of interest are not observed in the measurement data due to badly placed or insufficient sensors. Furthermore, as operational speeds of many production or process systems increase, these behaviours of interest get more complex, make it harder to maintain the high quality or completeness of measurements.
  Identifying measurement locations manually, in most situations, may lead to either incomplete measurements which do not capture behaviours of interest or a very large quantity of sensors that capture the system very well, at the expense of the project budget. With the help of *sensor location optimization* approaches, location identification can be done optimally; extracting maximum amount of information from the system with minimal number of sensors.
- **O3**: Most model updating and sensor location identification efforts are deterministic in nature and do not cover uncertainty in model parameters, measurements and the uncertain nature of engineering systems; *what happens when things change in real-life over time?* This has significant effect on the robustness of model updating and sensor location identification procedures and their omission may lead to inaccurate results in particularly if changes over time are considerable.

To the authors' best knowledge, the presented work is the first compilation of the above mentioned items **(O1** to **O3)** for fluid-structure interaction problems within the oil and gas industry and the inclusion of the uncertain nature, in the way described in Section 3.3, can be considered a novelty.

In the next section, a more detailed explanation is given to the listed problems. In Section 3, background information is presented on the currently available model updating and sensor location identification methods. These methods lay the theoretical basis for the adequate usage of digital twins. In Section 4, a relevant case study is presented, where the explained model updating techniques (in Section 3) and the results of a field survey are used to obtain a calibrated physical model of a failure-prone compressor system. The calibrated physical model is used to verify the root cause of the failures. Finally, in Section 5, the conclusions and recommendations are given.

2 Review of Technical Challenges

Approximating real life behaviour of systems and components, such as bridges and jet engines, with simulation models has been a focus of research for decades. Two major challenges have been identified in the process; updating simulation models to match measurement results and, subsequently, ensuring that the measurements (mainly the measurements locations) adequately capture behaviours of importance.

2.1 Model Updating

Real-life systems contain many details that are wrongly estimated or ignored to keep computational models as simple as possible. The exclusion or unrealistic implementation of these important details can adversely affect the accuracy of simulation results (**O1**). A few typical examples which result in modelling uncertainty in structural dynamics are mechanical damping, non-uniform material and element properties, properties of element joints and model constraints, e.g. welded, bolted, adhesive or friction based connections and boundaries[4].

In Figure 1, a simple example of modelling uncertainty is shown for a fixed cantilever pipe, clamped on both sides. In case (flexible) rubber is fit in between the pipe and clamp, the first natural frequency (f_n) of the structure may be significantly

by: A. van't Wel – PITPOINT; C. Tümer, P. Egberts – TNO

reduced (by factors of 2 to 5) as a function of rubber properties and thickness[5]. Such uncertain details present a challenge to simulation models and, usually, require validation. There are several investigations in the literature, for instance, on the effect of welded joints, and bolt torques at model boundaries[6] and the effect of non-uniform cross-sectional properties[7].

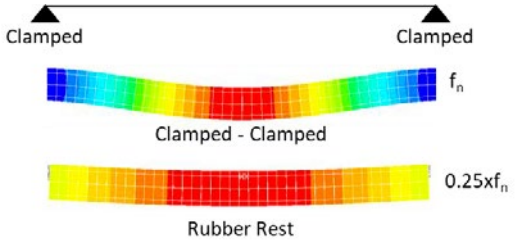

Figure 1: Effect of boundary stiffness on the first natural frequency of a cantilever beam. Red colors denote locations with larger movement (kinetic energy).

In order to account for the aforementioned complex or ambiguous details (viz. flexible model parameters), simulation models usually have to be *updated* with the help of either validation measurements or more accurate simulation models and with preference on the former.

Historically, there have been two main approaches in model updating; representational or insight-based. The former aims at *directly* arranging the physical model, e.g. mass and stiffness matrices in structural mechanics, such that they accurately match the measurements. However, any underlying physical modelling basis may be lost with this approach as the tuning is done on the "matrix level". Despite a good match between updated simulation model and measurements, any change to the mechanical layout or the effect of alternate loading conditions on the structure cannot be investigated with this approach.

The *insight-based* approach requires considerable physical interpretation skills. This approach is built on the identification of a set of *flexible* simulation model parameters, which can be tuned to match measurements. Compared to the previous approach, the emphasis is put on correcting the physically meaningful, although uncertain, modelling parameters. Hence, the aim is not only to mimic measurement results but to obtain accurate representations of the system of interest such that the updated model can also be used in the prediction of possible future layout improvements or in the identification of possible future problems. Insight-based approach is considered the most suitable for root-cause analysis purposes since the updated simulation model is aimed to be used for the evaluation of solution options.

Lastly, most of the reviewed work focuses on model updating with respect to (free) modal analysis results (natural frequencies and mode shapes) and not mechanical response to force excitation (e.g. frequency response functions). The primary advantage of modal analysis based model updating is the exclusion of damping modelling. However, it should be noted that damping plays an important role in the response of systems and its omission complicates the accuracy of the main root-cause analysis deliverable; pressure or vibration/stress responses of the system. Furthermore, systems with high modal densities impose considerable difficulty during mode identification and usually preclude the usage of modal analysis based model updating methods[8,9].

2.2 Sensor Location Optimization

As expected, the richness (*completeness*) of information contained in measurements determines the extent to which a numerical model can be improved by updating. In this context, completeness can be defined as the ability of the measurement setup to produce data that are relevant for describing the dynamic behaviour (*observability*) and for updating of physical model parameters.

The best illustration of observability can be given in the lack thereof. An extreme case of incompleteness occurs when sensors (or inputs) are present at vibration nodes but not at antinodes (**O2**). In Figure 2, the first three mode shapes of a fixed cantilever pipe can be seen. If the goal of the measurement is to capture the first two modes, it is evident that a single sensor at the middle of the pipe is not enough, as the second mode will not be observed by this sensor.

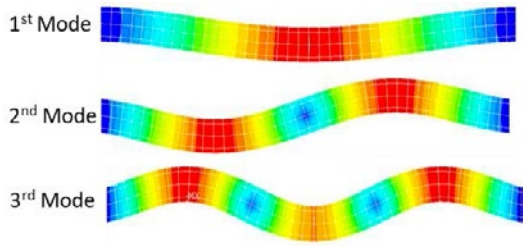

Figure 2: The first three mode shapes of a fixed-fixed beam.

It should also be noted that this reasoning, i.e. sensor placement at each vibration antinode, may lead to a significant amount of sensors (one for each wavenumber) in cases where many mode shapes need to be observed. Therefore, *sensor location optimization* must aim to optimally (within error margins) capture the dynamic behaviour of importance with minimal amount of sensors.

3 Used Methodology

3.1 Sensor Location Optimization Approach

There are numerous techniques in the literature that aim to find the optimum amount and location of sensors for a given problem.

The most commonly used scheme is the modal kinetic energy method[10]. The method is essentially built on the reasoning given in Section 2.2. In this

by: A. van't Wel – PITPOINT; C. Tümer, P. Egberts – TNO

method, the kinetic energy of a system is divided between modes and, to satisfactorily measure any mode, the kinetic energy at the sensor location must be a significant proportion of the total for a given range of modes. Even though the approach is intuitive and easy to use, the method does not offer a set of measurement locations by itself. However, the method gives an estimate on the validity of chosen locations, during the use of trial and error procedures.

Out of many reviewed methods, the Effective Independence Distribution Vector (EIDV)[11,12] method was found to be the most effective and practical. The mathematical basis of the method lies in the eigen vector solution itself. The finite element formulation of a continuous structure can be given as;

$$M\ddot{x} + C\dot{x} + Kx = f(t) \qquad (1)$$

where f represents forcing and M, C, and K are the mass, damping and stiffness matrices respectively. Assuming a solution as $x(t) = x(w) * e^{iwt}$, neglecting the damping, forcing and solving for the eigenvalues leads to the eigenproblem;

$$K\Phi_j = \lambda_j M\Phi_j \ , \qquad j = 1, \dots, n \qquad (2)$$

with Φ_j as the eigenvectors (of $M^{-1}K$) and λ_j as the corresponding eigenvalues ($w_j{}^2$). A modal matrix can be constructed with eigenvectors in the columns (n) and potential sensor locations (r) in the rows, giving an rxn matrix;

$$\Phi_{rxn} = \begin{pmatrix} \Phi_1(p_1) & \cdots & \Phi_n(p_1) \\ \vdots & \ddots & \vdots \\ \Phi_1(p_r) & \cdots & \Phi_n(p_r) \end{pmatrix}, \qquad (3)$$

where p_j denote the j[th] sensor location. The method is customizable as well; one has the ability to dictate where sensor placement is not desired (by removing corresponding rows) or to specify which modes need not be observed (by removing corresponding columns). These mentioned changes result in a reduced version of the model matrix, Φ_S. From here on, the Fisher information matrix, F_S, can be constructed as;

$$F_S = \Phi_S{}^T \Phi_S, \qquad (4)$$

where T stands for the transpose operation. In short, the larger the determinant of the Fisher information matrix (F_S), the more information the matrix contains. Thus, one should aim to minimize the number of sensor locations while maintaining a high value of the determinant; the best locations are those that result in most linearly independent modes and sensors are placed such that multiple modes are *observed* at the same time.

3.2 Parameter Estimation Approach

Several parameter estimation methods have been proposed in the literature for model updating purposes. They range from gradient based approaches, to genetic and machine learning algorithms[13].

Considering its simplicity and flexibility of usage, a gradient based Gauss-Newton optimizer, is selected as the optimization algorithm. The chosen optimizer iterates on the values of flexible parameters (e.g. the rubber stiffness of Section 2.1) such that an objective function is minimized. The objective function represents the difference (*distance*) between simulation and measurement results. Thus, the smaller objective function, the better the estimation of the model parameters. The used objective functions in this study are of Euclidean norms (straight distances between two points).

3.3 Deterministic vs. Probabilistic Approaches

The sensor location and model updating techniques, presented so far, are of deterministic nature. For instance, the optimal sensor locations are only ideal for a given set of model parameters. The robustness of the optimal sensor locations is dependent on the uncertainty of model parameters how much variation is expected in model parameters over time. For example, a support may get loose over time, resulting in different mechanical modes and, thus, degrading sensor location performance. The sensor location identification approach described in Section 3.1 is fast and allows for assessing robust sensor locations (**O3**), using e.g. a Monte-Carlo[15] technique to sample from assumed probability distributions of uncertain model parameters.

Moreover, deterministic model updating approaches result in a single set of optimal model parameters. The robustness of this single realization is also questionable as many problems are ill-posed and multiple sets of parameter values (multiple realizations) may converge to the measurement result. Thus, the obtained set of model parameters run the risk of being *nonunique*.

To deal with limitations in deterministic approaches, a Bayesian model updating technique[14] can be adopted that allows for a probabilistic description of measurements and prior knowledge of the flexible model parameters. Using Bayes method, a posterior parameter distribution can be derived. Then, the posterior distribution of model parameters can be sampled, e.g. with the randomized maximum likelihood method[16], and multiple realizations model parameters can be obtained, leading to increased robustness of results (**O3**).

To the authors' knowledge, using probabilistic sampling combined with deterministic optimization at each sample presents a novelty for model updating and sensor location identification approaches within fluid structure interaction problems.

4 Case Study

4.1 System and Problem Description

Severe vibrations, accompanied by frequent fatigue failures, were observed at a number of CNG compressor stations in the Netherlands. These stations

by: A. van't Wel – PITPOINT; C. Tümer, P. Egberts – TNO

all have the same type and brand of compressor package. The evaluated compression system is composed of two 4-stage, 2 cylinder compressors which supply pressurized gas to transportation vehicles. The cylinders each have 2 different stages at their head and crank ends, separately. The compressors have a fixed speed of 1060 RPM and are usually operated with one functioning and one standby (2x100%). The system operates with variable suction (1.2 bara to 6 bara) and discharge pressure (147 bara to 247 bara) ranges.

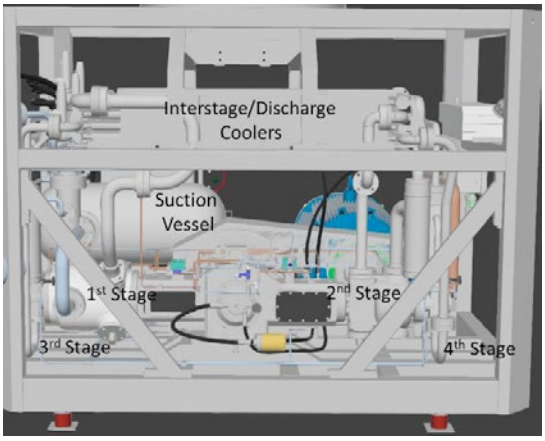

Figure 3: The overall layout of the compressor skid.

The 3D model of the system is visible in Figure 3. The system is designed to be relatively compact with all necessary equipment present within the skid itself.

Severe vibrations were observed in the piping near the compressor cylinder connections and, accordingly, the cylinder connections (at the weld locations) had damages, as seen in Figure 4. These failures lead to unplanned maintenance on the system and, thus, impose a burden on the operator.

Figure 4: The weld history at the 4th stage suction cylinder connection.

A field survey was conducted in order to get as much insight as possible to the problem, from both acoustic and mechanical perspectives. The observations and measurement results of the field survey are, then, used to improve the simulation model (*digital twin*) of the system, that forms the basis of reference of any possible to-be investigated improvement step. The following sections present the measurements, the calibration of the simulation model and the verification of the root cause of the failures. The given acoustic and mechanical recommendations, aimed to solve the experienced failures, are not within the scope of this paper.

4.2 Observations from the System

During the field survey, an inspection took place to identify locations that may result in modelling uncertainty at the simulation model and the identified locations are used as flexible model parameters in the subsequent work.

From Figure 5 to Figure 8, several of these spots can be seen. Firstly, the skid frame rests on several springs, as seen in Figure 5, that are designed to limit the mechanical transfer between the compressor and the foundation of the compressor building. Although the mechanical transfer to the environment is indeed limited, the springs create a very flexible boundary for the system.

Figure 5: A sample spring, at the bottom of the skid frame.

Both cylinders were found to be unsupported, as seen in Figure 6. Considering the large span between the crosshead guide and the cylinder outer head, the lack of cylinder supporting was expected (and later measured) to have an adverse effect on the mechanical response of the system. Therefore, the cylinders were also included in the measurement campaign and were later modelled with the available 3D model of the system to realistically include the stiffness and mass of the compressor.

Figure 6: The first and third stage cylinder.

by: A. van't Wel – PITPOINT; C. Tümer, P. Egberts – TNO

Additionally, the separators were mostly found to be overhanging. Some have connections to the top of the skid frame, as seen in Figure 7 and Figure 8. The construction with U-bolts and the flexible rubber imposes a significant amount of uncertainty, in terms of provided stiffness, to the mechanical model and were picked as flexible parameters for the model.

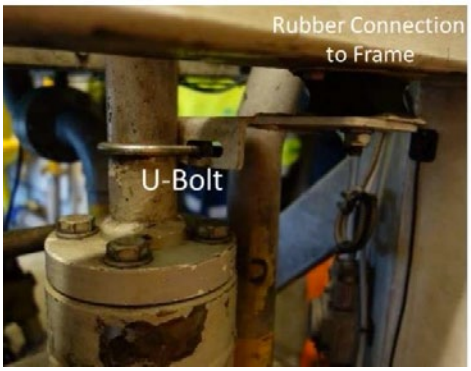

Figure 7: The supporting at the top of the 3rd stage separator, side view.

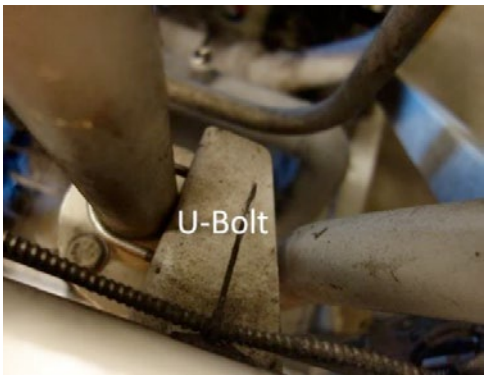

Figure 8: The supporting at the top of the 3rd stage separator, top view.

Furthermore, some separators are connected to the cylinder connection flanges by small plates, shown in Figure 9. These connections were reported to be damaged several times during the operation of the system, implying a high strain/stress problem near the cylinder connections.

Figure 9: The 2nd stage scrubber bottom connection to 2nd stage suction cylinder connection.

4.3 Measurements

The overall mechanical response of the system depends on the dynamic forcing as well as the mechanical properties of the system. The considered forcing in the analysis comes from the dynamic pressure field in the piping due to the pulsations generated by the compressors and the gas stretch forces in the cylinders. Accordingly, the conducted field survey contains both pressure pulsation and vibration measurements.

Pulsation measurements could only be done at 3rd and 4th stage cylinder outlets since the piping does not have any other connection available. However, due to the simplicity of the piping, a high wavenumber (high order mode shape) is not expected in the piping system (see Section 2.2 and Figure 2). Hence, it is possible to capture the acoustic response of this system with a limited number of sensors. Furthermore, the proximity of the pulsation measurement locations to the cylinders enable a close characterization of the pulsation source, i.e. compressor.

As opposed to the pulsation measurements, vibration measurements were done on a variety of locations, as seen in Figure 10. In summary, vibrations were measured at cylinder heads (V1 and V2) , tops of separators (V4, V5, V6) and the frame (V7, V8, V9). These locations were chosen based on a preliminary analysis of expected modes (see EIDV in Section 2.2) relevant to the motion around the cylinder connections (targeting the weld failures) and the motion of the frame.

A separate measurement was also conducted to quantify the mechanical transfer between the frame bottom and the foundation. This measurement helped to quantify the dynamic stiffness properties of the mechanical springs, shown in Figure 5.

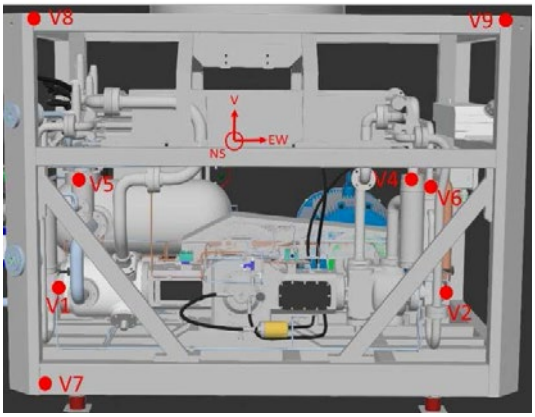

Figure 10: The fixed vibration measurement points.

The measured pressure pulsation levels can be found in Figure 13 and vibration velocities are presented in Figure 14 and Figure 15.

It should be noted that the measured pulsation levels were above the limits specified by API 618. The measured exceeding in pulsation levels, especially at

by: A. van't Wel – PITPOINT; C. Tümer, P. Egberts – TNO

these relatively high frequencies, is considered to be harmful.

Although not directly applicable for spring mounted compressors, EFRC Vibration Guidelines[18] were used as allowable levels for screening measured vibration levels. The measured vibration levels were found to be significantly exceeding the C/D zones of EFRC Vibration Guidelines. Furthermore, the relative motion between the 3rd stage separator (V5) and the 1st/3rd stage cylinder head (V1), shown in Figure 14, is considered to be excessive and could be seen as a direct root-cause of the fatigue failures at the suction cylinder connection – this is verified in the desktop analysis. Similar mechanical behaviour was also observed at other separators, see Figure 15.

4.4 Initial Modelling

The acoustic/mechanic modelling of the system was done based on the input received from the compressor vendor, the compressor valve vendor, and the operator.

The acoustic modelling was done with TNO software Pulsim. Pulsim is a method of characteristics solver for wave propagation problems in time domain. Pulsations are generated by the compressor, in this case, and are propagated within the system. In case pressure pulsations encounter reflecting boundaries, the system might experience acoustic resonances, so-called standing waves. The damping of these acoustic resonances, due to friction, is also captured with the solver due to its time marching nature. One of the largest uncertainties in acoustic modelling is the speed of sound of the medium. A sensitivity analysis is done by evaluating within a range of speeds of sound around a nominal value. This sensitivity is used in the model updating process later on while comparing measured and simulated spectral contents.

Subsequently, a mechanical model was created in ANSYS. The piping and the supporting layout were modelled with beam elements. The compressor, including the motor[17], was modelled with 3D elements and, then, *reduced* to a linear combination of mass and stiffness matrices, valid in the frequency range of interest (0-100 Hz). This reduced order modelling (ROM) approach allows fast and accurate calculations.

The uncertain items, listed in Section 4.2, namely the ground springs, the rubber based or U-bolt type connections are modelled as fixed in the initial model but are used as flexible parameters for model updating purposes later on. The considered excitation mechanisms are pulsation induced shaking forces in the piping and the gas stretch forces in the cylinders, that are computed in the acoustic analysis. Inertia forces are not included in the analysis.

The received CAD file and the final Pulsim model can be seen in Figure 11and Figure 12.

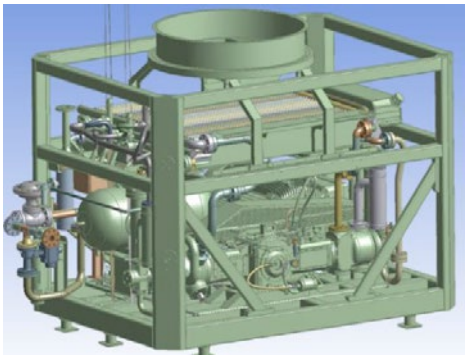

Figure 11: CAD model of the compressor skid.

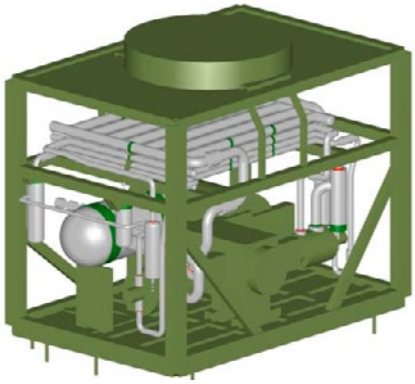

Figure 12: Pulsim model of the system. Mechanical beams, that represent the compressor, are for illustration purposes only.

4.5 Model Updating and Results

With the aim of getting the forcing right for the mechanical model updating, the initial model updating effort was conducted on the acoustic model.

The simulation results need to mimic the measured results both in terms of the relative contribution of frequencies to response (spectral content) and the absolute amplitudes at each frequency. From an acoustic standpoint, the spectral content is largely dependent on the acoustic resonance conditions and, accordingly, the speed of sound in a system. Firstly, an optimal speed of sound value was determined that gave the most spectrally coherent simulation results with respect to the measurements. The optimal speed of sound value was found to be -6% of the nominal. Afterwards, further optimization is done on the absolute amplitudes by slightly changing the acoustic damping within the system. The optimized simulation results show an overestimation of a maximum of 10-15% for the lower frequencies and larger for the higher frequencies, compared to measurements. The simulation results are displayed in Figure 13.

by: A. van't Wel – PITPOINT; C. Tümer, P. Egberts – TNO

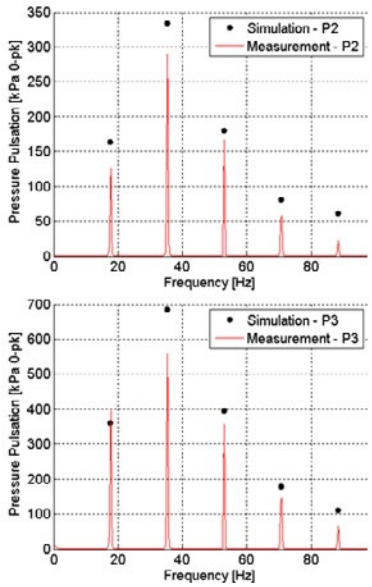

Figure 13: Measured vs. simulated pulsations at 3rd (top) and 4th stage (bottom) compressor outlets.

The next step in the analysis was to update the identified uncertainties within the mechanical model with the help of a Gauss-Newton optimizer. The items listed in Section 4.2 (modelled as springs, with 6 degrees of freedom each), and the flexibility factors of the (numerous) flanges within the pipe system were used as flexible parameters.

In total, the optimizer ran for over 20 different degrees of freedom at once, and optimal parameter estimations could be obtained in only a few hours; a feat not achievable manually **(O1)**. The simulation results with the updated model can be seen in Figure 14 and in Figure 15.

Looking at Figure 14 and Figure 15, one can conclude that the measured spectral content of the system was adequately captured by the updated simulation model. However, it should be noted that the updated model usually overestimates the mechanical response, with a maximum error of around 15% compared to the measurements. Further optimization could still be made over the used critical damping ratio (of 2%).

The calculated stress levels, resulting from the calculated vibrations (Figure 14 and Figure 15) range between 45 to 70 MPa at the cylinder connections and reach around 20 MPa in the main piping. The high stresses in the cylinder connections are caused by high local cyclic shear - large relative motion (vibrations) between separators and cylinder heads. The calculated values, especially at the cylinder connections, exceed allowable levels with respect to API 618 and, therefore, are concluded to be the root-cause of the fatigue failures (displayed in Figure 4).

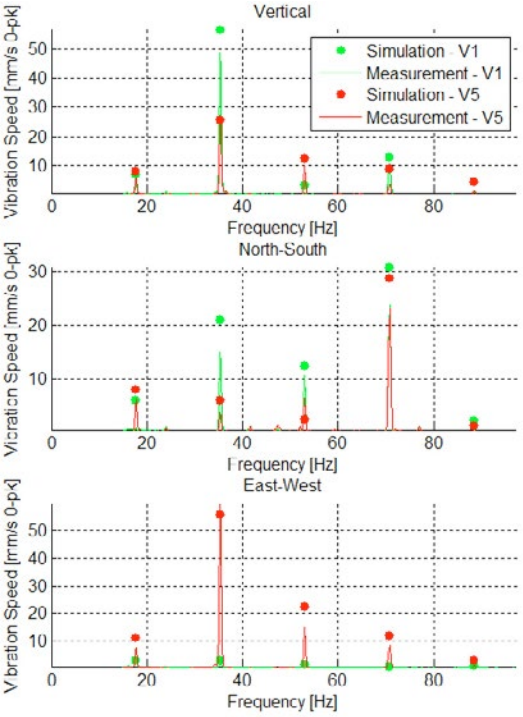

Figure 14: Measured vs. simulated vibrations at 1st/3rd stage cylinder (V1), 3rd stage separator (V5).

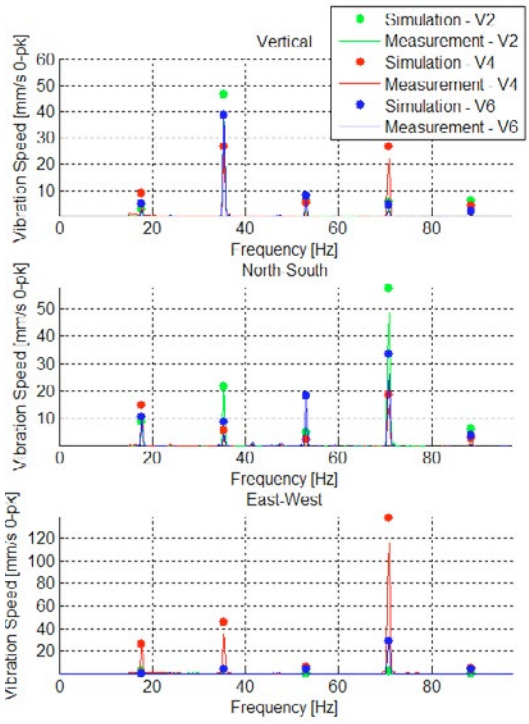

Figure 15: Measured vs. simulated vibrations at 2nd/4th stage cylinder (V2), 2nd (V4) and 4th (V6) separators.

During the analysis, it was found that the mechanical behaviour near the cylinder connection was to a larger extent influenced by stiffnesses of the rubber connections, seen in Figure 7, and to a lesser extent by the flange flexibilities in the high elevation piping. The obtained optimal translation stiffness values for the rubber connections are in the order of 1e5 kN/mm

by: A. van't Wel – PITPOINT; C. Tümer, P. Egberts – TNO

and the flexibility factors of flanges were found to be in the order of 0.2.

In Figure 16, the distance between the initial and updated mechanical simulation results can be found for the vibrations at the 3rd stage separator (V5). From a spectral perspective, it is clear that the initial model does not match the measured behaviour of the system. The measurement results indicate that the vibration levels are dominated by lower orders of the compressor speed than what is predicted by the initial model. The primary reason is that the higher frequency mechanical modes, from the standpoint of the initial model, are excited at much lower frequencies due to the flexibilities of the supporting layout, during the measurements. It can also be seen that, vibration amplitudes are underestimated by factors of 3 to 4 at the dominant frequencies. Thus, it can be concluded that standard, simplistic, mechanical modelling assumptions may lead to severe inaccuracies.

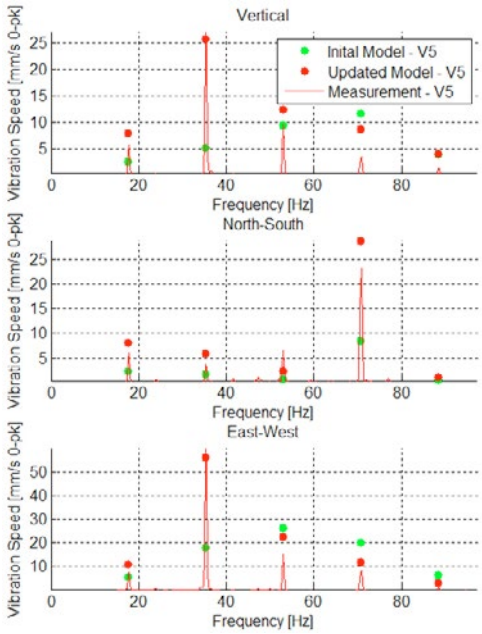

Figure 16: Initial model results vs the updated model results for the 3rd stage separator (V5).

Lastly, the good agreement between updated simulations and measurements imply that the measurements were complete and that the sensor locations were close to optimal for the considered frequency range and behaviours of interest. Furthermore, considering the large difference between the initial model (where the sensor locations were derived from) and the updated model (with large uncertainties accounted for), the chosen locations can also be considered robust (**O3**).

Although, the used set of sensors adequately observe the motion at the cylinder connections, they would be *blind* (**O2**) to the motion at high elevation piping, depicted in Figure 17, in case that motion also needed to be covered.

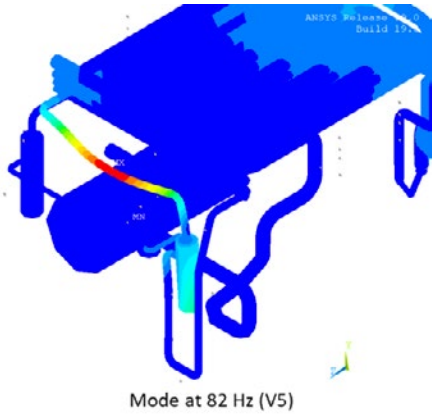

Figure 17: A high frequency mode near V5, around 4th harmonic of the compressor, that may not be captured adequately due to insufficient sensors.

5 Conclusions and Future Possibilities

A brief summary of conclusions is as follows;

- Automatic model calibration and sensor location identification methods were explained and used successfully in a root-cause analysis case study for a compact CNG system. The results of the calibrated model were used to confirm the root cause of the fatigue failures in the system and to shed light to improvement options. The latter was not in the scope of this paper.
- An inspection of the CNG system revealed irregularities within the piping system and the relevant mechanical properties of these irregularities were used as flexible parameters during the model updating process. The used Gauss-Newton optimizer handled over 20 flexible parameters at once and delivered an updated simulation model in a few hours. This process would have taken at least a few days, if done manually (**O1**). However, it should be noted that the issue of which parameters to choose for the updating process still remains subjective and case-based. The success of the model updating largely depends on the engineering judgment of the involved parties.
- Even though irregularities (with large uncertainties) were identified within the system, the chosen sensor locations were found complete and robust enough for model updating purposes (**O2**), considering the good agreement between measurement and updated model results.
  The Bayesian approach, given in Section 3.3, is a suitable way of including large uncertainties of model parameters in sensor location identification problems (**O3**).
- The desktop analysis, presented with this work, was done off-line. An alternative to this off-line approach is real-time condition monitoring.
  With an adequate initial model, continuous model updating and connection to a monitoring system can be sufficiently fast to track any harmful changes in operation and warn the

by: A. van't Wel – PITPOINT; C. Tümer, P. Egberts – TNO

operators in advance. This workflow could lead the way to defining predictive maintenance solutions or pre-emptive shutdown strategies.

6 Acknowledgements

The authors would like to acknowledge PitPoint B.V. for supporting this paper and giving the opportunity to present the results. This research was partially supported by TNO research funding. We would like to thank Ted Sertons from PitPoint B.V., Pieter van Beek and Andre Eijk from TNO for their valuable involvement in various aspects of this work.

References

1 Eijk, A., de Lange, D., Maljaars, J. (2014) : *Root Cause Analysis of the Fatigue Failures of the Pulsation Dampers of a large Underground Gas Storage (UGS) System*. Proceedings of 9th Conference of the EFRC, Vienna Austria.

2 Yi, T.-H., Li, H.-N., & Zhang, X.-D. (2015) : *Health monitoring sensor placement optimization for Canton Tower using immune monkey algorithm*. Structural Control and Health Monitoring. https://doi.org/10.1002/stc.1664

3 Teughels, A., & De Roeck, G. (2004): *Structural damage identification of the highway bridge Z24 by FE model updating*. Journal of Sound and Vibration. https://doi.org/10.1016/j.jsv.2003.10.041

4 Friswell, M. I., & Mottershead, J. E. (1995): *Finite element model updating in structural dynamics*. https://doi.org/10.1007/978-94-015-8508-8

5 N. Morman, Kenneth & Y. Pan, Tsung. (1988): *Application of Finite-Element Analysis in the Design of Automotive Elastomeric Components*. Rubber Chemistry and Technology. 61. 503-533. 10.5254/1.3536198.

6 Mottershead, J. E., Friswell, M. I., Ng, G. H. T., & Brandon, J. A. (1996): *Geometric Parameters For Finite Element Model Updating Of Joints And Constraints*. Mechanical Systems and Signal Processing. https://doi.org/10.1006/mssp.1996.0012

7 Moller, P. W., & Friberg, O. (1998): *Updating Large Finite Element Models in Structural Dynamics*. AIAA Journal. https://doi.org/10.2514/2.279

8 Allemang, R. J. (2003): The modal assurance criterion - Twenty years of use and abuse. Sound and Vibration. https://doi.org/10.1016/j.chemgeo.2006.02.014

9 Imregun, M., Visser, W. J., & Ewins, D. J. (1995): *Finite element model updating using frequency response function data - I. Theory And Initial Investigation*. Mechanical Systems and Signal Processing. https://doi.org/10.1006/mssp.1995.0015

10 Papadopoulos, M., & Garcia, E. (1998): *Sensor Placement Methodologies for Dynamic Testing*. AIAA Journal. https://doi.org/10.2514/2.7509

11 Kammer, D. C. (1991): *Sensor placement for on-orbit modal identification and correlation of large space structures. Journal of Guidance*, Control, and Dynamics. https://doi.org/10.2514/3.20635

12 Udwadia, F. E. (1994): *Methodology for Optimum Sensor Locations for Parameter Identification in Dynamic Systems. Journal of Engineering Mechanics*. https://doi.org/10.1061/(ASCE)0733-9399(1994)120:2(368)

13 Marwala, T. (2010): *Finite Element Model Updating Using Computional Intelligence Techniques*. Springer. https://doi.org/10.1007/978-1-84996-323-7

14 Beck, J. L., & Katafygiotis, L. S. (1998): *Updating Models and Their Uncertainties. I: Bayesian Statistical Framework. Journal of Engineering Mechanics*. https://doi.org/10.1061/(ASCE)0733-9399(1998)124:4(455)

15 Castro-Triguero, R., Murugan, S., Gallego, R., & Friswell, M. I. (2013): *Robustness of optimal sensor placement under parametric uncertainty*. Mechanical Systems and Signal Processing, https://doi.org/10.1016/j.ymssp.2013.06.022

16 Oliver, D. S. (2017): *Metropolized Randomized Maximum Likelihood for Improved Sampling from Multimodal Distributions*. SIAM/ASA Journal on Uncertainty Quantification, https://doi.org/10.1137/15M1033320

17 Kacani, V. (2017): *Vibration analysis in reciprocating compressors*. IOP Conference Series: Materials Science and Engineering, *https://doi.org/10.1088/1757-899X/232/1/012016*

18 European Forum Reciprocating Compressors (EFRC) (2017): *Guidelines for Vibrations in Reciprocating Compressor Systems*.

STASSKOL

SEALING EXPERTS SINCE 1920

STASSFURT GERMANY | HOUSTON USA

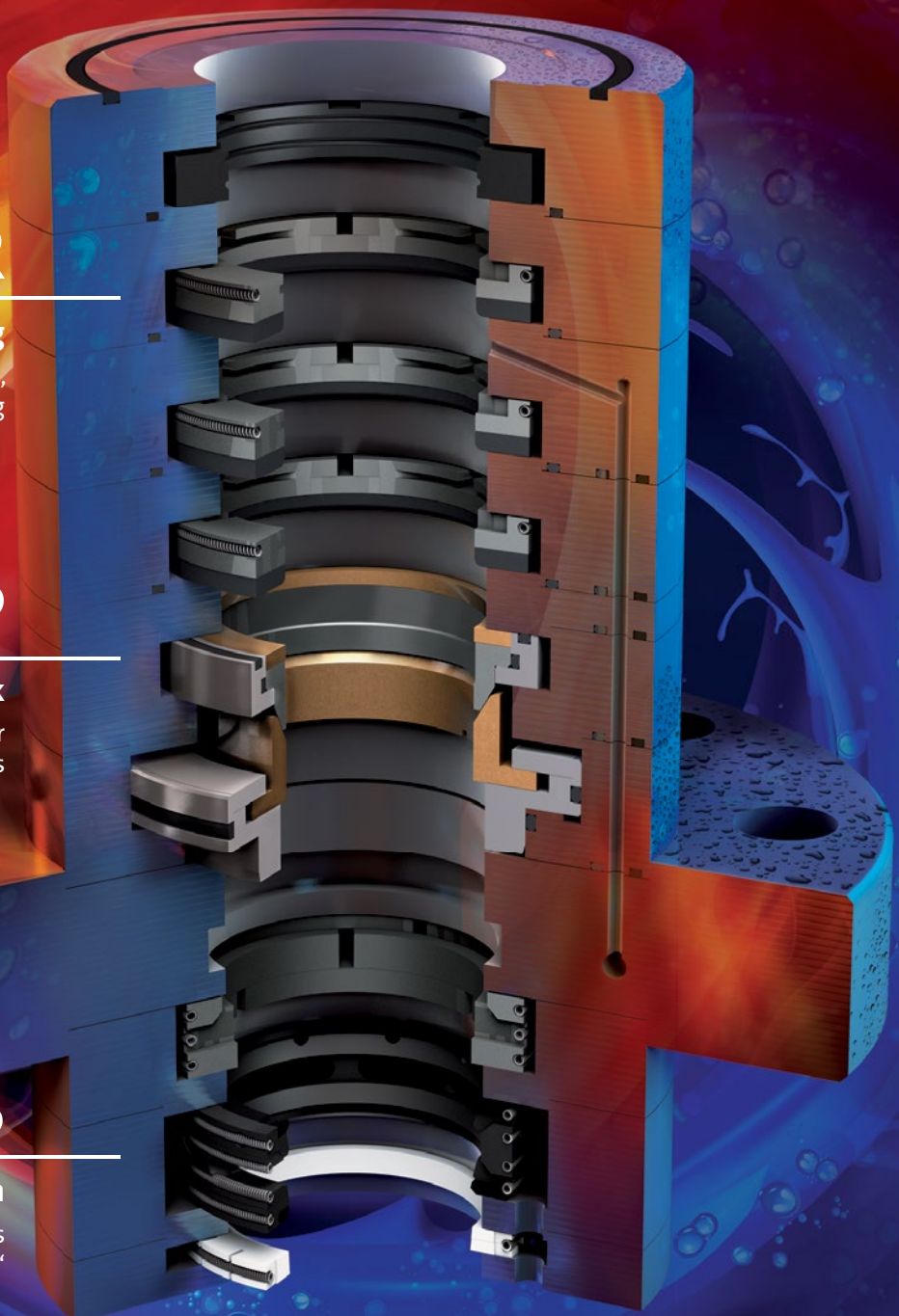

SSR

Patented Single Sealing Ring

Lower friction, longer service life time, reduced length of packing

SSP

Static Pack

Minimal leakage when compressor is not in process

BOSS

Balanced Oil Sealing Solution

High oil sealing efficiency with inherent gas tightness, “back pumping effect“

www.stasskol.de

EUROPEAN FORUM
for RECIPROCATING
COMPRESSORS

ENGINEERING OF COMPRESSOR PLANTS

Modularized Reciprocating Compressor Systems and the Factors That Influence Their Design

by:

Benjamin F. Williams
Process Sales and Market Development Specialist
Ariel Corporation
Mount Vernon, Ohio, USA
bwilliams@aa

11th EFRC CONFERENCE
September 13 – 14, 2018, Madrid

Abstract:
Although popular in the U.S. natural gas market for over 60 years, the modularization, or packaging, of reciprocating compressors is relatively new in other industries and elsewhere in the world. Unlike the traditional block mounted compressor system which generally requires a significant amount of field fabrication and assembly; a modularized compressor system results in an almost "plug and play" scenario. This offers significant benefits in both overall project cost and installation / commissioning time.

Identifying the application and selecting the appropriate compressor is just the beginning. The design of the compressor package is determined by a number of factors, including customer specifications, industry standards, the compressor manufacturer requirements, third party engineering studies and the installation location.

This paper will briefly describe the history of the compressor package, what makes up a compressor package, some of the factors that influence the design and will point out some of the things the Purchaser should look for when purchasing a compressor package. It will also briefly discuss the advantages and disadvantages of modularization.

by: Benjamin F. Williams – Ariel Corporation

1 Introduction

Reciprocating compressors have been around for a long time. They are in a wide variety of locations including onshore, offshore, in the jungle, in the desert, in the city, in the country, in gas plants, in refineries and chemical plants, etc. In other words, reciprocating compressors are located wherever gas compression is needed.

Initially, reciprocating compressors were block-mounted. In a block-mounted installation, the compressor and its associated components and auxiliary systems are shipped to site and assembled on a concrete block. This type of installation is still used today, primarily in refineries and chemical plants or in cases where very large compressors are utilized.

Another type of reciprocating compressor installation is a modularized compressor system. A modular compressor system, commonly referred to as a compressor package, includes all the items required for a complete compressor system, including the compressor, driver, pulsation dampeners, process gas coolers, moisture separation, auxiliary systems and the associated instruments and controls; all installed on a structural steel skid. This skid mounted compressor system is transported to site and minimal assembly is required; thereby reducing the installation cost and time to commission the unit.

The use of modular (packaged) compressor systems is becoming more popular in all phases of the oil and gas industry; including gas gathering application, on-shore and offshore facilities and increasingly, in refineries and petrochemical plants. These highly engineered systems have proven successful, regardless of the application, installation location, gas composition, and operating conditions.

This document will provide the history of the modularized (packaged) compressors and will describe the factors that go into their design. Please note that it is impractical to cover all aspects of package design in a single document but the intent is to highlight some of the factors that go into the design and to provide some guidance in what to consider when purchasing or specifying a compressor package.

Note, compressor module and compressor package have been used interchangeably in this document. The term “package” is used as either a noun (the compressor package) or a verb (to package a compressor means to assemble the complete compressor system on one or more structural steel skids).

2 History

The use of packaged compressor systems began with the development of the natural gas pipeline and transmission system in the U.S. at the end of World War II. Remote natural gas fields made it impractical to use large integral engine compressors for on-site installations.

Smaller, single throw, belt driven compressors, such as the Worthington HBGG and the Ingersoll Rand ES line were easier to install at remote locations. The success of these smaller compressors led to the large integral engine compressor manufacturers developing smaller versions of their large integrals, which could be skid mounted along with their piping, process gas and oil coolers and local control panels. These were the first compressor packages.

In the period from the late 1950’s through the 1960’s, short stroke, balanced-opposed, high speed compressors were developed by a number of companies, including Ingersoll Rand, Worthington, Cooper Bessemer and Ariel. These compressors were direct driven by existing industrial engines. Because of their smaller size, these compressor systems were very suitable for modularization. The module included the compressor, engine, piping, gas coolers, controls and auxiliary systems, installed on structural steel skids and then transported to and from locations with minimal disassembly. The packaged compressor concept became very popular and ultimately led to the decline of the integral engine compressor in the early 1990’s.

For over a century, the refinery, petrochemical and industrial gas industries have used long stroke, slow speed compressors almost exclusively. Due to their size and the size of their electric motor drivers, they are normally block mounted. Today, short stroke moderate speed compressors are becoming more popular. Because they are very suitable for packaging, they offer significant cost savings vs. the long stroke, slow speed block mounted units. According to multiple End Users, packaged moderate speed, short stroke compressors were typically 50-60% of the installed cost of the block-mounted, long stroke, slow speed compressors.

Although modularization began with smaller compressors for remote locations, today reciprocating compressors rated at 5 MW or more are routinely packaged and shipped. In addition to remote natural gas fields, compressor packages are now located anywhere in the world that gas compression is required.

Figure 1 shows multiple 6 MW compressor packages used in natural gas transmission service.

by: Benjamin F. Williams – Ariel Corporation

Figure 1: Multiple 6 MW compressor packages used in natural gas transmission service.

3 Package Scope of Supply

The primary factor in the design of the compressor package is the scope of supply. In simple terms, this comes down to the following questions:

- What is the gas?
- How much do you need to compress?
- What are the operating conditions?
- What type of driver do you want?
- What is the required run-time between shutdowns?
- What other specifications apply?
- Where is the compressor to be installed?
- Who is supplying what?

Customer specifications and datasheets will answer these questions. For this paper, we will assume the compressor Packager will supply all of the package related items.

3.1 Compressor Selection

It all starts with the compressor selection. The Request for Quotation (RFQ) will include customer specifications and requirements. It will also refer to any applicable industry standards, such as API 618, API 11P ISO 13631 or ISO 13707. These specifications may include supplements to these standards, specific to the project.

Upon review of the RFQ, the compressor manufacturer (or their respective distributor) will use proprietary software to make a compressor selection. Besides the operating conditions, other items considered when making the compressor selection are the type of driver; whether the compressor is lubricated or non-lubricated, capacity control requirements and the expected runtime between shutdowns.

3.1.1 Operating Conditions and Gas Composition

The gas composition, operating conditions and required capacity will determine the size of the compressor. The compressor must be large enough to deliver the required flow at the given pressures without exceeding limits imposed by the manufacturer, customer or industry specifications. These limits include discharge temperature, cylinder MAWP (maximum allowable working pressure) and rod load. Although rarely, if ever, used in the upstream oil and gas market, it is also common in the downstream compressor market to limit the compressor rotating speed and the average piston speed.

The gas composition is important because it effects the properties of the gas, such as the isentropic compression exponent (k-value) and the gas specific gravity. Combined with the operating conditions, these will determine how many stages are required and how much power is required. A gas with a higher k-value (or "n") will typically require more stages for a given set of operating conditions than a gas with a lower value, because of discharge temperature limits. In the case of hydrogen, which has a k-value of about 1.4, API 618 and ISO 13707 limit discharge temperatures in hydrogen rich service to 135°C (275°F). Unless specified, discharge temperature limits for other gases depend on the non-metallic wear part materials. It is quite common in the upstream oil and natural gas market to have discharge temperatures between 150 and 175°C (300 and 350 °F).

Gas composition will also determine the materials of construction, for both the compressor and the package. As an example, gases with hydrogen sulphide (H_2S) will require stainless steel. It is common for these sour gas applications to have stainless steel piston rods, valves and possible stainless process gas piping and vessels. This may also be the case with wet carbon dioxide (CO_2) applications, such as those in a fertilizer plant.

The specific gravity or molecular weight of the gas, combined with the cylinder displacement and speed of the compressor effects the differential pressure across the valves; therefore the rod load and power required. For a given cylinder displacement, a heavier gas will have a higher differential pressure across the compressor valves than a lighter gas, resulting in increased power losses across the valves. Similarly, for a given cylinder displacement, a higher speed compressor will result in higher valve power loss for the same gas.

Whether the gas is wet or dry determines the size requirements for inlet and interstage separators. Heavy hydrocarbon gases typically require significant separation vessels and their associated controls.

Low-pressure applications will require large cylinders, large diameter piping, valves and large diameter vessels.

3.1.2 Capacity Control

Capacity control of a reciprocating compressor can be accomplished a number of ways. These include

by: Benjamin F. Williams – Ariel Corporation

speed control, suction valve unloaders, adding clearance to a cylinder (spacers, clearance rings or clearance pockets) or by recirculation (bypass). These may require additional components or controls that affect the package design.

Clearance pockets and suction valve unloaders are normally manual, pneumatic, electronic or hydraulically operated. All automated clearance pockets will require additional controls, wiring, junction boxes, tubing etc. In the case of hydraulically operated devices, a closed loop hydraulic system is required. Control of these devices is either local, through a skid mounted control panel or remotely with an off-skid distributed control system (DCS).

Figure 2 shows a cylinder with a head end (HE) variable volume clearance pocket (VVCP) and suction valve unloaders (SVU) on both cylinder ends

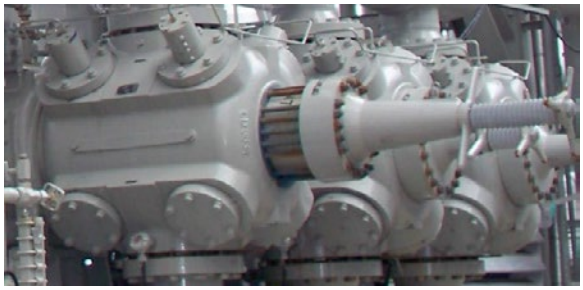

Figure 2: Cylinder with head end variable volume clearance pocket and suction valve unloaders.

Whatever the means of capacity control, the various load steps need to be included in the engineering studies performed on the package.in order to determine the impact on pulsation, natural frequency and torsional and mechanical vibration.

3.1.3 Purge and Vent Systems

The purposes of the distance piece purge and vent systems (along with the packing and distance piece arrangements) are to:

- Provide a means to prevent process gas leakage into the compressor crankcase and into the area surrounding the compressor. This is especially important due to environmental concerns and when compressing hazardous or toxic gas.
- Provide a means to prevent the distance pieces from filling with oil.
- Prevent contamination of the crankcase oil.
- Indicate the condition of the compressor piston rod packing.

There are a number of ways that the purge and vent systems can be designed. API 618, Annex I provides detailed recommendations for the purge and vent systems and includes schematic diagrams showing typical arrangements for single and two compartment distance pieces.

Figure 3 shows a distance piece vent and drain arrangement using individual vessels for collection.

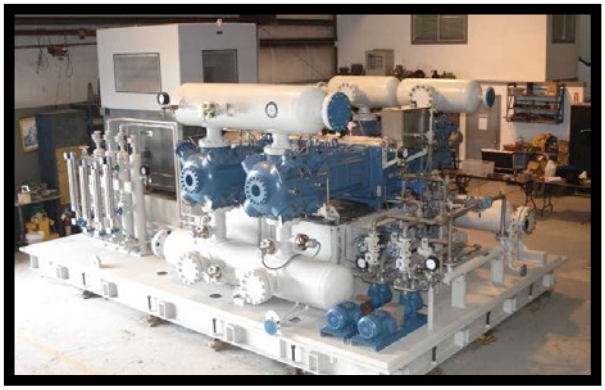

Figure 3: Compressor package showing vent and drain collection pots.

The compressor purge system may require a purge panel, as shown in Figure 4. This includes individual flow indicators and controls for each purge point.

Figure 4: Purge control panel.

3.1.4 Frame and Cylinder Lubrication

The design of the frame lubrication system will likely be either the manufacturer's standard or in accordance with the applicable industry standard (API 618, ISO-13631, ISO-13707 or API 614). The requirements for each will determine the number of coolers, pumps and controls required.

The "simplest" arrangement is using the main lubrication oil pump driven off the compressor crankshaft, a single cooler and filter arrangement. The more complicated systems, such as required by API 614 require dual lube oil coolers, dual element filters, two electric motor driven pumps and a backpressure regulator. This system will require significantly more space. Typically, API 614 lube oil systems are separate consoles; however if space permits, they can be part of the main compressor skid.

In general, cylinder lubrication systems are either divider block systems or pump to point systems. They receive their oil supply from the compressor crankcase or through a separate day tank. For the

by: Benjamin F. Williams – Ariel Corporation

same compressor and operating conditions, a pump to point lubrication system will be larger and take up more skid space than the divider block system.

Another consideration is make-up oil. This can be part of the package design or supplied during routine maintenance.

3.1.5 Cylinder and Packing Cooling

Whether or not a cylinder jacket water system is included in the compressor scope of supply will affect the layout and size of the package. Cylinder cooling systems will require additional piping, instrumentation, controls, pumps and coolers. If a closed loop cooling system is used, a stand tank will also be required.

Pressure packing may also require cooling. This will be determined by the operating conditions, whether the compressor is lubricated or non-lubricated or by manufacturer and/or customer requirements. In most cases, packing cooling systems are standalone, closed loop systems with a stand tank, pumps, cooler and valves.

3.1.6 Process Gas Cooling

For most multi-stage compressor systems, interstage gas coolers will be required. The cooler type will have a significant effect on the overall size of the package. Shell and tube type exchangers will require less area than an air exchanger (fin-fan) type cooler. With a gas engine driven compressor, it is normal to drive the cooler fan with the auxiliary end of the gas engine. Depending on the size of the compressor / engine, this cooler can be in excess of 10 meters (33 feet) in length and 5 meters (16 feet) in height.

Typically, the water supplied to shell and tube coolers is from cooling towers or rivers or in shipboard applications, the ocean. There are also cases where a closed loop, tempered water system is used, which may increase the overall package footprint. The type of cooler (ex. u-tube, single or double pass etc.) will determine the routing of the associated piping and therefore the package layout.

Other process gas coolers used (primarily on smaller compressors) include the plate and frame type and the spiral flow exchanger; both of which can significantly reduce the overall package footprint.

Cooling of the process gas between stages can result in liquid dropout. To prevent liquid carryover, properly sized interstage moisture separators will be required. These can be standalone vessels or incorporated in the suction pulsation dampeners or in rare cases, the process gas coolers. There are a number of process simulation programs available that can estimate the amount and composition of the liquid dropout at the suction and interstage of the compressor.

3.2 Driver

Although the operating conditions are crucial for the compressor selection, the driver type dictates the operating speed, which affects the compressor size and any associated forces and couples. The higher the driver speed the smaller the compressor. The most common drivers for reciprocating compressors are gas engines and electric motors. Compressors used in the refinery and petrochemical industries are almost exclusively electric motor driven, however because steam is available, steam turbine drivers are sometimes used. Natural gas compressors are primarily gas engine driven because the engine runs on the same gas compressed. The exception is those locations where electric power is readily available or when environmental or municipal regulations do not permit the use of engine drives.

Figure 5 shows a gas engine driven compressor package. Figure 6 shows an electric motor driven compressor package.

Figure 5: Natural gas engine driven compressor package.

Figure 6: Electric motor driven compressor package at a U.S. refinery.

3.2.1 Flywheel and Coupling

Regardless of the type of driver used, a torsional vibration analysis (TVA) is required to ensure the stresses caused by the rotation of the driver shaft and the compressor shaft are manageable throughout the entire speed range and operating conditions of the compressor. The drive arrangement is modelled on a mass-elastic basis (includes inertia and stiffness) to

by: Benjamin F. Williams – Ariel Corporation

predict the stresses in each drive component. The torsional vibration analysis will determine the need for additional inertia and stiffness.

If the torsional vibration analysis determines additional inertia is required, one option is an external flywheel. Gas engine drivers normally include a flywheel as part of their scope of supply; in most cases, electric motors do not. The size of the flywheel can affect the compressor centerline. As explained later in this document, the goal is to keep the height of the compressor package as low as possible. If the flywheel diameter is an issue, it may be possible to use a thicker external flywheel with a smaller diameter to add the same amount of inertia. Other options to add inertia include internal flywheels or torsional detuners, if the compressor crankshaft and crankcase design permit. In the case of flanged crankshafts, the torsional vibration analysis may require body-fit (minimal clearance) bolts to attach the flywheel or coupling adapter to the compressor crankshaft.

The torsional analysis also determines the need for a special coupling between the driver and the compressor. The most common coupling is a rigid, stacked disc type. The torsional analysis may also specify a "soft coupling". There are a number of these types available, each with different torsional dampening elements. These include special springs, rubber elements or viscous dampeners. Soft couplings are common when a variable speed drive is used. These couplings may reduce blocked speed ranges common with variable speed units. Review all operating cases in the torsional analysis, including start-up conditions.

It is important to note that with variable speed compressors, such as those using a variable frequency drive (VFD), the torsional vibration analysis may determine that certain rotating speeds must be blocked out due to torsional resonance. Although additional stiffness or inertia added to the drive arrangement may reduce the number of operating speeds blocked out, it may not be possible to run throughout the entire speed range.

Gearboxes add to the complexity of the drive train making the torsional vibration analysis more complicated.

Torsional failures can occur with the compressor crankshaft (and oil pumps driven off the auxiliary end), the electric motor shaft and the coupling arrangement. Figure 7 shows the results of a torsional failure on a compressor crankshaft.

Figure 7: Torsional failure of a compressor crankshaft.

3.3 Pulsation and Vibration Control

Once the compressor selection and the preliminary general arrangement is completed, the compressor system must be reviewed to determine the best means to reduce pulsations, vibrations and system excitations due to gas flow and the compressor rotation. The information gathered in the studies will determine the size and design of the pulsation control devices. It will also determine whether additional mass or stiffness is required to eliminate vibration or shaking, and provide detailed piping restraint requirements. It is very important to make sure these studies consider all operating conditions, especially any cases where the cylinders are single acting.

3.3.1 Mechanical Vibration Analysis

A reciprocating compressor generates a number of different forces, in a number of different directions. These include unbalanced forces and couples generated by the compressor frame or crankcase. Additional forces include those generated by the crossheads. The skid design must account for these horizontal and vertical forces and couples. The skid must be rigid enough to transfer them to the compressor foundation.

Mechanical studies will also determine the natural frequencies of the compressor package. The natural frequencies are determined to prevent compressor components, piping, vessels and tubing from becoming resonant. To prevent resonance, mass can be added to the skid by using thicker I-beam, adding concrete to the compressor pedestal or by skid mounted supports.

3.3.2 Pulsation Studies

API 618, API RP 688 and ISO 13707 describe the three design approaches for the pulsation studies and provides recommendations for when each applies.

Design Approach 1 uses empirical data to size the pulsation dampeners. Design Approach 2 includes an acoustic simulation and a piping restraint analysis. Design Approach 3 includes an acoustic simulation, a

piping restraint analysis plus a mechanical analysis of the system. (Design Approach 3 is required for most refinery and petrochemical installations.) In addition to pulsations caused by the gas, Design Approach 3 will review the natural frequency of the system to reduce vibrations caused by resonance.

The pulsation study will determine the size of the pulsation dampeners, as well as whether they require internals, such as baffles and choke tubes. The goal should be to keep the package height as low as possible to minimize vibration. This is because unless properly addressed, a small amount of movement at a lower elevation becomes significant at a higher elevation. In most cases, the diameter of the discharge pulsation dampeners establishes the height of the compressor centerline. Whenever large diameter, discharge pulsation dampeners are specified, you may want to consider longer dampeners with smaller diameters, if space allows.

In addition to suction and discharge pulsation dampeners, orifice plates are another means to reduce gas pulsations. Orifice plates will effect compressor power and pressure drop; therefore it is important that they be included in the compressor model..

3.3.3 Piping and Vessels

The pulsation and mechanical study will also review the piping and vessels to determine support locations and types. Some key points:

- In addition to the on-skid and interconnecting piping, off-skid piping details will be required for the analysis. Typically, the study will include off-skid piping up to the nearest pipe diameter increase or the nearest off-skid vessel.
- Piping runs should be kept as short and as low as possible. If long pipe runs are unavoidable, proper pipe supports are crucial.
- Smaller diameter connections or branches from larger piping or vessels can be problematic, if not properly gusseted or supported.
- Sightglasses and instrumentation require isolation valves. Note the weights of these items can be substantial and proper support is critical.
- Vertical vessels shall be as short as possible and fully skirted. These vessels should be welded or bolted to steel plate that is fully supported by skid beams. Do not weld or bolt vessels to the skid deck plate.

4 Controls and Instrumentation

Control and monitoring of the compressor package will be by a local control panel, a distributed control system (DCS) or a combination of both. Programmable logic controllers have become the standard for local control panels rather than the annunciator or switch gauge systems of the past. If no local control panel is provided, it is common to run all wiring to junction boxes located on the skid edge.

Customer specifications and manufacturer requirements will detail the required instrumentation. These will be either transmitters or local switches. The use of local gauges and temperature indicators is not as common as in the past with the advent of transmitters. However when they are, it may be better to locate these on a skid mounted gauge board which is easily viewed by the operator.

Instrumentation is subjected to vibration and pulsation from the compressor and that needs to be accounted for. The increased use of condition monitoring systems means larger control panels and more instrumentation on the compressor, piping and vessels. As mentioned previously, tubing and wiring associated with the devices must be properly supported and care taken to ensure they are not tripping hazards.

5 Installation Location

The location of the compressor installation can have a major effect on the design of the package. A compressor package going to the Middle East will have different requirements than one installed in Siberia. Similarly, an offshore compressor will have differing requirements than one installed in a refinery in Europe.

In addition to industry specifications, the package scope of supply may include items based on ambient conditions. Figure 8 shows a compressor package designed for installation in Northern Canada. Known as a “cold weather package”, it includes a building as part of the skidded package. The building includes catalytic heaters and gas detection. It is for the comfort of those working on the compressor in extremely cold weather. Provisions for makeup oil storage and drain collection are also part of the skid design.

Figure 8: Cold weather compressor package showing the skid and the inside of the skid mounted building.[1]

Tropical, arid (desert) and salt-water environments also require special consideration when designing the package. This may mean special paint and materials of construction are needed.

by: Benjamin F. Williams – Ariel Corporation

The Purchaser should identify potential space limitations in the RFQ package. This is especially important for installations in existing plants and those located offshore.

Another consideration for the package design will be any shipping limitations. Shipping limitations vary depending on the location. The Packager must be aware of shipping restrictions or limits when designing the package. This may even include designing the package to meet tunnel profiles when traveling by rail. (This primarily applies to Russian rail shipments.)

Standard (non-permit) shipping limits in Europe are as follows:

- The package should be a maximum of 2.55 meters (8.4 ft.) wide, 3.7 meters (12 ft.) high and 16-18 meters (52-59 ft.) long.
- The weight of the package should not exceed 44,000 kg (97,000 lbs.) including the weight of the truck.

Packages in excess of these dimensions will require special permitting. This can add significant cost and delivery time to the project. To meet shipping limits, it may be necessary to design the package with multiple skids or to disassemble the package prior to shipment.

5 Package Design Review

Current design technology provides excellent tools to review the package design, including 3-D models and virtual reality. With these tools, an End User can review the package layout and see where additional space is required for access and where safety hazards exist.

Having representatives of Operations and Maintenance involved in drawing review sessions can provide valuable insight and guidance into the package design. This can possibly prevent future disagreements between the procurement, operations and maintenance departments over the life of the equipment.

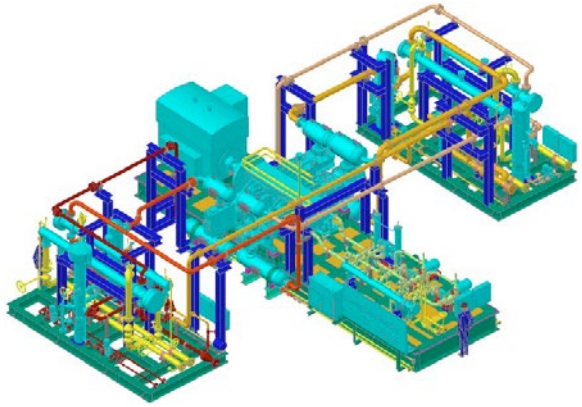

Figure 9: 3-D model of a multi-skid compressor package.[2]

Figure 9 shows a 3-D drawing of a multi-skid package and includes a human likeness to preview the package layout to look for accessibility and any tripping hazards.

6 Advantages and Disadvantages

A brief summary of the advantages and disadvantages of packaged compressors follows.

6.1 Advantages

- Lower cost of fabrication
- Eliminate the effects of weather on system fabrication, leading to higher quality.
- Reduced shipping cost compared to shipping individual components.
- Reduced time from installation to start-up.

All of these advantages result in overall reduced cost.. As previously noted, according to multiple End Users, packaged compressors were typically 50-60% of the installed cost of block-mounted, long stroke slow speed compressors for the same application.

Figure 10 shows a hydrogen compressor skid being installed at a chemical plant in the USA. The time from the compressor package arriving on site to bringing the compressor on-line was only 28 days. Prior to this, the facility only had block mounted compressors; since then, they have only purchased packaged compressors.

Figure 10: Compressor package installation at a U.S. chemical plant

6.2 Disadvantages

One perceived disadvantage is the use of third party companies for the design and manufacture of the compressor package. Although in the past, there may have been some small companies that did this, today the majority of these compressor "Packagers" are large privately owned or publicly traded companies. These Packagers are highly skilled and utilize the latest design tools. They are able to provide complete service and technical support to the End User. They are able to address all aspects of the

package design and have complete unit responsibility.

7 Conclusion

Modularization or packaging of reciprocating compressors began with the development of the natural gas pipeline system in the United States in the late 1940's. Since then, packaged reciprocating compressors have been installed at locations all over the world, including natural gas wellhead sites, gas processing plants, natural gas storage and transmission facilities, LNG facilities, power plants, refineries, chemical plants and other on-shore and off-shore facilities all over the world.

Because reciprocating compressors present unique design challenges due to the wide variety of forces, vibrations and pulsations inherent to their operation, there are a number of things to consider when designing a compressor package. Over 60 years of history has provided valuable insight into what makes a modularized compressor system work successfully and what to avoid. The compressor selection is only the beginning.

8 Acknowledgements

The author would like to thank the following people for providing information included in this paper:

Mr. Norm Shade – ACI Services, Inc. www.aciservicesinc.com/

Mr. Roger Wachter and Ms. Ionela Cioata – Euro Gas Systems - www.eurogassystems.com

Mr. Chris Mills – Oil and Gas Machinery, Ltd. - www.ogml.co.uk

9 References

[1] Cold weather package - Compass Compression – www.compasscompression.com

[2] 3-D Compressor Model – Enerflex Systems, Ltd. www.enerflex.com

HAUG Sauer Compressors

New Design of a completely oil-free high-pressure compressor series with a power up to 110 kW and a maximum pressure of 450 barg

by:

Thomas Heumesser
J.P. Sauer & Sohn Maschinenbau GmbH
Kiel, Germany
thomas.heumesser@sauercompressors.de

Bernd Schmidt
HAUG Sauer Kompressoren AG
St. Gallen, Switzerland
bernd.schmidt@haug.ch

11th EFRC CONFERENCE
September 13 – 14, 2018, Madrid

Abstract:
New design of a completely oil-free high-pressure compressor series with a power up to 110 kW and a maximum pressure of 450 barg.
The compressor series is designed as an absolutely non-lubricated, dry running machine, without any oil inside the crankcase and the cylinders. The gas industry has high demands for the gas quality, oil-free compressors can reduce operating costs and significantly reduce risks, because gas treatment and filtration downstream of the compressor is simple or, in some cases, not required at all. Oil-free compressors are therefore ideal for processes and applications which have high demands on the absence oil and on gas purity.
This special design includes gas tight crankcases up to a pressure of 20 barg. This crankcase eliminates the risk of environmental contamination due to gas leaks. The new design increases the delivery rate and discharge pressure of the existing series with 50 years of experience of completely oil-free and technical gas-tight process gas compressors.
This paper will describe the design and the technical solutions for this compressor series and also explain and show the running experience with the help of a new big data monitoring system.

by: Thomas Heumesser – J.P. Sauer & Sohn Maschinenbau; Bernd Schmidt – HAUG Sauer Kompressoren

1 Introduction

Gas industry clients are requesting higher suction and discharge pressures and larger flow rates for their non-lube process applications; hence a decision was made to develop a new completely oil-free and technical gas tight compressor to enlarge the product portfolio and to replace an existing lubricated cross-head design compressor. Although the new design is based on the existing and proven compressor technology several new developments had to be made.

2 Historical Investigations

Vitruvius was a Roman author, architect, civil engineer, famous for asserting in his book *De architectura* that a structure must exhibit the three qualities of *firmitas, utilitas, venustas* – in other words, to be solid, useful, beautiful. (Fig. 1) As drawn later by Leonardo da Vinci: the human body inscribed in the circle and the square (the fundamental geometric patterns of the cosmic order).

This statement remains over centuries and should have an influence on a new compressor design too.

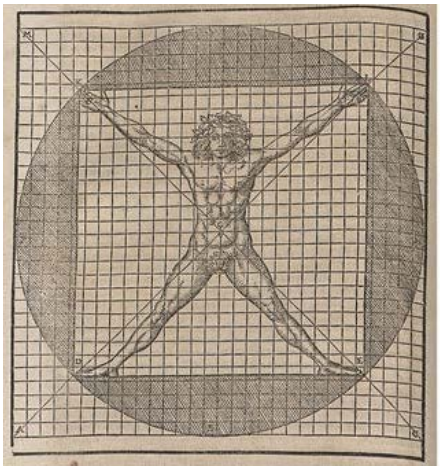

Figure 1: Walther Hermann Ryff interpretation of "The proportions of the human body according to Vitruvius", 1548

3 The fundamentals of Reciprocating Compressor Design

For numerous applications in the industry regarding gases, flow, pressures, there are mainly two different type of reciprocating compressor running gear set-ups.

a) Trunk piston

b) Crosshead

Remark: other related reciprocating compressor designs are hydraulic or pneumatic driven boosters and diaphragm compressor designs that are not considered in this paper.

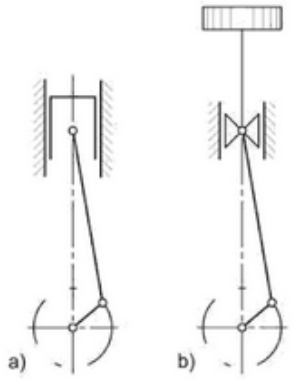

Figure 2: reciprocating compressor running gears

What is a trunk piston compressor?

Trunk piston compressors have a similar design to engines, simple and relatively low investment costs.

Suitable for smaller gas flows up to 2000 Nm^3/h and shaft powers up to 250 kW. Most of them, are lubricated, but for special applications non-lube and gastight is mandatory. Due to the relatively low shaft power, the cylinders are often air-cooled with an internal heat exchanger. Water cooled cylinders are available for special applications and high-pressure operation.

Reciprocating compressors with crossheads are much more complex design, larger and heavier. If applied for a non-lube process gas application there are always stuffing boxes required, that divide the lubricated driving part with the non-lube cylinders. Double acting pistons normally do require a crosshead execution.

Layout designs of trunk piston compressors:

For high-pressure applications, trunk piston compressor uses several cylinders connected in a multi-stage design.

by: Thomas Heumesser – J.P. Sauer & Sohn Maschinenbau; Bernd Schmidt – HAUG Sauer Kompressoren

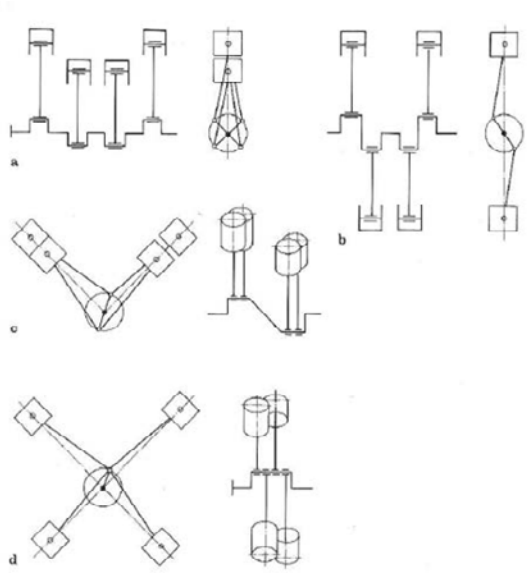

Figure 3: Typical compressor layout designs

Typical layouts of compressor frames, to be found in the industry, examples showed with trunk piston:

a) Vertical-design

b) Boxer-design, horizontal balanced opposed

c) V-design

d) Star-design (Fig.3, d)

The layouts of compressor frames are often a compromise between process & client requirements and manufacturing costs. Trunk piston compressors allow to set up a modular construction system of standardized driving systems and cylinders. With the modular system, the OEM is flexible to meet individual process requirements and to pre-fabricate compressor parts.

4 The market requirements for the new compressor design

- High flexibility to meet various applications (any gas) with a modular compressor design, up to 6 stages
- Suction pressure up to 20 barg and discharge pressure up to 450 barg
- Avoidance of product contamination requires a totally non-lube design for cylinder and compressor frame
- Technical gas tight compressor frame with a magnetic coupling (Leakage rate < 10^{-4} mbar*sec^{-1}). This crankcase eliminates the risk of environmental contamination due to gas leaks
- Water cooled cylinder system to cope with high differential pressures/temperatures
- Compact design in V- and Star-layout (Fig.3,d) optimized compressor dimensions
- Usage of proven design principles for long-term, trouble-free operation
- Compressor shaft power up to 110 kW. Rated rotational speed 450-900 min^{-1}, suitable for a frequency converter drive
- Low vibration level to meet ERFC vibration guidelines to allow foundation free set up
- Maintenance intervals that allow yearly inspection and/or exchange of wearing parts for continuous duty
- Design according to the EUROPEAN directives (Machinery, PED AD2000, ATEX). ATEX classification according to Ex II B T3, installation in Zone 1 and 2

5 The New Compressor Design

5.1 Compressor layout design selected

After an intensive evaluation process the star-design was chosen for the new compressor for several reasons:

- compact compressor design
- use of a proven crankshaft and magnetic coupling design
- generating of a more regular torque curve with four similar peaks with 90°offset, which is particularly advantageous for the use of a magnet coupling.
- low vibrations due to nearly 100 percent mass balance and due to low moments resulting in bearing supporting forces (Fig.4)

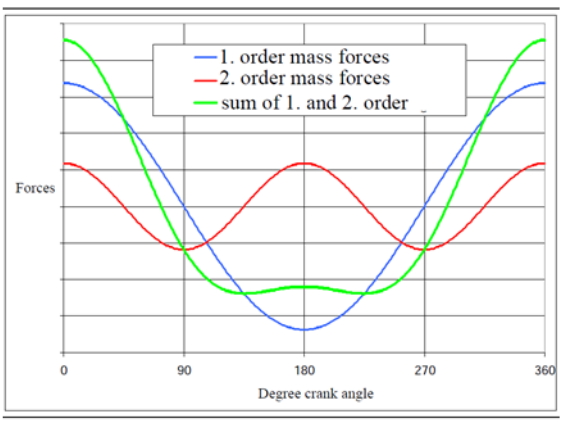

Figure 4: With the chosen star-design layout the 1+2.order mass forces are completely balanced; for the star design the resulting sum curve (green line) is a sinus curve that can be balanced completely with counterweights

by: Thomas Heumesser – J.P. Sauer & Sohn Maschinenbau; Bernd Schmidt – HAUG Sauer Kompressoren

The compressor is suitable to accommodate two or four cylinders in single or double acting executions. Double acting can be done with different cylinder diameters that allows up to max. 6 stages. (Fig.5)

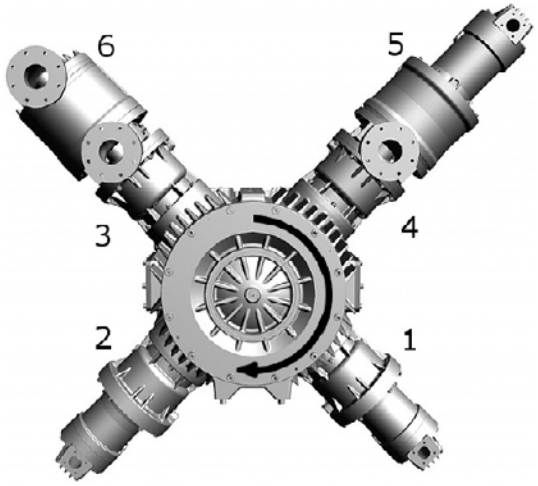

Figure 5: modular and flexible star-design, the exemplary configuration with two single acting cylinders (1 and 2), one double acting with different cylinders (4 and 5) and one double acting with identical cylinders (3 and 6)

5.2 Compressor frame design

In general compressor cylinders and frame housings are manufactured machine parts according to OEM engineering, manufacturing and quality assurance standards. They are not considered as pressure vessels as per PED and do not fall under such standards.

Nevertheless, calculations were carried out according to AD2000. The design calculation of the compressor cylinders and frame was performed using the finite element method. The program SOLIDWORKS was used, Version 2014.

Due to the pressurized compressor frame, not only the static and dynamic strength is of importance for the components. Exemplary a stress and deformation analysis of the compressor housing cover is presented in this paper. (Fig.6&7)

Compressor housing cover material selection:

Material Data Table									
Units: MPa	Ambient Temperature [°C]					Design Temperature [°C]			
	20					100			
Material Designation		Rm	K	f	E-Mod	Rm	K	fd	E-Mod
FN 10028-2 W-Nr 1.0425		410	265	176.6	212000	480	241	160.6	207000

Table 1 Material data EN 10028-2 W-Nr. 1.0425

Allowable stress calculation:

Allowable stress according to AD2000:

fd = K100/s = 241/1.5 = 160.6 MPa (1)

ftest = K20/s' = 265/1.05 = 252.3 MPa (2)

For this calculation, the pressure 30 barg is the design load. The structure has to fulfil the stress requirements of AD2000.

Test Load:

Test pressure according to PED 97/23/EG:

Ptest = (1.25*(176.6/160.5) * 30 = 41.236 barg (3)

or Ptest = 1.43 * 30 = 42.9 => max = 42.9 barg (4)

Because the term

(Re20/s')*(s/Re100) = (265/1.05)*(1.5/241) = 1.57

is greater than (Ptest/P) = (42.9/30) = 1.43 (5)

The design conditions are the governing conditions.

It turned out that the stresses and deformations at the compressor housing cover including the deformation of the bearing housing meet the requirements.

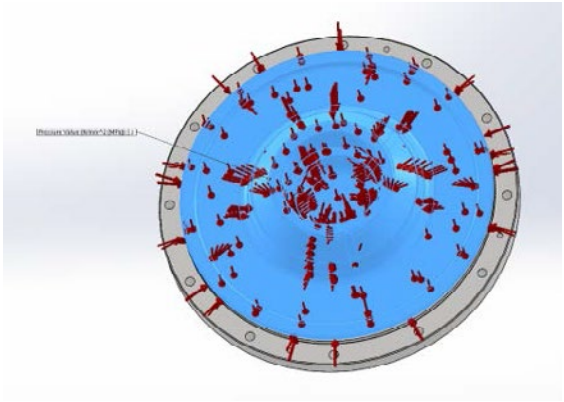

Figure 6: compressor housing cover with internal pressure

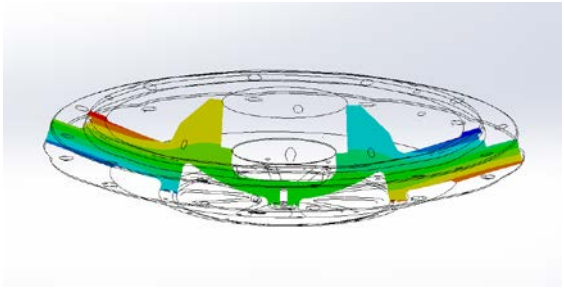

Figure 7 : Maximum displacement URES = 0.1648 mm

5.3 Modular compressor concept

A complete range of standard single and double acting set of pistons, cylinders, and cylinder heads was developed and engineered (Fig. 8).

The geometric series of cylinders is based on the required compression ratios of the focused process gas applications. In general, the diameters are based on the modular principle with same parts and standard interfaces. The cylinders diameters and compressor valves are standardized. The guiding

by: Thomas Heumesser – J.P. Sauer & Sohn Maschinenbau; Bernd Schmidt – HAUG Sauer Kompressoren

cylinders (Fig.9), similar to a crosshead design, are the same on all cylinders.

In total 23 standard cylinder diameters are available with diameter from 16 to 260 mm. By combining the standard cylinders in total 172 individual compressor configurations can be selected meeting clients process requirements. The advantages for the customers are a shorter engineering and manufacturing time and consequently a faster delivery time.

The modular system on the reciprocating compressors has been consistently adopted since the 1960s at all trunk piston compressor series and has been successfully implemented also in the new compressor development.

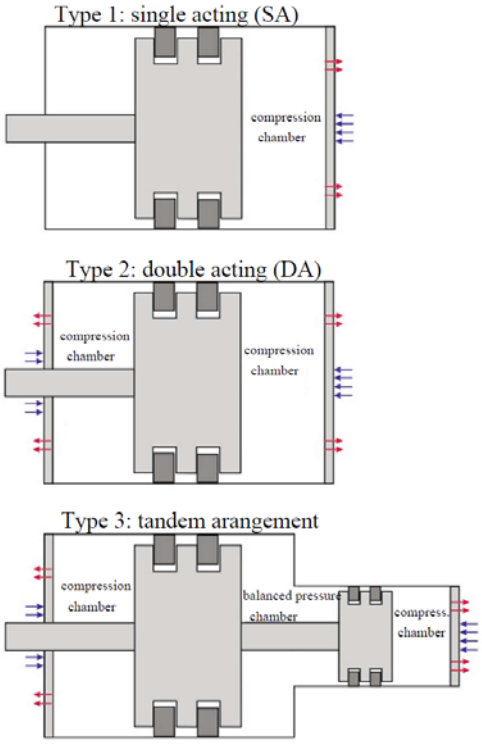

Figure 8: single- and double-acting cylinders, the tandem cylinder arrangement is a double-acting cylinder with two different cylinder diameters

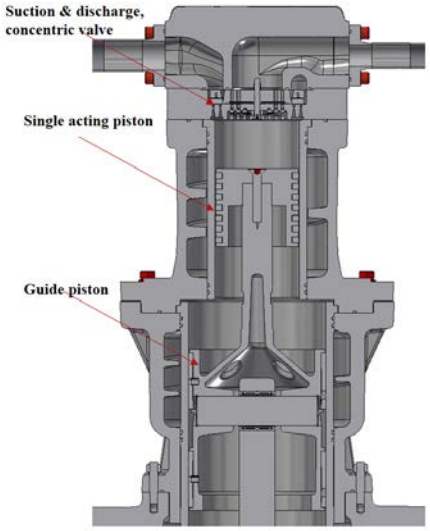

Figure 9: sectional view of type 1, single acting piston arrangement

5.4 High-pressure cylinder (450 barg)

Medium pressure applications 50 up to 150 barg piston are equipped with standard piston ring designs. For the high-pressure applications 150 up to 450 barg, a new series of single acting piston/cylinder sets have been designed. The goal was to find a design that can be integrated into the modular system of all non-lube piston compressor series and that can be adapted to very small piston diameters.

For very small diameters and high differential pressure, the sealing with non-lube piston rings is difficult to do and relatively expensive. To get enough sealing many piston rings have to be installed. Because of the small piston diameter, the mechanical stiffness of non-lube piston ring is difficult to achieve. Experiences have shown also a negative impact on the operational behaviour with piston ring wear that results in degradation of flow rate and forces to exchange piston rings in short time at applications with high discharge pressure.

The design alternatives for non-lube piston sealing are piston ring, labyrinth, and NanoLoc (Fig. 11). The challenge for all versions is beside the design engineering to apply the right material with the execution of a very accurate manufacturing.

After many years of testing the NanoLoc design has shown the best performance, stable flow rate and a long lifetime of the components.

The requirement of the NanoLoc piston design has to meet technical requirements as

a) the wide range of gas application, including wet gases and gas mixtures
b) stable flow rate
c) high efficiency
d) modular design
e) air and water cooled

by: Thomas Heumesser – J.P. Sauer & Sohn Maschinenbau; Bernd Schmidt – HAUG Sauer Kompressoren

f) discharge pressure up to 450 barg

To meet these requirements, the system design has to fulfill technical specification regarding

- a precision of NanoLoc and tolerances of machined parts (approx. 3 microns)
- optimized thermal independency of NanoLoc (operation range up to 200°C)
- wear resistance of NanoLoc (lifetime of 3000 to 6000 operation hours of the system depending on operation condition)
- low friction coefficient and chemical stability of the tribological system with various gases and gas mixtures
- extreme low lateral forces on the piston from the driving side to have low friction and wear

This is achieved through the combination of a piston with a metallic body and a low friction coating based on polymer compound. The cylinder sleeve consists of steel with a surface coating and finishing. The sleeve and piston is a matching pair that is manufactured and tested together and is exchanged always together. The selection of the material, the machining, and testing of the parts are the key technologies for this application.

The driving of the NanoLoc piston is done with flexible connection rod that results in almost no lateral forces on the piston. This flexible connection rod can be applied also for small piston diameters between 10 and 20 mm. The flexible connection rod is a modular and easy to handle system. The key technologies to realize it are in the dimensioning of the flexible connection rod, the selection of the material and the precise machining of the parts.

The material combination is also suitable for relatively high piston speeds, in particular preventing a blocking of the piston even in the case of a failure of the NanoLoc piston. A high operational security of the compressor is ensured.

Accordingly, a non-lube high-pressure piston with NanoLoc design can be achieved (Fig. 10 and Fig. 11) within a relatively large operating range and with a modular compressor system.

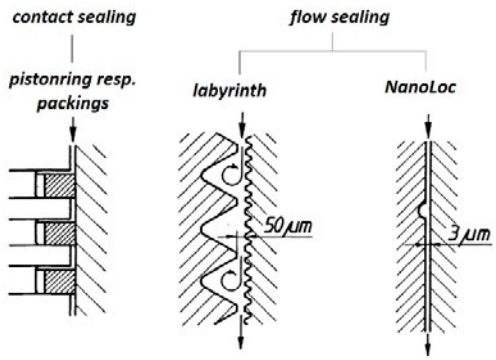

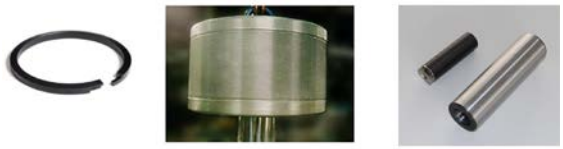

Figure 10: design alternatives for non-lube piston sealing

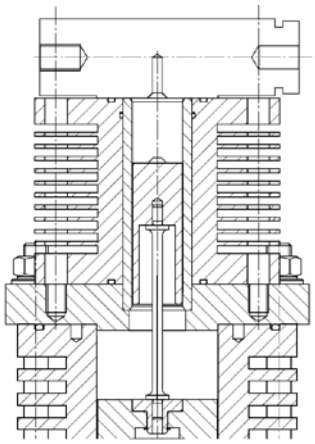

Figure 11: non-lube high-pressure piston with NanoLoc design

6 Compressor magnetic coupling

An oil-free compressor with oil-free crankcase consequently demands an oil-free shaft seal, which further needs to be leak- and maintenance-free for pressures up to 20 barg. These requirements can only be met by a magnetic coupling in place of the shaft seal. The magnetic coupling has the following features:

- oil-free, leak-free, maintenance-free
- no transmission or energy losses
- no sealing medium or energy required to operate
- modularly built coupling in combination with standard electric motors
- magnetic coupling acts as a safety clutch: in case of an override of the coupling due to a compressor overload or a blocked drive, the electronic shut down the motor using the signal from a sensor which checks the rotation of the compressor.

The coupling consists of two rotors with permanent magnets (see Fig. 13) and a non-metallic split pot (for example made of ceramic) in between the two rotors. The inner rotor is fixed directly onto the compressor crankshaft and the outer rotor is fixed to the motor shaft (see Fig. 14).

It ensures a technical gas-tight and permanent separation of the electric motor drive from the compressor lower part. For critical media like aggressive, toxic gases it serves as a reliable seal and prevents serious leakages occurring.

Another advantage of the design with magnetic coupling is the built-in “overload” protection. If the

by: Thomas Heumesser – J.P. Sauer & Sohn Maschinenbau; Bernd Schmidt – HAUG Sauer Kompressoren

compressor is running with too high load, then the magnetic coupling "slips" and the compressor is shut down safely and stops.

The dimensioning of the coupling depends on the inertia of the compressor drive and on the torque curve of the compressor shaft. The magnetic coupling is designed for a rated torque:

$$M_r = 9550 * P_r / n_r \quad (6)$$

where M_r is the rated torque (Nm), P_r the rated power (kW) and n_r is the rated motor speed (rpm).

$M_r = 9550 * 110 / 743 = 1414$ Nm

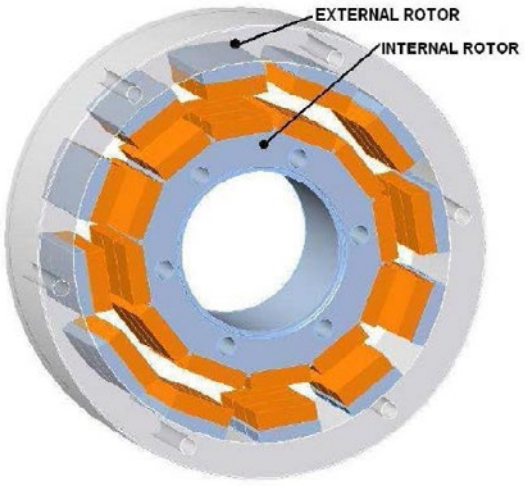

Figure 12: magnetic coupling, a schematic drawing with an inner and outer rotor with permanent magnets

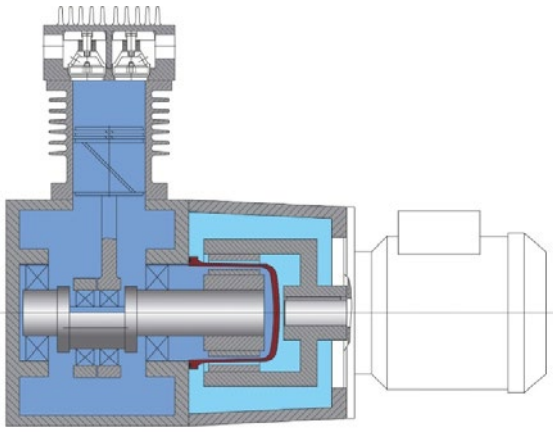

Figure 13: magnetic coupling, a schematic drawing of setting up with a crankshaft, inner rotor, split pot, outer rotor and electric motor

7 Running experience & Monitoring

The new compressor design has been tested with two configurations over about 3 years at the internal test field with around 10'000 operation hours in total. Because of the wide range of applications and operational data continuous testing is required. Besides checking the reliability and operation data of the new compressor design the main goal of testing was to compare the theoretical simulation with the real data and to understand root cause effects and trends.

For the test period, the compressor was equipped with an extensive monitoring system comparing measured data at the real compressor with the thermodynamic model of the virtual compressor (Digital Twin) on the simulation program (see Fig. 14 and 15).

Figure 14: compressor during the field test

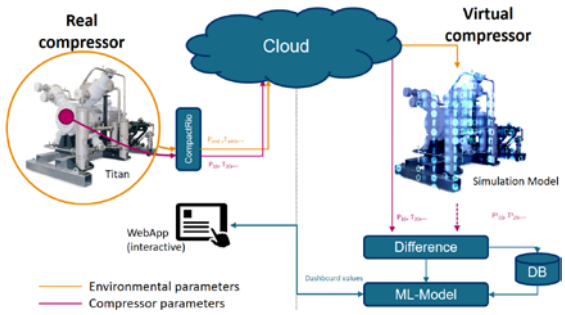

Figure 15: schematic concept of the monitoring, with data collection, evaluation, and comparison with the "Digital Twin"

In total 67 compressor operation parameters have been monitored with a sampling rate of 1 Minute. The measuring data includes gas and water volume flow rates, temperatures, pressures, vibrations, bearing performance, compressor speed and absorbed power.

To collect many data as possible was important from the beginning. The challenge was to understand and to find the right conclusions of the huge data collection. Very important was the optimal dimensional reduction method like

by: Thomas Heumesser – J.P. Sauer & Sohn Maschinenbau; Bernd Schmidt – HAUG Sauer Kompressoren

Principal Component Analysis (PCA) or Independent Component Analysis (ICA).

Considering Industry 4.0 and IoT (Internet of Things) a cloud solution with a connected database and a machine training and learning module was installed.

The "Digital Twin" is the virtual image of the real compressor that accompanies its physical counterpart simultaneously. This simulation model is thus assigned to an individual compressor and is fed with its real operation data resulting from the compressor sensors. Thus, the simulation model reflects the current, physical state of the equipment, but can provide more information than only the sensors.

This more in-depth consideration of the simulation model provides a wider view of the status of the compressor that is relevant to its life expectancy and wears profile of spare-parts.

In a first phase (training mode), process data derived from normal operation is used to learn a statistical model that includes non-interference variations in the process. As a result of the training phase, the simulation program creates 2 or 3 "Reference Values" that contain the several operation data. Operators can now easily monitor this "Reference Values" and understand trends and normal operation conditions, i.e. the conditions in which the training data was recorded (Fig. 16).

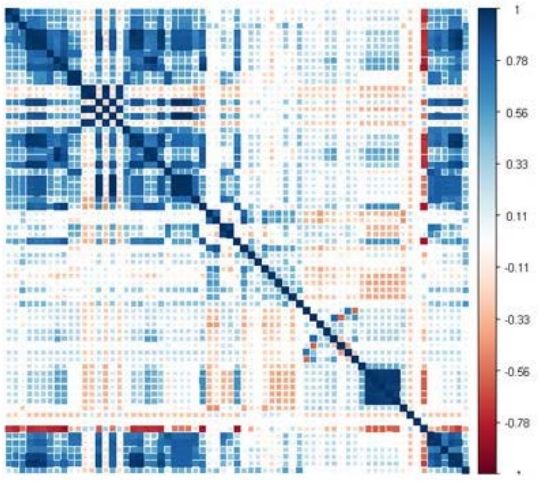

Figure 16: correlation matrix of the 67 sensor data for the system training duration

In the second phase (online operation mode), the model thus obtained is compared with online data from the process by calculating "Reference Values" for each new operation point and comparing them with the corresponding simulation. That allows to define operation limits and to detect "drift" of the process at an early stage.

As result of the field test experience, this program will be available and will provide an added value for the industry, customer as an up-to-date monitoring of valves, piston & guide rings and bearing wear for predictive maintenance services together with the historical data, combined and stored in a compressor lifetime diary including regular field service & spare parts reports.

8 Conclusion

A new stage-gate development process was started with the new design development.

The non-lube high-pressure piston 450 barg was designed and tested successfully at a smaller compressor of the existing series.

The simulation program and the data monitoring and evaluation system were also new and an important development step on this project. Soft and Hardware experience collected during the test phase will result in a new software for compressor 4.0 industrial demands.

With the completion of the new design development, the product range could be extended with a flow rate by factor of 3 to 4 compared to the existing series and extend the range of maximum discharge pressure from 100 barg to 450 barg. That is the worldwide largest completely oil-free and hermetical gas-tight piston compressor with magnetic coupling to meet client demands regarding environmental aspects and product quality.

References

[1] https://en.wikipedia.org/ historical research

[2] Karl-Heinz Küttner, (1991): Kolbenverdichter Auslegung und _Betrieb.

[3] T. Heumesser, Vortrag 14, 21. Kv.-Workshop, Rheine 2017

[4] NTB Interstaatliche Hochschule für Technik, Berichte, 2017

[5] https://recip.org/components-drive-mechanism/

[6] H. Baumann, Section 1: Application of process compressors @ Compressor Users International Forum Sept 2004

[7] EFRC-Guidelines-for-Vibrations-in Reciprocating -Compressor-Third-Edition

Engineering approach for world's largest hydrogen compression system

by:

Niek Albers
Howden Thomassen Compressors, Rheden, The Netherlands
niek.albers@howden.com

Leonard van Lier
TNO, Delft, The Netherlands
leonard.vanlier@tno.nl

Maarten van der Biezen
FLUOR, Hoofddorp, The Netherlands
maarten.van.der.biezen@fluor.com

11th EFRC CONFERENCE
September 13 – 14, 2018, Madrid

Abstract:
For a large new refinery project in the Middle East, the design and construction of a very large hydrogen compression unit was required. The compression unit design resulted in the requirement for six large reciprocating compressors operating in parallel, with a total installed electrical power close to 100 MW. The compressors have common suction and discharge headers and common headers for two side streams, with each compressor having 8 cylinders in a 4-stage configuration. The scale of the system and individual compressors required a dedicated engineering approach to handle the complexity of the project. This included a torsional analysis pre-study and the development of load-balancing and service life optimization features as part of the unit control system. From a pulsation perspective, the complex acoustic interaction between the various compressor trains, all possible capacity step combinations (exceeding 10.000) and the very large size of the complete system posed major challenges. Industry standards API 618, 5th ed., and API RP 688, 1st ed., do not provide any specific guidance on how to address these challenges. Therefore a new evaluation process was developed aiming to control the acoustic interaction between different compressor trains. This facilitated the selection of a realistic amount of analysis cases and appropriate evaluation criteria. The obtained acoustic separation between the compressor trains lead to an efficient pulsation and mechanical response analysis process.

by: Niek Albers – HOWDEN; Leonard van Lier – TNO; Maarten van der Biezen – FLUOR

1 Introduction

Hydrogen production and compression in the worldwide refining industry is impacted by changes in environmental regulations with regard to transportation fuel quality. The need for lower sulphur gasoline and diesel increases hydrogen demand for hydroprocessing operations. In addition, additional hydrogen is required to process heavier crude oils and to increase conversion capacity to match a changing demand balance, requiring less heavy fuel oil. Refineries may therefore require new or modified hydrogen production and compression facilities to provide the required compressed hydrogen supply.
As part of a major upgrade and expansion project at a refinery in the Middle East, very large scale hydrogen production and compression facilities were required to meet state-of-the-art refined product quality requirements and increase productivity. Hydrogen is supplied by several upstream hydrogen production units to an integrated hydrogen compression unit providing the hydrogen compression for different hydro-processing units. This integrated compression unit consists of six large reciprocating compressors, five operating in parallel and one spare machine. The total installed electrical power of the compression unit is close to 100 MW, resulting in the world's largest hydrogen compression system.

The scale of the system as a whole as well as the individual compressors required a dedicated engineering approach to handle the complexity of the project. This included additional analyses of the torsional characteristics of the compressor-driver system, the development of load-balancing and service life optimization features as part of the unit control system and a novel, dedicated approach for the process system design and pulsation and mechanical response analysis.

2 Compressor selection and design

The hydrogen compression unit is designed to compress hydrogen with a high purity. The low molecular weight (MW=2.1 g/mol) of the process gas in combination with the overall unit compression ratio of approximately 10 defines the choice for the applied compressor type. The suction pressure is 20 bar(a) and the final discharge pressure is 207 bar(a); each compressor has a rated capacity of 15500 kg/h. A centrifugal compressor for this duty would be very inefficient in this service and would require up to 90 impellers which is obviously not feasible, whereas a screw compressor would not be able to meet the required discharge pressure. A reciprocating compressor is therefore the only compressor type able to compress the required quantity of hydrogen gas to the required discharge pressure.

2.1 Reciprocating compressor design

The process demands in terms of suction and discharge pressures at battery limits, along with side streams from hydrogen recovery units and to different hydroprocessing units led to the selection of a four stage compressor configuration (Figure 1).

Figure 1: C-85.8, 8-cylinder, 4-stage reciprocating compressor in factory

Multiple configurations were analysed and rated on efficiency, footprint, maintainability and operating flexibility. Along with the applicable industry, customer and project specific standards, this resulted in an optimized design consisting of 6 parallel compressors, of which 5 are normally operating and one compressor is spare. Each individual compressor has four compression stages with two double acting cylinders per stage, thus 8 cylinders in total per compressor (Figure 2). The operating speed of the compressors is 333 RPM, with a rated driver power of 16600 kW.

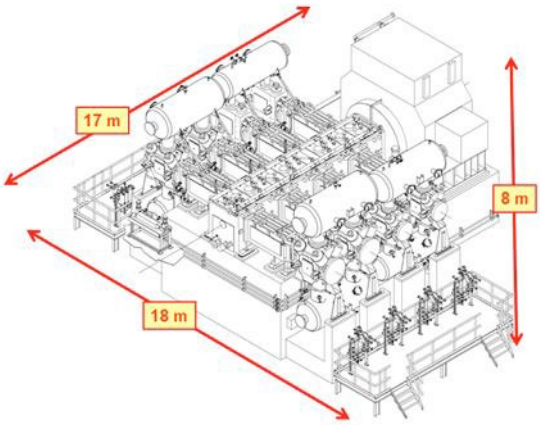

Figure 2: Main dimensions of the compressor unit

2.1 Torsional studies

Whilst operating well within the applicable design limits of the selected compressor type, the compressor system will include the largest reciprocating compressors built according to the American Petroleum Institute (API) Standard 618[1] to date. The physical size and associated costs and delivery time of the included components make it worthwhile to assess the component selection and design in an early stage. This pertains in particular to the selection and design of the electric motor.

by: Niek Albers – HOWDEN; Leonard van Lier – TNO; Maarten van der Biezen – FLUOR

2.2.1 Torsional pre-study

In line with API 618, section 6.7 requirements, a torsional analysis including calculation of torsional natural frequencies and possibly including a torsional stress analysis shall be provided during contract execution. The torsional characteristics of the complete compressor-driver system are governed by the compressor design and the specific design of the electric motor rotor, which can differ between motor size and design. Primary factors influencing these characteristics, such as rotor inertia and stiffness, are therefore already determined to a significant extent in a very early design phase. In order to validate the design of the compressor-motor combination upfront, a torsional pre-study using typical motor design information was performed. The indicative torsional natural frequencies and torsional stress levels provided by this early assessment of the torsional characteristics of the complete compressor-driver system ensured that the final design will meet all applicable design requirements.

2.2.2 Torsional analysis

The approach on torsional studies as outlined in API 618 primarily focusses on separation margins between torsional natural frequencies and dominant excitation frequencies. In this particular case, the final compressor and motor design led to a rotating system which complied with all the applicable separation margins. Though not formally required by API 618, a full torsional stress analysis including all normal operating and transient conditions was executed to ensure that the torsional vibration and stress levels are acceptable under all conditions. This analysis provides insight in the amplification caused by the systems torsional natural frequencies, even when meeting the specified minimum separation margins.

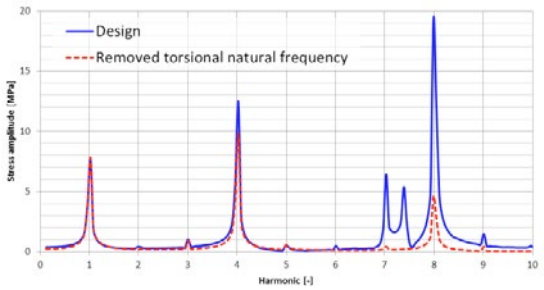

Figure 3: Frequency analysis of torsional stresses in normal operating conditions

Figure 3 illustrates this amplification effect showing the torsional stress amplitude in the crankshaft for the design analysis and an analysis with the torsional natural frequency artificially removed, by significantly increasing the shear modulus of the material. Whilst the design analysis meets the recommended separation margins, in this example the stress amplitude at the 8th harmonic increases with a factor 4 compared to the situation without any amplification from torsional resonance frequencies. Though the resulting torsional stress amplitudes are well acceptable, this underlines the importance of evaluating the torsional vibration and stress levels under all normal operating and also transient conditions, where amplification effects may be even more pronounced.

3 Control system design

The main stream of hydrogen (red coloured stream in Figure 4) is compressed from 20 bar(a) to 207 bar(a) in four compression stages. Additionally a 40 bar(a) admission side stream is introduced downstream the first stage and an additional extraction side stream is provided at a pressure level of 100 bar(a) (blue coloured streams).

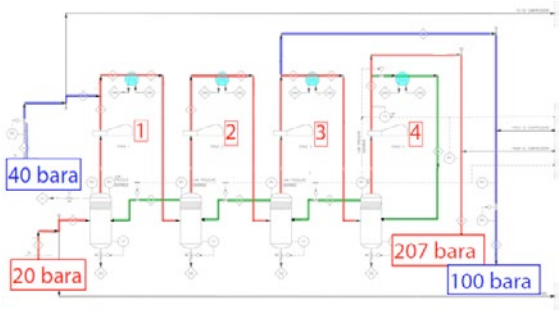

Figure 4: Layout of single compressor train (red coloured lines are the main process stream, blue coloured lines are additional admission and extraction streams, green coloured lines are recycle streams)

3.1 Capacity control system

Since the main process, 207 bar(a) hydrogen flow is fluctuating following the refinery demand similarly to the admission and extraction streams (even down to 0%), it became clear that the flow control would be rather complicated. Objective was to reduce recycling of compressed gas to the extent possible in order to maximize energy efficiency. This is achieved by allocating the overall capacity control of the complete compression system to an automated main control system, governing the overall capacity in a three tier approach:

- Stepped suction valve unloading
- Flow recycling
- Adjusting the number of operating compressors

Conventional five step suction valve unloading (0-25-50-75-100%) proved to be a good basis for design since there are normally five compressors in parallel operation, which increased the number of system load steps to 25 (5 steps x 5 compressors). This enables servicing the required hydrogen demand with increments of 5% of the plant load. In between the 5% increments stage recycling is added.

by: Niek Albers – HOWDEN; Leonard van Lier – TNO; Maarten van der Biezen – FLUOR

3.2 Operator support

Considering the scale and complexity in terms of operating configurations, certain operator support functions are integrated in the control system. This facilitates decision making by the operator, aimed to optimize system efficiency and maintenance.
The main control system is designed such that it automatically loads or unloads a cylinder side when a 5% flow increment is required or reduction is possible. In this way, the load is automatically balanced to the downstream demand whilst reducing the recycle flow rates to the extent possible. When the flow demand decreases significantly the operator is notified and may choose to put one or multiple machines in standby mode. An advise on the number of required operating compressors is provided based on the actual downstream hydrogen consumption. Additional service life optimization features are provided in the main control system. This includes advise on preferred compressor to start or stop, by monitoring and distributing running hours and start/stops between individual compressors.

4 Pulsation and vibration control

4.1 Guidelines and standards

The most commonly applied standard for the design of reciprocating compressor systems is API 618. With respect to pulsation and vibration control, this standard contains guidance on the best practice for the analysis, and also limit values for pulsations, vibrations and cyclic stresses. For systems containing multiple parallel compressors, pragmatic approaches were formulated in 1999 by TNO and SWRI in a joint paper[2]. Additional useful background information can be found in the API Recommended Practice 688[3].

4.2 Preliminary design review

At an early stage of the project, in a technical meeting the initial design concept of the system was reviewed, considering the aspects of pulsation and vibration control. The following aspects were considered within a multi-disciplinary team including rotating equipment engineers, process engineers, mechanical engineers and pipe stress engineers:

Pulsation damper volume: a large number of pulsation sources is expected in the system. For that reason, the pulsation damper volumes are oversized by the vendor during initial sizing, within the tolerable margins for additional weight and size.

Piping routing: Focussed on avoiding high-elevation piping, minimizing distance between inlet separators and the compressor's inlet and minimizing length of closed side branches, such as spillback lines, side streams and pressure safety valve lines. For pressure safety valves, other project specifications prevailed that dictated the pressure safety valves to be at high elevation (free draining of the flare header), thus increasing the length of the dead-leg branches to the PSVs.

Equipment: KO drums were positioned close to the compressor and spillback lines for compressor control are all attached to the KO drums and thus separated from the pulsation source and the main piping. Moreover, the location of flow measurement equipment was optimized, to suppress the disturbing influence of flow pulsations as much as possible.

Connection to the headers: Initially various concepts were discussed to stimulate acoustic separation between the compressor trains as much as possible. Theoretically, perfect separation would reduce the risk on pulsation issues in the common system and greatly facility the analysis effort. However, from a practical perspective, the separation techniques using volumes of additional vessels have a rather limited effect, due to the large speed-of-sound of the hydrogen gas. For example, also the design of a Helmholtz filter (assembly of 2 vessels separated by an interconnecting pipe, Figure 5) was considered. The resonance frequency of this 'Helmholtz' assembly is given by:

$$f_{HH} = \frac{c}{2\pi}\sqrt{\frac{A}{L}\left(\frac{1}{V_1}+\frac{1}{V_2}\right)} \qquad (1)$$

If the pulsation frequency is well above this resonance frequency, a very effective suppression of pulsation amplitude is achieved. However, given the low operating speed of the compressor (333 RPM), the high speed of sound c of pure hydrogen and the spatial restraints, achieving a f_{HH} sufficiently low appeared to be not realistic.

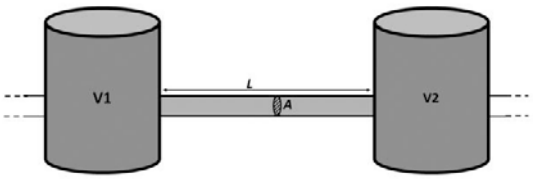

Figure 5: Helmholtz filter to suppress transfer of pulsations

Finally, the large size and considerable volume of the common headers was judged as a valid starting point for detailed numerical optimization.
In addition to the high-level optimizations that were achieved during this review, the meeting also enabled discussion and agreement on the detailed study approached that was deemed most suited for this special project.

4.3 Detailed approach pulsation study

According to the API 618 standard, by default the complete set of operating cases shall be contained in the analysis scope (section 7.9.2): "Pulsation levels shall be reviewed for all specified alternative

by: Niek Albers – HOWDEN; Leonard van Lier – TNO; Maarten van der Biezen – FLUOR

gases, operating conditions and loading steps to assure that pulsation levels will be acceptable under all operating conditions". It is also noted that in cases of multiple operating conditions, the pulsation levels shall be optimized for the conditions on which the unit must operate the greater length of time. Obviously, for the large system described in this paper, the number of operating cases will increase rapidly with increasing number of parallel compressors and increasing number of load steps. The total number of independent permutations P for a system of N parallel compressors (N>2) can be written as follows:

$$P = \sum_{i=1}^{N-1} \binom{N}{i} L^i, \qquad (2)$$

where L the number of compressor loads. To illustrate the implications of rigorously applying the API 618 method to simulate and analyse all independent combinations of N compressors with 4 load steps each (100%-75%-50%-25%), consider the table below.

N	1	2	3	4	5	**6**	7
P	4	8	60	368	2100	**11528**	61740

While up to 3 compressor trains running in parallel may still be manageable, for higher number of parallel compressors this approach requires a scope that 'explodes' beyond realistic proportions. The required analysis effort is considered excessive and also beyond efficient use of resources. Instead the following systematic and step-wise approach is proposed to handle the challenges of the pulsation analysis.

The first step is a pre-study of the compressor cylinders and the pulsation dampers, as stipulated by the API 618 standard (section 7.9.4.2.3.4). In this step, field piping is not yet included in the simulation models and for that reason the interaction between multiple compressors is ignored. Due to the basic assumptions for the boundary conditions at the line connections of the dampers, interaction between the compressors cannot be studied in this step. The purpose of the pre-study is to confirm the optimal design of the dampers by verifying pulsation levels at the line connections and pulsations at the cylinder flange (and in the Cylinder Gas Passage). Moreover shaking forces and unsteady flow losses are quantified and judged based on guidelines in the API 618 standard and experience. Essential part of the pre-study is the optimization of orifice plates at the cylinder flange and the layout of the damper internals (baffles, choke tubes, half pipes etcetera).

The next step is the pulsation analysis of a single compressor train. To this purpose, the simulation model of the pre-study is extended with the field piping and the relevant process equipment (KO drums, coolers). The model contains the first compressor train in full detail. Also, as a first evaluation of the interactions in the system, the simulation model is extended into the connected piping of compressor train #2 (Figure 6). To ensure proper numerical boundary conditions of this extension, the model for compressor train #2 contains the relevant KO drums, coolers and pulsation dampers. The other 4 compressor trains are included with closed isolation valves. This provides the longest possible dead-leg side branches and is considered the worst-case configuration.

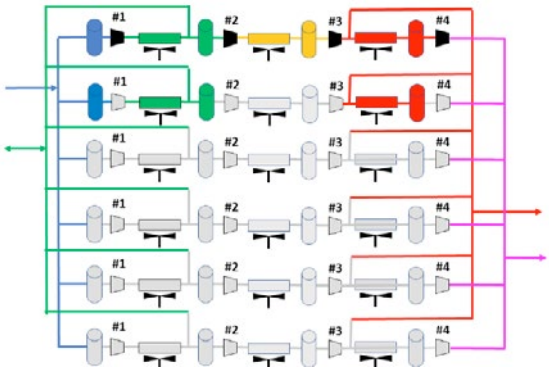

Figure 6: Single-compressor train simulation model (train #1 is shown on top)

The pulsation analysis using this simulation model allows for the optimization of the layout for the individual train. As the layout of the compressor trains are identical, the optimization will applied to all trains alike (to be verified in the next analysis step below). Moreover, the acoustic interaction (transfer of pulsations due to train #1 toward train #2) can be quantified. Finally the observations of the single-train analysis enable a robust selection of critical cases to be studied in the next analysis step (selection of loads and distribution of active compressors).

The next step will include the pulsation analysis on the parallel compressor trains. The simulation model for this task includes all 6 compressor trains and all relevant field piping (Figure 7).

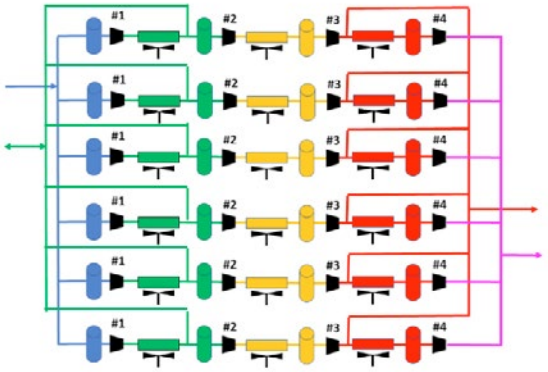

Figure 7: Multi-compressor train simulation model

by: Niek Albers – HOWDEN; Leonard van Lier – TNO; Maarten van der Biezen – FLUOR

For this model, a selection of compressor combinations and compressor loads will be defined, based on the results of the previous step (single-train analysis), by joint discussion of pulsation consultant, compressor vendor and EPC contractor. If required, additional measures to control the acoustic interaction between the trains will be proposed.
Finally, the mechanical response analysis will be performed. In this analysis step, the vibrations and cyclic stresses due to pulsation-induced forces will be computed and compared with applicable allowable limits. The mechanical analysis will be done for a single compressor train and the common field piping. Recommendations will be generalized for the other compressor trains, based on the single-train mechanical analysis and other previous evaluations.
If extension of the mechanical response analysis with the other compressor trains is judged mandatory, this will be recommended and substantiated.

In the API 618 standard, limit values are proposed for the evaluation of pulsation levels:

$$P_1 = \sqrt{\frac{c}{350}} \frac{400}{\sqrt{P_L \times D_I \times f}}. \qquad (3)$$

The limit value P_1 (in % peak-peak of the mean pressure) depends on speed of sound c, line pressure P_L, inner diameter D_I and frequency f. However, it is not explicitly specified how, in case of parallel running compressors, the summation of the pulsation levels shall be handled. Summation of pulsation levels for the evaluation of the pulsation levels is a cumbersome process for several reasons:

- Usually the contributions due to different compressors are calculated separately.
- The API 618 acceptance limit is a frequency-dependent criterion. In case of multiple sources, the summation procedure shall therefore be done for each frequency component.
- Correct summation requires the phase relation between the different pulsation sources. However, the real phase relation between the compressors is not known, and is in general also not fixed. This means that pulsation levels in the piping (the summation of the separate contributions) will display maxima and minima due to interference. The amplitude strongly depends on minute changes in the phase and in general will depend on the location in the pipe system.
- Compressors with the same nominal speed are usually not perfectly synchronized. Small differences in the speed will lead to additional modulation of the amplitude (beating).
- To account for all these uncertainties in the summation, usually the maximum amplitudes of the various sources are added, for each location in the pipe system. Comparing this overall maximum with the acceptance limit in API 618 results in a conservative approach. In particular in case of many parallel running compressors, this approach may be extremely conservative.

To avoid over-conservative estimates, the approach as suggested in an earlier EFRC paper[2] was followed for this project as well:

1. The contribution to pulsation levels by each compressor individually P_i shall not exceed equation (3).

$$P_i \leq P_1 \qquad (4)$$

2. The added pulsation levels due to N compressors shall not exceed equation (3) multiplied by the square-root of N.

$$\sum_{i=1}^{N} P_i \leq \sqrt{N} * P_1 \qquad (5)$$

In the mechanical analysis, which was done on an individual compressor train and the common headers, a strict screening criterion was applied for vibrations (40 mm/s peak-peak) and the stresses (36 N/mm^2 peak-peak). The 'square-root-of-N' approach may be applied to vibration levels. However, for cyclic stress evaluation it is strongly recommended to keep the conservatism, to absolutely ensure mechanical integrity even in case of parallel operation of many compressors.

4.4 Pre-study / damper check

After the preliminary sizing by the compressor vendor on the pulsation damper volumes, the simulation model for the pre-study was constructed using a dedicated digital calculation program (time-domain simulation based on method of characteristics). The models for the different stages are acoustically separated and can be considered independently. As an illustration, the 1st and 4th stage (high-pressure) stage cylinders and pulsation dampers are shown in Figure 8.

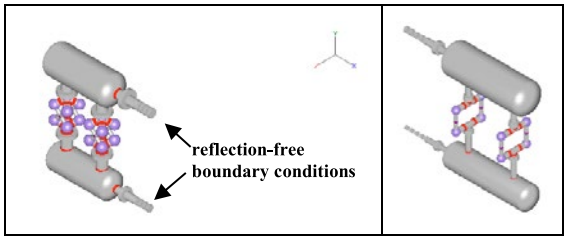

Figure 8: Simulation model for pre-study; 1st stage (left) and 4th stage (right)

by: Niek Albers – HOWDEN; Leonard van Lier – TNO; Maarten van der Biezen – FLUOR

A sufficiently large sensitivity range was applied for the speed-of-sound, fully covering the operating envelope. The pulsation levels at the line connections of the pulsation dampers are within the limits stipulated by API 618. Even over the large sensitivity range, the maximum pulsation levels is 60% of the API 618 limit for the field piping. This confirms the adequate and conservative damper volume, selected by the compressor vendor. By applying restriction orifices at the cylinder flanges, the high-frequency content in pulsations near the valves and in shaking forces was mitigated. Considering the simulation results, internals in the pulsation dampers (baffle plates, choke tubes, half pipes) were not required.

4.5 Pulsation analysis single compressor train

The full complexity of the process piping is illustrated in Figure 9. Including the full process gas pipe system into a single simulation model would be a large amount of complexity for a first screening.

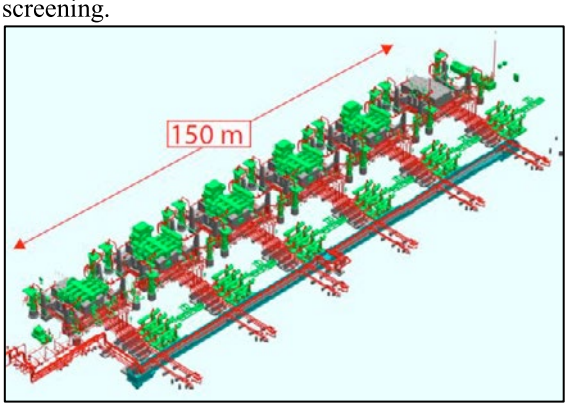

Figure 9: Illustration of the extent and complexity of the system (equipment in green and hydrogen lines in red)

As described before, the first compressor train #1 was selected for the preliminary analysis. The connection to train #2 is also included. This configuration results in the longest closed dead-leg side branch without flow. This is judged as the most realistic worst-case approach for the pulsations in the system.

Since the various parts of the system (suction, interstages and discharge) are acoustically separated, the analysis was split into separate parts, which reduced the complexity and calculation times, and thus sped up the optimization process. An example of the simulation model for the first interstage is shown in Figure 10. The common side stream is included in the model, which results in an acoustic interaction between the compressor trains.

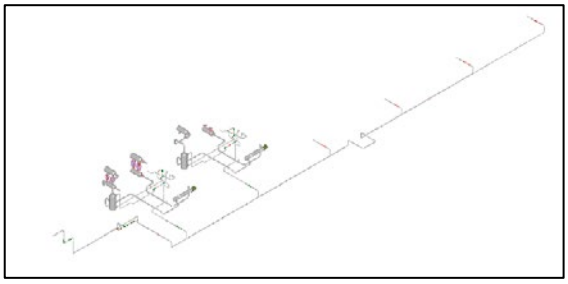

Figure 10: Single compressor train simulation model, for first interstage

For the simulations, the flow due to train #2 was included, to achieve a realistic estimate for the acoustic damping. The side stream flows were included based on the nominal values (compensating the unbalance in flow for the different stages, according to the datasheets).

Pulsation levels were compared with the limit values in the API 618 standard and a considerable exceeding was found (even due to a single compressor). Restriction orifice plates were optimized at the line connections of the dampers. Orifice plates are effective to reduce pulsation levels in the main lines to acceptable limits. For the lower part loads (50% and 25%) the effect of orifices is limited, due to the low pressure loss. Orifice plates in the relief lines were considered but rejected, in order to avoid obstructions in these pressure safety valve lines. As a consequence considerable shaking forces remain in the relief lines, that shall be controlled by mechanical mitigation measures. In the optimized layout, still some minor exceeding remains, but only in the spillback lines, connected to the KO drums. This exceeding may be accepted, since the acoustic interaction with the other trains is extremely weak in this area. Moreover, the piping mechanical layout is favourable (low-elevation, straight sections with multiple supports) and the dominant frequency is low (1st order) and therefore less critical. With respect to the acoustic interaction between the units, the results confirm that the pulsations of train #1 have a considerable effect in train #2. This is explained by the long dead-leg branches and the high speed of sound of hydrogen (large wavelengths and small damping effect).

by: Niek Albers – HOWDEN; Leonard van Lier – TNO; Maarten van der Biezen – FLUOR

4.6 Pulsation analysis multiple parallel compressor trains

The simulation model for a single train was extended with the complete field piping of the other trains, see Figure 11.

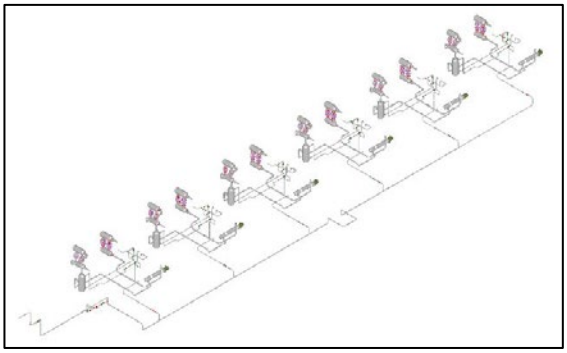

Figure 11: Multi compressor train simulation model, first interstage

Based on the results of the pulsation analysis on a single compressor train, the following list of case was considered fully representative for worst-case operation and selected for detailed analysis:

case	flow	N	T1	T2	T3	T4	T5	T6
1	150%	2	C	50%	100%	O	O	O
2	200%	2	O	O	100%	100%	O	C
3	250%	4	100%	50%	O	50%	C	50%
4	300%	4	O	C	50%	50%	100%	100%
5	325%	4	100%	100%	C	O	50%	75%
6	350%	4	50%	100%	100%	100%	O	O
7	375%	4	100%	100%	100%	75%	C	C
8	400%	4	100%	100%	100%	100%	O	C
9	425%	5	C	50%	75%	100%	100%	100%
10	450%	5	50%	100%	100%	100%	100%	O
11	475%	5	O	75%	100%	100%	100%	100%
12	500%	5	100%	100%	100%	100%	100%	C

This selection spans the total range of flow from 150% to 500% in sufficiently small steps (up to 100% was already verified in the single-train analysis). Note that the 25%, 50%, 75% and 100% load steps were already studied in full detail in the previous analysis step for the single compressor train. For each case, N calculations were run that allow to determine the individual contributions (in total 48 separate simulations). This selection reflected a good coverage of the positions of the sources in the system, the distribution of loads (25% load is only run shortly, and was discarded as an operational case), and the options for opened (O) or closed (C) isolation valves to the idle compressor trains. Though this selection of 12 case covers only 0.1% of all possible combinations, it was concluded that it is adequate for a complete screening of the system.

It was concluded that the sizing for the individual compressor train proved to be adequate also in case of the full parallel operation. The practical approach to weigh the statistical chances of worst-case addition of maximum pulsation amplitudes with the square-root of *N*, proved to be a realistic approach. Several arguments can be formulated that confirm that pulsation amplitudes do not scale linearly with the number of compressors. For example, the total flow in the system generally increases with increasing number of compressors, which enhances the acoustic damping and prevents a strong amplification of pulsations in resonance conditions. In addition, when multiple compressors are run, the amount of closed isolation valves is reduced and the number of strong acoustic resonators is limited. Of course, in the capacity control strategy, situations where multiple compressors are running at a very low load shall be avoided. For example, running 5 compressors at 25% is from a pulsation point-of-view worse than 2 compressors running at 75% and 50%.

Shaking forces in the optimized layout were considered acceptable. It was recommended to proceed with the final step in the analysis (mechanical response analysis).

4.7 Mechanical response analysis

This mechanical analysis was done on a single compressor train and the common headers, using all information from previous analysis steps with respect to the interaction between the compressor trains (addition of pulsations and shaking forces).

As input for the mechanical response analysis, the worst-case conditions have been selected from the results of the pulsation analysis. The conditions from the sensitivity range in the speed-of-sound that yield the largest shaking forces were used to excite the mechanical structure of piping, equipment and supporting.

Instead of modelling each pipe support with the details of the underlying steel structure, the effect of the pipe supporting structures was included as an effective stiffness for each support. In this way, the mechanical interaction of the various stages can be separated and again a modelling approach of separated systems (suction, interstages, discharge) is allowed. Because a large part of the piping is running over (very stiff) common supporting frames, the approach of an effective stiffness based on pipe line size is considered a conservative approach in these areas. On potentially critical areas, such as the high-elevation inlet into the suction dampers, the supporting structure was analysed in detail with Finite Element modelling, ensuring adequate separation of the mechanical resonance frequencies with the dominant 1st and 2nd order of the compressor speed.

by: Niek Albers – HOWDEN; Leonard van Lier – TNO; Maarten van der Biezen – FLUOR

Figure 12: Aerial view of compressor building construction

The interaction between the compressor was considered explicitly in the evaluation of the calculation results for vibrations and cyclic stresses. The evaluation of the interaction focussed on both the amplitudes and the frequencies. Even though the acoustic interaction between the trains is significant considering the *amplitudes* of the shaking forces, at the critical locations it appeared that often the higher orders of the compressor speed are most critical (for example the 4th order). The acoustic interaction for those higher orders is less strong, and as a consequences the analysis provided a robust argumentation that vibrations and stresses are within allowable limits, even in case of parallel operation.

The layout of the process piping was nearly identical for the different compressor trains due to the design of the compressor building, see Figure 12. The only exception was a small difference in the PSV lines (due to the inclined orientation of the flare header). The choice to apply the mechanical analysis on train #1, with the longest PSV line, is considered the worst-case assumption both from pulsation and vibration perspective.

The mechanical analysis model did not include the compressor frame, crosshead guides and cylinders. The intent of a mechanical natural frequency analysis of the combined compressor and pulsation suppression device mechanical model is avoiding mechanical resonances of this system at frequencies where high shaking forces exist. It is acknowledged that certain compressor designs, especially when mounted on a concrete foundation, can be considered as rigid and modelled as rigid elements.
It is known from prior simulations and field measurements that for the particular compressor type and mounting under consideration, the lowest natural frequencies are sufficiently removed from the dominant shaking force frequencies. Therefore the mechanical piping system model is extended to include the pulsation dampeners and starts at the cylinder flanges, which are assumed to be rigid. In addition, the pulsation-induced shaking forces are low and well within the applicable guidelines, ensuring that forced vibrations will not lead to excessive vibration levels.

4.8 Additional considerations

Another challenge that resulted from the requirements for this particular compressor system are the flow pulsations that occur near the flow metering equipment. It is known that pulsation measurement equipment may suffer from the effect of unsteady flow and standards are available to estimate the effect of the error[4]. Depending on the type of flow meter, prediction of the error once the flow pulsation amplitude is known is not a straightforward task and requires a large amount of detailed input information from the flow meter vendor[5]. The standards and guidelines generally address the measuring error, when the metering instrument is operated in its nominal flow range (Q_{NOM}). However, in the case of 'nearly zero flow' (Q_0~0), the *relative* flow pulsation levels may be excessive. In this system, this situation may occur in the spillback lines but more importantly in the side streams. In the side streams, the flow may be very small and (in case of the 1st interstage) even bi-directional. Reducing relative flow pulsation levels to very small values is then an unrealistic challenge. In particular at low part load the mean flow and as a consequence the side stream flow may be very small. Even a small flow pulsation amplitude will lead to large relative amplitudes and even flow reversal near the flow meter. In addition, the effect of the orifice plates will be limited at the lower part loads.
It is therefore recommended to assess the effect of the measurement uncertainty on the control system. In this case, mitigating measures have been applied in the control system to ensure control stability in 'near-zero flow' cases

Due to large dimensions of the system and the large capacity of the parallel compressor system the risk on flow-induced pulsation and vibration effects is more urgent than in smaller systems. Flow-induced pulsation issues may occur when high-speed and high-density gas is grazing along a closed side branch, see Figure 13. In case lock-in occurs (coincidence of flow instability with acoustic resonances inside the closed branch) large pressure pulsations and vibrations may be observed. Screening methods to quantify the risks can be

by: Niek Albers – HOWDEN; Leonard van Lier – TNO; Maarten van der Biezen – FLUOR

found in the Energy Institute AVIFF guideline[6]. For this system, in particular at the suction side, the local gas velocity in the headers is very considerable (up to 50 m/s). Though in systems with a dominant pulsation source (such as a reciprocating compressor or a plunger pump) incidents with flow-induced pulsation effects are reported very rarely it was flagged as a potential issue for this system. To control this risk the length of the pipe sections from the header to the isolation valves was minimized. It is not expected that acoustic resonances will develop inside the closed branches. Moreover, considering the low density (low kinetic energy) and the relatively low Mach number, the risk on flow-induced pulsation effects was judged as acceptable.

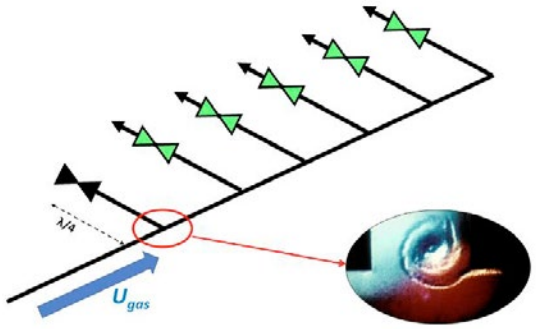

Figure 13: Layout with closed side branch with grazing flow with high gas velocity

5 Conclusions and recommendations

The engineering of very large compressor systems demands additional efforts to ensure an efficient project execution and reliable system and compressor design.
Sufficient attention needs to be given to the torsional characteristics of large reciprocating compressor, both in an early design stage as well as during the detailed design and analyses of the rotating system. Meeting basic separation margins do not rule out the consideration for further vibration and stress analyses to ensure long-term reliable operation. Control strategy and systems should be designed taking both process needs and compressor system optimization aspects as well as operator support into account.

The API 618 standard does not provide explicit guidelines for the pulsation and mechanical response analysis approach and the acceptance criteria for large compressor systems with many parallel compressors. This paper proposes a practical, systematic and cost-effective analysis approach starting from the optimization of a single compressor train.
For the parallel operation, a selection of the many possible combinations of compressors and loads must be made. This selection shall be based on the results of the analysis on the single compressor train. The selection shall include an adequate coverage of pulsating compressors, shall cover the full capacity range of the system, shall cover the range of loads and shall cover the various options for closed and opened isolation valves to the compressors and the side stream branches.

The contribution to pulsation levels by the individual compressors shall not exceed the limits in API 618. In general, the pulsation levels due to a single compressor in operation are most critical. In case of parallel operation, the individual pulsations are lower, due to the higher capacity and the subsequent larger acoustic damping. The acceptance criterion for addition of maximum pulsation levels in parallel operation (N compressors) was based on the API 618 acceptance limit, multiplied by the square-root of N.

Ensuring low relative flow pulsation levels may be difficult for the side stream branches, carrying a low flow. This is in particular true when the compressors are running at low part loads, due to the limited effect of the orifices plates in these conditions. A careful selection of the type of flow meter is essential. After the pulsation analysis, the flow pulsation levels shall be shared with the flow meter manufacturer to ensure an adequate design of the instrument and the control system.

In case of very large compressor systems, it is essential that the basic layout of the pipe system is chosen in a favorable way with respect to pulsations and vibrations. This requires a review with all concerned disciplines and parties at an early stage of the project; earlier than common practice for pulsation studies.

References

[1] API 618 standard, 5th edition (2007): Reciprocating Compressors for Petroleum, Chemical and Gas Industry Services.
[2] Smeulers, J.S.M; Blodgett, L.E. (1999): Improvements and Extensions to API 618, related to pulsation and mechanical response studies, 1st EFRC symposium, Dresden.
[3] API 688 recommended practice, 1st edition (2012): Pulsation and Vibration Control in Positive Displacement Machinery Systems for Petroleum, Petrochemical, and Natural Gas Industry Services.
[4] ISO/TR 3313 (1998), Measurement of fluid flow in closed conduits – Guidelines on the effects of flow pulsations on flow-measurement instruments.
[5] van Lier, L.J.; Crena de Iongh, R. (2012): Impact of pulsations on flow metering accuracy, 8th EFRC conference, Düsseldorf.
[6] Energy Institute (2008): Guidelines for the Avoidance of Vibrations Induced Fatigue Failure in Process Pipework, 2nd edition.

EUROPEAN FORUM
for RECIPROCATING
COMPRESSORS

EFRC

TECHNISCHE UNIVERSITÄT DRESDEN

Reversible Usage of a Reciprocating Compressor as Expansion Machine by the Application of new Force Actuated Valves

by:

Christian Stöckel, Christiane Thomas, Ullrich Hesse
Bitzer Chair of Refrigeration, Cryogenics and Compressor Technology
Technische Universität Dresden
Dresden, Germany
christian.stoeckel@tu-dresden.de

11th EFRC CONFERENCE
September 13 – 14, 2018, Madrid

Abstract:
Forced opening of the suction valve is a common known method for compressor capacity control. Redesigning the valves of a compressor in a way, that both suction and discharge valve can be forced actuated, the operation mode of the compressor can be switched in order to run the compressor reversible as expansion machine. This might be interesting for regaining energy from gas storage processes like for example in underground gas storages. The present paper deals with the first step of the experimental testing of such system. A compressor discharge valve, which can be forced actuated by impinging the sealing elements with a pneumatic pressure, was designed. The tests were performed within a compressor, which was equipped for that reason with additional measuring devices. At different discharge pressure levels the forced opening of the deliver valve was investigated. The results give a first experimental insight into the working principle and give directions for improvement of the control strategy and the valve design. The experimental data is also needed for design of suction valves which use a similar working principle. With both valves equipped the test compressor will be able to run reversible as expander.

by: Christian Stöckel, Christiane Thomas, Ullrich Hesse – TU Dresden

1 Introduction

Enhancing the efficiency of existing plants and machinery can lead to both ecological and economical benefit. Several possibilities for the improvement of reciprocating compressors in regard to efficiency were introduced in the past. Especially step less capacity control was one focus during the last years[1,2,3,4].A step even further is an actual research topic within the EFRC R&D-group that was presented during the last EFRC-Conference[5]: the during normal operation self-acting compressor valves, both suction and discharge valve, are redesigned to be capable of being forced-actuated. This enables a new operation mode of the existing compressor, in particular re-expansion of compressed gas, e.g. from underground gas storages, to recuperate energy.

Within the present paper actual results of the experimental testing of the abovementioned valves are canvassed, more precisely the testing of the discharge valves. Using them forced actuated a compressor flow control can be realized, however this is different to usual systems, where the suction valves are manipulated. In section 2 a summary about the new designed valves working principle is given. Afterwards the experimental setup is described in section 3. The results and their discussion is presented in section 4 and 5. Within section 6 the conclusions of the experimental testing and an outlook of the further test program are given.

2 Valve working principle

The initial layout of the new developed valve is a poppet valve. Different from commonly used poppet valves the small bores, which are bearing the sealing elements and their retention spring, are not connected directly to the valve pocket, but to an additional slider valve. By changing the position of that slider valve the pressure level inside the bores, subsequently named poppet control chamber, can be changed. In case of the compressor discharge valve the poppet control chamber can be connected either with the compressor discharge chamber or the suction chamber. During normal compression the pressure level in the control chamber is set to discharge pressure, therefore the valve is like an ordinary poppet valve self-actuated. By switching the pressure level in the poppet control chamber to suction pressure a lifting force is generated on the sealing element due to the pressure difference on the poppet surface facing the cylinder and its' opposite. A detailed description of the valve design and the working principle can be found in previous publications[5,6], a simplified schematic is shown in figure 1.

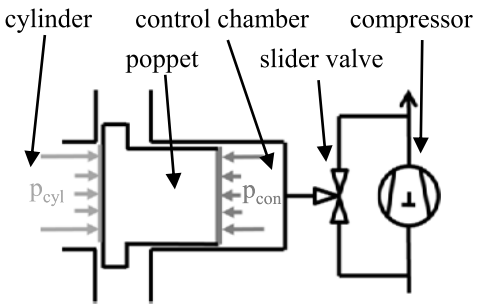

Figure 1: Simplified schematic of the poppet valve control

3 Experimental setup

The experimental testing was performed within an Atlas Copco AR1. It is a two stage compressor with two pistons, each double acting. The cylinders are arranged in an L-shape, with the axis of stage 1 vertical and stage 2 horizontal. Each working chamber is equipped with two suction and two discharge valves. An intercooler is mounted between the two stages. A sectional drawing of the compressor can be found in figure 2, the nominal compressor data of the 1st stage in table 1.

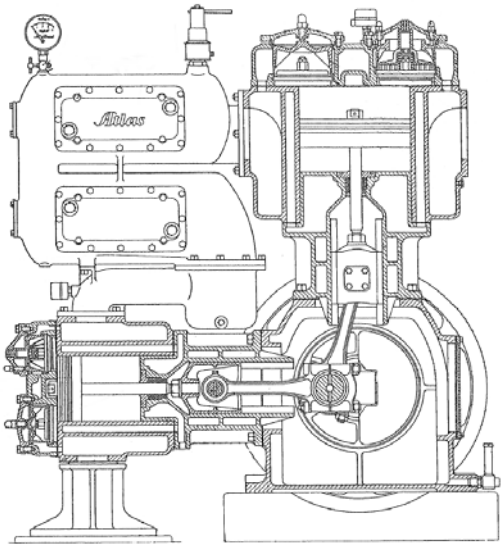

Figure 2: Sectional drawing of the test compressor Atlas Copco AR1[7]

Table 1: Nominal data of the 1st stage of the test compressor Atlas Copco AR1[7]

compressor speed	585 rpm
discharge pressure	2.8 bara
nominal flow	8.5 m³/min
piston diameter	285 mm
stroke	150 mm
piston rod length	295 mm

by: Christian Stöckel, Christiane Thomas, Ullrich Hesse – TU Dresden

The testing was performed only in the head ended working chamber of compression stage 1. To avoid interference with the other working chambers they were put out of operation by meaning of removing all valves from them, respectively the suction valves at the crank side working chamber of stage 1. The discharge valves of the 1st stage were replaced to the new developed ones, hence enabling the possibility of a reverse flow control by forced opening of the discharge valves.

Process monitoring was performed by means of various sensors. High speed pressure sensors were mounted to the working chamber as well as suction and discharge chamber of the 1st stage. Thermocouples were used to evaluate mean temperature values. A proximity sensor based on induction was utilized for determination of the top dead center position (TDC). The motor power was read directly from the PLC, which was used to control the motor. At the compressor outlet duct a filter was positioned to remove debris and oil droplets from the discharged gas. Afterwards the gas flow was measured by use of a calorimetric flow sensor. A screw-down non-return valve (SDNR) was used to set the pressure level at the outlet duct before the air was discharged over a muffler.

4 Testing procedure and results

The new developed valve was tested at different operating points. For that purpose on the one hand the discharge pressure of the machine was varied, on the other hand the end of the interval for forced opening was varied. Overall 12 different operating points were tested. A short overview is given in table 2.

Table 2: Overview of performed tests

discharge pressure level	tested opening intervals
l1: 2.0 bara	w/o, i1, i2, i3, i4, i5
l2: 2.5 bara	w/o, i1, i2, i3, i4
l3: 3.0 bara	w/o, i1, i2, i3

The intervals of crank angle variation are outlined in table 3.

Table 3: Crank angle intervals of forced actuation

label	**interval**
w/o	without actuation
i1	330° .. 10°
i2	330° .. 20°
i3	330° .. 30°
i4	330° .. 40°
i5	330° .. 50°

First analysis of the pressure curves has shown, that there is a strong deviation in the position were the discharge valve closes. That leads to variation in the cylinder pressure indicator diagram, as exemplarily shown in figure 3.

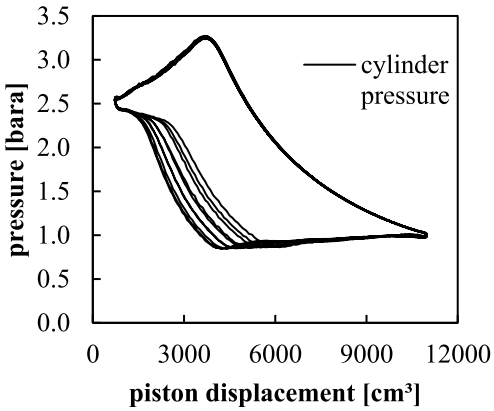

Figure 3: Example of the pressure indicator diagram for 10 serial crank turns

The cause for that deviation will be discussed later. However, for the further analysis the measured data of 100 serial crank turns was used to calculate a mean indicator diagram.

Figures 4 and 5 show the pressure-volume and the pressure-crank-angle-diagrams for discharge pressure level l1. The plots depict the mean values of the cylinder pressure. To enhance the visibility of the forced opening within the pressure-crank-angle-plot, the abscissa is only shown from 0° crank angle to 180° crank angle. Also only each 10° crank angle a data point is plotted for that purpose.

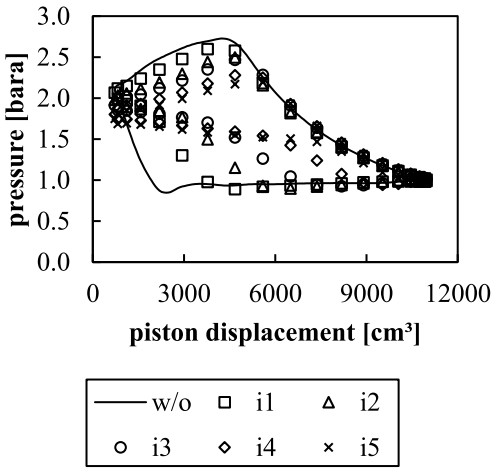

Figure 4: Cylinder-pressure over piston displacement for different operating points at discharge pressure level l1

by: Christian Stöckel, Christiane Thomas, Ullrich Hesse – TU Dresden

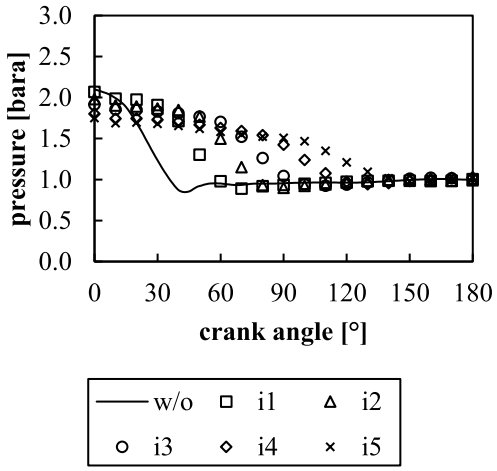

Figure 5: Cylinder-pressure over crank angle for different operating points at discharge pressure level l1

The indicator diagrams for the discharge pressure level l2 and l3 can be seen in figures 6 to 9.

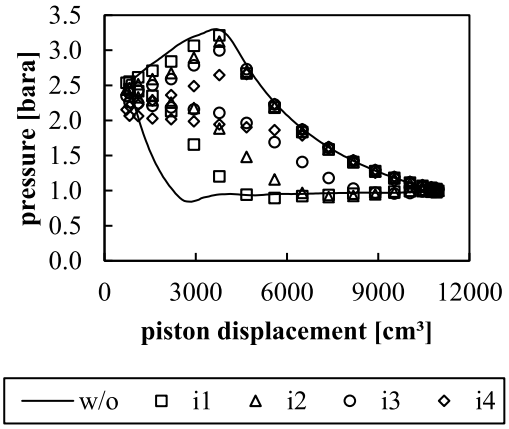

Figure 6: Cylinder-pressure over piston displacement for different operating points at discharge pressure level l2

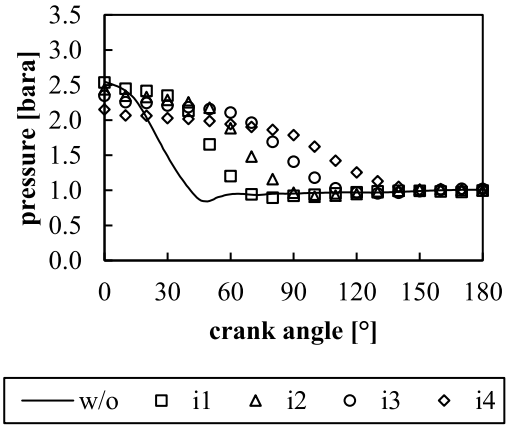

Figure 7: Cylinder-pressure over crank angle for different operating points at discharge pressure level l2

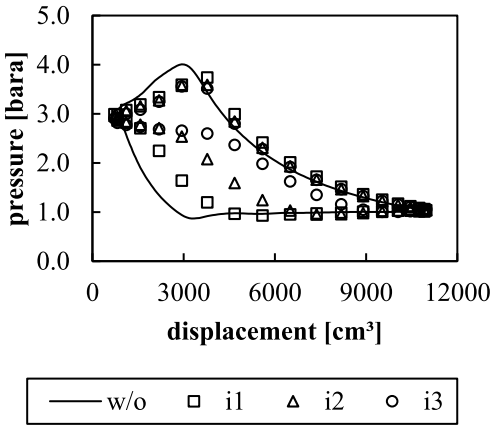

Figure 8: Cylinder-pressure over piston displacement for different operating points at discharge pressure level l3

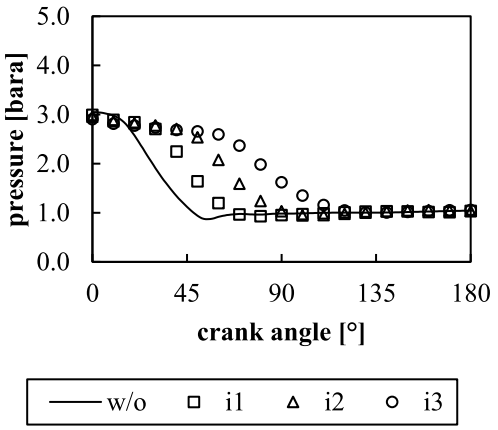

Figure 9: Cylinder-pressure over crank angle for different operating points at discharge pressure level l3

The internal work W_i within one crank turn can be calculated by integrating the cylinder pressure p over the piston displacement V:

$$W_i = -\oint_V p\, dV. \qquad (1)$$

The calculated values for all tested operating points can be found in table 4.

Table 4: Calculated internal work W_i for the tested operation points (in J)

	w/o	i1	i2	i3	i4	i5
l1	973	787	618	535	407	318
l2	1129	854	637	453	273	
l3	1215	1057	718	403		

The compressor speed n was calculated from the time difference between the TDC-signals and varied for all tests within a range of 614 rpm up to

by: Christian Stöckel, Christiane Thomas, Ullrich Hesse – TU Dresden

616 rpm. From compressor speed and internal work the internal power P_i can be calculated to

$$P_i = n \cdot W_i. \quad (2)$$

The results of that calculation are shown in table 5.

Table 5: Calculated internal power P_i for the tested operating points (in kW)

	w/o	i1	i2	i3	i4	i5
l1	9.97	8.07	6.34	5.49	4.18	3.26
l2	11.55	8.74	6.53	4.65	2.80	
l3	12.44	10.82	7.36	4.14		

The measured volume flow rate V for each data point can be found in table 6. The signal is transformed by the sensor internally into Nm³/min at standard atmospheric conditions.

Table 6: Measured volume flow rate for the tested operating points (in Nm³/min)

	w/o	i1	i2	i3	i4	i5
l1	3.96	3.37	2.80	2.11	1.20	0.39
l2	3.86	3.13	2.29	1.28	0.35	
l3	3.89	3.10	2.12	0.92		

The pressure levels in suction (p_s) and discharge chamber (p_d) were directly measured with fast reacting pressure probes. For calculation of the pressure ratio Π the averaged values over one crank rotation were used:

$$\Pi = \frac{p_d}{p_s} \quad (3)$$

Assuming the compressed air as ideal gas, with the specific heat capacity c_p and the isentropic coefficient κ, and knowing the compressor inlet temperature T_s from the measurement to be 20 °C the specific isentropic compressor work w_{is} can be calculated

$$\Delta w_{is} = c_p \cdot T_s \left(\Pi^{\kappa-1/\kappa} - 1 \right). \quad (4)$$

The internal efficiency η_i of the compressor can afterwards be derived from

$$\eta_i = \frac{\varrho \cdot \dot{V} \cdot \Delta w_{is}}{P_i}, \quad (5)$$

where ρ is the density of air under standard atmosphere. The calculated efficiencies of the operating points can be seen in table 7.

Table 7: Internal efficiency ηi of the compressor at different operating points

	w/o	i1	i2	i3	i4	i5
l1	0.53	0.54	0.52	0.43	0.28	0.11
l2	0.58	0.61	0.57	0.42	0.16	
l3	0.65	0.58	0.57	0.43		

The electrical power consumption of the motor for the compressor was monitored, the mean values for the different operating points are summarized in table 8. At pressure level l2 the power meter failed, hence the data is not shown.

Table 8: Motor power consumption (in kW) during operation at the different pressure levels l and opening intervals i

	w/o	i1	i2	i3	i4	i5
l1	8.65	7.66	7.00	6.25	5.64	5.11
l3	10.30	8.88	7.61	6.27		

5 Discussion

As already mentioned in the previous section, there is a deviation of the crank angle positions, where the forced opening of the discharge valve should end. This variation occurred between serial crank turns at a fixed value for valve closure. The slider valve, which changes the pressure inside the poppet control chamber, is electro-magnetically actuated. The signal for that actuator is generated by a control program which is running on a standard personal computer. Due to the operation speed of the control program on the PC there is some time difference in generation of the control signal, which then leads to varying actuation intervals. Since the starting point of the forced actuation is within the already opened discharge valve, that effect is not observed at that point.

From the indicator diagrams (figures 4 to 9) it can be seen that the 1st stage discharge pressure is decreasing when the forced opening interval is increasing. That effect is caused by the setting of the pressure level at the compressor outlet. By setting the pressure with the SNDR valve the flow rate is specified. However, the flow rate has also an influence on the internal compressor losses, means the pressure drop between 1st stage outlet and the measuring point for the discharge pressure is also changing. That effect leads to the abovementioned decrease of the discharge pressure of the 1st compression stage. Setting the pressure level by use of a pressure probe installed in the discharge chamber of the monitored stage will remove that effect at additional tests in the future.

by: Christian Stöckel, Christiane Thomas, Ullrich Hesse – TU Dresden

In figure 10 the motor power and the calculated internal power (tables 8 and 5) are plotted in one diagram. A discrepancy can be seen in the graph, since in some operating points the measured motor power is less the internal power, which is physically impossible. Pressure and temperature probes, as well as the flow meter are calibrated. That leads to the assumption, that the motor power meter is not working correct. A re-calibration is necessary for evaluation of the overall compressor efficiency.

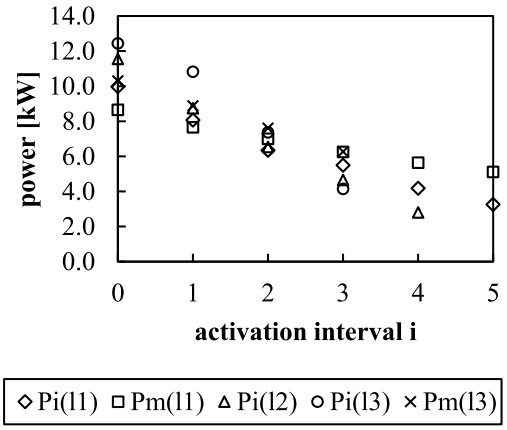

Figure 10: Calculated internal power P_i and measured motor power P_m for different operating points (interval i0 stands for no forced actuation)

However, only looking at the internal powers the trend of the data is as expected. With rising discharge pressure level the power is higher, by increase of the forced actuation interval the power consumption is decreasing with a nearly linear inclination.

The internal compressor efficiency (table 7) is largest at pressure level 3, which is near the nominal compressor working point. However, the high losses within the discharge valve, as can be seen from the pressure indicator diagrams (figures 4 to 9), lead to poor efficiencies. For the advancement of the design a flow-optimization needs to be done, by means of increasing the flow cross section and improving the geometry.

Plotting the flow rate (table 6) over the activation interval, as shown in figure 11, it can be seen that the volume flow of the compressor can nearly be decreased to idle mode. It is assumed that there are no irregularities in operation between the measured points, hence it is presumed that with the designed system a step less capacity control is possible. Also it can be seen that with increasing discharge pressure level a smaller activation interval is needed to achieve a similar flow rate.

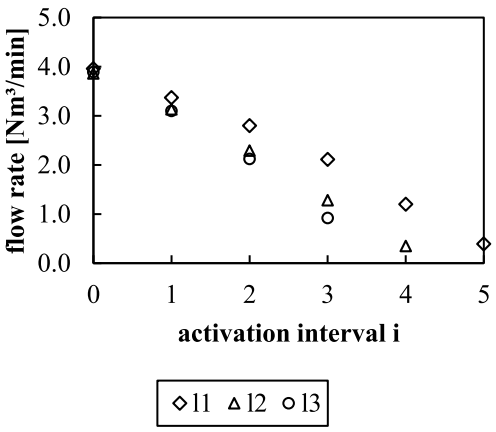

Figure 11: Flow rate for different operating points (interval i0 stands for no forced actuation)

From the plotted indicator diagrams (figures 4 to 9) the crank angle, where the discharge valve closes, can be determined. The data is shown in table 9.

Table 9: Discharge valve closing position for different operation points extracted from the pressure indicator diagrams

	i1	i2	i3	i4	i5
set	10°	20°	30°	40°	50°
l1	30°	50°	60°	80°	100°
l2	35°	50°	65°	90°	
l3	30°	45°	60°		

It can be seen, that there is a delay of the valve closure in relation to the set value. This delay is caused by the compressibility of the gas inside the poppet control chamber. However, unlike than expected the delay is increasing with increased opening interval. It was assumed, that the decrease of the cylinder pressure during forced opening leads to a higher pressure difference over the poppet, resulting in a larger closing force and hence faster movement of the sealing element. However, for better understanding of this effect an instrumentation of the poppet control chamber, by means of implementation of a pressure probe, is necessary. Also a sensor for measurement of the valve lift would lead to a more accurate statement on the closing delay. Actual the test compressor is being equipped with such sensors for further testing.

6 Conclusions and outlook

With the experimental testing of the new developed, forced-actuated discharge valves for a reciprocating compressor, the functionality of the basic design concept was proven. A step less capacity control could be achieved for a variety of operation points. It has also been shown, that the

internal efficiency of compression is decreasing with increasing interval of forced actuation.

However, the tests also have shown an extensive amount of optimization potential, especially in pressure losses, resulting into the need of further investigations. A stringent necessity is the enhancement of the signal for the slider valve actuation, which is switching the control pressure for valve actuation. The actual inaccuracy leads to a massive difference of valve closure point. Next step before further testing is for this reason the application of a new strategy for generation of the electrical control signal.

Afterwards the valve closure delay needs to be quantified for the different operation points for the discharge and also the suction valve. The experimental testing will be finished by application of the valve design to the 2nd compressor stage. However, in that stage the discharge valves will be mounted in the suction valve pocket and vice versa. That will allow to run the 1st stage of the test rig as compressor and the 2nd stage as expansion machine.

7 Acknowledgment

This work was supported by the European Forum for Reciprocating Compressors within the project “Valve systems for Piston Reversible Compression-Expansion-Machines”.

References

[1] Aigner, R., Voser, A., & Allenspach, A. (2010). Development of a Stepless Flow Control System. In Proceedings of the 7th EFRC Conference. Florence.

[2] Bin, T., Yuanyang, Z., Liansheng, L., Guangbin, L., Le, W., Qichao, Y., … Wenhui, M. (2013). Thermal performance analysis of reciprocating compressor with stepless capacity control system. Applied Thermal Engineering, 54(2), 380–386. http://doi.org/10.1016/j.applthermaleng.2013.01.036

[3] Schiavone, M., & Raggi, A. (2008). Electromechanical Actuator for Reciprocating Compressor Stepless Control. In Proceedings of the 6th EFRC Conference (pp. 180–187). Düsseldorf.

[4] Flade, G., Ritzen, F. J., & Hoff, K. (2011). Patent No. DE1020011079478A1. Germany: Deutsches Patent- und Markenamt.

[5] Stöckel, C., Nickl, J., Thomas, C., & Hesse, U. (2016). A novel valve design for combined reciprocating piston expansion and compression machines. In Proceedings of the 10th EFRC Conference (pp. 211–223).

[6] Stöckel, C., Thomas, C., Nickl, J., & Hesse, U. (2017). Investigations on pneumatically forced-actuated compressor valves. In IOP Conference Series: Materials Science and Engineering (Vol. 232). http://doi.org/10.1088/1757-899X/232/1/012031

[7] Atlas Copco (1969). Data Sheet Compressors AR1KT, AR4KT. Machine list No. 0856

TNO innovation for life

Identification and mitigation of Cylinder Gas Passage Pulsations

by:

Leonard van Lier
TNO, Delft, The Netherlands
leonard.vanlier@tno.nl

Jan Smeulers
TNO, Delft, The Netherlands
jan.smeulers@tno.nl

11th EFRC CONFERENCE
September 13 – 14, 2018, Madrid

Abstract:
Pressure pulsations are an intrinsic feature of reciprocating compressor systems, that may lead to various issues. The API 618 standard is the most relevant guideline for pulsation and vibration control during the design stage. However, the main focus of API 618 is on pulsation effects in the field piping, and less on the pulsations close to the compressor. Recent experiences indicate that these Cylinder Gas Passage (CGP) pulsations can lead to serious consequences, such as limited lifetime of compressor valves, high-frequency vibrations of the compressor manifold, reduced compressor performances and failure of compressor parts. To enhance awareness and to formulate best practices to identify and control CGP pulsations, a pre-competitive research project was assigned by EFRC's R&D group. The investigation included literature study, interviews with experts from industry and review of analysis and measurement techniques. A systematic discussion and demonstration of harmful effects is presented, along with best practices for numerical evaluation and field measurements. Furthermore screening techniques that do not require detailed simulation tools are presented, enabling a risk assessment very early in the design. The benefits and limitations of the common control techniques are discussed, along with potential benefits of more advanced control techniques.

by: Leonard van Lier, Jan Smeulers – TNO

1 Introduction

Reciprocating compressors are known to be an intrinsic source of pulsations. If the potential negative effects of pulsations are not carefully considered and mitigated, severe issues may be the consequence. Negative impact may occur on the field piping system and attached equipment (high vibrations, fatigue failure, issues with flow meters, erroneous PSV openings etcetera), but also more locally on the compressor itself (reduced efficiency, issues with integrity of the compressor valves and other components). For that reason, guidelines and standards have been formulated over the past decades, to analyse the effect of pulsations and mitigate the consequences to acceptable levels. The API 618 standard[1] is the most commonly used standard, to analyse and mitigate the effects of pulsations during the design stage. In addition to the development of industrial standards, also the capabilities of modelling tools have greatly improved over the past decades. Conventional techniques to mitigate pulsations include the design of pulsation dampers, optimizing the pipe system and the application of restriction orifice plates.

In spite of the availability of industrial standards and robust simulation tools, issues related to pulsations remain present in the industry. In particular in the gas passages within the compressor, excessive pulsations have been observed in field cases from recent history. In this paper, these pulsations will be called Cylinder Gas Passage (CGP) pulsations. Especially high-frequency CGP pulsations become more important and challenging due to increasing compressor speeds, larger spread in gas composition, larger cylinders and increased application of step-less flow control systems.

The EFRC Research Group has granted TNO an assignment to make an inventory of the present knowledge of CGP pulsations, its effects and control techniques. This was done by a literature survey and interviews with experts from the industry. This work has been carried out under EFRC contract and was reported to the EFRC R&D members[2]. A summary of the findings is presented in this paper.

2 Harmful consequences

The awareness on CGP pulsation effects as fundamental root cause is limited. The sense of urgency is relatively limited, at least among end users, EPC contractors and compressor vendors. However, some negative effects are observed in industry, for example by condition monitoring experts and pulsation consultants, though the relation with pulsations as root cause is not always clearly demonstrated.

Potential negative consequences that are specific for CGP pulsations include:

- Disturbance of the compressor valve operation: increased impact speeds, valve fluttering and reduced compressor valve life time.
- Mechanical vibrations on the compressor manifold (cylinders, pulsation dampers);
- Mechanical vibrations of Small Branch Connections (SBCs) in the vicinity of the compressor such as vents and drains on the pulsation bottles or instrument connections at the inlet/outlet piping of the compressor;
- Degraded compressor performance (increased power consumption and/or reduced capacity);
- Additional dynamic loading of compressor mechanical parts, such as piston, piston rod, cross-head pins and crank shaft.
- Excessive pulsations may influence also the rod reversal, and this has an impact on the lubrication of wearing parts of the compressor.
- Transfer of high-frequency pulsations, originating from resonance effects in the CGP, towards the field piping.

3 Guidelines and Standards

The API 618 standard[1] stipulates a relatively elaborate analysis approach to avoid pulsation and vibration issues. However, the focus of API 618 is on the field piping, and the guidelines for pulsations inside the compressor are very simplified and basic. Moreover, conventional measures are sometimes not adequate to resolve issues with CGP pulsations. Effective evaluation and mitigation of CGP pulsations may require a more robust and elaborate analysis approach, accurate at higher frequencies. It has been observed by recent field experiences that high-frequency pulsation-induced excitation forces in the cylinder and CGP play an important role in vibrations problems of the compressor manifold system. This has also been recognized by the API and in a future revision of the API 688[3] there will be more focus on this and requirements with respect to modelling will be more stringent.

API 618 stipulates (as a minimum) the following steps, in a design approach 3 study:

- Pre-study, ignoring the effects of the field piping and focussing on the cylinders and pulsation dampers.
- Pulsation analysis of the field piping.
- Mechanical response analysis of the field piping (may be extended with the

by: Leonard van Lier, Jan Smeulers – TNO

mechanical response of the compressor manifold).

The first step (pre-study) addresses the issues with CGP pulsations. This step is typically modelled with reflection-free boundary conditions at the damper line connections.

Though considered a good starting point that results in an adequate design in the majority of cases, some remarks shall be made before using the acceptance limits for CGP pulsations proposed in API 618. The API 618 stipulates a dedicated criterion for pulsations at the cylinder flange:

$$P_{cf} = 3R, \text{ or } 7\%, \text{ whichever is lower} \qquad (1)$$

with R the compressor ratio (P_{dis}/P_{suc}).

The criterion for pulsations in the field piping is:

$$P_{piping} = \sqrt{\frac{c}{350}}\frac{400}{\sqrt{P_L \times ID \times f}}, \qquad (2)$$

with c the speed-of-sound in the gas [m/s], P_L the line pressure, ID the inner pipe diameter [mm] and f the frequency [Hz]. Both limits shall be interpreted as % peak-peak of the mean pressure. Comparing these independent limits confirms that:

- The criterion (1) is limited to the cylinder flange only, implicitly assuming that location being representative for the complete cylinder area. Criterion (2) on the other hand is dedicated to each location in the field piping stipulating an appropriate limit for each location separately, considering the line pressure, pipe diameter and frequency.
- The criterion (1) specifies generally higher values than (2), which implicitly qualifies the performance of the pulsation dampers, to suppress the transfer of pulsations to the field piping. It also implicitly assumes that the mechanical layout in the immediate vicinity of the cylinders is sufficiently robust to withstand higher dynamic loading.
- The criterion (2) considers a frequency dependency that is absent for criterion (1). While in the field piping high-frequency pulsations are judged more strictly than low-frequency pulsations, this is not the case for pulsations close to the cylinders.
- The criterion (2) considers a speed-of-sound dependency that is absent for criterion (1). While in the field piping pulsation effects for heavy gases are judged more strictly than for light gases, this is not the case for pulsations close to the cylinders.

As the criterion (1) for the cylinder flange does not consider several aspects like gas composition, frequency and details of the position, increased awareness of the pulsation consultant is needed to avoid potential issues being overlooked.

4 Physical mechanisms and order-of-magnitude estimates

The definition of Cylinder Gas Passage pulsations is proposed as the unsteady flow and pressure effects occurring between the working chambers of the cylinder up to the volume of the pulsation bottles of the compressor, see figure 1.

Figure 1: Definition of CGP pulsation area.

4.1 Unsteady flow

A reciprocating compressor cylinder generates unsteady, pulsating flow at the inlet and outlet of the working chamber, due to the periodic movement of the piston, in combination with the action of the compressor valves. The connecting conduits between the compression chambers and the pulsation dampers can have a complex geometry. The impedance of these connecting conduits (CGPs) can be large and thus lead to high pressure pulsations near the valves, caused by the unsteady flow. Moreover, if an acoustic resonance is excited these pulsations can become very large. Acoustic resonances are most commonly observed as standing wave effect, where the distance between the compression chambers and the dampers acts as a ¼λ standing wave. At very high orders of the compressor speed, also more complex resonances may be triggered inside the CGP.

by: Leonard van Lier, Jan Smeulers – TNO

The pulsations that occur inside the CGP and near the compressor valves, are generally large (10-20% peak-peak of mean pressure are not uncommon). The dominant pulsation effects generally occur at high frequencies. Moreover, the amplitude of the pulsations depends on small geometrical details of the CGP, the flow characteristics of the compressor valves and the acoustic damping. Therefore it is challenging to correctly predict the absolute magnitude of the CGP pulsations. Still it is important to predict these pulsations accurately, to judge them as they can affect the compressor performance, the valve behaviour and may trigger harmful vibrations.

The strong CGP pulsations are caused by the sudden opening of the compressor valves. The steep flow pulse that occurs when a compressor valve opens, introduces high frequency pulsations up to (typically) 30 times the compressor speed.

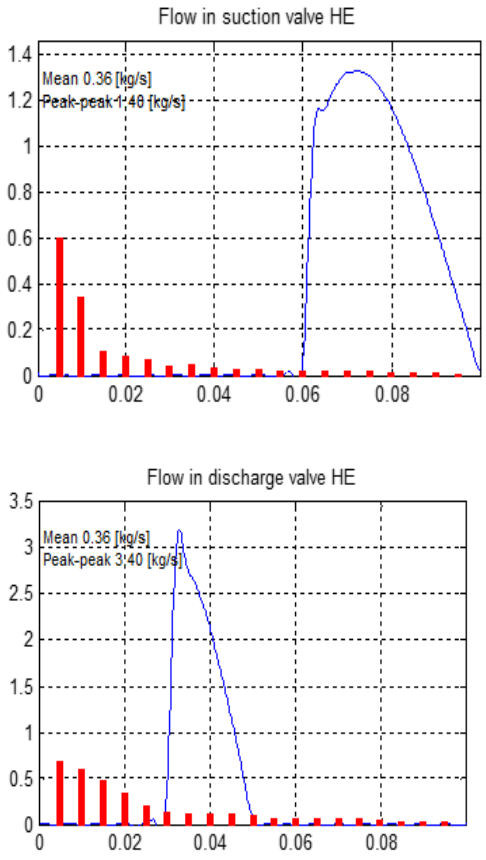

Figure 2: Flow pulses at suction (top) and discharge (bottom). Time signals of flow and frequency spectrum for the orders of the compressor speed (bars).

The high-frequency components of the discharge pulse are relatively higher than the suction pulse because the discharge pulse is shorter. In general the magnitude of the high frequency components depends on the steepness of the opening flank of the pulse. This steepness is related to the opening velocity of the valve and thus to the mass of the valve and the gas forces that act on the valve.

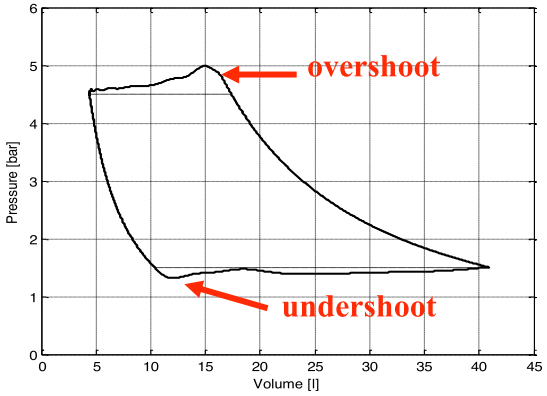

Figure 3. Normal PV diagram with excess pressures upon valve opening. Dashed line is the theoretical, ideal PV diagram.

The CGP pulsations cause extra power consumption, which is proportional to the area between the dashed and drawn lines in the PV diagram. The largest loss seems to occur at the discharge, but because the suction stroke is much larger than the discharge stroke the losses at suction and discharge are comparable. The pressure overshoot results from the flow amplitude times the total impedance. The total impedance is the sum of the static flow resistance in the valve and the CGP and the reactance, which can be considered as the dynamic resistance of the CGP and cylinder nozzle. In many cases, the (frequency-dependent) effect of the impedance is dominant over the effect of (static) flow resistance.

4.2 Acoustic resonances

If also acoustic resonances occur within the CGP, this strongly affects the shape of the PV diagram, as can be seen in figure 4.

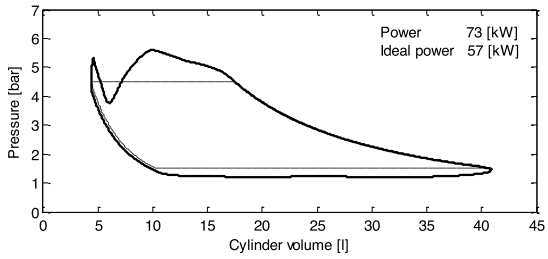

Figure 4: PV card in case of a strong CGP resonance.

A more detailed discussion on the features of the acoustic resonances in the CGP will be provided in the section on numerical modelling.

Comparison between simplified analytical expressions for resonance frequencies and detailed simulation models confirm that order of magnitudes can be estimated easily, but deviations increase for

by: Leonard van Lier, Jan Smeulers – TNO

increasing frequencies. For the lowest acoustic resonance modes, an acceptable correspondence is found.

As the dimensions of a CGP are in general relatively small compared to the acoustic wavelengths, resonances are excited by high-frequency components (harmonics) of the flow pulse. The value of these high frequencies (and the associated orders) depends on the compressor speed, the spatial dimensions of the gas passage and the speed-of-sound in the process gas (typical values for low-speed compressors: 4^{th} – 8^{th} order for heavy gases, such as natural gas or CO_2, and 10^{th} -20^{th} order for light gases such as hydrogen). The excitation of acoustic resonances inside the CGP can lead to high pressure amplitudes because the resonances are, without measures, poorly damped. The acoustic resonances in the CGP can amplify the high-frequency components of the compressor pulses.

Analytical models for estimation of acoustic resonance frequencies can be used for order-of-magnitude estimates. It shall be noted however, that in general detailed simulation models are preferred as these take into account correct diameter transitions and a better approximation of the impedance of compressor valves and the compression chamber.

In principle, also acoustic resonances inside the compression chambers of the cylinders can occur. In previous EFRC research projects, detailed prediction tools have been developed[4,5]. In some case, the assumption that pressure inside the compression chamber is homogeneous fails. The sudden opening of (in particular) the discharge valves generates large dynamic pressure differences across the compression chamber. Also the compression at maximum piston speed will lead to a pressure surge ('gas inertia effect') that can be observed in dynamic pressure measurements inside the cylinder. If acoustic resonances inside the working chamber are triggered by these effects, a strong amplification of the amplitude will occur. In most practical cases however, the acoustic resonance effects occur at a much higher frequency and can only be observed as a second order effect, in particular during the re-expansion phase with closed valves.

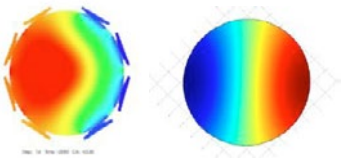

Figure 5. Snapshot of pressure fluctuation in working chamber (left) and acoustic resonance (right).

These effects are most relevant for large cylinder diameters, low speed-of-sound (heavy gases) and high rotational speeds. In case of excessive pulsation effects inside the working chamber, forces on the piston and bending of the piston rod shall be investigated in more detail. A screening method to assess this risk is given in a paper by Hinchliff[6].

4.3 Power consumption and efficiency

CGP pulsations will affect the capacity, power consumption and efficiency. It is well known that flow resistance in the inlet channel leads to a lower gas pressure filling the cylinder and thus a reduction of the capacity. However, if the flow can be considered quasi-stationary, i.e. the flow in the suction system follows the piston speed then the pressure upon closing of the suction valve will be exactly the suction pressure, because the flow velocity and therefore the pressure losses are exactly zero when the suction valve closes (at the BDC). However, when dynamics plays a role the pressure variations at the suction valve can, and in most cases will be out of phase with the piston speed. Then, at closure of the suction valve the pressure at the suction valve can be higher or lower than the ideal suction pressure, which will lead to a higher, respectively lower capacity. Another cause of a reduction of the capacity is late closure of the suction valve, due to valve dynamics or stiction effects. In reality, the effective flow loss will be a combination of the above mechanisms, which cannot be separated a priori within a single measurement of the PV diagram.

In first order, the pressure surge during the opening of the discharge valve, due to the impedance of the CGP can be estimated as follows. The impedance of the CGP is based on the effective cross sectional area, based on average volume and a typical acoustical length of the CGP:

$$A_{eff} = \frac{V_{CGP}}{L_{ac}} \qquad (3)$$

Then, the pressure increase at opening of the valve $\Delta P(t_{open})$ is:

$$\Delta P(t_{open}) = \rho c \frac{\Delta Q(t_{open})}{A_{eff}}, \qquad (4)$$

with ρ the density [kg/m^3], c the speed of sound [m/s] and $\Delta Q(t_{open})$ the increase in volume flow through the valve.

In case of acoustic resonances, the pressure surge will be higher, and an amplification factor

by: Leonard van Lier, Jan Smeulers – TNO

(typically 10-20) shall be included to account for the resonance effects. Beyond the scope of this paper, approximate guidelines are presented in the EFRC R&D report[2].

For a typical example, based on realistic input values, the analytical formulas have been compared with the results of a detailed simulation model.

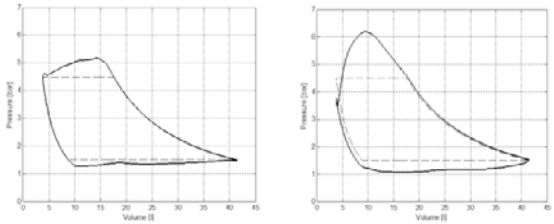

Figure 6: Calculated PV diagrams with pressure overshoot without resonance (left) and with resonance (right).

The analytical model predicts a pressure overshoot of 0.39 and 1.3 bar, respectively. This is in reasonable accordance with the more detailed numerical simulation results. In the full report also analytical expressions to estimate the pressure surge due to valve resistance and orifice plates are presented.

5 Numerical analysis

Though analytical expressions can be valuable for a general understanding of the mechanisms and quick order-of-magnitude estimates, robust numerical simulation tools are available and commonly used to evaluate design of reciprocating compressor systems in the petrochemical industry.

5.1 Purpose of the analysis

For evaluation of new compressor systems, a pulsation study is part of the detailed design, usually dictated by the stipulations in the API 618 standard. The purpose of the study, in particular with respect to CGP pulsation effects can be summarized as follows:

- Evaluation of the pulsations at the cylinder connections. Comparison with API 618 limit.
- Evaluation of pulsations near the compressor valves. This result determines the need for more detailed compressor valve analysis (in case of high pulsations).
- Evaluation of shaking forces on dampers, cylinders and internal passages. This result determines the need for more detailed mechanical analysis of the compressor manifold.
- Evaluation of PV card and power consumption.
- Quantify extra dynamic loading on piston and piston rod due to pulsation effects.

The last two points shall be shared with the compressor manufacturer for information.

5.2 Challenges

For adequate numerical modelling of the detailed effects occurring in the CGP, the pulsation consultant is faced (even with state-of-the art simulation tools) with some challenges.

A straightforward translation of a complex-shaped cylinder into a 1D simulation model can be troublesome. Compare for example a forged high-pressure cylinder layout (left) with a more curved cast low-pressure cylinder (right).

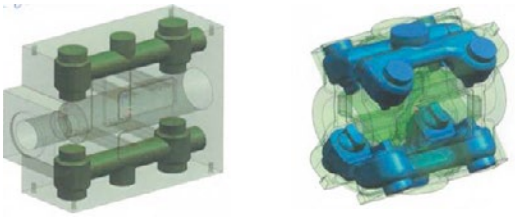

Figure 7: example of simple '1D' cylinder layout (left) and complex '3D' cylinder layout (right).

The '1D' layout is conveniently modelled, but for the '3D' layout several modelling options can be used. Based on experience, the best match for similar geometries is achieved with an H-pattern wireframe[7]. A full benchmarking study with realistic cylinder geometries, 1D and 3D acoustic simulation tools is considered a valuable topic for future research.

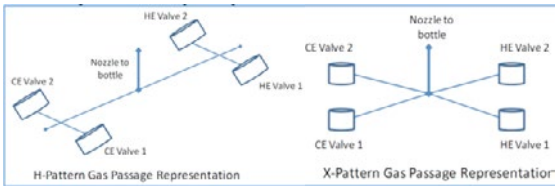

Figure 8: H- and X-pattern simulation models for the CGP.

Nevertheless, this shall be considered on a case-by-case basis, using the following generic strategy: 1) the total volume of the CGP shall be provided by the compressor manufacturer 2) the prevailing acoustic length scales in longitudinal direction shall be estimated as accurately as possible 3) the effective diameter shall be chosen to correctly represented the CGP volume. In case the compressor vendor delivers a schematic wire-frame sketch of the CGP, the dimensions shall be reviewed, in conjunction with the cylinder drawings for consistency. In any case, the spatial and

by: Leonard van Lier, Jan Smeulers – TNO

temporal discretization in the simulations shall be sufficiently fine, to capture the relevant length and time scales. This requirement is generally more strict for CGP pulsations than for pulsations in the field piping.

In industry, both time-domain and frequency-domain simulation tools are used. Though frequency-domain codes may be adequate for basic screening and orifice optimization, a time-domain approach is considered most suitable to represent the complex pulse shapes of the source, the essential non-linear behavior of compressor valves and to handle non-linear damping mechanisms which are essential for pipe flows.

Acoustic damping in complex geometries and flows is a challenging topic that is vivid topic of research. The flow in the CGP is highly complex, and the pulsation amplitudes are generally very high, so application of linear theory for the acoustic damping has limited accuracy. The flow resistance of compressor valves is usually provided by the vendor of the valves. Modelling of resistance in the curved conduits in the CGP is usually based on experience. As a general guideline, it is advised to apply for each obstruction/deviation in the flow path a pressure loss coefficient of the order of the dynamic pressure $\frac{1}{2}\rho U^2$.

5.3 Examples

To illustrate the most relevant mechanisms and to present some typical results that are obtained during numerical analysis (in particular during the pre-study) a representative case is defined.

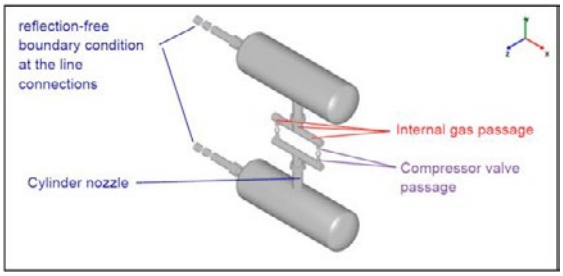

Figure 9: typical simulation model.

The pulsation dampers are empty bottles, without internals. Representative figures are used for the compressor data (pressure ratio, bore, stroke, clearance). The dimensions of the cylinder passages are slightly exaggerated, to have a 'pronounced' response due to the compressor pulses.

The first example is a light gas (hydrogen) with MW=2, and a high speed-of-sound (1400-1600 m/s). To verify the sensitivity of the results for small fluctuations in the operational conditions, a range around the nominal conditions was investigated, from -20% to +20% around the nominal speed-of-sound. The results for the pressure amplitude in the CGP (near the compressor valves) are shown in figure 10. The highest pulsation amplitudes are found at the discharge side. The amplitudes are considerable, up to 10% of the mean pressure.

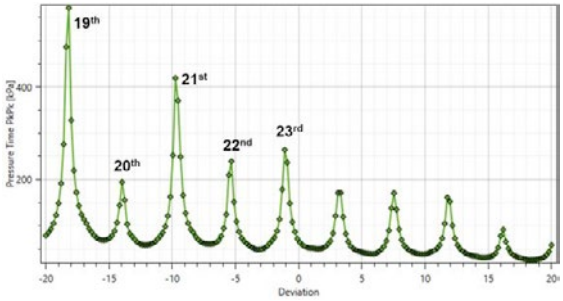

Figure 10: Pulsation amplitude as a function of speed-of-sound (hydrogen example).

A typical feature are the peaks that correspond to acoustic resonance conditions that are triggered at particular gas conditions. The peaks are relatively sharp and narrow, which indicates resonances with a high quality factor. This illustrates the importance to use a sensitivity range with sufficiently small steps, to avoid underestimation of the resonance effects.

The peaks are identified as higher orders of the compressor speed. The main feature of the resonance is a standing wave, originating from the compressor valves (high pressure pulsations amplitude) toward the damper volume (low amplitude), see figure 11.

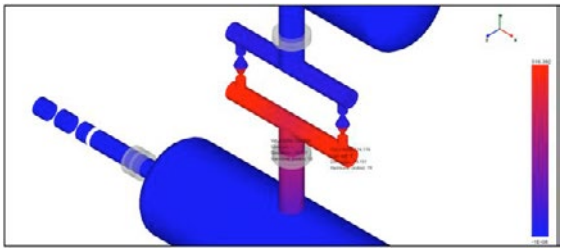

Figure 11: Illustration of acoustic resonance.

This also illustrates the difference in pulsation amplitude that can occur between the cylinder flange (the API 618 target location) and other areas in the CGP, in particular near the compressor valves.

The simulation results, including the frequency information, can be most conveniently presented in a 2D color plot. Figure 12 contains the speed-of-sound (horizontal) and the frequency (orders of compressor speed, vertical). The pulsation amplitude is shown in the color scale.

The inclined curve is a single type of acoustic resonance that is triggered at different frequencies, depending on the value of the speed-of-sound. In this example the resonance is a $\frac{1}{4}\lambda$ standing wave (figure 11), that is called Cylinder Nozzle

by: Leonard van Lier, Jan Smeulers – TNO

Resonance (CNR). Other resonances are not observed, up to the 32rd order of the compressor speed.

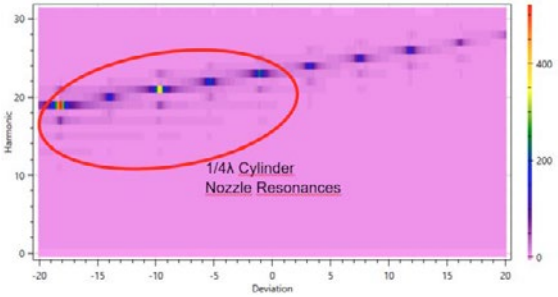

Figure 12: Pulsation amplitude as function of speed-of-sound and frequency (hydrogen example).

The pulsation effect is also clearly present in the PV card, which also allows to judge the impact on the consumed power. Based on the results the consultant can estimate the dynamic loads on the piston and piston rod.

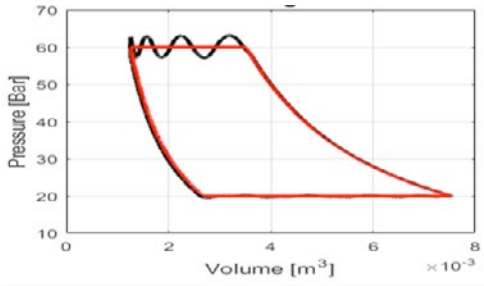

Figure 13: PV card highlighting acoustic resonance on discharge side (hydrogen example).

In a second example, a natural gas application is considered, with the same simulation model. Now, due to the heavier gas, the speed-of-sound is considerably smaller (450-500 m/s). Again the pulsation amplitudes show several peaks. However, these are found at a variety of orders of the compressor speed. The lowest orders (6th, 7th, 8th) are associated with ¼λ resonances (CNR). Also higher orders are found that are associated with a different type of acoustic resonance mode. Here, the resonator is fully trapped inside the CGP, being a ½λ standing wave between HE and CE: Gas Passage Resonance (GPR).

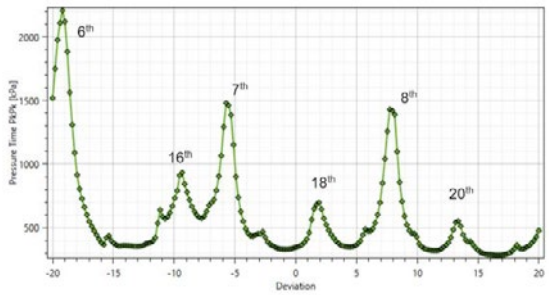

Figure 14: *pulsation amplitude (natural gas example).*

The 2D plot highlights multiple resonance effects:

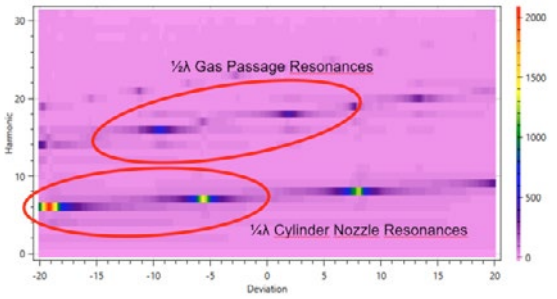

Figure 15: Pulsation amplitude (natural gas).

The Cylinder Nozzle Resonance has the highest amplitude and occurs at lower frequencies. The Gas Passage Resonance (GPR) is weaker and occurs at higher frequencies. Despite the smaller amplitude, the GPR has some features that may be critical. The mode is trapped, and the amplitude at the cylinder connection flange is nearly zero. For the judgement of these resonances, the API 618 criterion at the flange is not adequate. Moreover, this trapped resonance cannot be suppressed conveniently with a restriction orifice plate at the cylinder flange. Finally, the shaking force due to this trapped mode can efficiently trigger the cylinder, due to the phase difference of the pressure fluctuation at HE and CE. If a mechanical resonance frequency in piston-direction coincides with the shaking force frequency, severe vibration issues (cylinder stretch) may be observed.

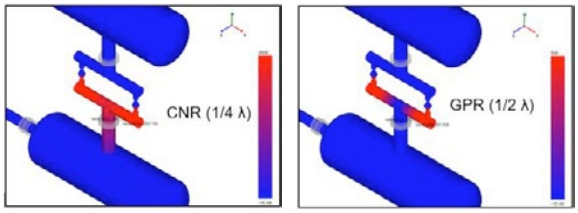

Figure 16: Acoustic resonances: Cylinder Nozzle and Gas Passage resonances.

Finally, the PV card illustrates the resonance effect and (in this case) a considerable increase in consumed power. Note that this acoustic resonance effect is not easily separated from high losses due to unsteady flow. In this example, the overshoot is not due to the flow resistance in the valves or CGP but due to an acoustic amplification.

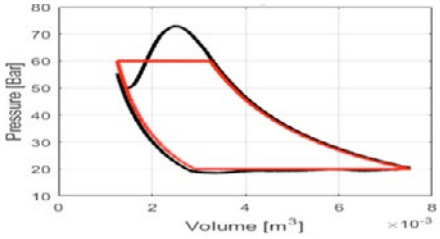

Figure 17: PV card highlighting acoustic resonance on discharge side (natural gas example).

by: Leonard van Lier, Jan Smeulers – TNO

Once the diagnosis of acoustic resonances and flow resistance in the CPG has been done, optimization steps can be performed with the numerical model. The beneficial effect of a restriction orifice can be assessed, and the bore can be optimized. During the optimization of the bore, the extra pressure losses due to unsteady flow effects shall be carefully considered.

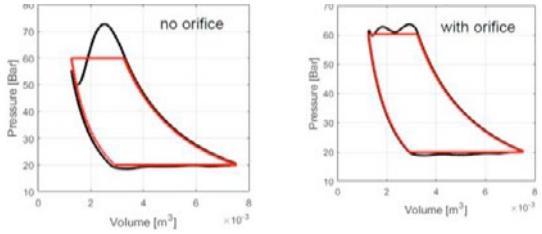

Figure 18: Beneficial effect of restriction orifice.

While restriction orifice plates are effective for the majority of CGP pulsation issues, in case of trapped modes orifice plates are not effective. Less conventional techniques to control these pulsations effects are a re-design of the CGP, introduction of a restriction inside the CGP (insert), additional volume on the valve covers, or a tuned side branch absorber. For specific conditions, a side branch absorber can be effective to detune the resonance and relocate the area of high pressure fluctuations away from the critical compressor valves. To suppress the amplitude the absorber must contain a restriction which shall be optimized with the simulation model. In any case, the absorber must be a tunable device, to be effective over a large range of process conditions.

6 Dynamic valve response

As the valve behavior is affected by both the mechanical properties of the valve and the fluid forces, the modelling can be complex. However, in most practical cases the valve behavior is dominated to a large extent by the fluid forces. It appears that often for the major part of the opening cycle the fluid forces are much larger than the mass and spring forces. Only when the valve is about near closing, the mass spring behavior of the valve is dominant. Therefore the pulsations in the CGP, and sometimes the pulsations inside the cylinder, govern the valve behavior. Whatever the valve properties are, the valve movement is determined by the fluid forces, i.e. the pressure difference across the valve. This means that comparing the mechanical resonance frequency of the valve with the acoustic resonance frequency of the CGP and avoiding that these coincide is not an adequate way to avoid adverse valve behavior.

This is shown in the figure 19 in which three cases are compared with the same CGP but a variation of the valve resonance frequency. In the base case the resonance frequency of the valve is approximately equal to an acoustic resonance frequency of the CGP. In the second case the mass of the valve plate is half, the resonance frequency is 40% increased. The response changes, but is still quite similar. Increasing the mass of the valve by a factor of two, i.e. eigen frequency is reduced by 40%, gives a change of the curve, but the unstable valve behavior remains.

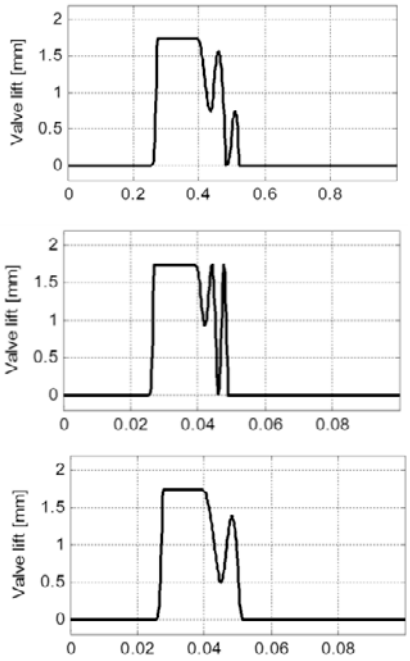

Figure 19: Effect of valve mechanical properties to the same fluid forces. Top: base case. Middle: higher resonance frequency. Bottom: lower resonance frequency.

In addition to this, considering the mechanical resonance frequency of the valve based on the mass and spring constant does not comply with reality. This is because the valve is restrained by seat and limiter (non-free and non-linear behavior). See the illustration in figure 20, where an ideal valve movement is shown. The total opening time is in this case approximately ¼ of the full rotation time of the crank shaft. The valve opening and closing times are even smaller fractions of the discharge stroke (a few percent). Only in these two short time intervals the valve can move freely.

In the figure also the typical time scale of a free mechanical oscillation of the valve is shown. It is clear, that the valves resonance frequency is ‘too slow’ to be effectively triggered, since triggering can only occur in the very last phase of the valve opening when the flow reduces to zero. In other words, for the interaction with the mechanical properties of the valve (mass, spring) the higher frequencies in the pulsation spectrum shall be considered. This pleads for a careful evaluation and control of the high-frequency pulsations. To study the acoustic-mechanical interaction in detail a fully coupled calculation method is mandatory which

by: Leonard van Lier, Jan Smeulers – TNO

considers both the pulsation effects in the CGP and the mechanical valve properties.

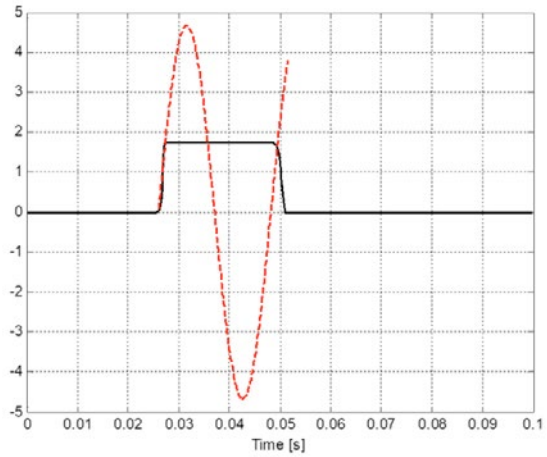

Figure 20: Valve position (black) and free-movement valve oscillation (red).

7 Conclusions and recommendations

Based on the literature survey and interviews with experts, the following observations were brought forward during the inventory.

Awareness and urgency. The awareness of CGP pulsation issues is generally limited. It is noted that often only the consequences of CGP pulsations can be seen, and often not directly the root cause. Excess power consumption often remains unnoticed. Condition monitoring engineers and pulsation consultants are most often confronted with CGP pulsation issues, while compressor vendors and end user indicate that the issues do occur but on a limited scale. Pulsation effects associated with Cylinder Nozzle Resonances can generally be identified and controlled in the design stage with state-of-the-art engineering tools.

Negative consequences. The integrity of compressor valves remains a key aspect of the reliability of the reciprocating compressor. In case of issues with compressor valves, often a combination of adverse conditions is found (high pulsations, fouling, off-design operation) and causes cannot always be clearly separated. Also the integrity of piston rods has been raised by several experts. Dynamic loading due to pulsation effects is generally considered in generic safety margins

Importance of the pre-study. The state-of-the art numerical tools for the detailed pulsation study can be used to identify and control the majority of the pulsation effects during the detailed design of the compressor system. In addition to pulsation effects (resonances) also the resistance of the CGP can be evaluated, including losses over valves and orifices. The excess power consumption quantified in the pre-study can be considered in the evaluation of Operation Expenditure (OPEX cost). Based on the pre-study as stipulated by API 618, the need for a more detailed dynamic valve analysis and a more detailed compressor manifold analysis shall be substantiated, and discussed with the client.

Occurrence of trapped modes. Though more rarely, the occurrence of higher-order CGP pulsation resonance effects ('trapped' Gas Passage Resonances or acoustic modes inside the working chambers) is observed in the field. If these coincide with mechanical resonances of the compressor manifold, vibration problems may be very hard to mitigate. Accurate modelling of these high-frequency resonance effects is very challenging, due to the limitations in the state-of-the-art engineering tools. Also the possible solutions to these issues are more demanding and rarely encountered in industrial application.

Modelling complex geometries and acoustic damping. To quantify high-frequency effects, such as the pulsation amplitudes of trapped GPR modes, the basic engineering tools have limited accuracy. To overcome the limitation, many aspects ask for a more substantial investigation, such as the challenge to model complex geometries with 1D models and to have reliable acoustic damping at high frequencies.

Existing standards and guidelines. In general standards are considered adequate for the majority of cases found in practice. Increased emphasis on certain critical aspects in the existing standards and guidelines is considered valuable, such as evaluation of pulsation levels near compressor valves and simplified calculation methods of pressure loss of restriction orifice plates in dynamic conditions.

New techniques to suppress vibrations. If the source of high-frequency vibrations cannot be reduced, solutions are required to control the vibrations. Conventional techniques such as pipe supports and bracing clamps have limited effect at high frequencies. In these case, an increased mechanical damping is considered more effective. A practical guideline to enable the application of special visco-elastic damping materials to enhance performance of mechanical supports (for example to suppress vibrations on Small Branch Connections) is considered valuable. As a general recommendation, SBCs shall be avoided wherever possible in the immediate vicinity of the compressor. In any case, length and overhung mass shall be minimized and adequate bracing shall be applied in accordance with good engineering practice.

Finally, the predictive value of condition monitoring systems can be enhanced by application the available physical and numerical models for the interpretation of the dynamic conditions in the vicinity of the compressor.

8 Acknowledgement

The authors wish to thank the EFRC R&D group for supporting this work and their approval to present a summary of the results in this paper.

References

[1] API 618 standard, 5th edition (2007): Reciprocating Compressors for Petroleum, Chemical and Gas Industry Services.

[2] TNO report TNO-2018-R10344 (2018): Literature survey on identification and mitigation of Cylinder Gas Passage pulsations (funded and supported by EFR R&D group).

[3] API 688 recommended practice, 1st edition (2012): Pulsation and Vibration Control in Positive Displacement Machinery Systems for Petroleum, Petrochemical, and Natural Gas Industry Services.

[4] R. Aigner, Internal Flow and Valve Dynamics in a Reciprocating Compressor, PhD thesis, Technischen Universität Wien, Institut für Strömungsmechanik und Wärmeübertragung. June 2007.

[5] T. Müllner, Flow Patterns and Valve Dynamics in Multi-Valve Reciprocating Compressors, PhD thesis, Technischen Universität Wien, Institut für Strömungsmechanik und Wärmeübertragung, December 2015.

[6] M. Hinchliff, S. Greenfield, W. Bratek “A discussion on the various loads used to rate reciprocating compressors”, GMRC 2014.

[7] M. Nored, Gas Passage System Pulsation Analysis for Modern Reciprocating Compressors. Proceedings of 7th EFRC Conference 2010.

EUROPEAN FORUM
for RECIPROCATING
COMPRESSORS

MEASURING AND MODELLING

TECHNISCHE UNIVERSITÄT DRESDEN

Experimental and numerical study on the thermodynamic behavior of a reciprocating compressor

by:

Konrad Klotsche, Gotthard Will, Ullrich Hesse
Bitzer-Chair of Refrigeration, Cryogenics and Compressor Technology
Technische Universität Dresden
Dresden, Germany
Konrad.klotsche@tu-dresden.de

11th EFRC CONFERENCE
September 13 – 14, 2018, Madrid

Abstract:
This paper applies both experimental and numerical approaches for a horizontal balanced-opposed test compressor. Experiments are conducted at a typical operating condition (speed: 1000 min-1, pressure ratio: 3.5). The compressor's thermodynamic behaviour is then determined with the calculation program for reciprocating compressor plants – KVA – and the calculation results are validated using the measured data. Finally, the temperatures of the compressor components are determined by a FEM simulation in Ansys.
This combined analysis of the compressor lead to a significant gain in accuracy. The respective advantages of each method complement each other and results in a more comprehensive analysis of the compressor. Furthermore, the FEM model is used to show the cooling of the piston rod sealing by variation of the thermal properties of the piston rod. This also reveals the advantage of simulation tools compared to experimental measurements considering time, effort and cost for the investigation of different configurations.

by: Konrad Klotsche, Gotthard Will, Ullrich Hesse – TU Dresden

1 Introduction

The knowledge of thermodynamic processes and important operating parameters of reciprocating compressors is essential for an economical and low-maintenance operation as well as for compressor research and development. The relevant operating data can be derived from either experimental investigations or theoretical calculation methods. However, each technique is characterized by its advantages and disadvantages concerning accuracy, required time, effort and consequently costs.

Experimental investigations provide direct results from the compressor. However, they often require comprehensive instrumentation and complex measurements particularly in case of thermodynamic studies. This is due to the fact that the heat transfer depends on the three-dimensional geometry as well as on the three-dimensional temperature distribution and its temporal dependency. Calculations and simulations, on the other hand, allow comparatively reproducible results but require validation of the results by measurements.

The aim of this work is to show the combination of both experimental and numerical approaches applied on a reciprocating test compressor. This shows that the individual advantages lead to an increased understanding of the compressor's thermal behaviour. The three-dimensional thermal simulation of the compressor is then used to conduct a parameter study which would be difficult and costly to realize by experiments. Based on the thermal simulation model it is shown to what extent the heat transfer along the piston rod is influenced by its thermal and geometric properties and how this affects the packing and the cylinder cooling.

2 Information on the experimental conditions

2.1 Setup and instrumentation of the test compressor

The test compressor used in this study is shown in figure 1. It is a balanced-opposed crosshead type, double-acting, single-stage and dry-running piston compressor with two horizontal throws. It sucks in ambient air and pumps it against a high-pressure control valve which is located at the facility outlet and which is used to adjust the back pressure. One peculiarity of the compressor is the position of the piston rod packing, which is located at an intermediate piece due to its comprehensive instrumentation.

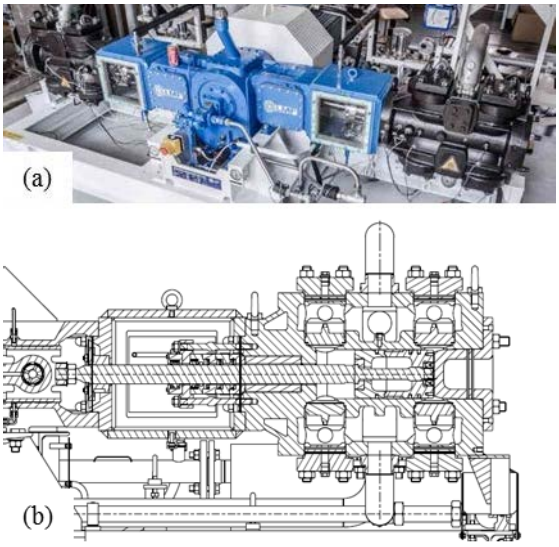

Figure 1: Photograph (a) and sectional view (b) of the test compressor

Essential compressor operating data:

- Nominal flow rate: 150 $m^3\ h^{-1}$
- Power consumption: 15…30 kW
- Speed range: 500…1500 min^{-1}
- Average piston velocity: 1.66…5 m s^{-1}
- Typical suction pressure: 1 bar_a
- Max. discharge pressure: 5.5 bar_a

The compressor is equipped with high speed pressure transducers (max. sample rate 100 000 samples per second) for each cylinder collecting the pressure data from the suction and discharge chamber as well as from the head end and crank end working chambers. In addition, both piston rod packings are each equipped with high speed pressure sensors, which record the pressure values in front of and between the individual sealing ring packages. In total, the operating behaviour of the compressor was measured with 16 pressure measurements at the relevant locations in the compressor at high-frequency (50 kHz). In this way, that all relevant pressure pulsations are covered. The gas temperatures were recorded with thermocouples (type K) at the similar locations as the pressure sensors. In addition, the solid-state temperatures in the metallic packing ring chambers were measured at the piston rod packing. Due to their thermal inertia, they were sampled at a sample rate of 1 Hz. Furthermore, a mass flow sensor is installed at the discharge line and two volume flow meters are located at the flare lines of the piston rod packing to record any air leakage.

2.2 Measurements

A typical operating point for reciprocating compressors was selected for this study. The speed was set to 1000 min^{-1} and the back pressure to

by: Konrad Klotsche, Gotthard Will, Ullrich Hesse – TU Dresden

3.5 bar_a to achieve a high thermal load for the compressor. Three measurements were carried out for the operating point and the results of these measurements were averaged within steady-state operation. Some of the results are shown in figure 4 – figure 8.

The measurements are intended to validate the results of steady-state KVA calculations and Ansys simulations. Therefore, the compressor was operated under constant boundary conditions until a quasi-stationary operating state was reached. This state means that the mean values of the temperatures do not change. For evaluation of the thermal behaviour, the temperatures are averaged over 60 minutes (3600 values), to ensure meaningful results. In this state, the high-frequency pressure measurements (50 kHz) were also carried out to record p,V diagrams and other pressure fluctuations in the suction and pressure chambers as well as in the piston rod packing chambers.

3 Calculation of the compressor's thermodynamic behaviour by means of KVA

The experimental results of the thermocouples provide information about the local temperatures at the measuring points and they can be used for the analysis of the thermal situation. For example, the direction of heat flows or local thermal hot spots can be determined by the temperature gradients. In addition, they can be compared with calculated results to check and verify them. The high-frequency pressure measurements in the working chambers and the suction and pressure chambers also enable the analysis of the temporal thermodynamic condition of the gas.

However, the measurement results do not allow a complete assessment of the thermal boundary conditions of the compressor, which is necessary for a comprehensive characterization of the compressor's behaviour. For the compressor components, these boundary conditions are the convective heat transfer, characterized by heat transfer coefficients (HTCs) and the temperature of the surrounding fluid, but also the frictional power that occurs at the sealing rings. They were determined based on the calculation program for reciprocating compressor systems KVA.

3.1 KVA's working principle

The analysis tool for compressor systems KVA (in German: "Kolbenverdichteranlagen") is a development of the Bitzer-Chair of Refrigeration, Cryogenics and Compressor Technology and aims at calculation of the entire compressor system.

The calculation procedure is based on a network model with each relevant gas-filled volume considered as one node. This includes all working chambers, the suction and pressure chambers and other volumes (buffer tanks, mufflers, crankcase, etc.) that are relevant to the compressor's thermodynamic behaviour. In this analysis all thermodynamically relevant volumes were considered since a more complete simulation leads to a more precise calculation of the compressor's thermodynamic behaviour. All properties of these volumes (p, V, T, m, h, s) are time-dependent and location-independent within each volume.

The volumes are interconnected by links which may represent pipes, valves and sealing. They are gas-filled elements which are mostly characterized by the flow through them. Volume boundaries are represented by wall elements in KVA. They represent the compressor component structure and allow a consideration of heat transfer between the gas and the compressor walls. The heat conduction between adjacent wall elements may also be included. All KVA calculations are based on the general gas equation and the first law of thermodynamics. The explicit formulation for the time-dependent behaviour of the pressure and temperature within each gas volume is given by Equations (1) and (2).

$$\frac{1}{p}\frac{dp}{dt} = \frac{K}{K-1}\left(\frac{p}{m*K*R*T}\frac{dQ}{dt} - \frac{1}{V}\frac{dV}{dt} - \frac{1}{K}\frac{dK}{dt}\right), \quad (1)$$

$$\frac{1}{T}\frac{dT}{dt} = \frac{K}{K-1}\left(\frac{p}{m*K*R*T}\frac{dQ}{dt} - \frac{1}{V*K}\frac{dV}{dt} - \frac{1}{K}\frac{dK}{dt}\right) - \frac{1}{m}\frac{dm}{dt} - \frac{1}{R}\frac{dR}{dt}. \quad (2)$$

The change of heat over time dQ/dt for each volume accounts for all heat flows and enthalpy flows across the volume boundaries. The governing equation for the law of mass conservation is $dm/dt = \sum \dot{m}_j$ which considers every mass flow $\dot{m}_j$ across the volume boundaries. The thermodynamic state over time is calculated by a time-step method over several crankshaft turns which uses a step size between 0,01° and 1,0°. The flow through the valves is calculated with a general nozzle flow approach given by Equation (3) [1].

$$\dot{m} = h_V * l_V * \alpha_{fl} * \psi_f * \sqrt{2 * p * \varrho} \quad (3)$$

The valve (e.g. lamella, ring plate, poppets or similar elements) movement is based on the time dependent forces. The heat transfer between the gas volumes and the surrounding walls is determined by HTCs. They are calculated using a general Nusselt number approach $Nu = f(Pr, Re)$ based on the Prandtl number Pr and the Reynolds number Re. The latter considers the piston speed and the equivalent speed for the kinetic energy of the gas.

This approach for the HTCs has shown a good agreement of experimental and simulation results of

by: Konrad Klotsche, Gotthard Will, Ullrich Hesse – TU Dresden

an air compressor [2]. For more information about the working principles of KVA see [2].

3.2 KVA model of the test compressor

For the calculation of the test compressor, the structure of the internal flow path shown in figure 2 (b) was designed. This structure composed of the essential volumes that flow through the gas from inlet to outlet but comprises only one cylinder due to the symmetry of the compressor design. For all modelled volumes the actual dimensions were adopted, so that the size of the volumes and the surfaces correspond with those of the real compressor. Note, that the piston rod packing consists of three volumes (P1, P2, P3) that are separated by two packing rings.

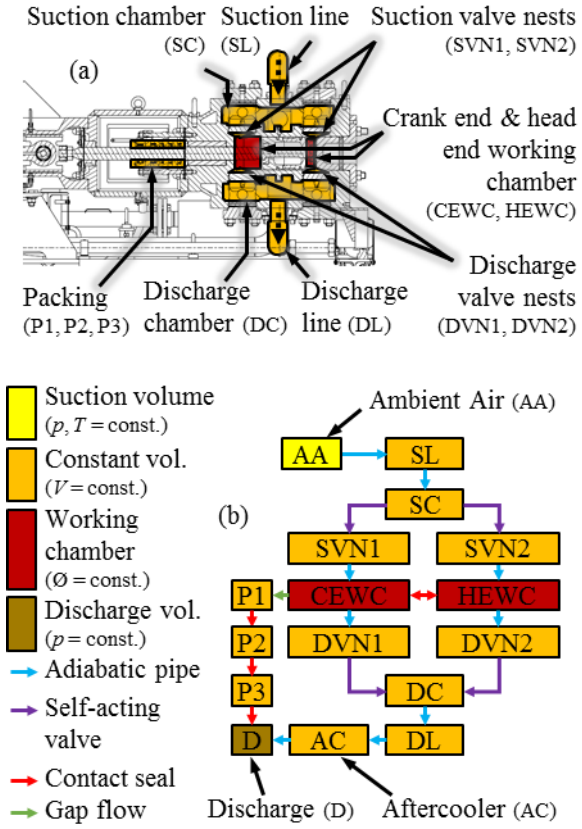

Figure 2: Assignment of the gas volumes in the sectional view of the test compressor (a) to the corresponding KVA gas flow network (b)

For the heat transport mechanisms, all relevant components were implemented as walls in the calculation model. Figure 3 (b) shows the discretization of the wall elements, which was derived from the cylinder geometry and which reflects the geometry and position of the components in a simplifying way. The oscillating assembly, consisting of the piston, piston rod and crosshead, was modelled in the middle position. The volumes which are limited by the wall elements can be seen in figure 3 (b). These volumes and the circumjacent wall elements are thermodynamically connected, so that heat is transferred between them depending on the geometric conditions (contact surface, dimensions) and the temperature differences. This heat transport also takes place between the wall elements that are in contact with each other in figure 3 (b).

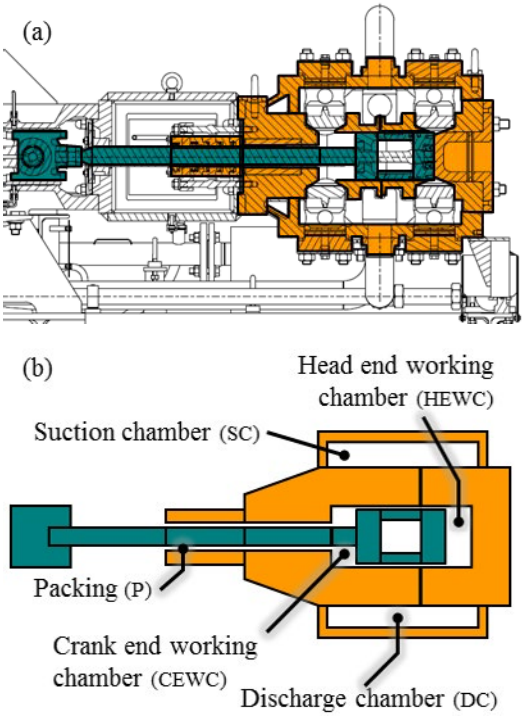

Figure 3: Assignment of the compressor components in the sectional view of the test compressor (a) to the corresponding KVA wall elements (b)

For the thermodynamic calculation of the compressor, a step size for the crank angle of 0.1° was selected. In total 100 complete crank revolutions were calculated, so that a stationary state was achieved for all elements. However, an almost stationary state was already achieved after 25 crank turns, so that only minor changes occurred in the subsequent calculation steps.

3.3 Comparison of measurement and calculation results

Figure 4 and figure 5 show the comparison of the measured (with suffix “Meas”) and calculated pressure curves (with suffix “KVA”) from the cylinder area and from the packing. The good correspondence of the curves shows that the thermodynamic processes of the gas can be reliably reproduced with the aid of the KVA calculation.

Figure 6 shows the relevant averaged temperatures from the measurement in the steady-state of the compressor both cylinders. These values are compared with the KVA calculation. The deviations are in the order of a few Kelvin. Only the temperatures at the crank end working chamber (CEWC) show larger deviations, which is probably due to the special position of the packing and due to

by: Konrad Klotsche, Gotthard Will, Ullrich Hesse – TU Dresden

gas pulsations in the annular gap between the crank end working chamber and the first sealing ring of the packing that are difficult to grasp.

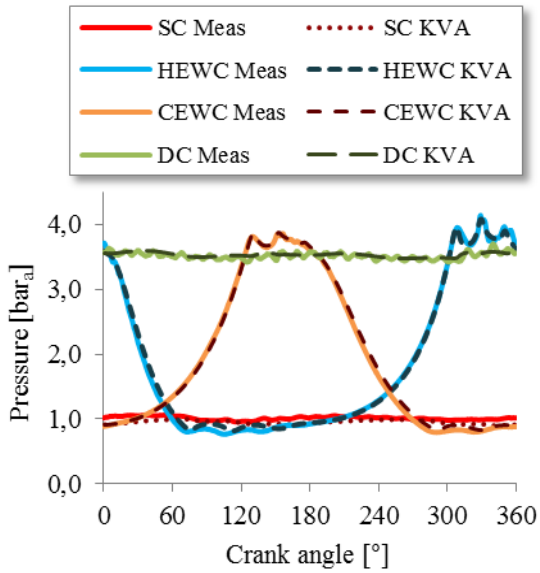

Figure 4: Comparison of measured and calculated pressure curves from the cylinder

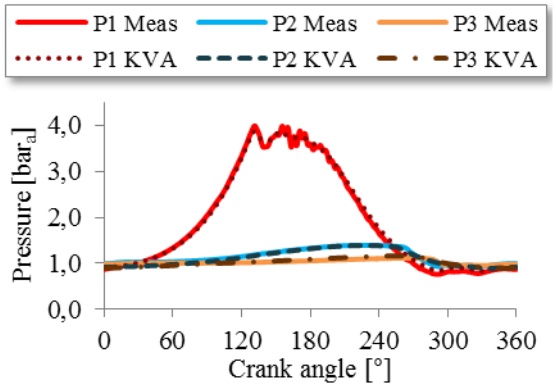

Figure 5: Comparison of measured and calculated pressure curves from the packing

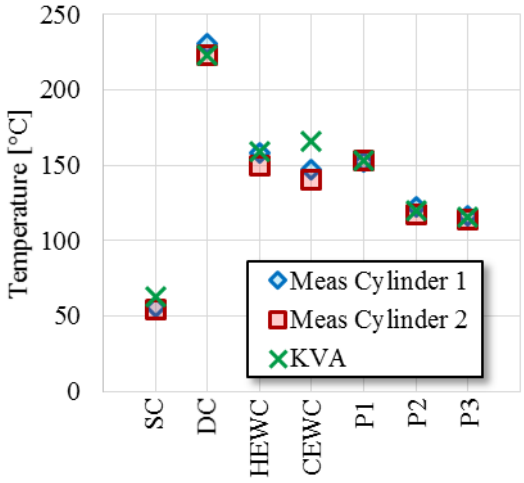

Figure 6: Comparison of averaged measured and calculated (KVA) gas temperatures

Some performance parameters are shown in figure 7. The deviations between the measurements and the KVA calculation for the mass flow and indicated power are below 5 % and are therefore in a reasonable range.

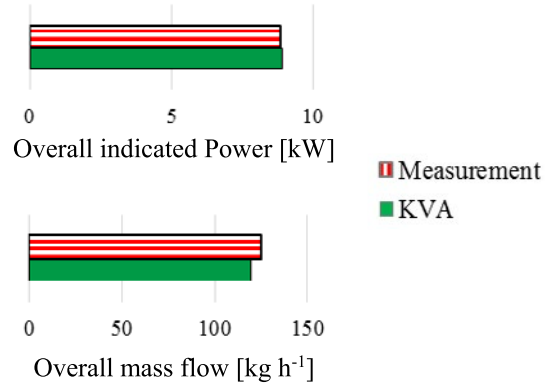

Figure 7: Comparison of averaged measured and calculated (KVA) performance parameters

Figure 8 shows the calculated time curves of temperatures and the heat transfer coefficients for both working chambers. These parameters can be determined by measurements only with great effort. Therefore, the calculation using KVA represents a time- and cost-saving alternative. Furthermore, special phenomena become visible, e.g. that the temperature temporarily rises above 250 °C during the discharge phase.

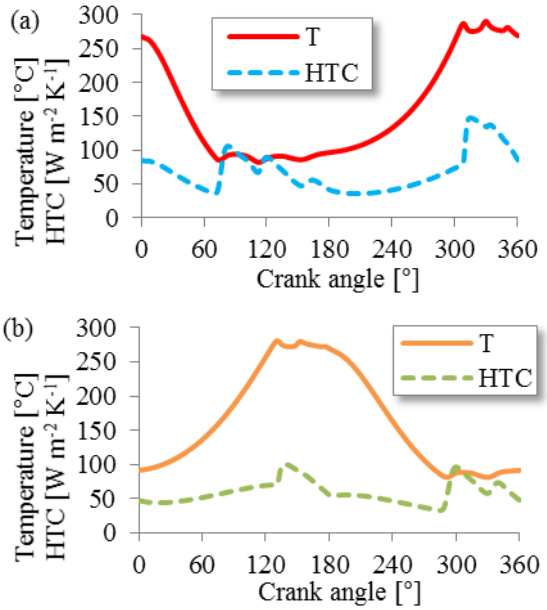

Figure 8: Calculated temperature curves (T) and heat transfer coefficients (HTC) over one crank turn for the head end working chamber (a) and for the crank end working chamber (b)

The comparison between the measured and calculated results by means of KVA shows that based on a simplified model structure a good and reliable correspondence of the calculated values with those at a real compressor can be achieved. A validation of the calculated values based on

by: Konrad Klotsche, Gotthard Will, Ullrich Hesse – TU Dresden

measured data is not strictly necessary but is recommended if possible.

In conclusion, the calculation results enable a more precise analysis of the compressor behaviour, as all relevant thermodynamic parameters are determined with high temporal resolution. Thus, for example, the temperature progression in the working chambers can be shown, which changes highly dynamically and can only be measured with great effort. In addition, many parameters that are difficult to measure can be determined, e.g. all the heat and exergy flows for all volumes and wall elements, heat transfer coefficients, valve behaviour, pressure pulsations in pipelines, etc. With the help of a calculation tool like KVA, it is possible to precisely determine which phenomena cause the biggest losses and how existing potentials can best be used.

4 Thermal compressor simulation by means of ANSYS

In order to enable a more precise examination of the component temperatures, a solid model was created in Ansys that takes the compressor components into account as realistically as possible (see figure 9).

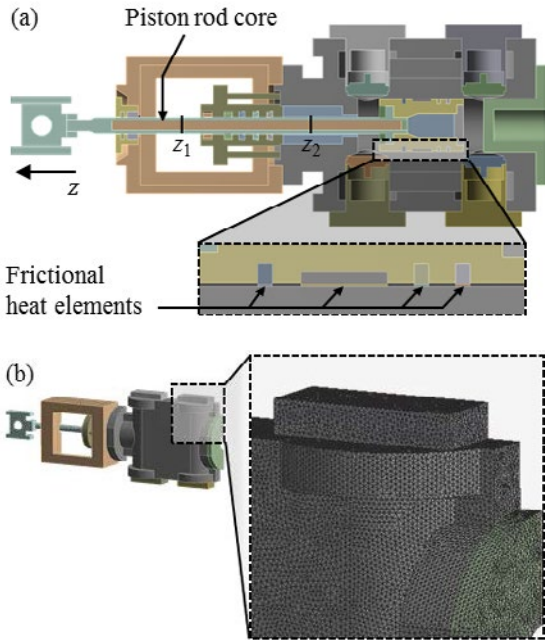

Figure 9: Ansys model of the compressor cylinder (a) and detailed view of the cylinder meshing (b)

For example, only connecting elements (e.g. screws) or other small parts were omitted and minor simplifications were made to complex components (e.g. the cylinder). Furthermore, due to the mirror symmetry along the vertical mean sectional plane, only half of the model was modelled in order to keep the number of elements and thus the calculation time as low as possible. Since the oscillating compressor assembly is not moved in the simulation, it is positioned in the middle position between the two dead positions (BDC and TDC), as with the KVA model. Figure 9 (a) shows that the core of the piston rod has been modelled as a separate component which can be varied in terms of both the thermal conductivity (λ_{core}) and the diameter ($Ød_{core}$). This is used for a parameter study in which the impact of changed properties of the piston rod core on various component temperatures is investigated.

For the boundary conditions on all free surfaces of the model, the measured temperatures and HTCs determined with the aid of KVA were used. In addition, the thermal loads resulting from friction of the sealing rings on the mating surface are applied (assuming a friction coefficient μ_{fric} of 0.1). For this purpose, very thin elements (see figure 9 (a)) were modelled, which are provided with a heat source density corresponding to the frictional power.

5 Parameter study with regard to piston rod heat transfer

With the help of the simulation model 14 different simulations were carried out. Table 1 shows an overview of the simulated configurations and the corresponding labels.

Table 1: Overview of parameter configuration for the Ansys simulation model and their labels

	Thermal conductivity of the piston rod core [W m^{-1} K^{-1}]						
$Ød_{core}$	Original	10^2	$3*10^2$	10^3	10^4	10^5	$5*10^5$
15 mm	„15-Orig“	„15-2“	„15-3*10^2“	„15-3“	„15-4“	„15-5“	„15-max“
25 mm	„25-Orig“	„25-2“	„25-3*10^2“	„25-3“	„25-4“	„25-5“	„25-max“

The temperature distributions of the whole model are compared for the configurations "15-Orig" and for "25-4" in figure 10. The contour plots show that the increase of the diameter and of the thermal conductivity of the piston rod core have a significant influence on the temperatures of the components. For example, there is a significant cooling in the packing area, so that the maximum temperature of the model (red label) shifts from the packing area to the cylinder area. In addition, the temperature gradient along the piston rod is significantly reduced. This also cools the piston at its crank end side.

by: Konrad Klotsche, Gotthard Will, Ullrich Hesse – TU Dresden

One of the most important objectives of the internal piston rod cooling is heat dissipation from the packing area. In order to investigate the influence of both parameters, the maximum temperature occurring in the packing area $T_{pack,max}$ was evaluated. The results for all simulations are shown in figure 11.

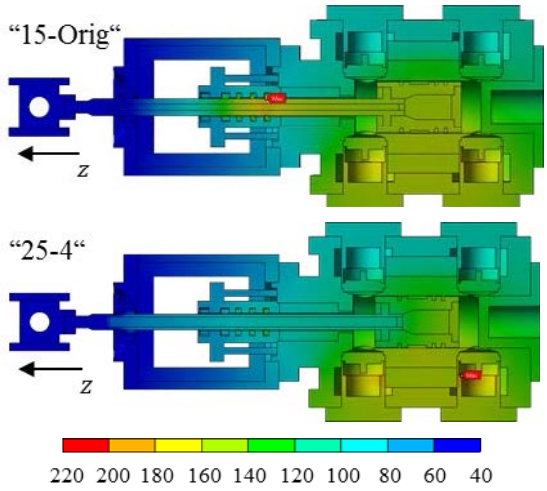

Figure 10: Comparison of the temperature distribution for the simulations "15-Orig" and "25-4"

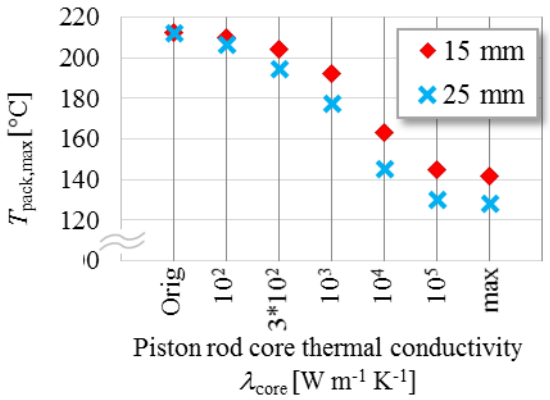

Figure 11: Comparison of the maximum temperature $T_{pack,max}$ at the packing for all simulations.

Figure 11 shows a reduction of the maximum packing temperature for both diameter configurations as the thermal conductivity of the piston rod core λ_{core} increases. As expected, the cooling is greater with the larger diameter. Replacing the original core of the piston rod with a pure copper core (approximately $3*10^2$ W m^{-1} K^{-1}) [3] would reduce the maximum packing temperature approximately 8 K or 18 K for a core of 15 mm or 25 mm, respectively. An increase in thermal conductivity to 10^4 W m^{-1} K^{-1} which is given as an approximate magnitude for a piston rod internal cooling with a two-phase cooling fluid [4] would lead to a temperature reduction of 49 K ($Ød_{core}$ = 15 mm) and 67 K ($Ød_{core}$ = 25 mm). It is shown that higher thermal conductivities of the piston rod core of up to 100 000 W m^{-1} K^{-1} would lead to a significant cooling. Beyond that, there are only minor changes, although this order of magnitude cannot be currently achieved by any type of internal cooling. In the long term, maybe graphene or carbon nanotubes could also be used as technical materials for the core material. These relatively new materials have high thermal conductivities of up to 5 000 to 6 000 W m^{-1} K^{-1} (at room temperature) [5].

Another important criterion for the internal cooling of the piston rod is the heat transport along the piston rod. For the evaluation, the heat flux density in the piston rod core (not in the circular ring-shaped cross section of the actual piston rod) in the direction of the cylinder axis (z-axis) was averaged at two characteristic locations z_1 and z_2 (see $\bar{\dot{q}}_{core}$ in figure 12 (a). These two positions are shown in figure 9 (a). The axial heat flux density in the cross sections of the piston rod is in the range of a few kilowatts per square meter and is therefore not shown here. In addition, it remains almost constant for all configurations. The total heat flow $\dot{Q}_{tot}$ ($\dot{Q}_{tot} = \dot{Q}_{core} + \dot{Q}_{rod}$) at both positions z_1 and z_2 is shown in figure 12 (b) for all configurations. It can be determined based on the respective area proportions of the piston rod and its core.

Figure 12 (a) shows that the axial heat flux densities between 100 and 1500 kW m^{-2} that can be dissipated from the packing through the piston rod to the crosshead for realistic thermal conductivities of the piston rod core material λ_{core} = 300...10^4 W m^{-1} K^{-1}. The values at position z_1 are always higher than for z_2, which also applies to the total heat flows shown in figure 12 (b). This indicates that the heat flow from the packing towards the crosshead (position z_1) is larger than the heat flow from the crank end working chamber towards the packing (position z_2). The difference between these two heat flows represents the heat dissipated from the packing rings for the respective diameter.

This results in heat flows of approximately 20 to 40 W from the packing for a 15 mm piston rod core in the range of realistic thermal conductivities of the piston rod core of 300...10^4 W m^{-1} K^{-1}. For a 25 mm core, the heat flow rejected from the packing increases to approximately 50 to 200 W.

by: Konrad Klotsche, Gotthard Will, Ullrich Hesse – TU Dresden

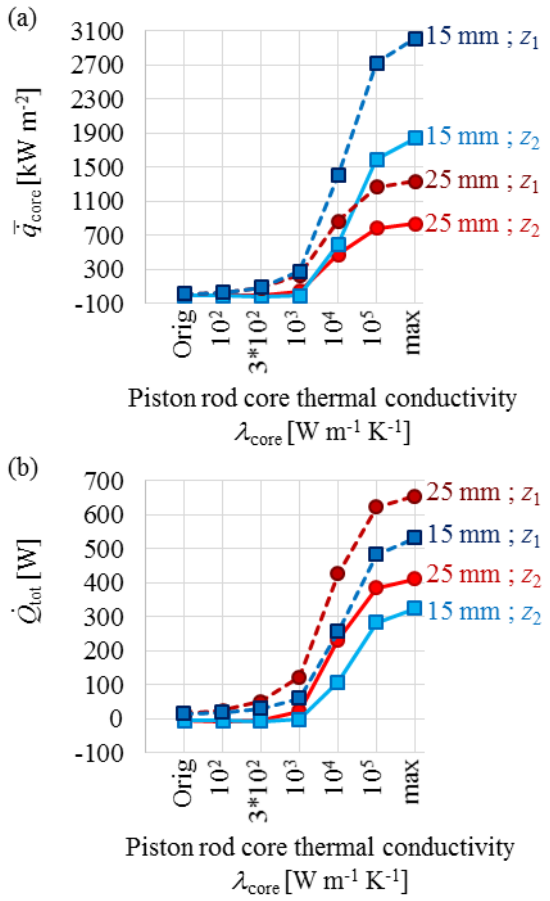

Figure 12: Averaged axial heat flux of the piston rod core ($\bar{q}_{core}$) and total axial heat flow through the piston rod core and through the piston rod ($\dot{Q}_{tot}$) at position z_1 and z_2.

6 Conclusion

Using a reciprocating test compressor, this study shows how measurement and computational methods can be used to determine the compressor's thermodynamic behaviour more precisely.

With the help of the measurement results, the calculation model for the determination of time-dependent temperature and heat transfer coefficients could be verified. These in turn were used as boundary conditions, which are required for a realistic simulation of the component temperatures within a FEM simulation model.

Using this simulation, the influence of the internal piston rod cooling on the thermal behaviour of the compressor was investigated. This approach is based on a piston rod core with improved thermal properties to increase the heat transfer through the oscillating assembly. The influence of the diameter and the thermal conductivity of the piston rod core are evaluated. It was found that the maximum packing temperatures were reduced by 8 to 18 K and 49 to 67 K in the range of realistic thermal conductivities of the piston rod core (λ_{core} = 300...10^4 W m^{-1} K^{-1}) for piston rod core diameters of 15 mm and 25 mm, respectively. The heat flows that are dissipated from the package and that lead to this cooling range of 20 to 200 W for those configurations.

7 Acknowledgements

Sincere thanks are expressed to Ms. Shaimaa Hefny for substantial help with the Ansys simulation model.

References

[1] Surek, D.; Stempin, S. (2014): Technische Strömungsmechanik. Springer Vieweg.
[2] Will, G.; Hesse, U. (2014): Thermodynamic Calculation of Reciprocating Compressor Plants. 9th EFRC Conference.
[3] Hoff, K.; Knop, G.; Langela, M. (2016): A new piston rod design to improve packing lifetime for non-lubricated reciprocating compressor applications. 10th EFRC Conference.
[4] Thomas (née Hammer), C. (2013): Innenkühlung der Kolbenstange von trockenlaufenden Kolben-verdichtern. Dissertation. Technische Universität Dresden.
[5] Balandin, A.; Ghosh, S.; Bao, W.; Calizo, I.; Teweldebrhan, D.; Miao, F.; Lau, C.N. (2008): Superior Thermal Conductivity of Single-Layer Graphene. Nano letters. 8(3). 902-907.

Diagnosis of a capacity control problem that appeared randomly

by:

Luis Sancho Gómez, Juan José García Pérez
Iberian Lube Base Oils Company
Valle de Escombreras, s/n
30350 Cartagena Murcia

11th EFRC CONFERENCE
September 13 – 14, 2018, Madrid

Abstract:
This paper describes case study about the detection, root cause analysis and lessons learned of random appearance reciprocating compressor capacity control problem.

After one year or trouble-free operation of a reciprocating compressor, a random appearance control problem arises. Due to the complexity and infrequent appearance of the problem the diagnosis and solution took a year. This article shows the methodology and the root cause analysis developed by ILBOC for a general, hidden failure, control problem solution. It also explains how the PV diagram was the key tool to identify the problem.

by: Luis Sancho Gómez, Juan José García Pérez – ILBOC

Introduction

One year after commissioning and start-up of ILBOC Group III Base Oils Plant, one of the two H2 compressors started to randomly experience abnormal capacity control problems. Up to that time, the compressor performance was excellent without any issues. The other compressor also had flawless performance and didn't show that problem.

The Iberian Lube Base Oils Company, SA (ILBOC) is a company incorporated in 2012, 30% owned by Repsol Petróleo and 70% by SK Lubricants, to produce state-of-the-art Lubricants (LBOs) (group II and III) at its plant in the Escombreras Valley in Cartagena.

Repsol Petróleo is the leading refining company in Spain, and with its investment in this plant, it has reinforced its strategy of developing the lubricants business.

SK Lubricants is a pioneer company in South Korea and world leader in the high-quality lubricant base oil market.

ILBOC produces more than 500,000 tons per year of high-quality base oils for the manufacture of high-tech lubricating oils with significant advantages over conventional oils.

Description of the system:

Two (1 plus spare) 4-cylinder reciprocating compressors (Figure 1)

- 1MW power
- 180kg/cm2 discharge pressure
- Medium: H2 gas
- Service: supply for make-up (cylinders 1 and 3) and recycle (cylinders 2 and 4) gas
- Function of the compressors is the supply of the H2 necessary for the catalytic reaction in Dewaxing reactors for manufacturing group III lubricants
- Stepless + spillback capacity control

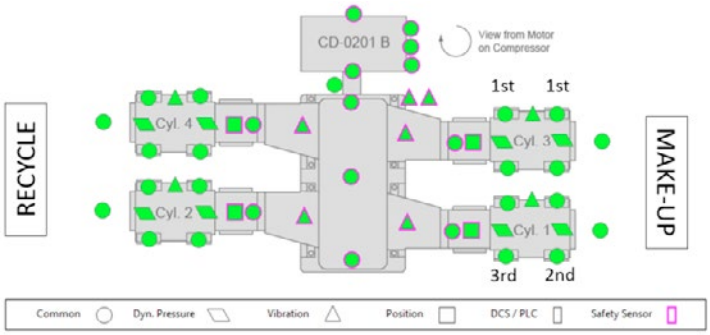

Figure 1 -Compressor scheme

Description of the problem

The flow capacity demanded by the DCS of the plant and the flow capacity calculated by the PLC of the compressor (1st, 2nd stage), as can be seen in Figure 2, is stable. Suddenly (in less than 1 minute), 1st and 2nd stage capacity increased from 70% to near 100%.

This capacity increase is confirmed by plant main pressure transmitter and plant hydrogen flowmeter. After a few minutes, the operation and capacity control return to normal. No alarms were issued.

It seems that the compressor capacity control system had a temporary malfunction. This problem appeared randomly and repeatedly; sometimes with days in between, sometimes with weeks.

by: Luis Sancho Gómez, Juan José García Pérez – ILBOC

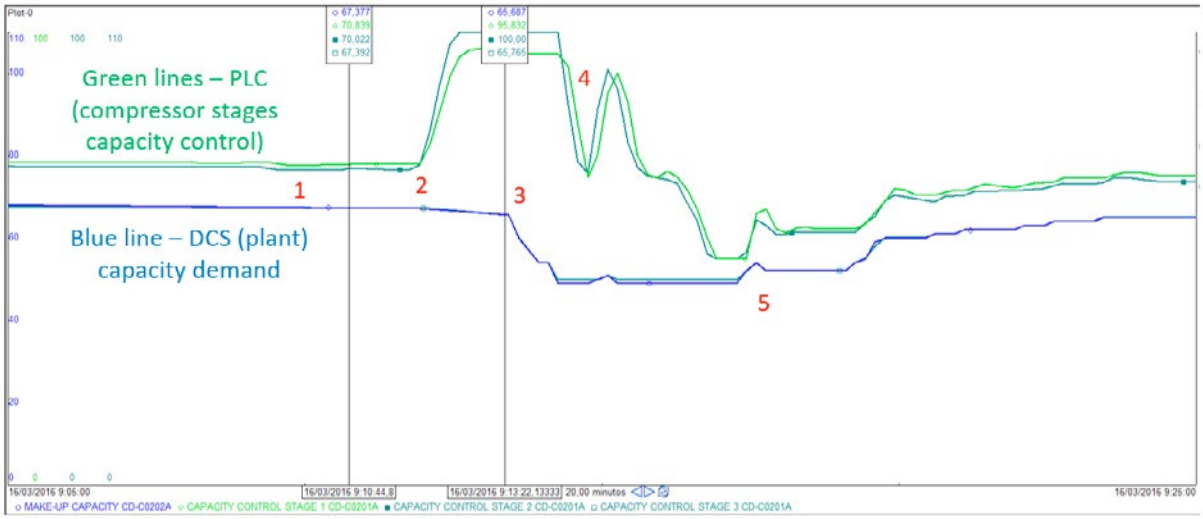

Figure 2 – Graphic description of the problem. 1st and 2nd stage capacity oscillation.

The blue line is the needed capacity of the compressor (plant – DCS demand). The green lines are the capacities of each stage that the PLC calculates to supply DCS demand (green line trend must follow blue line trend).
1.- The plant capacity demand is stable (blue line) and the compressor capacity is also stable (green line)
2.- The plant capacity demand is stable (blue line) but the compressor capacity increases suddenly (green line) to near 100%
3.- The plant capacity decreases (blue line) as the DCS reacts to undesired increase in plant pressure
4.- The compressor capacity (green line) oscillates up and down very fast.
5.- Finally the compressor capacity (green line) follows plant capacity (blue line) as it should be.

Description of the capacity control system

The capacity control system of the compressors is quite complex. Plant DCS sends a signal to local compressors PLC to reach the desired plant pressure setpoint. The local PLC makes the calculations to adjust the capacities of each stage. Depending on the capacity needed step-less control systems and spill-back valves work together or separated. The step-less control system governs hydraulic actuators that are mechanically linked to the valves (see Figure 3).

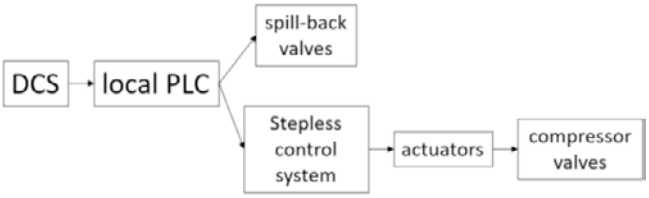

Figure 3 - Scheme of the capacity control system

DCS, local PLC, spill-back valves and stepless control systems are state of the art systems with diagnosis capacities and communication of alarms and events. Unfortunately, none of the previous mentioned systems showed any alarm.

by: Luis Sancho Gómez, Juan José García Pérez – ILBOC

As the capacity control problem duration was normally less than 5 minutes and it happened randomly in time and with days or weeks in-between, it was very

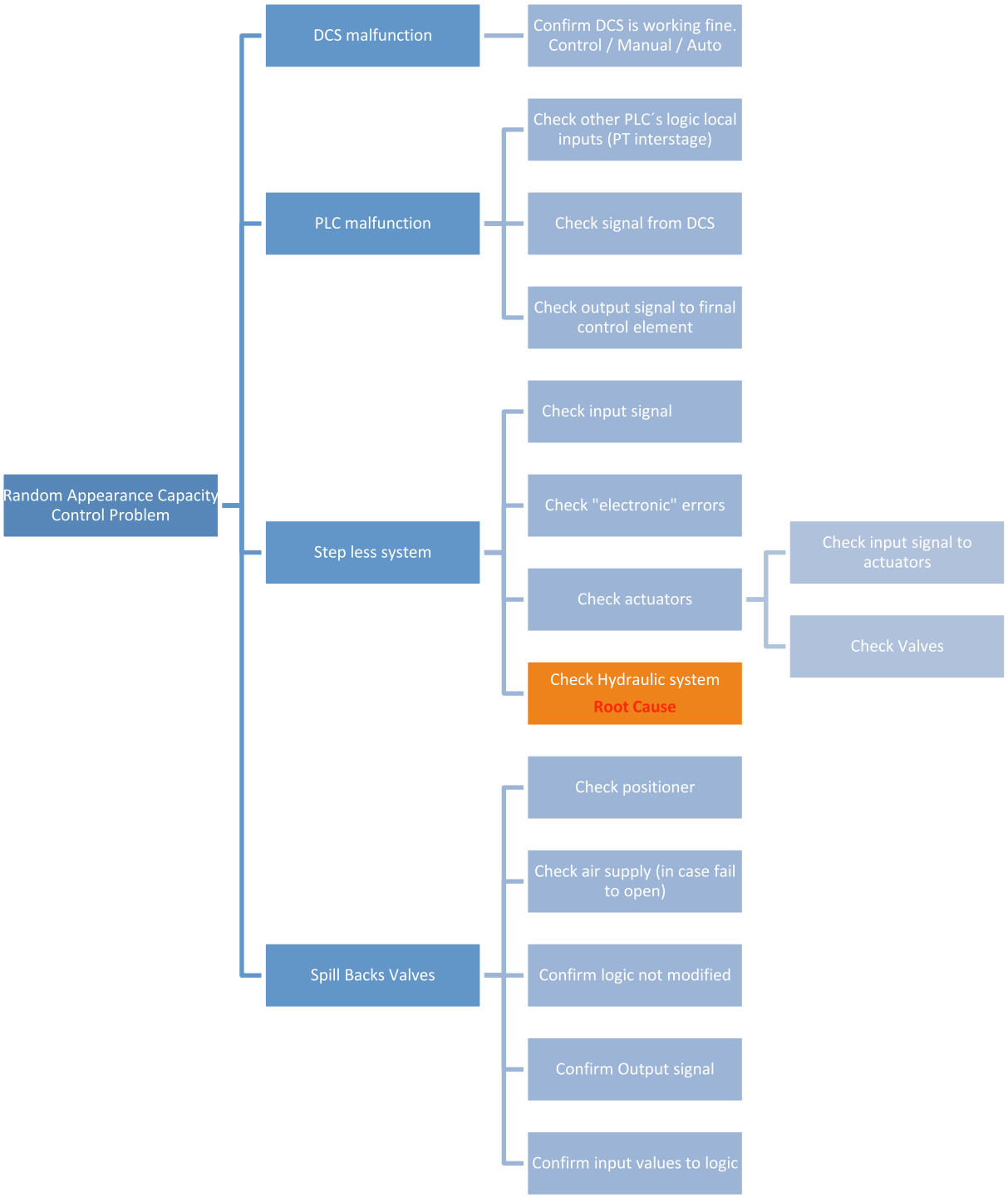

Figure 4 - root cause analysis tree of the problem

by: Luis Sancho Gómez, Juan José García Pérez – ILBOC

difficult to have the luck of diagnose the systems in real time in person.

In few cases the problem near tripped the whole plant. A task force team between operations, maintenance and reliability departments, with a lot of support of the manufacturers of each of the elements of the system, was stablished to solve the problem.

As there was no clear suspect of what element could be failing, a complete RCA (root cause analysis) was performed and the root cause tree is attached as Figure 4.

All of the elements of the route cause tree where checked (signals, logic programs, …), in some cases replaced (for example wirings) and in some cases exchanged by the warehouse spare ones (electronic cards, pressure transmitters, …) to find, by a simple trial and error methodology what was the element failing.

This methodology took months to be fully implemented and, unfortunately, it didn't work to find the failing element.

How the problem was solved

After several months we assumed that it was not possible to discover where the failure was using the current methodology, so we started to look for other tools.

The Condition Monitoring Software system installed at ILBOC is connected also to the DCS and the PLC system to get process values and capacity control system data for better diagnosis of the system. One of the capabilities of the Condition Monitoring system is the ring buffer that is continuously recording all raw data of all signals for the last 10 minutes.

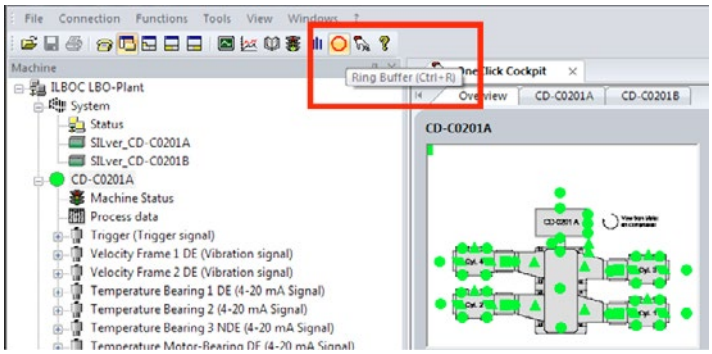

Figure 5 - Condition Monitoring Software User Interface showing the ring buffer capability

We waited to the next event to happen and remotely we recorded a Ring Buffer.

In collaboration with the Condition Monitoring Software manufacturer, we analyzed all the raw data to find any abnormal signal and what was discovered is that, actually, the problem was only in 3rd stage. For some reason, the 3rd stage went to 100% but DCS, local PLC, and stepless control system was demanding a lower capacity (eg. 70%). First and second stage where working at the capacity that DCS, PLC and stepless system was demanding. That insight focused us to the third stage and it was clear for us that the problem was only in third stage and first and second stage sudden increase in capacity was commanded by the PLC, as a reaction, just to supply the gas third stage was suctioning.

That insight was discovery thanks to another Condition Monitoring Software capability that is the representation of the PV diagram (see Figure 6), that was also recorded in the Ring Buffer.

by: Luis Sancho Gómez, Juan José García Pérez – ILBOC

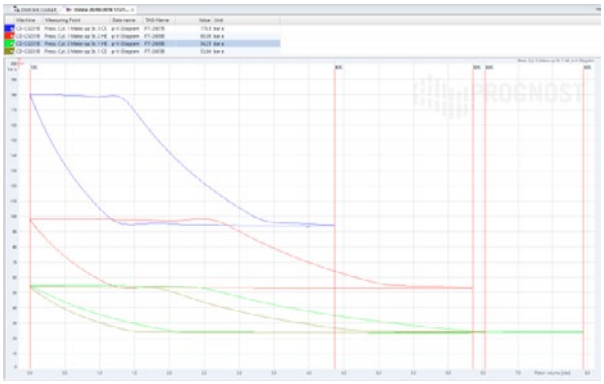

Figure 6 - Condition Monitoring Software User Interface showing the PV diagram of the 3 stages of the compressor

As the problem was only in third stage, additional and redundant instrumentation was installed to fully monitor third stage operation and we discovered that hydraulic pressure to the actuator was stable most of the time but suddenly started to oscillate.

We discovered that the problem was in the pressure regulation valve of the hydraulic system (see Figure 7) such that sometimes, it started to oscillate in a resonance mode. The low-pressure peaks of the pressure resonance behaviour were so low that the actuator was unable to keep the valve open (the design of the compressor/actuators is Fail To Load).

The solution was simply to replace the hydraulic pressure regulator. In a further examination of the regulator it was found that the internal spring was a defective and suffered relaxation over time.

We also discovered that for the pressure transmitter of the hydraulic system, the refresh rate was too low to reveal the lack of pressure.

Figure 7 - hydraulic pressure regulator

What we have learnt

Machinery monitoring systems like the showed before are a great tool to analyse not only mechanical problems but also, capacity control related problems. They help to analyze the problem from the bottom to the top

It is a good practice to connect the machinery monitoring system to plant and local control systems to also monitor process and control parameters and be capable to analyze at the same time process versus mechanical response.

References

- Hydromechanical resonant frequency and cylinder speed. https://www.hydraulicspneumatics.com © 2018 Informa USA, Inc.

Customized Thermoplastic Components for Reciprocating Gas Compressors

EGC Critical Components has engineered and manufactured customized components and seals for compressors for over 50 years.

Our strong materials portfolio ensures that EGC has the material best suited for your API618 or PET compressor application – refining, petrochemical and specialty gases. From cryogenic liquid natural gas (LNG) to high pressure/high temperature (HPHT) service - EGC has experience, expertise, and technology to ensure your most critical parts meet your performance requirements.

EGC engineers have decades of experience in fitting the best materials to some of the most challenging applications. Our custom in-house blending capabilities mean that if we don't have the material you need, we can make it. . .

- Rider rings • Piston rings • Packing rings • Poppets
- Valve plates and rings • Oil wipers

Learn more about our compressor component solutions at EFRC 2018, booth No.2
www.egccomponents.com

EGC CRITICAL COMPONENTS
Materials. Engineering. Precision.
Europe +39 327 4910056
USA +1 281-774-6100

Burckhardt Compression

Measuring dynamic pressure of a mechanical seal of a LDPE reciprocating compressor

by:

Felix Ragg, Ricardo Cruz
R&D
Burckhardt Compression AG
Winterthur, Switzerland
Felix.Ragg@burckhardtcompression.com

11th EFRC CONFERENCE
September 13 – 14, 2018, Madrid

Abstract:
During production of low-density polyethylene (LDPE), ethylene gas is compressed up to 3200 bar. At the core of this process is a combination of two reciprocating compressors which are monitored by condition based monitoring systems. The secondary compressor, called a Hyper, compresses the gas in two stages from 300 bar up to 3200 bar and has to be capable to operate reliably in such dynamic environment. On the Hyper compressor the gas is compressed via a packed plunger which is lubricated via a forced lubrication system. The Hyper high pressure packing and its behavior is of vital importance as its main function is to seal the compression space from the atmosphere. The high pressure packing is in essence, a mechanical seal typically made up of one radial split pressure breaker ring and five radial/tangential split ring pairs. In this case, one cylinder was equipped with pressure transducers on the high pressure packing in order to dynamically measure the pressure drop between each sealing element. This article discloses a measurement campaign currently underway on a fully operational Hyper compressor and provides a valuable insight to the dynamic behavior of high pressure packing. The first results show a changing sealing activity of the different rings, revolution by revolution. During the observed periods, some of the sealing rings are inactive and become active just a few compressions strokes later with no signs of hindered performance. Furthermore, the wear pattern of the packing will be interpreted with respect to this extreme dynamic behavior and also compared to a previous measurement campaign.

by: Felix Ragg, Ricardo Cruz – Burckhardt Compression

1 Introduction

The production of polyethylene of low density (LDPE) requires gaseous ethylene at very high pressures of up to 3200 bar. To achieve this high pressure, a combination of two reciprocating compressors is applied. The primary compressor brings the gas from atmospheric pressure to 300 bar, from where on the secondary compressor, called Hyper, compresses the gas in two stages from 300 bar up to 3200 bar. Due to the lack of redundancy, often both compressors are equipped with condition based monitoring systems. The gas on a Hyper compressor is compressed via a packed plunger type design. The plunger, made out of solid tungsten carbide, is lubricated directly at its locations of friction via a forced lubrication system. The compressed gas is sealed against the environment by a high pressure packing and a low pressure packing. The high pressure packing, which lies in the focus of this article, contains an arrangement of six mechanical sealing elements. The lifetime of the sealing elements is of vital importance, not only for operational efficiency and mean time between overhaul (MTBO) reasons, but also to prevent catastrophic failures at this high pressure. The lifetime of a high pressure packing varies greatly due to intrinsic design and extrinsic operational factors. To improve the lifetime of these sealing elements, one must understand the behavior of the packing and the underlying mechanism of sealing very high pressures. Therefore, a cylinder equipped with additional sensors and especially pressure transmitters inside the high pressure packing, will provide an insight into the operational characteristics of the packing. The first measurement campaigns were conducted by Scheuber[1] and Traversari[2] in the late 1970s. As a next step, a special monitored cylinder was mounted on a K8 Hyper compressor in 2015 and brought into operation in 2016. Figure 1 shows the Hyper compressor during assembly on site with the monitored cylinder in gray color. This article discloses the latest results of a measurement campaign currently ongoing on this Hyper compressor in normal production operation. The focus lies on setting up such complex measurement system and begin to gain understanding of the pressure distribution inside the packing.

Figure 1: K8 Hyper compressor with the monitored cylinder in gray color on the left hand side.

2 The Monitored Cylinder

2.1 Typical Pressure Distribution

To discuss the mechanism working inside a high pressure packing it is advantageous to introduce the definition of dynamic and static pressure component. In general, a sealing element, or ring, will face two different pressure components, the

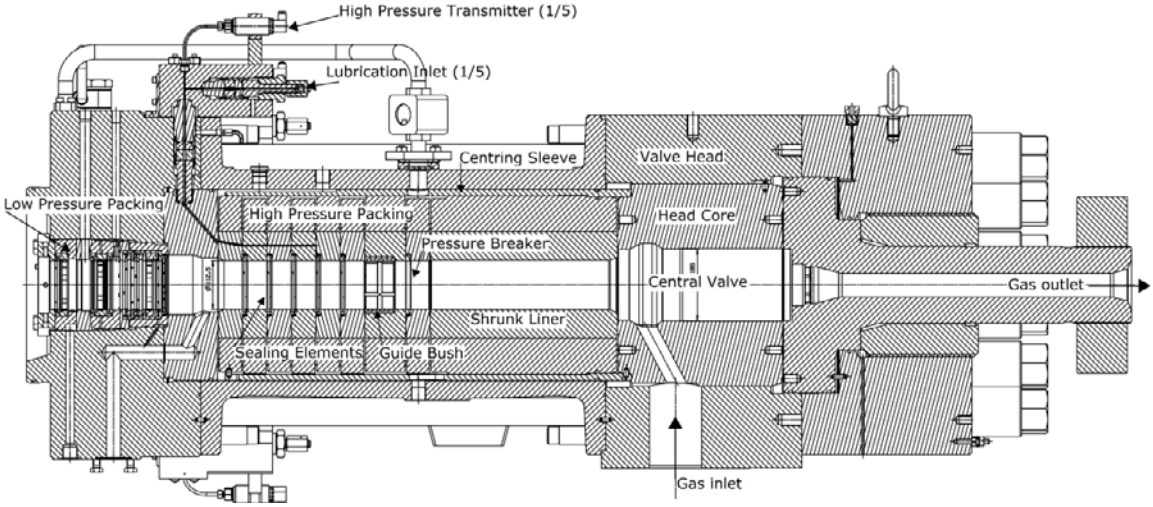

Figure 2: Cut through the monitored cylinder and description of parts.

by: Felix Ragg, Ricardo Cruz – Burckhardt Compression

altering component, called dynamic pressure, which is the difference of suction and discharge pressure and which alters revolution by revolution. The second component is the static component which is the difference of suction and atmospheric or

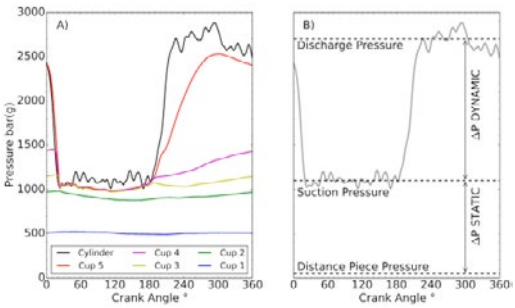

Figure 3: Ideal pressure distribution A) and definition of dynamic and static pressure component B).

distance piece pressure. Figure 3-B illustrates this definition.

Beside the altering dynamic pressure component, the tribological system is covering several lubrication regimes during one stroke due to the reciprocating motion of the plunger (referred to the *Stribeck* curve). The two pressure components differ considerably in terms of influence on the sealing characteristic of the rings as well as the operational behavior of the entire sealing system[3]. The separation of the pressure components allows the optimization of the sealing system and hence the use of rings for each pressure component (specific load). This ends up into a heterogeneous sealing concept where the pressure drop over one sealing element is distributed more evenly across the entire packing. This concept is implemented by inserting different types of rings across the packing. In front of the packing, facing upstream, a pressure breaker (PB), which operates as gap flow type sealing, reduces the dynamic pressure component by throttling it. The subsequent true sealing elements (SE) should only face the static pressure component, if the pressure breaker is designed

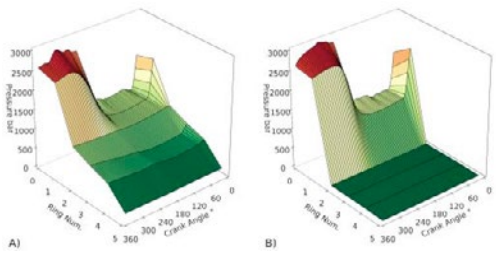

Figure 5: Pressure distribution across packing and over crank angle. A) optimized distribution, B) unfavorable distribution where first ring seals entire pressure.

correctly. Figure 3-A and Figure 5-A gives an idea how the pressure distribution ideally looks like when the first rings throttle the dynamic pressure and the last rings only face the static component. With this kind of pressure load splitting, the lifetime of the rings can be increased by preventing the sealing elements to fail by fracture. Without partitioning the load, one sealing element will take the complete pressure load, dynamic and static pressure like shown in Figure 5-B. Consequently, the highly loaded ring will fail and the subsequent ring takes over, until compressor alarm is given or catastrophic failure occurs.

2.2 High Pressure Packing

The high pressure packing of a Hyper compressor is in essence a mechanical seal composed of five sealing elements, one pressure breaker and one guide bush. Each sealing element is a ring pair of a cover ring, radially split, and a tangentially split sealing ring shown in Figure 4. When implemented into the packing, the two rings are twisted to each other to seal the joints of the segments. The pressure breaker is separated radially like the cover ring. Distinct grooves on top of the pressure breaker and cover ring, facing upstream, allow the gas to

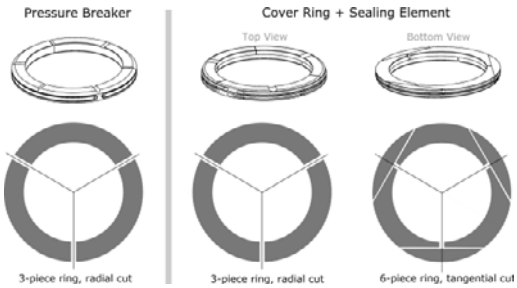

Figure 4: Pressure breaker ring and sealing element with location of cut.

flow back during expansion stroke. All rings are made from special bronze alloys optimized for low friction coefficient and good thermal conductivity but still high strength. The segments of the rings are held in place by garter springs, not only for assembly but also for start the sealing activity when pressure drop across the ring is not sufficient during start-up. Between the sealing elements and the pressure breaker, the guide bush is located. Deep by-pass grooves prevent the bush from taking any sealing function hence its duty is guiding the plunger. Rings and guide bush are housed in an arrangement of high-strength cups with special grooves for lubrication. The lubricant is highly refined mineral oil or synthetic oil with additives for wear resistance and anti-oxidation. Upstream of the high pressure packing is the shrunk liner where

by: Felix Ragg, Ricardo Cruz – Burckhardt Compression

the compression of the gas by the plunger takes place. Downstream of the high pressure packing, the low pressure packing is located. Figure 2 gives an overview of the test cylinder with the high pressure packing. The plunger diameter of the compressor being heavily monitored is 111 mm with a stroke of 450 mm. The Hyper compressor runs at a speed of 200 revolutions per minute. The plunger system design shows some advantages compared to the traditional piston ring system design. One is the direct lubrication where lubricant is injected exactly between the sealing elements while in the piston ring system a controlled injection at the sealing elements is not possible, or difficult to implement.

2.3 Test Packing Measurement Setup

The condition based monitoring system installed on the Hyper compressor provides online data of all implemented sensors as well as an event triggered ring buffer of high resolution. The trigger can be defined by the customer as start/stop, alert, unsafe or even based on customized performance data gained from sensors. Access to the data will be provided through a distribute control system (DCS) on site. In a normal application the condition based monitoring system comprises of several sensors per cylinder as well as sensors for trigger, line temperature and line pressure data. Crank angle information is provided by a trigger switch installed at the fly wheel of the compressor. Two acceleration sensors, one on the cylinder and one on the frame next to the crosshead deliver vibration data. Eddy current sensors measure horizontal and vertical plunger position. A strain gauge ring delivers cylinder pressure data in high resolution for p-V diagrams and valve action analysis. The highly monitored cylinder discussed here, has additional specially adapted sensors to understand the operational behavior of the plunger and packing more in detail. Plunger temperature is measured which indicates, among others, the thermal load acting on the plunger. Leak gas flow provides direct information about the sealing efficiency of the packing rings. Figure 7 shows the locations of the sensors installed. Packing pressure is measured directly at each lubricant injection point inside the packing. Therefore, two additional lubrication bores, which do not contribute to packing lubrication, are implemented to monitor the pressure at each single sealing element. Figure 6 illustrates the high pressure packing in detail including the lubricant injection positions. The color scheme of Figure 6 represents the one used for plots. The pressure transmitters are commercially available and widely used in automotive industry. The highly resolved pressure data as well as the ring buffer data is recorded with a sampling rate of 25kHz. Long term trends are generated from the highly resolved data by averaging on hourly base.

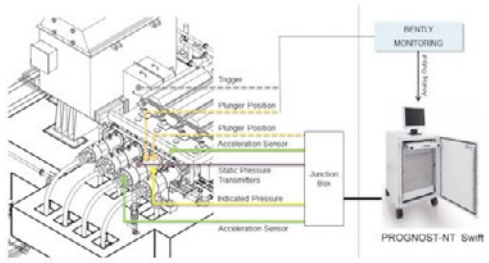

Figure 7: Measurement setup and sensor location (courtesy of Prognost).

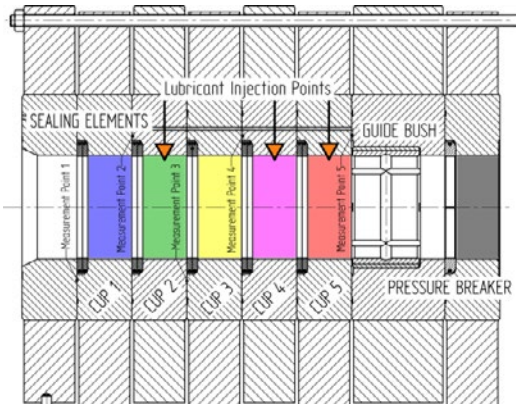

Figure 6: Detailed view of high pressure packing with measurement and lubrication points. Color scheme of cups valid for plots throughout the article.

3 Results

3.1 Pressure Distribution

From a period of almost one year, representative data was selected. During the test period no adjustments were made to the packing. Shutdowns were mainly due to scheduled plant maintenance and cleaning of the low pressure separator unit. These disruptions are visible as such in the operational pressure data in Figure 9-C where all pressure signals go to zero. The long term trend data was continuously recorded during the operational time of the test packing which was 6585 hours. When analyzing the long term packing pressure data in Figure 9-A, it is peculiar that no uniform or even constant pressure distribution is kept for more than approximately thirty days. This means, the total pressure difference across the packing is not equally divided by the number of rings and not each sealing element faces the same pressure load. On the contrary, one sealing element (SE4) takes the entire load for a long period, see

by: Felix Ragg, Ricardo Cruz – Burckhardt Compression

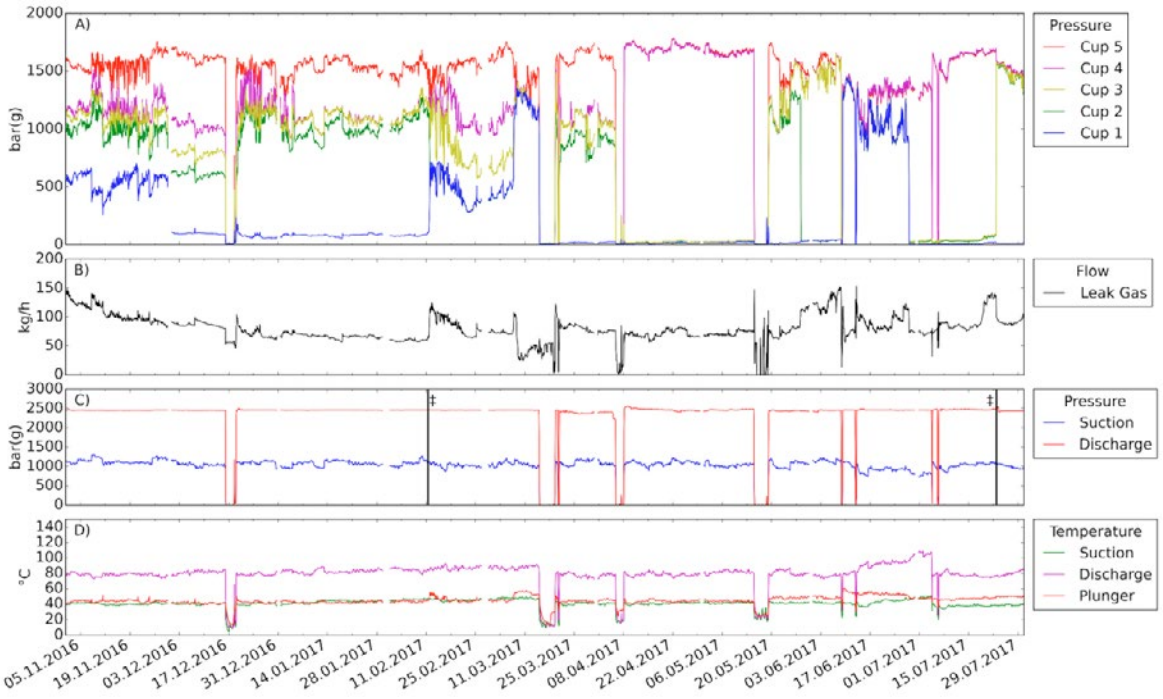

Figure 9: Long term data of packing. A) packing pressure, B) leakage flow of packing, C) operational pressure, D) temperatures of packing.

Figure 9-A, from begin of April to end of May, while the other elements are idling. Changes in the sealing activity are triggered mainly by compressor shutdown and restart. After each restart of the compressor a new sealing layout is formed. This has also an impact on the gas leakage flow (Figure 9-B) through the packing. The leakage flow increases right after restart of the compressor and swings back to a lower level.

But not only changes in operational mode of the compressor induce a switch of ring sealing activity. Sudden changes can also occur if the compressor runs steady, which can be seen in Figure 9 at the dates of 11.02.2017 and 22.07.2017 (marked in Figure 9-C by vertical lines and ‡). Figure 12 is a snapshot of the event from 22.07.2017 and illustrates the change in sealing activity when pressure in cup three (yellow line) and two (green line) increases rapidly from 80 bar to 1550 bar (Figure 12-A). At the same time the leakage flow decreases by 40 kg/h (Figure 12-B). Subsequently, the plunger temperature increases (Figure 12-C) since the leak gas flow cools the plunger as can be seen in Figure 12 where the plunger temperature follows timewise the leak flow decrease. Plunger position shows a deflection when the ring change takes place (Figure 12-D).

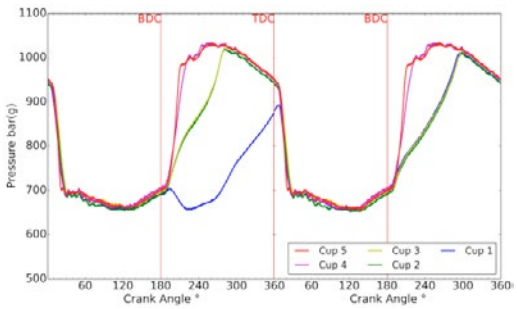

Figure 8: Packing pressure data of two consecutive revolutions during start-up phase.

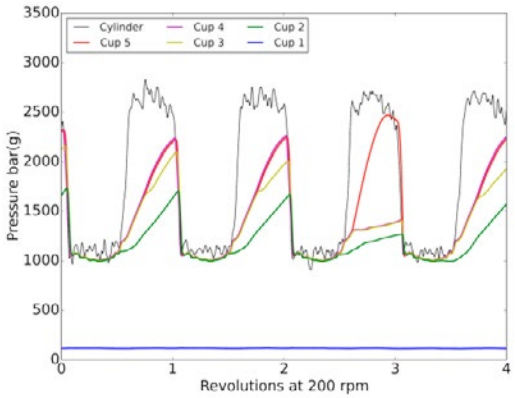

Figure 10: Highly resolved packing pressure data during normal operation.

The highly resolved pressure data support the above finding of non-uniform pressure distribution inside the packing. During the instable start-up phase of the compressor (Figure 8), the sealing sequence of the rings changes rapidly. SE1 (blue) starts its sealing activity at 270° crank angle during the first

by: Felix Ragg, Ricardo Cruz – Burckhardt Compression

revolution and at 180° crank angle during the second revolution (Figure 8). During expansion stroke the pressure in all cups follows the cylinder pressure fast with almost no delay. Pressure relief grooves ensure the gas to flow back upstream hence no gas of higher pressure is trapped.

During normal operation the same idling ring phenomena can be observed. Figure 10 shows four consecutive revolutions. During the first and second displayed revolution, the pressure breaker could throttle the dynamic pressure well (pressure difference between black line and red/magenta line), whereas SE5 (red line) was idling. The proximate revolution the pressure breaker declined its throttling action (less pressure difference between black and red line) but SE5 woke up and sealed a pressure drop of around 1000 bar. The next revolution the initial arrangement was reestablished. This shows the extreme dynamic of the process. A ring is able to change its status within 0.3 seconds (at 200 rpm) without any sign of hindered performance.

3.2 Wear

After 6585 hours the test packing, still fully functional, was dismantled and all sealing elements were carefully examined and wear measured. The averaged wear was measured in units of length (thickness) and not in weight because rings can break and hence corrupt the results. The most wear shows the sealing element one (SE1) at the crank end in cup one (Figure 11-A). One possible explanation for the enhanced wear of SE1 could be the exposed position at the end of the packing

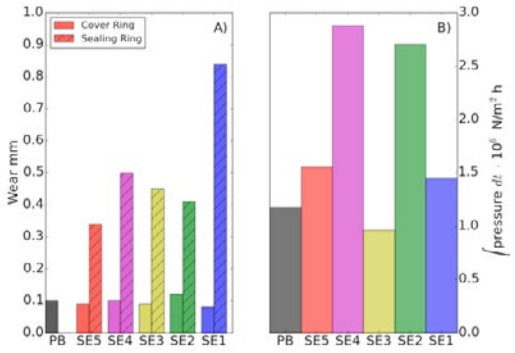

Figure 11: Wear of test packing A) and load of packing which is integrated averaged pressure drop across each sealing element over time B).

where first, no oil is kept back by following rings and secondly, less oil arrives, since the last oil injection point is in front of SE2. All radial split rings, which are cover rings and pressure breaker, show very little wear of 0.1 mm in average.

When comparing the wear pattern to the effective

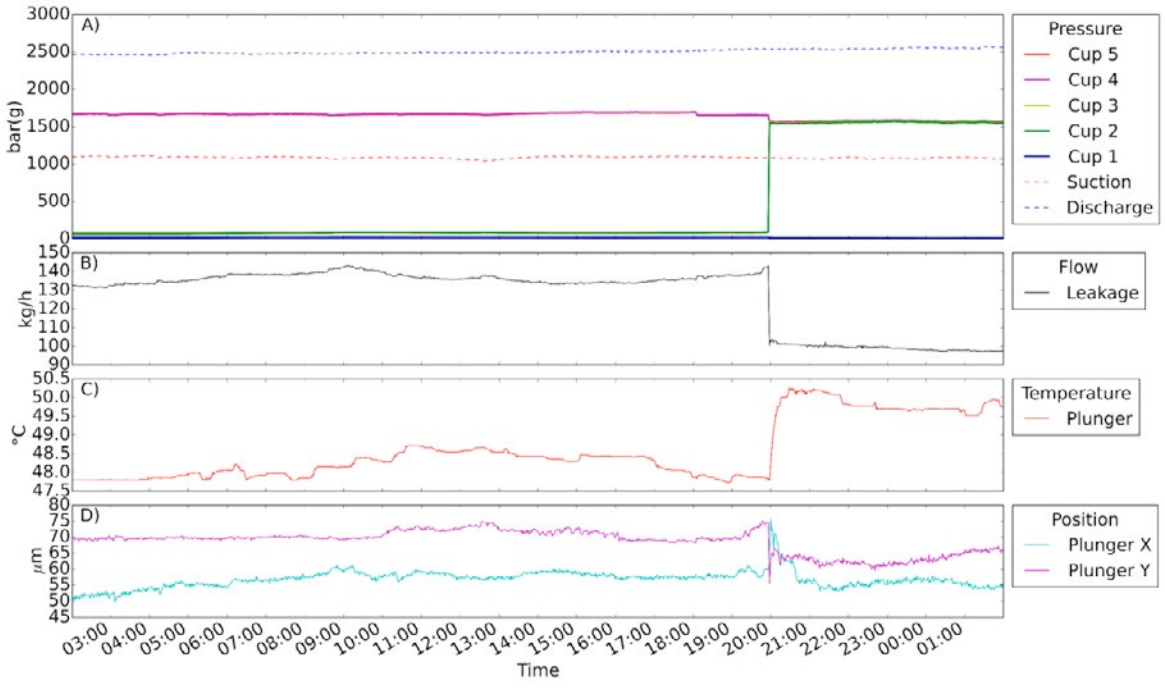

Figure 12: Long term data of the day 22.07.2017. A) packing and operational pressure, B) leakage flow, C) plunger temperature, D) plunger position.

by: Felix Ragg, Ricardo Cruz – Burckhardt Compression

load of all sealing elements (Figure 11 A and B), which is the integrated averaged pressure drop across each element over time, the load correlates well with wear, except for SE3 and SE1 which do not comprise a lubricant injection point inside their cups (compare Figure 6). But wear mechanism comprises more than only pressure drop.

The wear characteristic of the present test packing is contrary to the one measured in 1970[1] by Scheuber where the most wear was observed at the pressure breaker (compare Figure 13). A main difference between the packing setup from 1970s and the current one, is the implemented solid pressure breaker ring with a scarf which tends to close and hence wear more. Enhanced packing

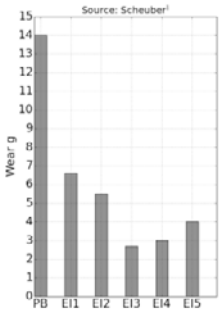

Figure 13: Wear of 1970s packing by Scheuber.

design and heterogeneous sealing concept is able to balance wear on sealing rings. As the principal task of the pressure breaker is to throttle the dynamic pressure component, its wear shall not overshoot the wear of the true sealing rings.

4 Conclusion

With sophisticated measurement technique it is possible to gain profound insights into the behavior of a high pressure packing of a Hyper compressor. A special cylinder with a test packing equipped with pressure transmitters shows the extreme dynamic behavior of the sealing activity of the rings. Sealing elements that are actively sealing become inactive a compression stroke later without any sign of hindered performance. The same pattern is distinguishable in long term data. One single sealing element can face the entire pressure load for long time. Sudden changes of ring activity occur as well as changes after compressor restart. Leakage flow data, plunger temperature and plunger position show distinct impact of ring activity change.

The sealing conditions were found to be unstable, this reflects the causal relationship to the tribological nature of the system. A phenomenon directly linked to such dynamic behavior is possibly stick-slip effects across a change in lubrication regime. Furthermore, temperature effects or an accumulation of oil additives on sealing ring surface can also cause or contribute to the extreme dynamic behavior of the sealing elements. But keeping in mind the abrupt change of status, from idling to seal full pressure, a geometric reason is most likely. This can be, for example, ring tilting or clamping.

The examination of one packing and its sealing elements does not form a base for final statements, but results lead to a hypothesis that lubricants support the sealing function of the rings. Rings which are not lubed directly like SE3 and SE1, show high wear but low load (Figure 11). To distribute the load more evenly across the packing, one possibility could be, to dispense the lubricant more evenly in order to bring further stability to the tribological system. This could be achieved by changing the surface structure by laser ablation to reduce the speed dependent threshold for lubrication regime. The work presented is the baseline for further testing of laser structure surfaces and to better evaluate their effectiveness. But as investigation is at the beginning and the measurement campaign is still ongoing, more precise explanations will turn to light.

References

[1] Scheuber, K.: Dynamic Pressure Distribution in the Cylinder Packing of Compressors for Very High Pressures. Sulzer Technical Review 3/1980.

[2] Traversari, A. and Giacomelli E.: Some Investigation on the Behavior of High Pressure Packing Used in Secondary Compressors for Low Density Polyethylene Production. Proceedings of the 2nd Int. Conf. on H. P. Engineering, University of Sussex, Brighton, England, July 8–10, 1975, pp. 57-58.

[3] Vetter, G. and Feistel N.: Investigation of the operational behaviour of dry-running piston-rod sealing systems in crosshead compressors. 3rd EFRC Conference, Vienne, Austria, 2003, p. 141-149.

EUROPEAN FORUM
for RECIPROCATING
COMPRESSORS

PULSATIONS AND VIBRATION

Application of a Constrained Layer Damping to reduce Pipe Vibrations of a Reciprocating Compressor System

by:

André Eijk, Hajo Pereboom
Heat Transfer & Fluid Dynamics
TNO
Delft, NL
andre.eijk@tno.nl; hajo.pereboom@tno.nl

Jörg Fröbel
ESK GmbH
Freiberg, Germany
J.Froebel@rwe.com

11th EFRC CONFERENCE
September 13 – 14, 2018, Madrid

Abstract:
At an Underground Gas Storage (UGS) plant, a 2-stage four-cylinder reciprocating compressor is installed with a maximum power of 5 MW. The system can operate at many different pressures, from a suction pressure of 31 bara up to a discharge pressure of 168 bara. The flow is controlled by means of different fixed speeds in combination with step less flow reversal control. Since start-up of the system in 2012, there were several vibrations issues, leading to trips of the compressor.
The dominant vibrations of parts of the system occurred for different frequencies around 100 Hz. These high frequency vibrations were caused by rather small cylinder displacements which excited mechanical resonances of parts of the system. It is known that high frequency vibrations are rather difficult to mitigate with traditional measures such as pipe supports or by stiffening of mechanical the supporting structures. The vibration amplitudes at resonance are determined mainly by the mechanical damping ratio. In a research project carried by TNO, it was shown that a Constrained Layer Damping (CLD) device can be used very effectively to increase the local damping at rather low costs. To reduce the high frequency vibrations to acceptable levels, a CLD has been applied to a part of the piping in the system. Field measurements have shown a reduction of the vibrations to run safe and reliable for the long term. This paper describes the effective application of a low cost CLD device and the results of field measurements with and without CLD.

by: André Eijk, Hajo Pereboom – TNO; Jörg Fröbel – ESK

1 Introduction

Innogy Gas Storage new, operates an Underground Gas Storage (UGS) system in Staßfurt since many years. To increase the capacity, an additional reciprocating compressor was installed in 2012, see photo in figure 1.

Figure 1 Photo of the compressor system

During start-up of the system, several vibration problems were experienced. Measurements have shown that the highest vibration levels occurred at high frequencies, around 100 Hz. By means of additional vibration reduction measures, such as the installation of additional pipe supports and suction damper bracing, the vibration problems were reduced.

A step less reverse flow control system is installed on the system and this type of capacity control can cause high frequency pulsations and vibrations[5]. To further reduce the vibrations of this system, the flow control scheme was changed, and subsequent measurements showed a considerable reduction in vibrations.

Since pressure in the cavern of the UGS system does not varies much in a short time, the vibration measurements can only be carried out for a small number of pressure ratios and flows. That means that the maximum vibrations (worst-case situations) for all possible occurring pressure and flow conditions cannot be measured during one field survey. For that reason, it was decided by the operator to carry out a detailed compressor manifold analysis according to the Design Approach 3 of the 5th edition of the API Standard 618[1]. u A large amount of operating conditions were investigated to determine the worst-case conditions, also focussing on the high frequencies caused by the step less reverse flow control system This has been done for both the original and modified flow control scheme The calculated results showed that, depending on the operating conditions, a reduction of the vibrations with a factor of 1.5-12 can be achieved with the new flow control scheme. As a result of the analysis, it was recommended to install several additional pipe supports to reduce the vibration levels of several parts of the system.

Further on, it was shown during this analysis that fatigue failure could occur at the unbraced Small-Bore Connections (SBC's) for certain process conditions for frequencies around 100 Hz. Stiff and robust braces have been implemented to avoid fatigue failure.

The calculation results for the investigated modifications showed that the maximum vibration levels still exceed the allowable levels according to the ISO 10816-8[2]. It was shown that this will occur only for a limited number of process conditions. The results of the cyclic stress calculation showed that fatigue failure will not occur for the vibrations which exceeds the ISO 10816-8 limits. For that reason, higher vibration levels have been accepted for this system. Several permanent vibration sensors have been installed on several critical parts of the system to guarantee that higher vibrations levels will not occur for the complete operating envelope.

However, after the implementation of the recommendations the system tripped several times during start-up of the system and during a change of the flow setting for certain process conditions. This was caused by the fact that the maximum vibrations exceeded the trip level of one of the permanent mounted vibration sensors of the vertical inlet pipe of the suction 1st stage.

In general, transient loads occur during start-up of a compressor or by an abrupt change to another flow setting. These transient loads resulted in a temporarily increase of the vibration levels with high frequencies, leading to trips of this system. This was observed after the installation of an additional pipe support in the vertical part of 1st stage inlet piping (see figure 14 in section 4.2).

Further modifications to reduce the high frequency vibrations were shown not to be effective and it was decided to remove the additional pipe support. The consequence was that the pipe vibrations increased by a factor two for the stationary conditions.

The target was to find a feasible solution to avoid trips and to reduce the (stationary) vibrations of the vertical inlet pipe. It is well known that the amplitude of a mechanical vibration at resonance is strongly determined by the mechanical damping ratio: larger damping ratios will lead to lower vibrations. It has been demonstrated that an increase in damping ratio can be achieved effectively by the application of a Constrained Layer Damping (CLD) device[3].

This paper describes into detail the effective application of this low cost CLD device and the results of the field measurements with and without the CLD.

by: André Eijk, Hajo Pereboom – TNO; Jörg Fröbel – ESK

2 System description

The system consists of one natural gas reciprocating compressor with 4 cylinders. The compressor is used for a two-stage storage mode with 2 cylinders on both stages. The one-stage storage and withdrawal mode use 4 cylinders.
The suction pressures in the system varies between 31-56 Bar. The discharge pressures are also variable and are between 57-81 Bar for the 1-stage mode and between 57-168 Bar for the 2-stage mode.
The speed of the compressor is a function of the suction pressure, both for the 1-stage and 2-stage mode, as follows:

- fixed speed of 585 rpm for a suction pressure below 36 bara;
- fixed speed of 501 rpm for a suction pressure between 36-44 bara;
- fixed speed of 400 rpm for a suction pressure equals and larger 44 bara;

For each fixed speed, the flow can be controlled further with a step-less flow reverse control system. At the lowest control setting, the flow can be reduced further by a turndown of the speed to minimum of 400 rpm and by bypass control. The capacity range for the 1-stage mode is from 100.000-150.000 Nm3/hr and for the 2-stage mode from 20.000-75.000 Nm3/hr.

3. Constrained Layer Damping (CLD)

3.1 Some background[3]

A passive Constrained Layer Damping (CLD) device consists of a sandwich of a visco-elastic damping layer in between 2 structural constraining base layers (in general steel) as shown in Figure 2. In this case, the base layer is the pipe wall. The deformation of the structure will lead to a shear strain in the visco-elastic material, which will increase the damping ratio and thus lower the vibration and cyclic stress levels, if designed well.

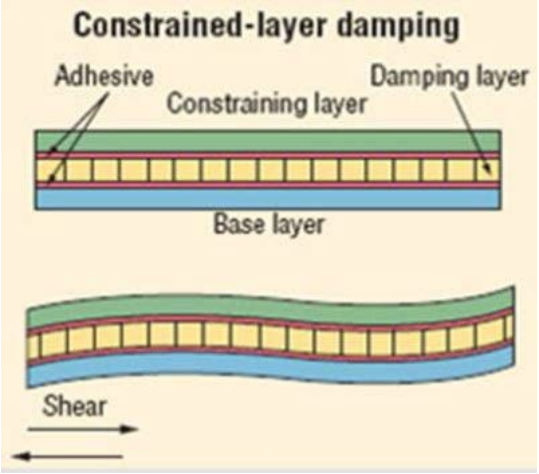

Figure 2 Example of a Constrained Layer Damping

CLD is already applied for several decades in the automotive and aerospace industry but as far as known not yet for reciprocating compressors. The effectiveness of the CLD for pipe systems has been demonstrated in a recent research project[3].

It was shown[3] that a significant increase in damping ratio can be achieved for a very broad frequency range. Besides that, CLD is a very cost-effective method. It shall be noted that the application of a CLD device is most effective for locations and associated modes with a damping ratio smaller than 1-2%.

The required reduction in vibration levels of the 1st stage inlet pipe as shown in Figure 3, shall be at least two. The CLD device can be glued and clamped to the pipe. Valuable experience was built up by using clamps instead of glue. The advantage of using clamps is that a larger radial force can be applied to the viscoelastic material, tightening the visco-elastic layer and leading to an increased shear strain and a higher mechanical damping ratio.

The CLD device shall cover the entirely vertical length of 5 meter of the suction pipe. The CLD is divided into several smaller parts for easy mounting purposes. To avoid a loss of preload of the clamps, preloaded springs have been applied. An overview of some details is shown in the photos in Figures 4 and 5.

by: André Eijk, Hajo Pereboom – TNO; Jörg Fröbel – ESK

Figure 3 Vertical inlet pipe of the suction 1st stage

Figure 4 CLD mounted to the pipe

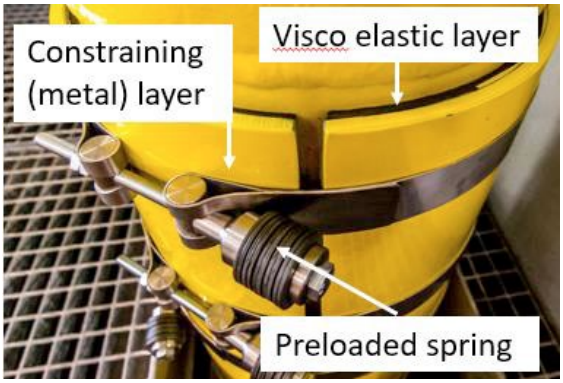

Figure 5 Some details of the applied CLD

3.2 Temperature effect

Viscoelastic materials, like polymers and rubbers, show substantial changes in properties with temperature variation. If used in the right temperature regime, they can generate high damping properties. Therefore, prediction of thermal-mechanical stresses and deformations require the input of accurate temperature dependent properties. At lower temperatures, the polymer is in its glassy state, while in the transition region the material possesses the highest damping performance. At higher temperatures the polymer behaviour is rubber like. For this reason, the temperature effect of the damping properties shall always be considered during the design of a CLD.

Measurements were carried out for several visco-elastic materials. Figure 6 shows the results of the quality factor Q at resonance of the applied visco-elastic material. The quality factor is inversely proportional to the damping ratio; hence, a lower Q factor means a higher damping ratio. From Figure 6, it can be concluded that the highest damping ratio occurs at approximately 60 degrees Celsius.

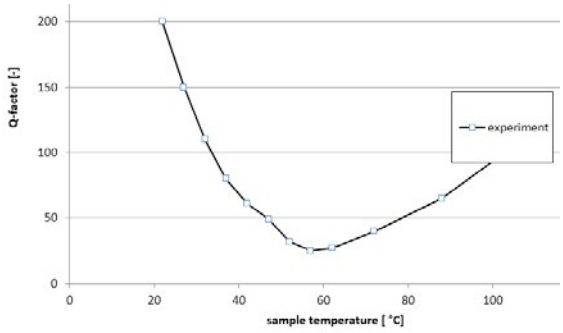

Figure 6 Measured quality factor as a function of temperature for a material

The required material data of the viscoelastic material shall be provided by the manufacturer. However, the experience is that the provided data is not always correct or is insufficient. It is, therefore, strongly recommended to measure the required material properties at different temperatures. This is normally done with a Dynamic Mechanical Analyser[4] (DMA). DMA, also known as dynamic mechanical spectroscopy, is a technique used to

by: André Eijk, Hajo Pereboom – TNO; Jörg Fröbel – ESK

study and characterize materials and is very valuable for studying the viscoelastic behaviour of polymers. A sinusoidal stress is applied to the sample and the deflection of the specimen is measured, allowing one to determine the material properties such as complex modulus and the damping ratio.

4 Measurements

4.1 Experimental modal analysis

At first, the dynamic behaviour of the vertical inlet pipe of the 1st stage is investigated with an experimental modal analysis, for the pipe with a without the CLD. With such an analysis, the so-called frequency response functions (FRF) are measured, which give clear insight in the resonance frequencies, modal damping and general dynamic behaviour of the installation (e.g. mode shapes).

To determine the FRF's, the structure is excited with a known dynamic force and the response is measured with vibration transducers. In this case the structure is excited with an impact hammer with a built-in force transducer. The resulting vibration response is measured in the directions where the highest vibrations are calculated and measured: in the piston rod and crankshaft direction.
The measurements have been carried out on location A1-A5 as shown in picture 7. Finally, the measured response is normalized to the input force, resulting in the excitation independent FRF per direction and location.

Figure 7 Measuring locations

Experimental FRF analysis is a rather time-consuming activity because each location and direction must be excited multiple times to get a statistically reliable FRF. Moreover, to minimize the sensitivity to external noise, in general such an analysis is performed on an installation in which no other vibration sources are present. The quality of the measurement can be indicated with the spectral coherence function. This frequency dependent function describes the correlation between the input (force) and output (vibration).

4.1.1 Results

The FRF's for the piston rod and crank shaft direction are shown in Figures 8-13 for several of the measured locations. Sensor 2 is mounted at location A2 and measures the vibrations in the piston rod direction.
It can be concluded that there are many Mechanical Natural Frequencies (MNF's) present in the investigated frequency range. This was measured during several field surveys and calculated with the compressor manifold analysis. It can also be concluded that the amplitudes for most of the frequencies for the pipe with the CLD are lower than those of the pipe without the CLD. The largest reduction of the amplitudes, which means a higher mechanical damping ratio, is measured for frequencies between 40 and 130 Hz. The measured amplitude with the CLD is approximately a factor 2-3 lower in the piston rod direction and a factor 2 lower in the crankshaft direction.
It can also be concluded that several MNF's of the pipe with the CLD are shifted to lower values. This is mainly caused by the added mass of the CLD which is approximately the same as the mass of the pipe for this system.

It can be concluded further that the amplitude for some frequencies of the pipe with the CLD are larger than without the CLD with no shift in frequencies. The largest ratio (≈2.4) is measured for location A3 for a frequency of approximately 22 Hz. That means that the vibration level will increase if the MNF of 22 Hz will be excited. This phenomenon was not calculated and measured during the research project[3] and is not been explained yet. However, the excitation of the MNF at 22 Hz was not addressed as a worst-case situation from the calculations nor from the measured vibrations during several field surveys. Besides that, a permanent vibration sensor is installed to avoid unacceptable levels.

by: André Eijk, Hajo Pereboom – TNO; Jörg Fröbel – ESK

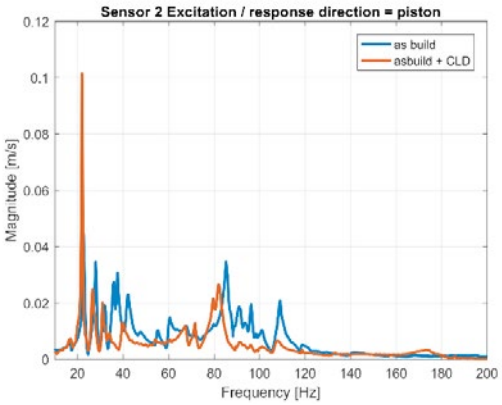

Figure 8 FRF at location A2 in the piston rod direction

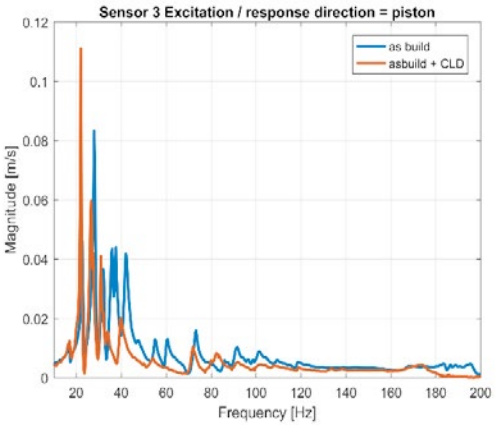

Figure 9 FRF at location A3 in the piston rod direction

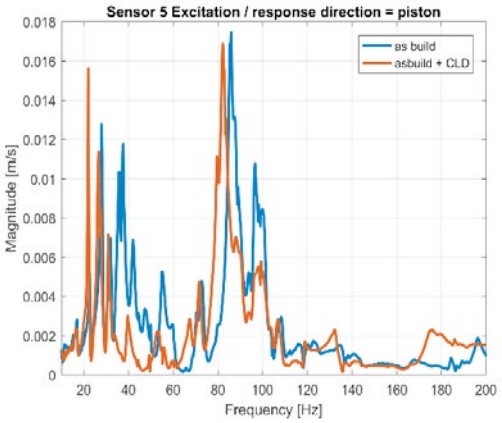

Figure 10 FRF at location A5 in the piston rod direction

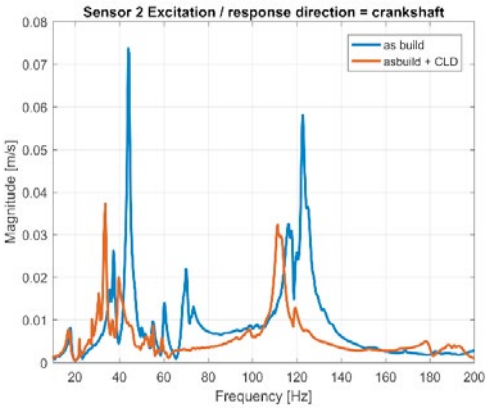

Figure 11 FRF at location A2 in the crankshaft direction

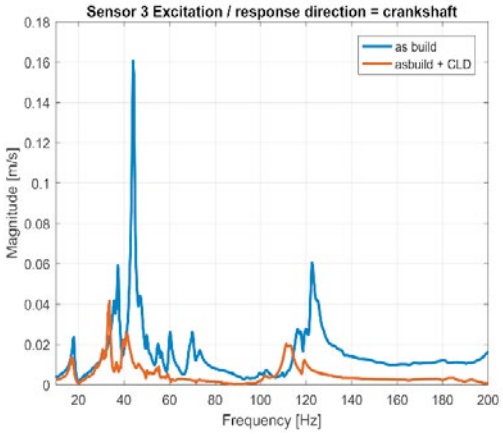

Figure 12 FRF at location A3 in the crankshaft direction

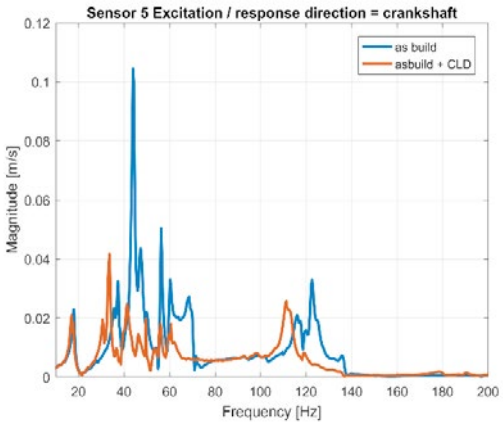

Figure 13 FRF at location A5 in the crankshaft direction

4.2 Vibration measurements

4.2.1. Results of the pipe without the CLD

Vibration measurements have been carried out for the system with and without the CLD. Both measurements have been carried out at the same operating conditions where the trips occurred.

The additional recommended pipe support, as shown in Figure 14, which was the cause of the trips, was removed before vibration measurements were taken.

A summary of the measured vibration levels is given in Table 1 (see Figure 7 for measurement locations).

The system tripped on the vibrations of the permanent sensor on a too high vibration level in the piston rod direction after a change of the flow control setting. The sensor of the vibrations of location A2 is mounted near the permanent installed vibration sensor.

by: André Eijk, Hajo Pereboom – TNO; Jörg Fröbel – ESK

Figure 14 Recommended additional pipe support

From the detailed results of the vibration measurements, it was shown that the frequency of the highest vibrations at location A2 (sensor 2) is 107 Hz. Figure 15 shows the calculated mode shape at 116.8 Hz which is rather close to the measured mechanical frequency of 107 Hz. It is shown that this is a MNF with maximum deflections in the piston rod direction.

Table 1 Vibrations levels without CLD

Location number	Vibration velocity mm/s rms		
	Vertical	Crankshaft	Piston Rod
A1	26	5	25
A2	8	21	>50[1]
A3	25	19	22
A4	19	19	39
A5	-	16	9

[1]compressor tripped

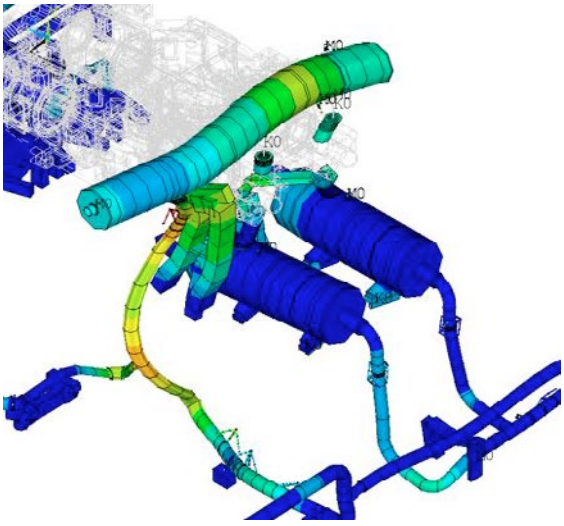

Figure 15 Mode shape @ 116.7 Hz

4.2.2. Results of the pipe with the CLD

The CLD was mounted to the pipe and the vibration measurements were repeated. The system did not trip during start-up and during a change in the flow control setting, therefore this was already a significant improvement.

A summary of the measured vibration levels is given in Table 2. It can be concluded that the maximum vibrations are decreased for most of the locations in one or more directions.

The largest reduction is approximately a factor of two times for location A2 in the piston rod. This was the location and direction for which the start-up trips occurred.

The general conclusion is that the required vibrations reduction of a factor of two has been achieved with the CLD device. After implementation of the CLD, trips did not occur up to now.

It should be noted that higher damping ratios could have been achieved for this system if the gas temperature would have been higher than 15 degrees Celsius (see also section 3.2). For systems with a low gas temperature which require a larger damping ratio, a possible solution could be achieved with the installation with e.g. an electrical heating device which is mounted on the constraining layer of the CLD. Although a further increase in damping was not required for this system, it could be a solution for other systems.

Table 2 Vibrations levels with CLD

Location number	Vibration velocity mm/s rms		
	Vertical	Crankshaft	Piston Rod
A1	24	5	27
A2	9	20	26
A3	21	10	20
A4	11	11	24
A5	10	20	8

5 Conclusions

High vibrations were experienced after start-up of the compressor system. Measurements have shown that the high vibrations occurred at high frequencies around 100 Hz. The high frequencies were mainly caused by the step less reverse flow control system.

The vibrations were reduced considerably after the installation of suction damper braces, additional pipe supports and by changing the step less flow reverse control scheme.

The question was if the (reduced) vibrations would be acceptable for all possible pressure and flow conditions. This shall normally be investigated during the design phase of these systems with a detailed compressor manifold analysis according to the Design Approach 3 of the API Standard 618.

by: André Eijk, Hajo Pereboom – TNO; Jörg Fröbel – ESK

However, this was done for this system at a later stage to further reduce the vibrations for all worst-case conditions.

The analysis showed that several additional pipe supports were necessary and that an exceeding of the ISO 10816-8 vibration level at some parts of the main piping could be accepted because it would not lead to fatigue failure.

Further on, the calculations showed that fatigue failure of Small Bore Connections (SBC's) could occur for certain process conditions and stiff robust braces were implemented.

After implementation of all recommended modifications, the system tripped several times during start-up and during a change of the flow settings for certain process conditions.

An inspection of the vibration measurements and calculation results revealed that this was caused by an excitation of a mechanical natural frequency (MNF around 107 Hz of the inlet 1st stage piping.

The vibrations have been reduced by the application of a Constrained Layer Damping Device. Vibration measurements showed that the vibrations were reduced with a factor of 2 and trips did not occur anymore.

The advantages of CLD devices are that they can be produced at rather low costs, are very easy to install and are very effective for a very broad frequency range.

CLD devices can be applied for pipe systems, Small Bore Connections (SBC's), steel structures, braces, plate type structures etc. when the mechanical damping ratio is low (≈<2-4%).

References

[1] API Standard 618, 5th edtion "Reciprocating Compressors for Petroleum, Chemical, and Gas Industry Services"

[2] ISO 10816-8" Mechanical vibration — Evaluation of machine vibration by measurements on non-rotating parts"- Part 8: Reciprocating compressor systems.

[3] A. Eijk, D. de Lange, J. de Vreugd, D, E. Slis. Non-traditional vibration mitigation methods for reciprocating compressor systems. 3rd International Rotating Equipment Conference (IREC) Pumps, Compressors and Vacuum Technology Düsseldorf, 14 – 15 September 2016

[4] Kevin Menard, Dynamic Mechanical Analysis: A Practical Introduction, 2nd Edition, CRC Press, 2008

[5] H. Korst, Pulsation effects of capacity control options, Compressor Control Workshop, EFRC Conference Prague 2007

LEADING COMPRESSOR TECHNOLOGY AND SERVICES

www.burckhardtcompression.com

Compressors for a Lifetime™

Burckhardt Compression

New adjustable vibration absorber – First application on site

by:

Dr.-Ing. Patrick Tetenborg, Dr.-Ing. Johann Lenz
Machinery and Plants
KÖTTER Consulting Engineers GmbH & Co. KG
Rheine, Germany
p.tetenborg@koetter-consulting.com

11th EFRC CONFERENCE
September 13 – 14, 2018, Madrid

Abstract:
Reciprocating compressors are used for several processes in the oil and gas industry. The working principle of reciprocating compressors induces a pulsating flow. Therefore pulsation dampers are always installed on the suction and discharge side next to the compressor for decreasing the pulsation level. But also low pulsation levels or mechanical dynamic forces often involve increased vibrations of the attached piping system if resonances occur.
Different measures can be used to decrease this vibration level. In many cases additional supports are used to tighten the piping. But in some cases it is not possible or very expensive and uncomfortable to install additional piping supports or damping devices. Another very effective measure is the use of vibration absorbers1. Especially vibration absorbers with an implemented damping characteristic enable a significant optimization of the vibration characteristic in the whole frequency range.
In this paper a newly designed vibration absorber is presented. The vibration absorber is adjustable on site in a wide frequency range with different mass configurations. The design is introduced and a case study shows the vibration reduction effect in the field.

by: Dr. Patrick Tetenborg, Dr. Johann Lenz – KÖTTER

1 Introduction

In several industries increased vibrations often occur at pumps, compressors or turbines and also at the connected piping systems. These vibrations can have different causes. In many cases structural resonance effects are an essential mechanism for an increased vibration level. Resonances occur, when a vibratory system is excited in its natural frequency. Often even a slight excitation – e.g. pulsations in a pipeline – is sufficient to evoke critical dynamic stress of the structure.

A possible measure to eliminate resonance problems is the detuning of the system. By changing the stiffness or the mass the natural frequency is shifted. However, to be effective, these measures have to be individually planned, manufactured and installed. That costs time and can lead to production losses and high costs at critical plant conditions.

KCE took this time and cost factor as a challenge to develop a solution for operators that can be implemented in a short time – even during a measurement: The patented device[2] is a variable two-dimensional vibration absorber that can be universally configured on site.

2 Usage of vibration absorbers

There are several different measures for vibration reduction. The most effective solution always depends on the root cause. In case of resonances with low damping (often at pipelines) a vibration absorber enables an effective vibration reduction. Vibration absorbers are not only used for industrial applications but also in everyday life, for example to improve unwanted vibrations at cabriolet roofs or to protect bridges and buildings against storms and earthquakes.

For analysing the dynamic effect of a vibration absorber a dynamic model with two degrees of freedom is usually used, see figure 1.

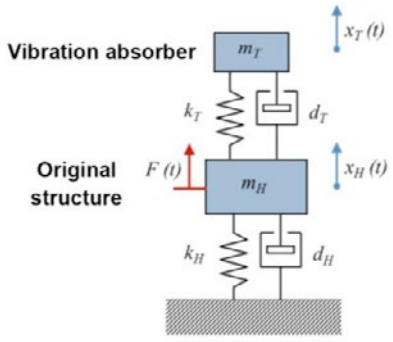

Figure 1: Principle dynamic system consisting of the original structure with a coupled vibration absorber.

The original structure without the coupled vibration absorber - as an example for various dynamic structures - has got one degree of freedom. If the system is excited harmonically with its natural frequency, resonance occurs. The resonance case (see dominant peak in figure 2) often leads to enhanced vibration, which may end in cracks or other damages.

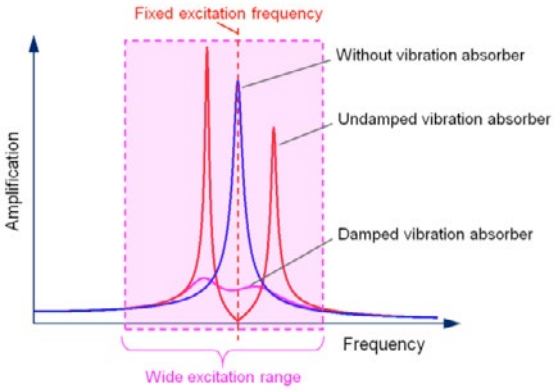

Figure 2: Response characteristics of an original structure and the modified behaviour with a vibration absorber.

In case of fixed excitation speed additional stiffness or mass enables the tuning of the natural frequency and therefore a common measure to improve the dynamic behaviour. Another possibility with a nearly total compensation of single-frequency vibrations is the use of an undamped vibration absorber. An undamped vibration absorber is able to compensate the excitation forces by a counterforce. The result is visible in figure 2. With an undamped vibration absorber the response of the original structure is almost eliminated but only at one fixed frequency.

Today many machines – especially reciprocating compressors – are changing their operating speed in dependency of the operating conditions. Thus, there is a wide range of possible excitation frequencies.

In this case tuning of the system often only changes the critical operating point but does not solve the resonance problem. The use of an undamped vibration absorber also leads to two new resonance cases. Therefore, other modifications are necessary.

One very effective measure in case of low dampened resonance is the use of a damped vibration absorber. In contrast to the undamped configuration of a vibration absorber no further dominant resonance frequencies of the new dynamic system occur. The typical optimized response behaviour is shown in figure 2. This absorber enables the machine operation in a very wide range without further restrictions.

by: Dr. Patrick Tetenborg, Dr. Johann Lenz – KÖTTER

3 Design of new vibration absorber

The design is made for high flexibility. The focus is on multiple parameter variation during the vibration investigation on site. All functionally relevant components are placed in an encapsulated casing, see figure 3.

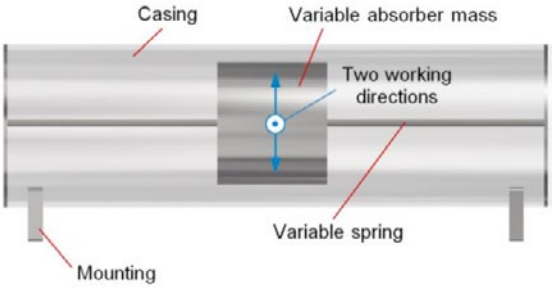

Figure 3: Design of the new vibration absorber.

The main components of the absorber are the variable mass and the connected spring with its tuneable stiffness. Both are integrated in the casing that can be connected to any critical structure by changeable mountings.

The on site installation can be divided in three main steps. At first, a suitable absorber mass is selected depending on the vibrating structure. Then the natural frequency of the absorber system is set with variable elements. In a final step the damping is adjusted via a matched damping oil. A damping ratio of up to 25 % can be reached with a special lamellar contour inside of the casing. The frequency range, at which the vibration absorber can be implemented, is up to 150 Hz.

Resonance induced vibration overshoots of pipelines are a typical application. These often have – because of their symmetry – two adjacent natural frequencies with orthogonally oscillating mode shapes. The two-dimensional mode of action also enables an effective reduction of the vibration level at more dimensional mode shapes.

4 Laboratory investigations

A test structure was set up for a first view on the vibration reduction potential of the new vibration absorber. This test structure consisted of a piping section with an additional mass at the top, see figure 4. For the excitation of the structure an unbalanced motor with variable speed was used.

For the laboratory investigations the unbalanced motor was driven with a frequency sweep from 10 Hz up to 40 Hz. The dynamic behaviour of the test structure was analysed without the vibration absorber in a first step. For the original test structure two dominant resonance frequencies occurred at 25 Hz and at 26.5 Hz (see figure 5).

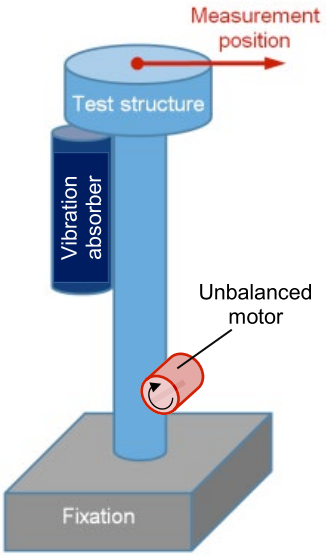

Figure 4: Test rig with experimental setup.

Vibrations of up to 115 mm/s RMS were measured in this initial state. The enormous vibration level resulted from the two original resonances (without absorber). These correspond to the already mentioned orthogonally oscillating mode shapes of the pipeline.

For the assessment of pipeline vibrations the standard VDI 3842[3] and ISO 10816-8[4] are proven. In this case the VDI 3842 standard is used. This gives frequency dependent guideline values for allowable pipeline vibrations. The comparison with the measured effective vibration velocities shows an unallowable vibration level, figure 5.

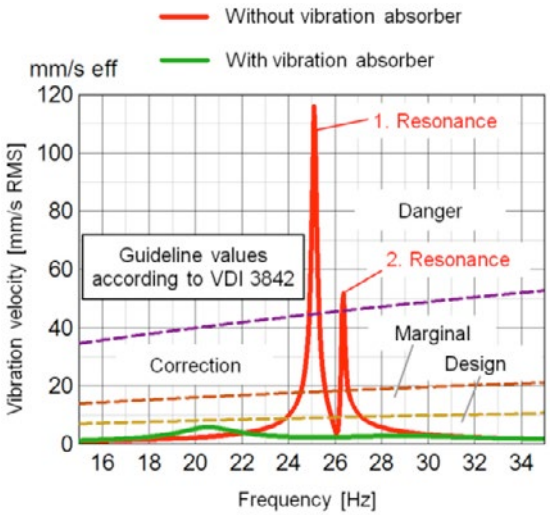

Figure 5: Reached vibration reduction for the experimental setup.

To reduce the increased vibrations, the vibration absorber was installed without further ado. The comparison with the original situation shows that the vibration level of the test structure could be reduced with a factor of more than 20. According to the assessment with VDI 3842 the vibration level now is in the design range, at which a flawless "operation" can be ensured from the vibration-technical point of view.

by: Dr. Patrick Tetenborg, Dr. Johann Lenz – KÖTTER

5 Case study

After the successful laboratory investigations the vibration absorber was installed on site for the first time. In this case a metrological investigation of three reciprocating compressors for ethylene was carried out. Each of the vertical compressors has got two cylinders and two stages. The power of each unit is 1.5 MW and the fixed running speed is 498 RPM. In dependency from the ethylene consumption of the connected chemical plant many different operating conditions are possible. The suction and discharge pressures are changing continuously. Single and parallel operation of up to three compressors are also possible.

Within the scope of the investigation increased pipeline vibrations were found in the ethylene compressor station. The maximum pipeline vibrations of up to 51 mm/s RMS occurred in a section (DN 150, PN 100) located almost 4 m high near the cooler of the second compressor stage.

A comparison to the guideline values according to VDI 3842 showed a clear exceedance of the allowable vibration velocities for the measured vibration frequency of 16.6 Hz, see figure 6.

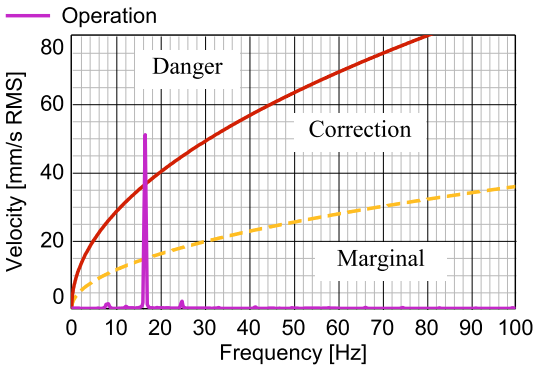

Figure 6: Measured spectrum of the local vibration level at the critical measurement position compared to VDI 3842 guideline values.

To analyse the reason for these increased vibrations, a harmonic response analysis was done during shut down. The mobility of the piping section was determined by bump tests. Figure 7 shows the recorded data of one bump test.

A single beat by a hammer was used to excite the structure, which vibrated with its natural frequency. To get information about the excitation force, a load cell was used. The vibrations were collected with a common vibration transducer. The recorded data could be used for the determination of the structural mobility (special type of transfer function) after some repetitions of the bumps.

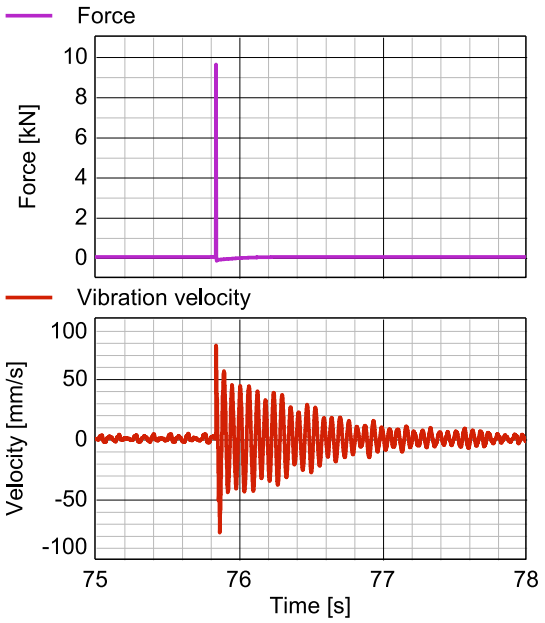

Figure 7: Measured force and vibration during a bump test.

The structural mobility is calculated by a mathematical method using spectral transformations from the time domain into the frequency domain. As a result the structural dynamic behaviour of the system is described by a complex response with a frequency depending magnitude and phase. Figure 8 shows the spectrum of the magnitude for these bump tests.

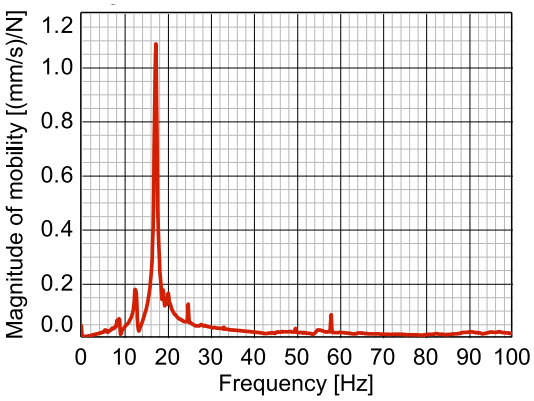

Figure 8: Magnitude of the local mobility at the critical vibration position as a result of the measured bump tests.

The critical piping section had a dominant natural frequency of 17 Hz. This natural frequency is close-by the measured vibration frequency of 16.6 Hz during operation, which is the second harmonic of the compressor speed. Thus, the increased vibrations occur due to this structural resonance. A low modal damping ratio $D < 2\ \%$ could also be detected by analysing the mobility.

by: Dr. Patrick Tetenborg, Dr. Johann Lenz – KÖTTER

To reduce this vibration level, several measures were possible. The challenge was to optimize the mobility at the dominant excitation frequency of 16.6 Hz. One possible solution was the detuning of the system by additional stiffness or additional mass. Additional stiffness was quite difficult in this case because of several other pipelines nearby. Furthermore, the strut had to be stiff enough to work in a height of 4 m. Additional mass was another possibility to shift the natural frequency downwards. This was not preferred because in the original condition the natural frequency was slightly above the excitation frequency. The additional mass had to be really heavy to get far below the critical excitation frequency.

Thus, another solution was suggested in this case: The installation of a vibration absorber.

One advantage of the new vibration absorber is that it can be applied on any structure and does not need any support to its surrounding. So it did not matter that the critical vibrations occurred in a height of 4 m with difficult support possibilities. Another advantage corresponds to the realization of a damped vibration absorber. There is no more dominant resonance peak in the frequency spectrum when using the damped vibration absorber to solve vibration issues. This is an additional advantage for sometimes critical start-up conditions when machines have to pass through resonance frequencies. This advantage should also be taken in this case.

To get a well working design of the absorber, the modal parameters of the original structure must be known. Therefore, a curve fitting tool is used to calculate the relevant structural parameters: stiffness, damping and mass of the piping section.

For the design of the vibration absorber the modal mass of the original structure and its damping ratio are the most important design values. The damping ratio was already known ($D < 2\ \%$) and the calculated modal mass was about 180 kg.

Knowing these parameters, the vibration absorber was configured on site with a mass of 14 kg, a natural frequency of 16.6 Hz and a damping ratio of about 7 %. These values are based on our long-term experience and recommendations from technical literature[5,6]. Subsequently, bump tests were carried out to check the influence on the modified structure.

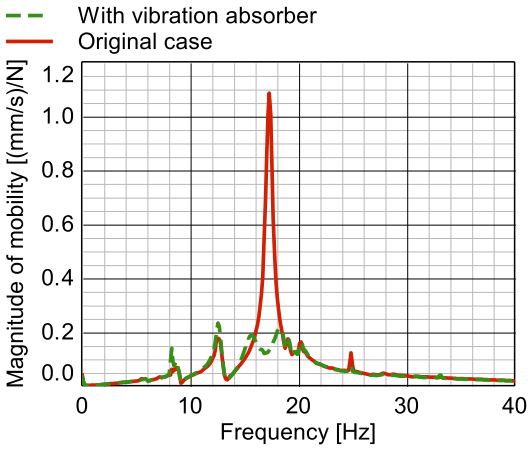

Figure 9: Comparison of the mobility with and without damped vibration absorber.

Figure 9 shows the improving influence of the vibration absorber very clearly. There was no more dominating resonance peak. Thus, the modified structure was ready for permanent operation.

To check the function and the performance of the vibration absorber over a long period of operation, a long-term measurement was installed for more than a month. Figure 10 shows a time line of the RMS vibration value for the before critical measurement position. The improved vibration level was far below the guideline value of the VDI 3842 for permissible vibrations. The different vibration levels during this long-term measurement were a result of the varying operating conditions of the three reciprocating compressors.

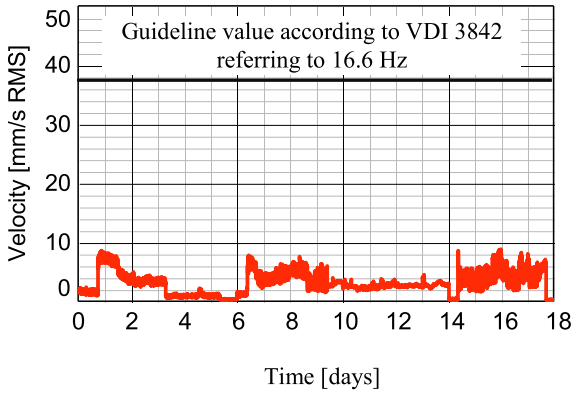

Figure 10: Vibration level during long-term measurement (time excerpt).

The maximal effective vibration level is now about 8 mm/s RMS. Figure 11 shows the installation position and compares the original case with the optimized case to visualize the effect on the vibration level.

by: Dr. Patrick Tetenborg, Dr. Johann Lenz – KÖTTER

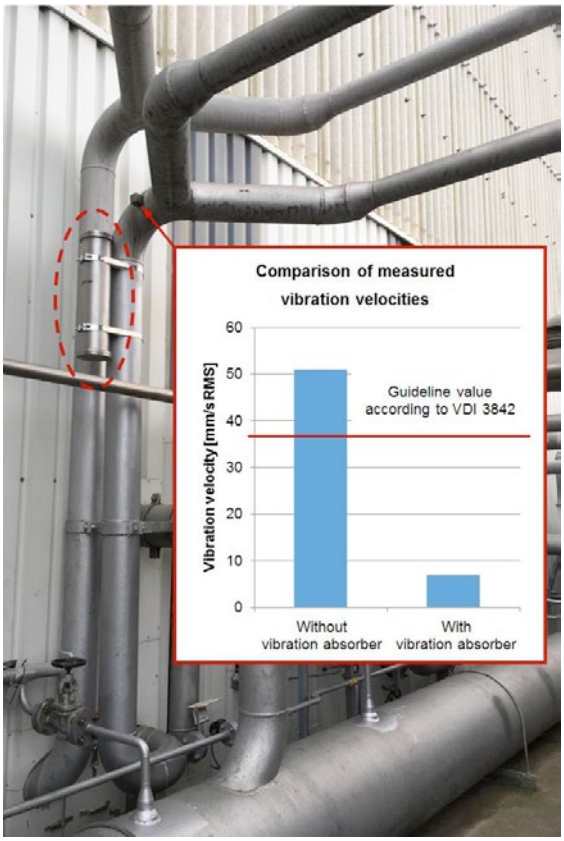

Figure 11: Installation and measurement position of the vibration absorber with comparison of vibration velocities.

6 Conclusion

In this article a newly designed vibration absorber has been presented. Its general design has been chosen to obtain high flexibility regarding damping parameters: natural frequency, absorber mass and absorber damping.

After some laboratory investigations a first installation at a pipeline of a reciprocating compressor has been performed. This first installation has been checked very accurately by a long-term measurement, which confirmed the long life fatigue strength and also the well operating behaviour of the new vibration absorber. A total reduction of the critical vibration level from about 51 mm/s RMS down to 8 mm/s RMS has been realized in this case.

Further applications for the vibration absorber are possibly all areas of machinery and plants.

Additional installations on site have already been realized.

References

[1] Lenz, J.: Three-dimensional vibration absorber to eliminate high vibrations in pipelines. In: Gas Machinery Conference. 6th October 2008, Albuquerque, New Mexico.

[2] KÖTTER Consulting Engineers GmbH & Co. KG: Schwingungstilger oder Schwingungsdämpfer. Inventor: Patrick Tetenborg und Johann Lenz. DE, Patentschrift: DE102014006193B4. 2014.

[3] VDI 3842: Schwingungen in Rohrleitungssystemen. 2004-06.

[4] ISO 10816-8: Mechanical vibration - Evaluation of machine vibration by measurements on non-rotating parts - Part 8: Reciprocating compressor systems. 2014-07.

[5] Petersen, C.: Dynamik der Baukonstruktionen. Vieweg & Sohn Verlagsgesellschaft. Braunschweig / Wiesbaden. 1996.

[6] Den Hartog, J. P.: Mechanische Schwingungen. 2. Auflage. Springer Verlag. Berlin. 1952.

Effect of cylinder nozzle location on orifice performance

by:

Author: **Tim Norden**
Central Division of Technology
Neuman & Esser
Maschinenfabrik Wurzen GmbH
Wurzen
Germany
tim.norden@neuman-esser.de

Co-Author: **Gerhard Knop**
Central Division of Technology
Neuman & Esser
GmbH & Co. KG
Übach-Palenberg
Germany
gerhard.knop@neuman-esser.de

11th EFRC CONFERENCE
September 13 – 14, 2018, Madrid

Abstract:
The mitigation of pressure pulsations and pulsation-induced vibrations plays an important role in reciprocating compressor plants. A very powerful and simple device to mitigate pressure pulsations is a restriction orifice plate (RO). The effectiveness strongly depends on its location. A general approach is to place an RO at a location with low pressure-pulsations and high flow-pulsations e.g. vessel entrances. The distance between the compression chamber and the RO highly influences the performance as well. This was detected by commissioning a compressor equipped with a double-acting cylinder with suction valve unloaders, a cylinder nozzle located at the crank-end side and a RO at the cylinder nozzle. The vibration levels at the pulsation bottles were analysed. Even though all values were very well below limits, the vibration levels were 2 times higher with the crank-end unloaded than with the head-end unloaded. A 1D acoustic simulation evaluating the pressure pulsations in the cylinder nozzle showed the same phenomena. Thus, to completely understand the physical problem, a fully turbulent 3D URANS CFD calculation was performed.

by: Tim Norden, Gerhard Knop – Neuman & Esser

1 Introduction

Reciprocating compressors create pressure pulsations due to the discontinuous compression. In the connected piping system, pressure pulsations can create unbalanced forces at e.g. elbows, reducers, vessel entrances, etc. These unbalanced forces can lead to high vibrations of the piping system. Thus, it is mandatory to bring the pressure pulsation to an uncritical level. This is done by performing a pulsation study according to API 618[1] during the design phase of the compressor plant. The pressure pulsations are calculated and if they exceed the API 618 limits mitigated. The most common damping devices to mitigate pressure pulsations are pulsation bottles close to the compressor cylinders. Another very often used damping device is the restriction orifice plate (RO). In the RO, the flow area is reduced generating a region of strong vorticity in which the acoustic energy is dissipated[2]. On the negative side, this causes a pressure drop over the orifice plate. Despite that, orifice plates have many advantages. They are cheaper than other damping devices and very easy to install since they do not need much space. The efficiency of an orifice plate strongly depends on its location within the pipe system. It is most efficient at locations with high flow fluctuations and low-pressure pulsations e.g. vessel entrances[2].

Apart from these general pulsation and vibration phenomena, sometimes, interesting unusual findings give rise to a closer look at what is happening. In a discharge pipe section, it was noticed by vibration measurement that there was a significant difference between head end and crank end side cylinder operation. The special discovery was a difference of about a factor of two of the vibrations velocity and this for nearly every harmonic. Different from other, more typical, vibration issues in reciprocating compressor systems, this seemed to be no resonance driven phenomenon.

In this paper, the observed event is investigated using different approaches like 1D and 3D fluid dynamic simulations as well as acoustic wave calculations.

2 Measurements

2.1 General arrangement of compressor

The objective of this investigation is a two-crank, two-stage horizontal reciprocating compressor. The main operating data are listed in Table 1.

The cylinders are double-acting and each compression chamber is equipped with two suction and two discharge valves. Normally, the cylinder nozzles are located in the middle between the two compression chambers. As opposed to this, in this compressor, the cylinder nozzles are located at the crank end. This setup was chosen considering general design aspect like:

- cylinder length and weight (effect on dead weight and mechanical natural frequencies)
- maintenance accessibility
- thermal nozzle loads

Even though it was not in focus during the cylinder design, it turned out later that this unsymmetrical design also creates a better pulsation performance at crank end operation (as shown in this paper).

The general arrangement of the compressor, the cylinder nozzle locations and the arrangement of the pulsation dampers can be seen in Figure 1.

Table 1: Main data of the compressor

Gas composition	CO_2 43.75 kg/kmol
Suction pressure	39 bar(a)
Interstage pressure	100 bar(a)
Discharge pressure	240 bar(a)
Rated capacity	102885 kg/h
Power at shaft	3400 kW
Rotational speed	370 1/min
Control	Suction valve unloading

The point of interest in this report is the 1st stage discharge side, which is on the back of Figure 1 but has the same arrangement as the 2nd stage in front. At the cylinder nozzle, a restriction orifice with an open area ratio of $\alpha = 0.35$ is installed. This was an outcome of the pulsation study during the design phase.

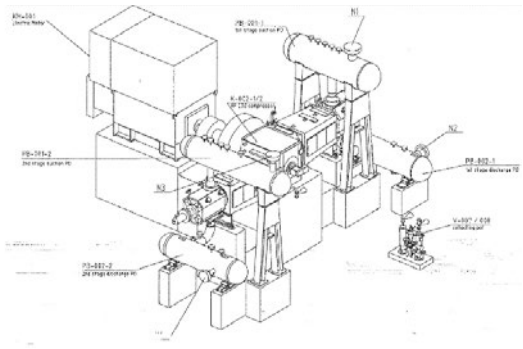

Figure 1: General arrangement of the compressor

by: Tim Norden, Gerhard Knop – Neuman & Esser

2.2 Measurements at commissioning

The compressor runs at a high discharge pressure and carbon dioxide is a high molecular weight gas tending to a higher probability of pulsation and vibration problems. Therefore, at the commissioning of the compressor, several measurements were carried out. Among others, the vibration levels at the pulsation dampers were measured and compared to the EFRC guideline[3]. The frequency spectrum of the vibrations at the pulsation damper 1st stage discharge side, perpendicular to the damper axis is shown in Figure 2 with head end compression chamber acting and the crank end unloaded and in Figure 3 vice versa. A measurement of 100% load could not be taken due to plant restrictions.

The overall vibration velocities were 24 mm/s RMS for head end (HE) acting and 13 mm/s RMS for crank end (CE) acting. 24 mm/s RMS is situated on the higher end of the EFRC guideline[3] but since stress verification proved sufficient margin to the limit, there was no reason for doing adjustments.

Nevertheless, it can be seen that the vibration levels differ strongly between the two chambers acting. The vibration level of the crank end (CE) side acting is nearly half of the head end (HE) acting. This can also be recognized in the frequency spectrums. Nearly every harmonic order of the frequencies is reduced for the crank end side up to the 13th harmonic. Thus, just by looking at the measurements, a resonance can be excluded.

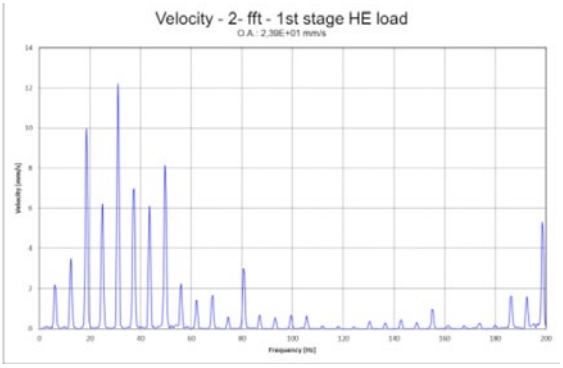

Figure 2: Vibration velocity spectrum. HE acting.

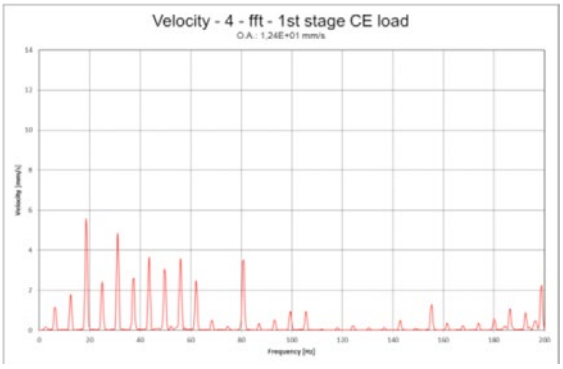

Figure 3: Vibration velocity spectrum. CE acting.

Several explanations were analysed e.g. failing of the valve unloader but were precluded. The only reason left, is the unsymmetrical location of the cylinder nozzle. To evaluate this assumption, flow simulations are carried out in the next sections.

3 1D flow simulation

3.1 Computational methods

In this chapter, a flow simulation is conducted. Thus, the governing equations for flows have to be solved numerically. The conservation of mass, momentum and energy read the following by using the Einstein notation, which implies summation over the indexed terms in the formula.

$$\frac{\partial \rho}{\partial t} + \frac{\partial (\rho u_i)}{\partial x_i} = 0 \tag{1}$$

$$\frac{\partial (\rho u_i)}{\partial t} + \frac{\partial (\rho u_j u_i)}{\partial x_j} = \frac{\partial \tau_{ij}}{\partial x_j} - \frac{\partial p}{\partial x_i} + \rho f_i \tag{2}$$

$$\begin{aligned} \frac{\partial \rho \left(e + \frac{1}{2}u^2\right)}{\partial t} + \frac{\partial \left(\rho u_i \left(e + \frac{1}{2}u^2\right)\right)}{\partial x_i} \\ = -\frac{\partial q_i}{\partial x_i} - \frac{\partial p u_i}{\partial x_i} \\ + \frac{\partial (\tau_{ij} u_j)}{\partial x_i} + f_i u_i \end{aligned} \tag{3}$$

where $\tau_{ij} = \mu \left(\frac{\partial u_i}{\partial x_j} + \frac{\partial u_j}{\partial x_i}\right) - \frac{2}{3}\mu \frac{\partial u_j}{\partial x_j}\delta_{ij}$ is the viscous stress tensor, f_i is an external volume force, e is the internal energy and q_i is the heat flow.

A 1D simulation of the flow in the pipe system is conducted to analyse and evaluate the measured behaviour. Therefore, the governing equations are simplified to only one dimension along the flow stream. The simulation approach used, employed some simplifications, like neglecting the advection term of the momentum equation (2) and considering a constant speed of sound. The latter allows for dropping the energy equation (3) since the derivative of pressure p with respect to density ρ is assumed at constant entropy s[4]:

$$c^2 = \left(\frac{\partial p}{\partial \rho}\right)_s \tag{4}$$

The 1D simulation model (see Figure 4) starts at the cylinder nozzle of the 1st stage suction side and contains the cylinder including the gas passages and valve pocket volumes. Furthermore, it comprises the 1st stage discharge cylinder nozzle including the restriction orifice plate, the pulsation damper and the connecting piping between cylinder and damper. The model starts and ends with a reflection-free

by: Tim Norden, Gerhard Knop – Neuman & Esser

boundary condition. The characteristic impedance Z at the end of the line is defined as[4]

$$Z = \frac{p_B}{Q_B} = \frac{c}{A} \qquad (5)$$

where p_B is the pressure at the boundary, Q_B is the imposed mass flow at the boundary, c is the speed of sound and A is the cross-section area of the pipe.

Figure 4: 1D simulation model

Two simulation cases are evaluated: head end (HE) acting and crank end (CE) acting.

3.2 Results 1D

The most interesting results to look at are the shaking forces / unbalanced forces in the horizontal connection between the cylinder and the pulsation damper. These forces excite the vibrations measured in the previous section of this report. The frequency spectrum of the shaking forces acting on the pulsation damper 1st stage discharge side, perpendicular to the damper axis is shown in Figure 5 with head end compression chamber acting and the crank end unloaded and in Figure 6 vice versa.

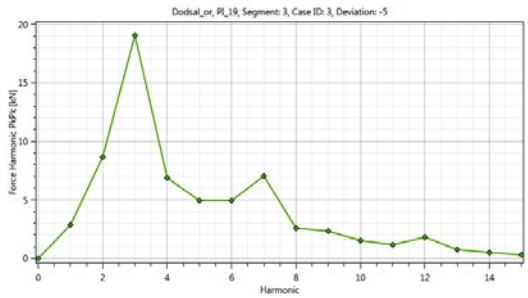

Figure 5: Shaking force spectrum of the horizontal connection between cylinder and pulsation damper. HE acting.

The same behaviour as in the measured vibrations (see Figure 2 and Figure 3) can be seen. The overall shaking force value for head end acting is 41.6 kN peak-to-peak and 23.7 kN peak-to-peak for crank end acting. The shaking force, as well as the vibration velocity, is for the head end (HE) acting nearly twice the value as for the crank end (CE). Hence, the simulation confirms the measured results.

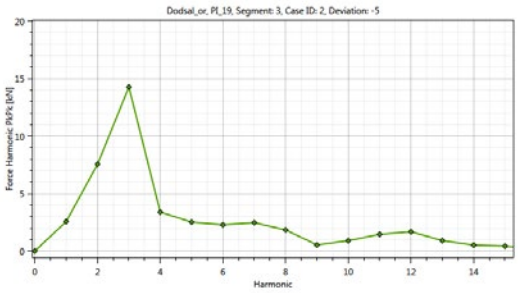

Figure 6: Shaking force spectrum of the horizontal connection between cylinder and pulsation damper. CE acting.

A significant difference in the results between the two modes of operation is the acoustic resonance with the 3rd harmonic number of the rotational frequency of the compressor. In both modes of operation, the resonance can be found in the spectrum (see Figure 5 and Figure 6). For the head end (HE) acting case the shaking force at the 3rd harmonic is 19 kN peak-to-peak, whereas, it is 14 kN peak-to-peak for the crank end (CE) acting. There is a perfect quarter wave resonance between the pulsation damper, which acts as an open end, and the head end valve, which acts as a closed end. The quarter wavelength for an acoustic resonance can be calculated as follows considering the operational data from Table 1:

$$\frac{\lambda}{4} = \frac{c * 60}{4 * 3 * n} = \frac{313\frac{m}{s} * 60s}{12 * 371} = 4.22m \qquad (6)$$

The length between the pulsation damper and the head end valve is 4.23m and thus, a resonance occurs. For the crank end (CE) acting, the same resonance between the head end (HE) valve and the pulsation damper occurs. However, the shaking force value for the 3rd harmonic is lower. The excitation for the latter case is generated at the crank end (CE) valve and hence, not at the antinode of the standing pressure wave. The excitation of the resonance is lower, whereas for the head end (HE) acting the excitation is exactly at the pressure antinode.

On the one hand, an acoustic resonance with the 3rd harmonic occurs, but on the other hand, in the measured data, the vibration velocities are in an equal range between the 3rd and 8th harmonic. Hence, there is no mechanical resonance at the 3rd harmonic of the compressor speed. This was also confirmed by the theoretical mechanical vibration analysis according to API 618[1], which was performed during the design phase.

Despite the acoustic resonance at the 3rd harmonic, it can be seen in Figure 5 and Figure 6 that also for the harmonic orders up to the 8th, the shaking force values are higher for head end (HE) acting as for

by: Tim Norden, Gerhard Knop – Neuman & Esser

crank end (CE) acting. This also represents the measured results.

4 Visualization

In this section, the reason for crank end side (CE) operation creating lower shaking forces than head end side (HE) operation, for most harmonics, is illustrated.

For this purpose, a simplified calculation model was created consisting of

- Cylinder gas passage
- Orifice
- Nozzle pipe
- Damper vessel

The model starts with a velocity boundary condition (10 m/s as unity load for every harmonic separately) at the compressor valves and terminates with an anechoic (non-reflecting) boundary condition downstream the pulsation damper. The pulsation damper is not shown in Figure 7 and Figure 8 in order to have a better (magnified) view on the relevant pipe sections.

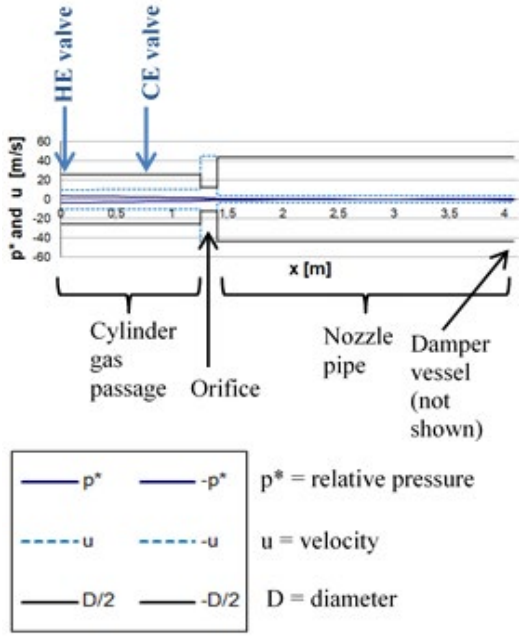

Figure 7: Description of Figure 8

The calculation method[5] makes use of the acoustic wave equation for pressure p and velocity u. They are related to each other by $p = \rho c u$ with ρc being the constant acoustic impedance as the product of density and speed of sound. The pressure p is related to the impedance in order to get the same scaling and the same unit (m/s) as the velocity u

$$p^* = \frac{p}{\rho c} = u \qquad (7)$$

That way p^* and u have the same amplitudes but a phase shift of 90°.

Cross section area changes shift the phase of both p^* and u which is nothing different than a reflection of a certain share of the incoming wave.

Figure 7 describes the model.

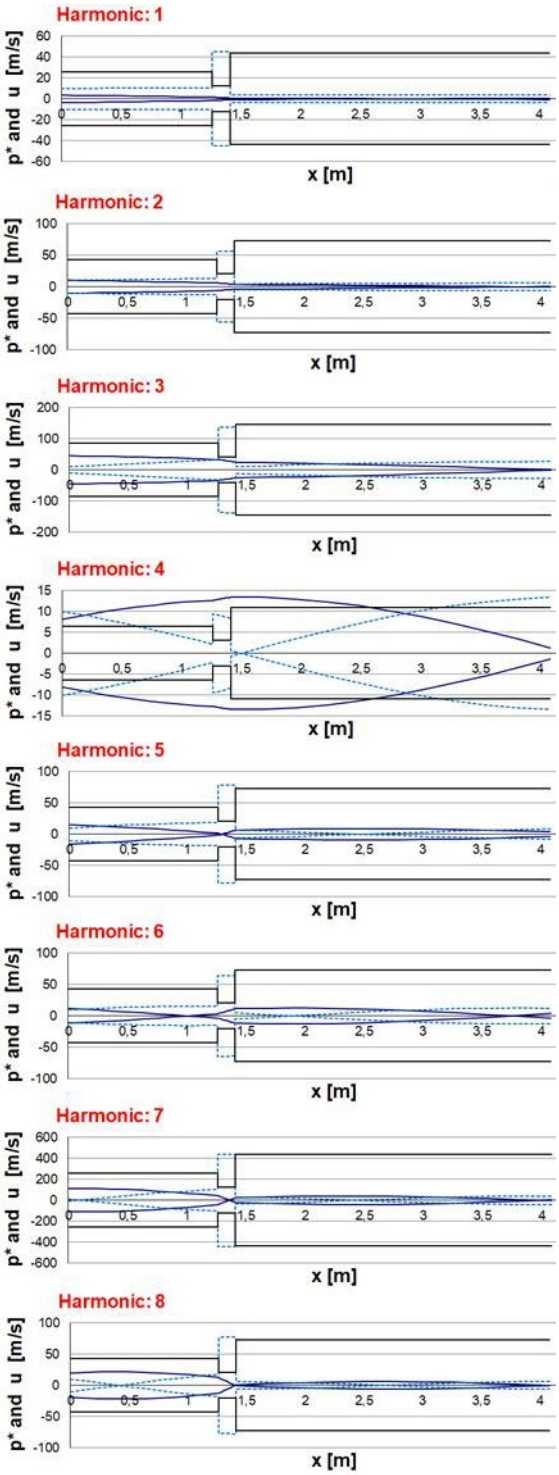

Figure 8: Pressure and velocity waves of different harmonics

The difference between head end (HE) and crank end (CE) operation is the location of the excitation (the compressor valves). In the first case (HE), the excitation is at the very left of the model, in the

by: Tim Norden, Gerhard Knop – Neuman & Esser

second case it is more to the right (refer to Figure 7 indicated as 'CE valve').

It is known that a system is more excitable at locations where the pressure pulsations are high. This is the reason why pulsation damper vessels preferably have their cylinder nozzle in the axial centre of the vessel as there is a pressure node of the λ/2 standing wave pattern.

In the subject system, it turns out that for most harmonics, the pressure pulsation is higher at the location of the HE valve. This can be seen in Figure 8 when comparing the locations 'HE valve' and 'CE valve' as shown in Figure 7. This finding indicates that the given standing wave pattern (which is independent on the location of the excitation) is more excited by the head (HE) valve than the crank end (CE) valve at most harmonics.

It must be noted that this calculation has only been carried out for better understanding. Due to its simplifications, results may differ quite significantly from the 1D and 3D simulations.

5 3D flow simulation

5.1 Computational methods

A 3D CFD approach is used to get a better insight into the flow and to visualize the mechanism of the restriction orifice plate. To determine the unsteady effects in the region of the orifice plate and to solve the governing equations (1), (2) and (3), the Unsteady Reynolds Averaged Navier Stokes equations (URANS) algorithm developed by Osborne Reynolds is applied. The turbulence of the flow is modelled statistically. The actual value of a flow variable ϕ is divided in a time-averaged value $\langle\phi\rangle$ and its fluctuations ϕ'

$$\phi = \langle\phi\rangle + \phi' \tag{8}$$

The implementation of the averaging of the flow variable to the equations (1), (2) and (3) is exemplarily shown for the conservation of momentum

$$\frac{\partial(\rho\langle u_i\rangle)}{\partial t} + \frac{\partial}{\partial x_j}\left[\rho\langle u_i\rangle\langle u_j\rangle + \rho\langle u_i'u_j'\rangle - \mu\left(\frac{\partial\langle u_i\rangle}{\partial x_j} + \frac{\partial\langle u_j\rangle}{\partial x_i}\right)\right] = -\frac{\partial\langle p\rangle}{\partial x_i} + \rho f_i \tag{9}$$

Due to the averaging of the conservation equations, new terms $\rho\langle u_i'u_j'\rangle$ are created. They are called Reynolds stresses. Due to the new terms, the URANS equations cannot be solved. There are more unknown variables as equations. This is the so-called closure problem and suitable approximations for the Reynolds Stresses are needed. In this investigation a two-equation model is applied which uses the Boussinesq-Approximation by modelling the Reynolds stresses analogical to Stokes law[6]

$$\rho\langle u_i'u_j'\rangle = -\mu_t\left(\frac{\partial\langle u_i\rangle}{\partial x_j} + \frac{\partial\langle u_j\rangle}{\partial x_i}\right) + \frac{2}{3}\rho\delta_{ij}k \tag{10}$$

where μ_t is the eddy viscosity and $k = \frac{1}{2}\langle u_i'u_j'\rangle$ is the turbulent kinetic energy. The closure problem is still not solved, since μ_t and k are unknown.

There are several turbulence models available to solve the eddy viscosity and the turbulent kinetic energy[7]. In this work, the k-ω-SST model developed by Menter[8] is used, because it is very applicable for flows in engineering applications[7]. In the k-ω-SST model, the near wall flow is treated by using the k-ω-model[9], whereas the far flow is treated using the k-ε-model[6]. The equations for the eddy viscosity μ_t, the turbulent kinetic energy k and the turbulent frequency ω read as[8]

$$\mu_t = \rho\frac{k}{\omega} \tag{11}$$

$$\frac{\partial(\rho k)}{\partial t} + \frac{\partial}{\partial x_j}\left[\rho\langle u_j\rangle k - \left(\mu + \frac{\mu_t}{\sigma_k}\right)\frac{\partial k}{\partial x_j}\right] = P_k - \beta^*\rho k\omega \tag{12}$$

$$\frac{\partial(\rho\omega)}{\partial t} + \frac{\partial}{\partial x_j}\left[\rho\langle u_j\rangle\omega - \left(\mu + \frac{\mu_t}{\sigma_{\omega1}}\right)\frac{\partial\omega}{\partial x_j}\right] = \frac{\alpha_2}{\mu_t}P_k - \rho\beta_2\omega^2 + (1 - F_1)\frac{2\rho}{\sigma_{\omega2}\omega}\frac{\partial k}{\partial x_j}\frac{\partial\omega}{\partial x_j} \tag{13}$$

where σ_k, β^*, $\sigma_{\omega1}$, α_2, β_2, and $\sigma_{\omega2}$ are model constants, $P_k = \mu_t\left(\frac{\partial\langle u_i\rangle}{\partial x_j} + \frac{\partial\langle u_j\rangle}{\partial x_i}\right)\frac{\partial\langle u_i\rangle}{\partial x_j}$ is the production rate of the turbulent kinetic energy and F_1 is a switching function which switches based on the wall distance between the k-ε-model and k-ω-model.

For the discretisation of the governing equations in space and time a second order limited central difference scheme is used. Since the flow domain of the whole cylinder including the compression chambers and the gas passages is very big, the compression chamber was not included in the computational domain due to restricted computational resources. Despite that, symmetry effects of the cylinder and the nozzle between the cylinder and pulsation damper were used to keep the model as small as possible. The flow domain is shown in Figure 9.

Unstructured grids are generated to discretise the flow domain. The generated grids consist mostly of hexahedron cells, but also prism and polyhedron cells were generated in regions of complex geometry. A special focus was paid to the region around the restriction orifice (RO) plate at the

by: Tim Norden, Gerhard Knop – Neuman & Esser

cylinder nozzle. In this region high-velocity gradients occur due to the high decrease of the hydraulic diameter. A fine mesh is needed to calculate these gradients correctly. For the flow domain in Figure 9 five different grids were generated in the cell size from 100-kilo cells to 5000-kilo cells. Grid independence check was performed to avoid numerical errors due to the dependence of the results on the numerical grid. It was achieved for a grid with 2300-kilo cells.

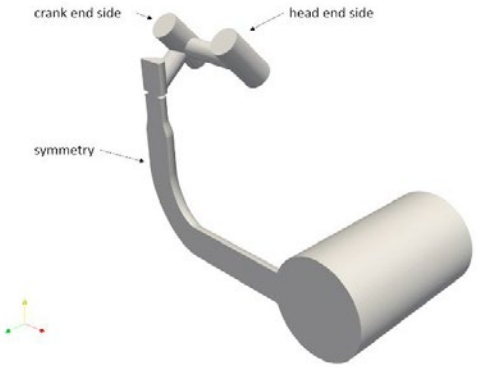

Figure 9: Flow domain of the compressor using symmetry effects and a simplified cylinder model

Since the compression chamber is not included, inlet boundary conditions are applied at the valve seats. Dirichlet boundary conditions are adopted for the velocity by calculating the flow velocity at the valve due to the piston motion and the opening of the valve. The inlet velocity for the head end and crank end side are shown in Figure 10. The inlet velocity of the head end (HE) side is higher than the velocity of the crank end (CE) side, due to the smaller volume of the compression chamber at the crank end side. There, the capacity is decreased by the piston rod. However, the different inlet velocities respectively volume flows are not the reason for the different vibration behaviour of the two ends acting. A simulation with the same inlet conditions at each side checked this.

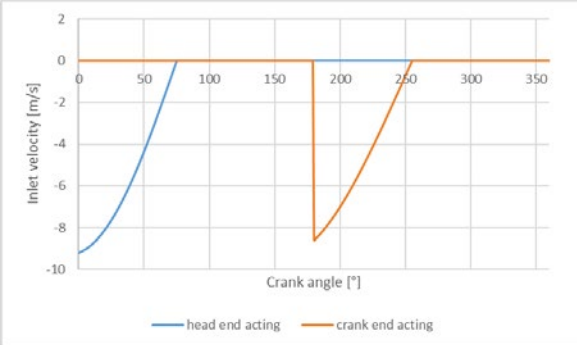

Figure 10: Inlet velocity at the head end resp. crank end valve

Dirichlet boundary conditions are also applied to the turbulent parameters and the inlet temperature, whereas Neuman boundary conditions were adopted for the pressure. In the outlet face, Dirichlet boundary conditions were adopted for the pressure and Neuman boundary conditions for the velocity, the turbulence parameters and the temperature. Ordinary no-slip conditions were used as hydrodynamic wall conditions. Despite that, the heat transfer between the fluid and the walls is neglected.

Two simulation cases are carried out. In the first, the flow is coming from the head end (HE) side and in the second, it is coming from the crank end (CE). Five compression cycles are simulated for each case to achieve an independence of the numerical errors at the beginning of the simulation.

5.2 Results 3D

5.2.1 Integral values

First, the results of the static pressure drop over the orifice plate are compared to the results of the 1D simulation. The results are listed in

Table 2. The static pressure drop is the pressure loss at stationary flow. In the 1D approach, it follows $\Delta p = K_W \frac{\rho}{2} u^2$ with flow velocity u in the main pipe diameter.

The pressure drop coefficient K_W is found empirically depending on the open-area ratio α. For orifice plates, Kramer's approximation can be used[10]:

$$K_W = 2.7 \frac{(1-\alpha)(1-\alpha^2)}{\alpha^2} \qquad (14)$$

Table 2: Static pressure loss. Comparison of different calculation approaches.

	Head end	Crank end
1D/3D simulation	1.053	1.027

The results are in good accordance and the deviation between the different approaches is very small. The pressure drop ratio of HE to CE is 1.21 with the more accurate 3D simulation.

The efficiency of a restriction orifice plate in terms of mitigating pressure pulsations strongly depends on the velocity fluctuation in the orifice plate as already described in chapter 1 of this work. Therefore, the velocity in the orifice is sampled for both simulation cases over the time and averaged over the orifice bore area. The velocity perpendicular to the orifice plate axis is shown in Figure 11 for one revolution of the compressor crankshaft. As already mentioned, the velocity of the head end acting is higher than for the crank end acting. This is also applicable to the flow through the orifice plate. The velocity curves in the orifice plate look different from the curves of the inlet velocity. They are wider and consist of more maxima. The

by: Tim Norden, Gerhard Knop – Neuman & Esser

reflection of the pressure and velocity waves at the vessel entrance and at the closed valves is responsible for that. Despite that, in both modes of operation, velocities with a positive algebraic sign can be noticed. This represents a counter-flow through the orifice plate also caused by the reflection at the entrance of the vessel.

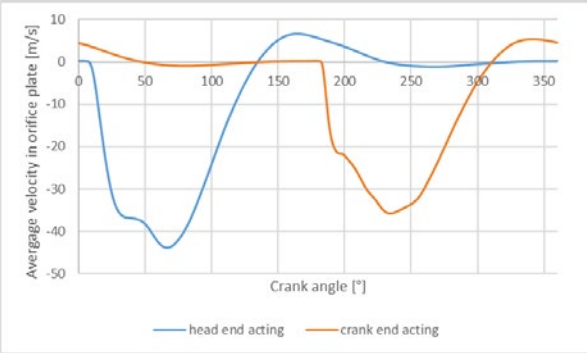

Figure 11: Velocity in the orifice plate bore

The sampled data from Figure 11 is transferred to the frequency domain by conducting a Fourier analysis. This gives a better overview of the velocity fluctuations. The spectrum for both run cases is shown in Figure 12. Head end acting leads to a higher mean velocity and higher velocity fluctuations in the orifice plate than crank end acting.

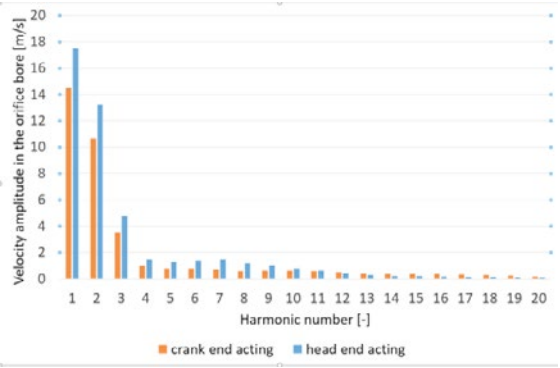

Figure 12: Velocity in the orifice plate in frequency domain

5.2.2 Streamlines

A restriction orifice plate dampens pressure pulsations due to static and dynamic pressure loss. Regions of strong vorticity are created downstream of the orifice plate and dampen the acoustic energy[2].

These regions of strong vorticities can also be recognized in the streamline pictures (see Figure 13). At the top, the streamlines for the highest flow velocity are shown for head end (left side) and crank end acting (right side). The main part of the fluid is driven through the orifice bore. Due to the relatively low velocity, vortices upstream of the orifice plate are not created.

Close downstream of the orifice a counter-flow is noticed due to the sharp edges inducing a relatively stable recirculation zone. In these zones, the acoustic damping takes place due to dissipation. The size of the recirculation zone strongly depends on the total velocity (mean + fluctuations). Since for the head end acting, both the mean velocity and the fluctuations are higher (compare Figure 11 and Figure 12), the recirculation zone is also greater. The latter has a length of 0.08m for head end (HE) acting, whereas, it has a length of 0.06m for the crank end (CE) acting. The same behaviour applies for the counter-flow displayed at the bottom of Figure 13.

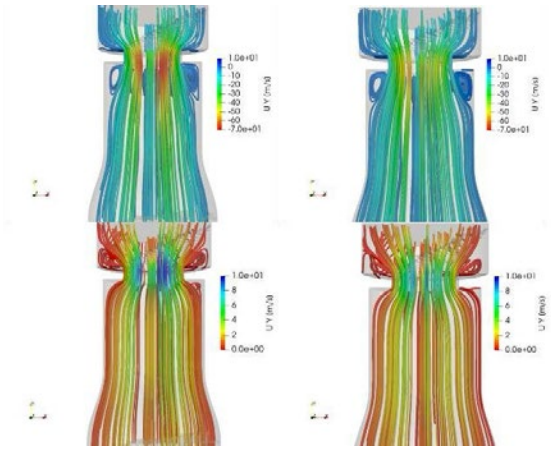

Figure 13: Streamline pattern through the RO. Top: Maximum velocity in main flow direction. Bottom: Maximum velocity at counter-flow. Left: HE acting. Right: CE acting.

6 Conclusion

The investigations performed to explain the interesting finding of seemingly harmonic independent shaking force differences between head end (HE) and crank end (CE) operation yield the following results.

Measurement vibration readings could be reproduced by 1D fluid dynamic simulation.

3D CFD simulations confirmed the 1D results and provided a deeper understanding of the behaviour of the cylinder flange orifice plate. It indicates the following. Higher velocity fluctuations create:

- a stronger vortex creation,
- more reverse flow and
- a higher pressure drop.

A simplified acoustic wave calculation yielded a clear indication that with most harmonics, the pressure wave shape in the cylinder gas passage is of a kind that pressure amplitudes are higher at the HE side compressor valve (which is more remote to the orifice plate) than at the CE side valve (closer to the orifice). Therefore, the excitability of pulsations is higher at HE side than at CE side.

It might be subject to further investigations whether the latter finding is something general or just specific to the subject system. The study of this work also

by: Tim Norden, Gerhard Knop – Neuman & Esser

supports the thesis that an orifice plate at the cylinder flange is more suitable for the purpose of mitigating a wide range of harmonics as opposed to an orifice plate at the pulsation damper vessel which is certainly much more effective on acoustic resonant conditions (i.e. standing waves).

An unsymmetrical cylinder, heaving the nozzle at crank end (CE) side rather than in the centre of HE and CE creates especially low pulsations when operating at CE side. If HE side operation is also needed, this however provides no advantage in total. Nevertheless, this is an interesting finding which can be certainly used in other cases.

Based on the findings presented in this work, more detailed investigations will be conducted to get a better insight in this phenomena.

References

[1] API 618 5th edition, Reciprocating Compressors for Petroleum, Chemical and Gas Industry Services, December 2007

[2] Peters M.C.A.M. (2001): Evaluation of Low Frequency Pulsation Damping Devices. 2nd EFRC Conference, Den Haag, Netherlands.

[3] EFRC Guidelines (2017): Guidelines for Vibrations in Reciprocating Compressor Systems

[4] Smeulers, J. (2017): Unsteady Flow in Pipe Systems and Fluid Machinery, TNO

[5] Kuhlmann, Harmonsiche Schwingungen in Rohrleitungen, Hochschule der Bundeswehr Hamburg

[6] Launder, B.E., Spalding D.B. (1974): The Numerical Computation of Turbulent Flows. Comput. Methods Appl. Mech. Eng., 3:269-289.

[7] Versteeg, H.K., Malalasekera, W. (2007): Introduction to computational fluid dynamics. Pearson/Prentice Hall, Harlow. 2. Edition.

[8] Menter, F.R. (1994): Two-equation eddy viscosity turbulence models for engineering applications. AIAA Journal, 32(8), 1598-1605.

[9] Wilcox D.C. (1988): Reassessment of the Scale-determing Equation for Advanced Turbulence Models. AIAA Journal, 26(11), 1299-1310.

[10] van Lier, L., Korst H. (2007): Mitigation of high-frequency pulsations, using Multi Bore Restriction Orifices, 5th EFRC Conference, Prague, Czech Republic

Modelling of transmission loss characteristics of reactive pulsation dampers

by:

Warzyńska Urszula, Kollek Wacław
Faculty of Mechanical Engineering
Wrocław University of Science and Technology
Wrocław, Poland
urszula.warzynska@pwr.edu.pl

11th EFRC CONFERENCE
September 13 – 14, 2018, Madrid

Abstract:
The article presents a method for modelling transmission loss characteristics in four basic types of passive pressure pulsation dampers: a chamber damper, a damper with an orifice, a damper with internal choke tube and a low-pass filter. It also compares the characteristics obtained by means of a one-dimensional model based on the plane wave equation solved in the frequency domain with the characteristics obtained from a three-dimensional model based on the Helmholtz equation. The article considers the influence of the positioning of the nozzles on the received attenuation characteristics, includes a discussion of the results obtained, and indicates in which cases the simplification for damper modelling in 1D space can be applied, and when it is unfavourable.

by: Urszula Warzyńska, Wacław Kollek – Wrocław University

1 Introduction

Gas pressure pulsation dampers are indispensable devices in any compressor installation exposed to high amplitudes of pressure and flow pulsation. Uncontrolled pressure pulsation in gas installations carries the risk of damaging the system components and serious cost-generating failures. In the case of single-chamber dampers without internal damping elements, the minimum damper volume can be determined from the formulas included in the API 618 std. (5th edition). In practice, more complicated damper constructions with internal elements (orifices, choke tubes) are also often used. In order to determine the optimal dimensions of the damper and internal damping elements, transmission loss characteristics are determined depending on the frequency.

2 Mathematical models - fundamentals

2.1 Helmholtz resonator theory

The simplest way to model a pulsation damper is by deploying a linear model with lumped parameters, also called the Helmholtz model[1]. The Helmholtz resonator theory can be applied to the system components consisting of a small volume and a short neck, modelled as lumped parameters: acoustic compliance – compressible gas in the volume acting as a spring, and acoustic inertance – incompressible plug of gas in the neck behaving as a vibrating mass (Figure 1).

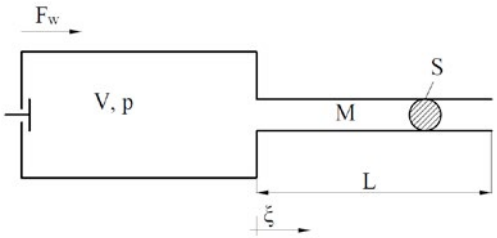

Figure 1: Schematic of a chamber pulsation damper

The resonant frequency of the damper can be determined from models with lumped parameters (Eq. 1). This formula is widely used in industrial practice to pre-estimate the dimensions of the chamber damper.

$$\omega_0 = c\sqrt{\frac{S}{LV}} \tag{1}$$

where ω_0 – resonant angular frequency, c – speed of sound, S – cross-sectional area of the neck, L – equivalent length of the neck with end correction, V – static volume of the cavity.

In order to determine the dynamic properties of a chamber damper, it is possible to plot a frequency characteristic in the form of a transfer function, defined as the ratio of the Laplace transform of the output signal to the Laplace transform of the system input signal at zero initial conditions. Replacing the Laplace transform with the Fourier transform (due to harmonic excitation), operator transmittance can be transformed into spectral transmittance. The spectral transmittance module is equal to the amplitude ratio, and the argument is the phase shift between the output and the input signal for a given frequency. The transmittance module describes the amplification of the system, which in this case is determined by the following dependence (Eq. 2):

$$|H(j\omega)| = \left|\frac{P_2(j\omega)}{P_1(j\omega)}\right| = \frac{1}{\sqrt{\left(1-\frac{\omega^2}{{\omega_0}^2}\right)^2 + 4\zeta^2\frac{\omega^2}{{\omega_0}^2}}} \tag{2}$$

where ω_0 - the resonant angular frequency of a damper, ω - the angular frequency of a excitation, ζ – damping coefficient; $\zeta = \frac{k}{2M\omega_0}$, k – viscous damping, M – acoustic mass.

For higher efficiency of pressure pulsation damping, a system consisting of two chamber dampers connected in series or a two-chamber damper with a baffle and internal choke tube can be used (low-pass filter). The transmittance module for such a system is determined by the dependence (Eq. 3):

$$|H(j\omega)| = \left|\frac{P_2(j\omega)}{P_1(j\omega)}\right| = \frac{1}{\sqrt{\frac{1}{\omega_{01}^2\omega_{02}^2}\omega^4 - \left(\frac{1}{\omega_{01}^2}+\frac{1}{\omega_{02}^2}\right)\omega^2 + 2\frac{\omega_{01}^2}{\omega_{02}^2}}} \tag{3}$$

where ω_{01} – resonant angular frequency of the first damper, ω_{01} – angular frequency of the second damper.

2.2 Plane wave theory in 1D

A limitation on the use of Helmholtz resonator theory is the wavelength of the highest frequency of oscillation, which has to be predicted. The largest dimension of the resonator should be less than ¼ of this wavelength in order to achieve accurate results. If the restriction is violated by selecting a much longer neck of a damper, resonances (standing waves) occur, which cannot be predicted by the Helmholtz model. Therefore, models with distributed parameters (continuous system approach) should be used[2,3,4,5]. This approach is based on the plane wave equation in one dimension. In large systems, one-dimensional approach is considered to be a good assumption in necks or long pipes, and to save computational time.

The use of the plane wave equation requires the following assumptions:

- the constant and the variable component of each variable can be separated over time,

by: Urszula Warzyńska, Wacław Kollek – Wrocław University

- values of variable components are small compared to average (below ± 20% of the average pressure),
- when deriving wave relationships, constant component is omitted and only variable components are modelled in time, assuming the possibility of applying the superposition principle,
- the flow is one-dimensional, and waves of pressure pulsation do not form transverse modes, i.e. no pulsations perpendicular to the axis are generated in a pipeline.

Pressure pulsation can be described by the damped wave equation in the following form (Eq. 4):

$$\frac{\partial^2 \xi}{\partial t^2} + \bar{\nu}\frac{\partial \xi}{\partial t} = c^2 \frac{\partial^2 \xi}{\partial x^2} \quad (4)$$

where ξ – displacement in x-axis, $\bar{\nu}$ – equivalent viscous damping coefficient, c – speed of sound.

The value of $\bar{\nu}$ can be determined from the Helmholtz-Stokes model (Eq. 5):

$$\bar{\nu} = \frac{2}{D}\sqrt{2\nu\omega} \quad (5)$$

where D – effective diameter of a pipe, ν – kinematic viscosity, ω – angular frequency.

The wave equation solution is known in the form of (Eq. 6):

$$\xi(x,t) = A_1 e^{-ax} e^{j(\omega t - kx)} + B_1 e^{ax} e^{j(\omega t + kx)} \quad (6)$$

where k – wave number: $k = \frac{\omega}{c} = \frac{2\pi}{\lambda}$, a – damping factor: $a = \frac{\bar{\nu}}{2c}$, j – imaginary unit: $j = \sqrt{-1}$, A_1, B_1 – complex constants calculated on the basis of boundary conditions.

Defining the wave propagation coefficient as $\gamma = a + jk$ and taking into account the above relations, the equations of pressure and flow pulsation may be obtained as follows (Eq. 7, 8):

$$p(x,t) = -\rho c^2 \frac{\partial \xi}{\partial x} = \rho c^2 \gamma [A_1 e^{-\gamma x} - B_1 e^{\gamma x}] e^{j\omega t} \quad (7)$$

$$q(x,t) = j\omega S [A_1 e^{-\gamma x} + B_1 e^{\gamma x}] e^{j\omega t} \quad (8)$$

2.3 Helmholtz wave equation in 3D

In recent years, attempts have been made to model installation elements, e.g. dampers or short sections of the installation by means of a three-dimensional acoustic simulation based on the Helmholtz equation, which has been implemented in engineering software packages based on the finite element method (FEM) [6,7,8,9,10]. The methods of multidimensional 3D simulation can be complementary to one-dimensional methods, if individual elements or short sections of the installation are analysed[11].

In the FEM-based 3D acoustic simulation, the fluid momentum (Navier-Stokes) equations and continuity equations are simplified to obtain the acoustic wave equation using the assumptions that the fluid is compressible (density changes due to pressure variations) and no mean flow of the fluid is taken into account. Viscous dissipation is included using the Stokes hypothesis (the lossy wave equation). The wave equation is reduced to the inhomogeneous Helmholtz equation and the finite element formulation is obtained from a testing wave using the Galerkin procedure. In harmonic response analyses, the following equation is resolved for pure acoustic problems (Eq. 9):

$$(-\omega^2[M_a] + j\omega[C_a] + [K_a])\{p\} = \{f_F\} \quad (9)$$

where:
$[M_a]$ – acoustic fluid mass matrix,
$[C_a]$ – acoustic fluid damping matrix,
$[K_a]$ – acoustic stiffness matrix,
$\{f_F\}$ – acoustic fluid load vector.

3 Simulation models

The numerical analyses were performed for exemplary conditions of a reciprocating compressor operation. The medium was natural gas. The main parameters of the medium used for the calculations are presented in Table 1.

Table 1: Parameters of medium

Parameter [Unit]	Value
Speed of sound [m/s]	426
Density [kg/m^3]	30.60
c_p/c_v [-]	1.43
Dynamic viscosity [kg/m·s]	$1.18 \cdot 10^{-5}$
Molar mass [kg/kmol]	16.78
Polytrophic exponent [-]	1.33

For both 1D and 3D analyses, identical general dimensions of dampers were assumed: the damper chamber length with caps l=1570mm and the diameter d=508mm. However, in the case of 1D simulation models, some geometry simplifications had to be included. Firstly, the elliptical caps were not modelled, and because the volume of a vessel is a dominant parameter in damping efficiency, diameter corrections were applied to assure the same volume of the damper as in a 3D simulation. The same approach was adopted for the internal elliptical baffles. No reducers were included in 1D geometries. The end corrections were set for 1D models with internal tubes.

3.1 Acoustic 1D models

The 1D analyses for the present study were performed on the basis of the in-house script. The wave equation was solved in frequency domain with the assumption that the long transmission line may be represented by a linear acoustic four-pole network with two inlets (P_0 and Q_0) and two outlets (P_L and Q_L). The transmission loss characteristic of

by: Urszula Warzyńska, Wacław Kollek – Wrocław University

a damper can be then computed using the transfer matrix approach[3]:

$$\begin{bmatrix} Q_0 \\ P_0 \end{bmatrix} = \begin{bmatrix} A & B \\ C & D \end{bmatrix} \begin{bmatrix} Q_L \\ P_L \end{bmatrix} \tag{10}$$

where:

$$A = \cosh \gamma L = D \tag{11}$$

$$B = \frac{1}{Z_f} \sinh \gamma L \tag{12}$$

$$C = Z_f \sinh \gamma L \tag{13}$$

- acoustic wave impedance:

$$Z_f = \frac{\rho c^2 \gamma}{j\omega S} \tag{14}$$

The diagrams of dampers modelled with simple elements of specified lengths and diameters as well as four-field matrices describing them are presented below (Figs. 2–5, Eqs. 15–18). At the inlet the unitary flow rate was applied, and at the outlet the anechoic boundary condition was selected (Eq. 19).

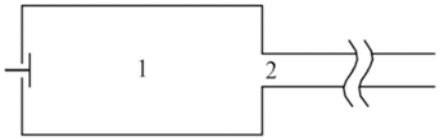

Figure 2: Schematic of a single chamber damper

$$\begin{bmatrix} A_T & B_T \\ C_T & D_T \end{bmatrix} = \begin{bmatrix} A_1 & B_1 \\ C_1 & D_1 \end{bmatrix} \tag{15}$$

Figure 3: Schematic of a damper with an internal tube

$$\begin{bmatrix} A_T & B_T \\ C_T & D_T \end{bmatrix} = \begin{bmatrix} A_1 & B_1 \\ C_1 & D_1 \end{bmatrix} \begin{bmatrix} 1 & 1/Z_{200} \\ 0 & 1 \end{bmatrix} \begin{bmatrix} A_3 & B_3 \\ C_3 & D_3 \end{bmatrix} \tag{16}$$

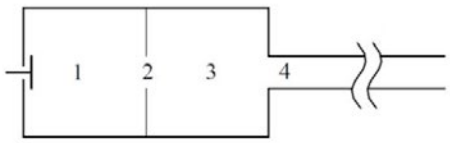

Figure 4: Schematic of a damper with an internal baffle

$$\begin{bmatrix} A_T & B_T \\ C_T & D_T \end{bmatrix} = \begin{bmatrix} A_1 & B_1 \\ C_1 & D_1 \end{bmatrix} \begin{bmatrix} A_2 & B_2 \\ C_2 & D_2 \end{bmatrix} \begin{bmatrix} A_3 & B_3 \\ C_3 & D_3 \end{bmatrix} \tag{17}$$

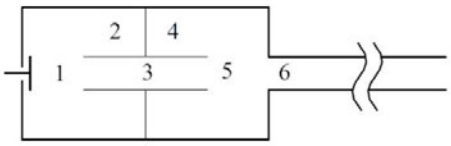

Figure 5: Schematic of a low-pass filter

$$\begin{bmatrix} A_T & B_T \\ C_T & D_T \end{bmatrix} = \begin{bmatrix} A_1 & B_1 \\ C_1 & D_1 \end{bmatrix} \begin{bmatrix} 1 & \frac{1}{Z_{200}} \\ 0 & 1 \end{bmatrix} \begin{bmatrix} A_3 & B_3 \\ C_3 & D_3 \end{bmatrix} \cdot \cdot \begin{bmatrix} 1 & \frac{1}{Z_{400}} \\ 0 & 1 \end{bmatrix} \begin{bmatrix} A_5 & B_5 \\ C_5 & D_5 \end{bmatrix} \tag{18}$$

Anechoic boundary condition:

$$q(0,t) = \frac{S}{c_0 \rho_0} p(0,t) \tag{19}$$

3.2 Acoustic 3D models

In the FEM method, normal surface velocity (inhomogeneous Neumann condition) was applied as an inlet boundary condition (Eq. 20):

$$v = V \rightarrow V = -\frac{1}{j\omega\rho} \frac{\partial p}{\partial x} \tag{20}$$

At the inlet and at the outlet ports, the radiation boundary condition was applied (Robin boundary condition).

The geometrical models of dampers used for the simulations are presented in Fig. 6.

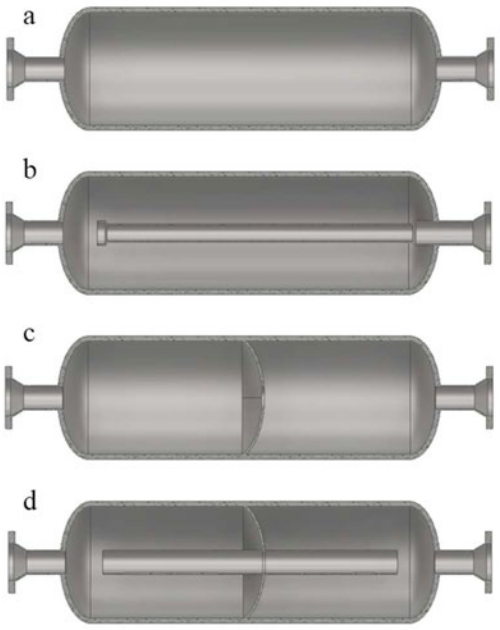

Figure 6: Geometrical models for the 3D simulation: a – single-chamber damper, b – damper with an internal tube, c – damper with an internal baffle, d – damper with an internal baffle and a choke tube

by: Urszula Warzyńska, Wacław Kollek – Wrocław University

For the purpose of acoustic 3D simulations, fluid domain models were prepared, based on the dampers geometry (internal volume of gas medium). The obtained fluid domains were then divided into finite elements forming the discrete models (Fig. 7). All analysed types of dampers were meshed with the use of identical mesh parameters.

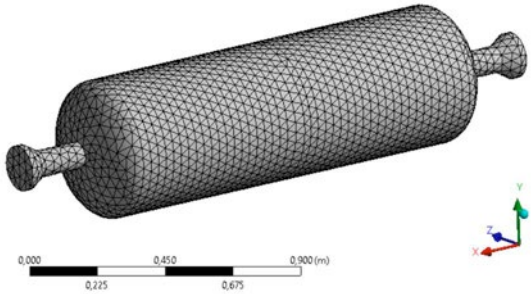

Figure 7: Finite element domain of the damper

4 Results

As a result of 3D simulations, the acoustic pressure level may be plotted in order to visualise the resonance and antiresonance modes. The acoustic pressure level (L_p) is a logarithmic measure of the effective pressure of a sound (p – RMS value of pressure) relative to a reference value (p_0) for a given harmonic of the signal (Eq. 21):

$$L_p = 20log\left(\frac{p}{p_0}\right)\ [dB] \qquad (21)$$

The pressure level contour plots enable the visualisation of standing wave phenomenon for each resonant frequency. In the pictures (Figs. 8–11) the selected results of the first resonance and antiresonance modes of a single-chamber damper and a low-pass filter are shown.

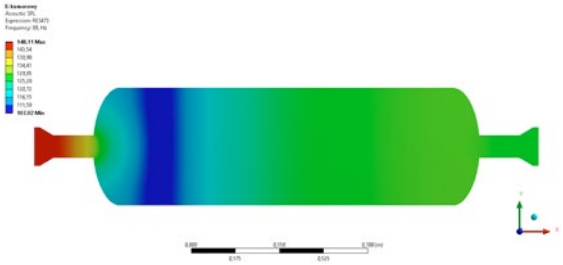

Figure 8:Acoustic pressure level contour plot of the first antiresonance at 89Hz of a single-chamber damper

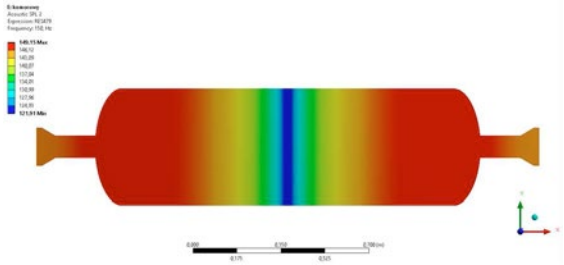

Figure 9: Acoustic pressure level contour plot of the first resonance at 150Hz of a single-chamber damper

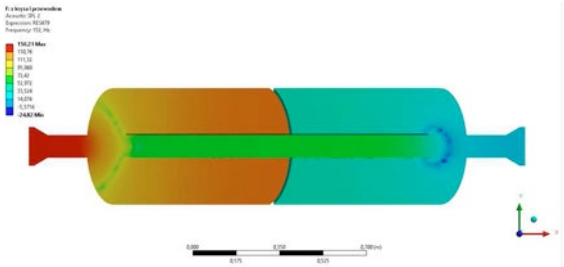

Figure 10: Acoustic pressure level contour plot of the first antiresonance at 152Hz of a damper with an internal baffle and a choke tube

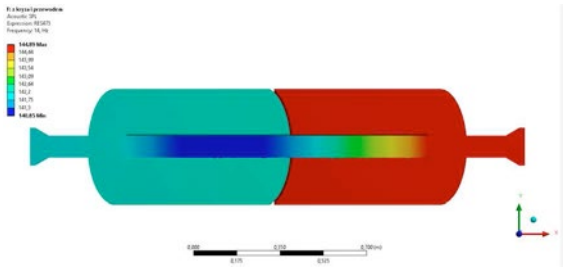

Figure 11: Acoustic pressure level contour plot of the first resonance at 14Hz of a damper with an internal baffle and a choke tube

The simulations performed, both in 1D and 3D approach, allowed obtaining the transmission loss characteristics of the analysed types of reactive pulsation dampers. The transmission loss (TL) of a damper determines the decrease in the strength of the acoustic signal between the inlet and the outlet from the pulsation damper and is most often determined from the ratio of the amplitudes of the pressure pulsation at the inlet (P_0) and at the outlet (P_L) for a given harmonic of the signal (Eq. 22):

$$TL = 20 \cdot log\frac{P_0}{P_L}\ [dB] \qquad (22)$$

If the amplitude of the pulsation at the outlet is much greater than the amplitude of the pulsation at the inlet, the transmission loss function reaches the minimum, which indicates the damper resonance – amplification of the pulsation in a given frequency. The maximum of a transmission loss function determines the highest attenuation in a given frequency.

by: Urszula Warzyńska, Wacław Kollek – Wrocław University

4.1 Comparison of 1D and 3D results

Figs. 12–15 show the comparison of transmission loss characteristics obtained from 1D and 3D simulations. The maximum value of a frequency range was set to 500Hz, which corresponds to the maximum rotational speed of a reciprocating compressor n=1500rpm and the number of significant excitation harmonics - i=20 ($f = n \cdot i/60$).

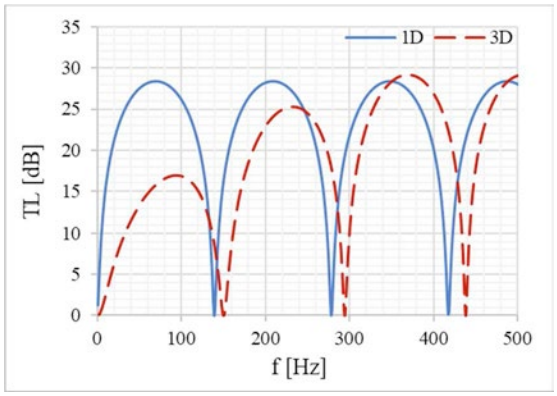

Figure 12: Transmission loss characteristics of a chamber damper obtained by 1D and 3D approach

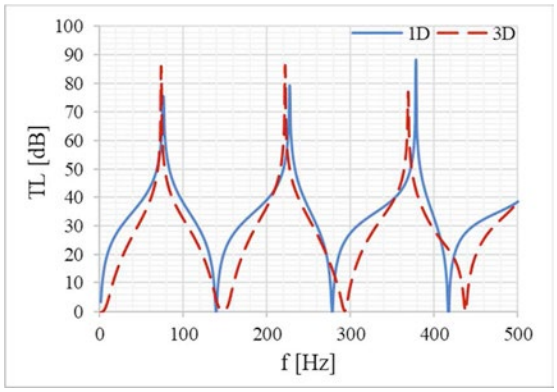

Figure 13: Transmission loss characteristics of a damper with an internal tube obtained by 1D and 3D approach

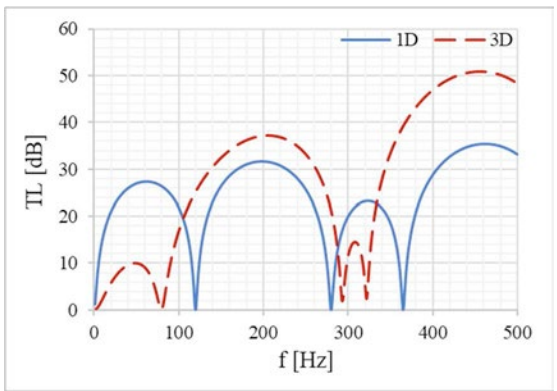

Figure 14: Transmission loss characteristics of a damper with an internal baffle obtained by 1D and 3D approach

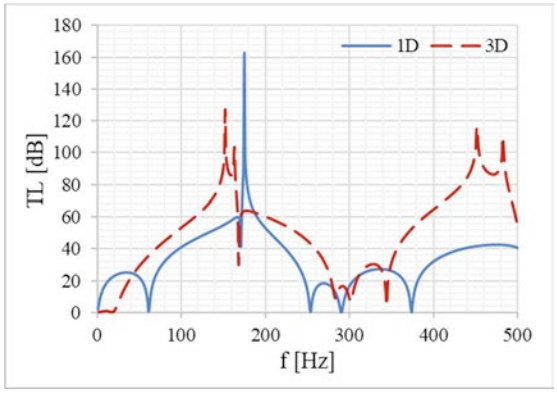

Figure 15: Transmission loss characteristics of a damper with internal baffle and choke tube obtained by 1D and 3D approach

The analysis of the simulations results indicates that 1D modelling with simplified geometry assumptions provides some differences in attenuation characteristics as compared with the results from 3D models. Of greatest importance are the differences in the natural frequencies of selected dampers, which should not be coincident with excitation frequencies in order to avoid resonance. In the case of a chamber damper and a damper with a choke tube (Figs. 12 and 13), a shift in the natural frequencies can be seen, which results from the damper caps geometry – a simplification of the elliptical caps in 1D formulation. The higher the frequency, the bigger the shift between the 1D and the 3D results. In particular, the highest natural frequency obtained in 1D simulation is 417Hz, while in 3D it equals 437Hz. The highest attenuation frequencies associated with choke tube length are reasonably consistent in both simulation methods (Fig. 13). Much larger differences in natural frequencies are visible in the characteristics of dampers with internal baffles (Figs. 14 and 15). The internal baffle geometry representation has a significant impact on the damper resonances as well as the transmission loss values.

4.2 Influence of nozzle position in 3D

Subsequent comparative analyses concerned the influence of inlet nozzle position on the transmission loss characteristics of the dampers. A series of computations was performed with the use of 3D approach including previously specified damper types with the change of inlet nozzle position from axial position to the side position in relation to the main axis of a damper chamber (Fig. 16). In a chamber damper and in a damper with a choke tube, the side nozzle was positioned in the middle of damper length, while in a damper with a baffle and in a low-pass filter, the side nozzle was situated in the quarter length of damper, due to the baffle position (in the middle of the chamber).

by: Urszula Warzyńska, Wacław Kollek – Wrocław University

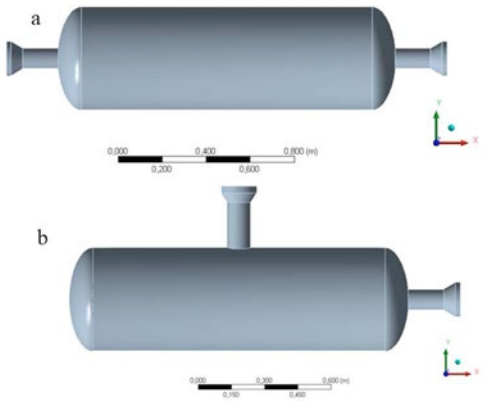

Figure 16: Schematic of the inlet nozzle position: a – axial position of the nozzle, b – side position of the nozzle

The general dimensions of the dampers as well as simulation parameters and discrete models were analogous to those previously described in subsection 3.2.

Figs. 17-20 show the comparison of transmission loss characteristics obtained with the 3D approach including the impact of the inlet nozzle position.

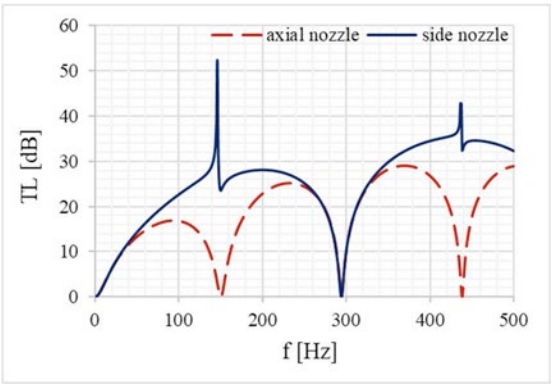

Figure 17: Transmission loss characteristics of a chamber damper with axial and side inlet nozzle position

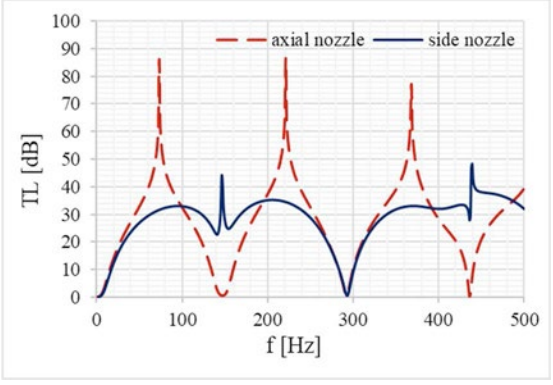

Figure 18: Transmission loss characteristics of a damper with an internal tube with axial and side inlet nozzle position

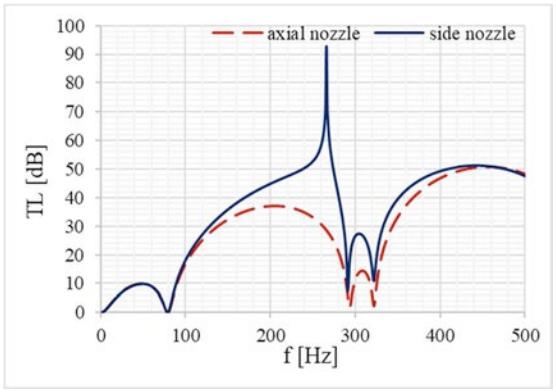

Figure 19: Transmission loss characteristics of a damper with an internal baffle with axial and side inlet nozzle position

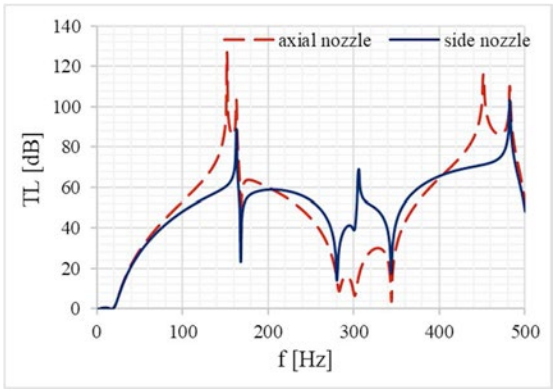

Figure 20: Transmission loss characteristics of a damper with internal baffle and choke tube with axial and side inlet nozzle position

The analysis of the presented attenuation characteristics demonstrates that a change of the inlet nozzle position has a significant influence in the case of a single-chamber damper and of a damper with an internal tube (Figs. 17 and 18). In the case of the axial nozzle position, the transmission loss function has two additional minimums relative to the side nozzle position case, which occur at 150Hz and 438Hz. At the same frequencies, the transmission loss function achieves a maximum for the side nozzle type dampers. This phenomenon results from the side-branch resonator effect, which is created by the chamber situated perpendicular to the inlet nozzle. For the above reasons, these types of dampers (chamber damper and a damper with an internal tube) should be designed with asymmetric nozzles in order to achieve wider frequency range of attenuation. In the case of a damper with an internal baffle and a low-pass filter, the transmission loss characteristics obtained in both simulations are similar. The resonance frequencies of the dampers have the same values for both the axial position of the nozzle and the side position of the nozzle.

by: Urszula Warzyńska, Wacław Kollek – Wrocław University

5 Conclusions

Three-dimensional acoustic simulation methods are currently not used for the modelling of entire compressor installations due to high demand for computing power and long calculation time. Although linear one-dimensional methods already have their established position among the currently used engineering programs, it seems reasonable to develop algorithms combining 3D and 1D models. The weakest point of algorithms based on 1D simulations consists in the correct modelling of compressor cylinder internals and passive pulsation dampers geometry, which may have a significant impact on further acoustic analyses of the compressor installation.

The results of the simulations presented in the paper indicate that some simplifications of damper geometry assumed in 1D models, in particular in the case of elliptical caps and baffles, may have a significant influence on the calculated transmission loss characteristics. In the case of single chamber dampers and dampers with an internal choke tube, geometry simplifications have an impact on resonant frequencies, and therefore it seems reasonable to take into account the resonance span of about 20% from the resonant frequencies obtained in 1D simulations (with the geometry simplifications). The transmission loss characteristics obtained from 1D and 3D simulations for a damper with an internal baffle and a low-pass filter have shown high difference in resonant frequency values and damping values, between those modelling methods. Therefore, in such cases, the 3D approach should be used in order to achieve more accurate transmission loss characteristics. The simulations of the influence of the inlet nozzle position on the transmission loss characteristic have shown the side position of the inlet nozzle in relation to the main axis of the damper and the outlet to be more favourable. The greatest benefit of this solution is evident in the case of a chamber damper and a damper with an internal tube where no additional resonances are present, as in the case of an axial inlet nozzle position.

6 Acknowledgements

Calculations have been carried out using resources provided by Wroclaw Centre for Networking and Supercomputing (http://wcss.pl), grant No. 223.

References

[1] Atkins K.E., Pyle A.S. and Tison J.D. (2004): Understanding the Pulsation & Vibration Control Concepts in the New API 618 Fifth Edition. Gas Machinery Conference in Albuquerque.

[2] Kadam P., Kim J. (2007): Experimental formulation of four poles of three-dimensional cavities and its application. Journal of Sound and Vibration, 307, 578-590.

[3] Soedel W. (2007): Sound and vibrations of positive displacement compressors. CRC Press.

[4] Wang C.N., Wu C.H., Wu T.D. (2009): A network approach for analysis of silencers with/without absorbent material. Applied Acoustics, 70, 208-2014.

[5] Wu T.W., Zhang P. (1998): Boundary element analysis of mufflers with an improved method for deriving the four-pole parameters. Journal of Sound and Vibration, 217 (4), 767 – 779.

[6] Selamet A., Radavich P.M. (1997): The effect of length on the acoustic attenuation performance of concentric expansion chambers: an analytical, computational and experimental investigation. Journal of Sound and Vibration, 201(4), 407-426.

[7] Barbieri R., Barbieri N. (2006): Finite element acoustic simulation based shape optimization of a muffler. Applied Acoustics, 67, 346-357.

[8] Liu B., Feng J., Wang Z. and Peng X. (2012): Attenuation of gas pulsation in a reciprocating compressor piping system by using a volume-choke-volume filter. Journal of Vibration and Acoustics, 134, 5.

[9] Mehdizadeh O.Z. and Paraschivoiu M. (2005): A three-dimensional finite element approach for predicting the transmission loss in mufflers and silencers with no mean flow. Applied Acoustic, 66, 8, 902–918.

[10] Tsuji T., Tsuchiya T. and Kagawa Y. (2002): Finite element and boundary element modelling for the acoustic wave transmission in mean flow medium. Journal of Sound and Vibration, 255 (5), 849–866.

[11] Linkamp A., Deimel C., Brümmer A., Skoda R. (2016): Non-reflecting coupling method for one-dimensional finite difference/finite volume schemes based on spectral error analysis. Computers and Fluids, 140, 334-346.

BORSIG

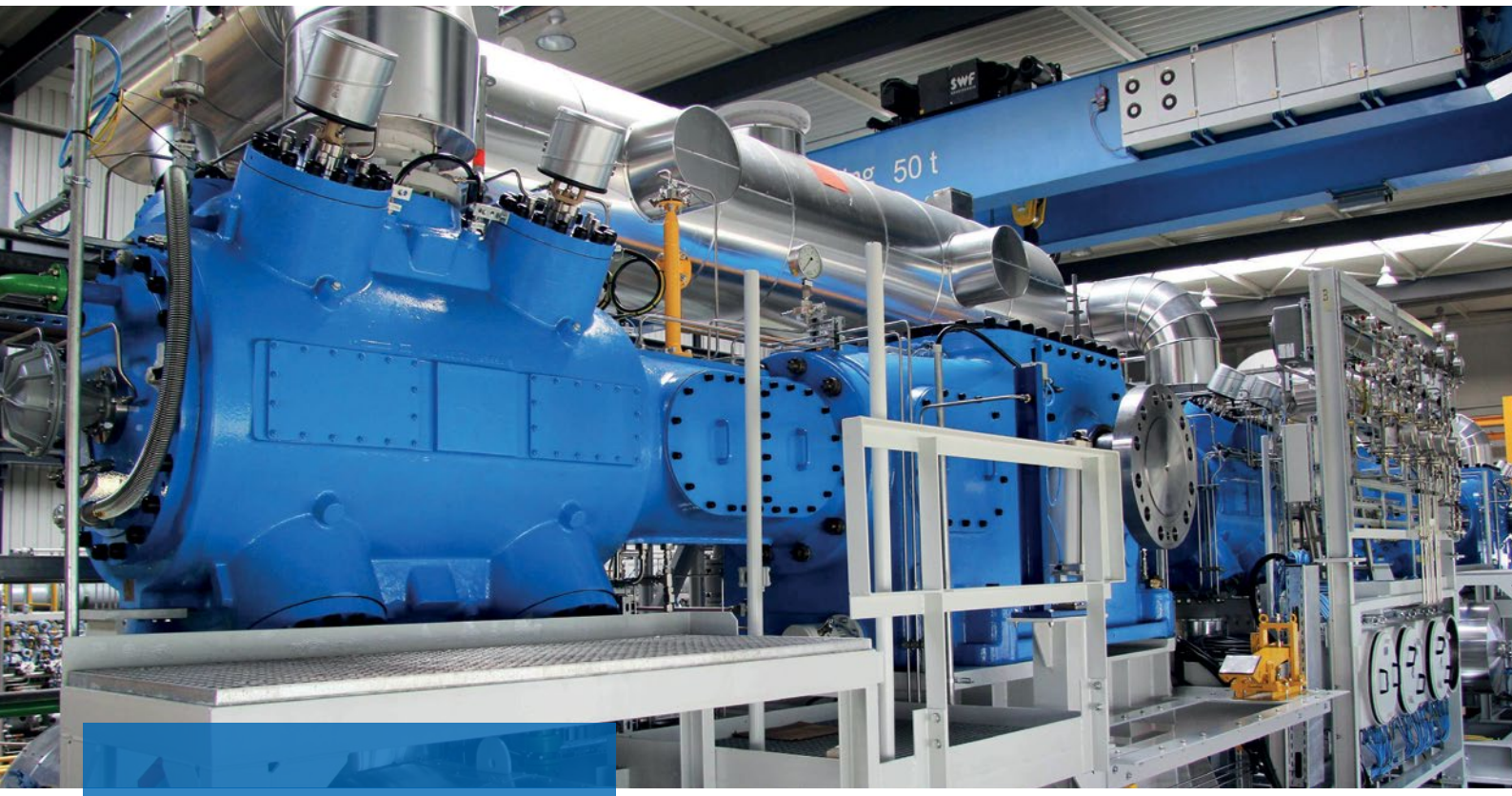

PROCESS GAS COMPRESSORS

API 618
Reciprocating Compressors

API 617 & 672
Integrally Geared Centrifugal Compressors

We, at BORSIG ZM Compression GmbH, design and manufacture tailored compressors for innovative process gas compression solutions.

BORSIG ZM Compression GmbH

↘ To learn more, please visit
www.borsig.de/zm

Pulsation optimization by dynamic variable orifice & Recips starting phase selection

by:

Author: **Marco Passeri**
RC Consulting Engineer/Technologist, Baker Hughes, a GE company, Florence – Italy
Marco.passeri@bhge.com

Co-Author: **Ludovica Guerrini**
RC Engineer, Baker Hughes, a GE company, Florence – Italy
Ludovica.guerrini@bhge.com

Co-Author: **Christian Rossi**
Machinery & Packages Dpt., SAIPEM SpA, Fano – Italy
Christian.Rossi@saipem.com

Co-Author: **Michele Mazzoli**
Electrical Dpt., SAIPEM SpA, Fano – Italy
Michele.Mazzoli@saipem.com

Co-Author: **Giancarlo Ferrari**
Electrical Dpt., NIDEC – ASI Spa, Cinisello Balsamo – Italy
Giancarlo.Ferrari@nidec-asi.com

Co-Author: **Sebastiano Melis**
Energy Engineer, Florence University, Florence – Italy
Sebastiano.melis.ing@gmail.com

11th EFRC CONFERENCE
September 13 – 14, 2018, Madrid

Abstract:
In a compressor installation of Ital Gas Storage S.p.A. at Cornegliano Italy, injection and extraction of natural gas in/from the reservoir are performed using four reciprocating compressors working in parallel with common piping. The complexity of that plant derives from the presence of multiple operating conditions in single or double stage compressor configurations with variable operating pressures, possible on/off assets, compressor capacity control, different injection/extraction conditions. In this environment, to minimize the pulsation induced forces and allow a smooth and safe operation of the plant, a refined solution to comply with API 618 requirements in terms of pressure drop and residual pressure pulsation limits was needed. The first issue is that, due to the wide operating range, the use of hole orifices at fixed diameter does not allow the compliance with pressure drop limits for all certified conditions. That challenge was solved by using dynamic variable orifices (valves), which can adjust the pressure drop as a function of versus the compressor operating conditions. Another important aspect is to minimize the total pressure pulsation when compressors are running simultaneously. That requirement can be solved by calculating the best phase among compressor crankshafts (electric motors phase start synchronization) to minimize the total generated pressure pulsation and relevant pulsation induced forces. This selection allows to finally limit vibration requirements.

by: M. Passeri, L. Guerrini – Baker Hughes GE; C. Rossi, M. Mazzoli – SAIPEM; G. Ferrari – NIDEC; S. Melis – Florence University

1 Introduction

The demand for Natural Gas is constantly increasing. To meet this demand importing States are forced to diversify supply sources. The Cornegliano Laudense plant is one of the Italian projects for increasing natural gas storage capacity. The plant is the result of the use of the best technologies present in the Oil & Gas sector, being able to boast a layout designed to respect the environment, current regulations and to save energy. The design phase has imposed numerous challenges due to the plant complexity and the numerous operating conditions. The pressure and flow requirements have been met by using four reciprocating compressors. As well known, reciprocating compressors generate a pulsating gas flow, whose harmonic components may interact with the plant piping and equipment so to induce resonance conditions. The effects of resonance include high vibrations, poor performance, noise, and high risk of fatigue failures [3,4]. Accurate plant pressure pulsations and mechanical analysis are the means for protecting plant operation from pressure or mechanical resonance, by limiting their effect with proper damping and/or stiffening of supports. Pulsation Dampers are commonly used in these systems and they are placed upstream and downstream of the compressor. These dampers are typically designed according to Pre-Study (API 618 5th ed. para 7.9.4.2.3.4) [1], with the piping system replaced by an infinite length to verify that the pulsations requirements are achieved with a sufficient margin. This approach usually allows the minimization of the modifications required by the final acoustical study. Then the changes will be limited to the insertion of single or multi-hole plates (Fix Hole Orifices; FHO) and/or to the piping size increase for small sections, with no changes in the overall layout to detune the local acoustic resonance. In this application, the vast differences in operating conditions coupled with the possibility to work in single or double phase make inadequate the use of traditional FHO orifices (plant resonances damping solutions) to fully comply with API618 requirements in terms of pulsation suppression device pressure drop and residual pressure pulsations. In this system, the classic pulsation damping solutions have been refined to obtain full compliance with the stringent contractual API 618 and flexibility operations requirements. Specifically, at some locations valves that work as “Dynamic Variable Orifice (DVO)” (adaptive valve) have been used. These allow for variation in the orifice pressure drop, in function of the compressor operating condition, by varying their passage cross-section. The use of DVO imply a higher initial cost investment compared to the cost of classic solutions, but it allows for a more efficient use of the compressors, guaranteeing, in addition to compliance with the regulations, the lower energy consumption needed to power the compressors. In this case, the energy saving achieved with the use of DVO allows the recovery of the initial investment in a short time.

In a plant configuration with several compressors, the maximum pressure pulsation is obtained by the sum of the pulsations of the individual compressors. In this case, the sum of pulsations produces a quite high pulsation induced forces in the common piping. To efficiently control the sum of pressure pulsations, another refined acoustic solution was introduced by the investigation of the best phasing between the compressor shafts. The selected phase is applied through a system solution that requires a precise start coupling of each compressor electric motor.

The use of DVO coupled with the selection of the best start-up phase between compressors allows for the lowest pulsation induced forces on the system. Lower forces applied to the system results in reduced mechanical vibration study recommendations.

2 Plant description

The objective of this project is to store natural gas in the depleted gas reservoir at Cornegliano Laudense, Lodi, Italy. The storage facility is connected to the Italian gas grid and provides seasonal storage of natural gas.

2.1 Plant Overview

In Principle, gas is pumped into the reservoir during summer and pumped out during winter.

The company Ital Gas Storage S.p.A owns the concession to exploit the reserve for a period of forty years. The plant reuses a Natural Gas field discovered in 1951, exploited until 1997, and is therefore classified in the category of storage facilities. As it is known, storage facilities follow the seasonal trend of natural gas demand; Figure 1 shows a typical gas demand trend. Demand increases during winter (greater demand for the domestic sector) and decreases in the warmer months.

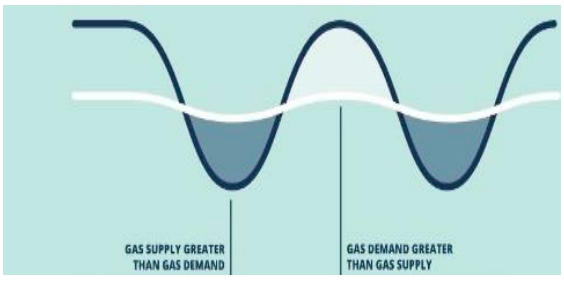

Figure 1: Annual gas demand

The storage site provides flexibility to the national gas distribution network and helps to prevent some undesired scenarios including sudden cold peaks and interruption of import services for geopolitical reasons. The Cornegliano plant increases the annual Italian storage capacity by 10% (daily 8%).

The facilities are situated at two main geographical locations: Central Station & Wellheads Cluster A (Central Area) and Wellheads Cluster B (Cluster B)

by: M. Passeri, L. Guerrini – Baker Hughes GE; C. Rossi, M. Mazzoli – SAIPEM; G. Ferrari – NIDEC; S. Melis – Florence University

which is approx. 2 km away and is connected to the Central Station by means of a 24" pipeline and a fiber optic cable. Each Cluster has seven wells for a total capacity of 28 million Sm^3/day.

2.2 Operating configurations

The plant has three basic operating configurations:

- **Injection:** Importing gas from the Snam Rete gas grid and injecting/storing it into the depleted gas reservoir via the wellheads located at Clusters A and B using compressors.
- **Production:** Exporting stored gas from the reservoir back to the Snam Rete gas grid using the reservoir pressure as free flow.
- **Extraction:** Exporting stored gas from the reservoir back to the Snam Rete gas grid using the compressors in a parallel configuration. This mode is used when the reservoir pressure is not enough-to get the gas back to the gas grid under free-flow conditions.

When the grid pressure is higher than the wellhead by an adequate margin (~ 5 bar), **Free Flow** into the reservoir is possible. The gas flow from/to the grid is measured by a three-line bi-directional ultrasonic fiscal meter.

2.3 System characteristics

The plant as reported in paragraph 2.2 has two phases (Extraction and Injection) for which it is necessary to use compression systems. The compression system consists of four identical parallel duty two-stage single-casing reciprocating compressors (model 6HG/2), using common piping. Each compressor is driven by a 15 MW synchronous electric motor and can compress 7 MSm^3/day from 55 barg to 170 barg. Double-stage compression is used in the Injection phase when the pressure in the reserve reaches the value of 107 barg; other pressure limits to be met are shown in table 1.

Table 1: Compressors Operating Pressure

Config.	Suction (OP)	Discharge (OP)
Injection	37 ÷ 74 barg	50 ÷ 174* barg
Extraction	25 ÷ 75 barg	41 ÷ 78 barg

* Theoretical maximum but due to the limit within the reservoir, initially imposed by the authority leads to a compressor max discharge pressure equal to 150 barg. The compressor must be able to achieve 174 barg, in case the authority will later allow that run.
To satisfy those pressures and flow limits, the compressors make the capacity control adjustments shown in table 2. In case of parallel run all the cylinders work in single stage.
Adjustments in between the steps and below 50% of the flow capacity are carried out by recirculation valves lines.

Table 2: Compressor Capacity control

Injection (above 107 barg) Series Run		
	1st stage Cylinder 2,4,6	2nd stage Cylinder 1,3,5
1	100%	100%
2	83%	100%
3	83%	83%
Extraction/Injection (up to107 barg) Parallel Run		
	1st stage Cylinder 2,4,6	1st stage Cylinder 1,3,5
1	100%	100%
2	83%	100%
3	83%	83%
4	66%	83%
5	66%	66%
6	50%	66%
7	50%	50%

Interstage air-coolers and discharge air-coolers keep the gas temperature at 45°C. The two stages of each compressor can operate in series or in parallel, depending on the operating mode and conditions. The gas coming from the wells, where hydrate formation is prevented injecting methanol during start-up, passes through five separators and is dehydrated in four columns, counter-current with Tri-Ethylene Glycol (TEG), before being delivered to the grid, after heating and pressure reduction, or after compression. The TEG is regenerated, in a closed loop, using three gas-fired units. The produced water from the wells is treated and then stored in a dedicated Tank, before being disposed of via truck. A gas recovery compressor reinjects into the process the gas leaking from the main compressors' mechanical seals, thus avoiding discharging it to the vent system.

2.4 API 618 acoustic requirements

API 618 5th edition approach 3 requires that the maximum allowable Pressure Drop based on steady flow through a pulsation suppression device, shall be limited to 0.25% of average absolute line pressure or the value determined by the following formula (para 7.9.4.2.5.3.1, Equation 13), whichever is higher:

$$\Delta P = 1.67 \left(\frac{R-1}{R}\right) \% \qquad (1)$$

Where ΔP is the maximum pressure drop % and R the stage pressure ratio.

These limits shall be increased by a factor of two when the pressure drop is calculated using the total flow, where the total flow is the sum of the steady flow plus the dynamic flow components, provided that the static component still meets the above criteria.
API618 also specifies that the peak to peak pressure pulsations levels for normal operating conditions

by: M. Passeri, L. Guerrini – Baker Hughes GE; C. Rossi, M. Mazzoli – SAIPEM; G. Ferrari – NIDEC; S. Melis – Florence University

shall satisfy the following formula [para 7.9.4.2.5.2.2.2., Equation 8).

$$P_1(\%) = \sqrt{\frac{a}{350}} * \left(\frac{400}{(P_L * ID * f)\text{^}1/2}\right) \qquad (2)$$

Where P_1 is the maximum allowable peak-to-peak level of individual pulsation components, expressed as a % of mean absolute line pressure, a is the gas speed of sound (m/s), Pl is the absolute line pressure (bar), ID is the inside diameter of line pipe (mm) and f is the pulsation frequency (Hz).

2.5 Compression system design

The selected Reciprocating compressors satisfy the flow and pressure data sheet requirements, but they generate pulsating flow and pressure. So, just after the compressor/s selection, the second step of the design is the limitation of the pressure pulsation plant propagation/amplification through proper pulsation suppression device sizing according to API618 requirements. The selection of the damper type (empty volume or filter) and size is performed by a dedicated preliminary sizing program [5,6] that, taking data directly from the compressor sizing software, calculates the volume, the diameters, and length of chokes and the relevant pressure drop, optimizing the results for all the operating conditions. Having chosen the most effective main dimensions and applying the best practice design to minimize shaking forces inside the dampers (e.g. by internal pipes or by baffles) a preliminary General Arrangement design (see figure 2) is made to accommodate these dampers into the compressor.

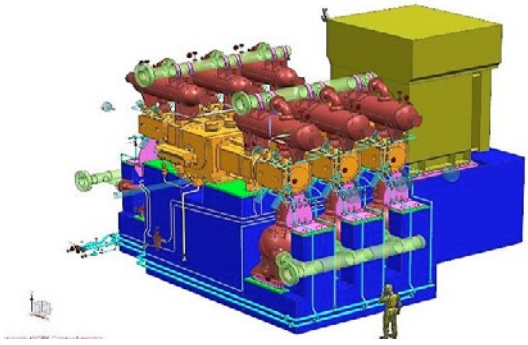

Figure 2: Compressor General Arrangement

This must be done in close cooperation with the compressor manufacturer and the Pulsation/vibration specialist who must verify compliance with the following API 618 requirements and, if necessary, introduce modifications:

- Damper check of the selected geometry to verify compliance with the allowable pressure pulsations limits (para 7.9.4.2.3.4 “pre-study).
- Forced Mechanical response analysis of the Compressor Mechanical Model (Finite Element Model according to para 7.9.4.2.4.3) to verify vibrations and cyclic stress. This is achieved by preliminary cylinder manifold forced response study considering the following forces applied:

  a. Pressure pulsation induced forces
  b. Cylinder gas loads due to compression
  c. Dynamic forces induced at the foundations

In the latter verification, the critical forces are those generated by the compression (cylinder gas loads), which are strictly related to compressor data sheet, cannot be adjusted unless the change of data sheet requirements. Cylinder gas loads have high force amplitudes on high harmonic components, which frequencies may easily interfere with the Mechanical natural frequency of the compression system, resulting in mechanical resonance phenomena. For this reason, that verification needs to be performed at an early stage of the project, to guide the General Arrangement design of the compressor and to avoid discovering excessive vibrations levels too late when modifications to the system are no longer feasible. When this step is positively verified, the Design of the compression system and dampers layout can be released for construction [7,8].

2.6 Pulsation study system difficulties

The pressure pulsations generated by the compression system, even if properly reduced by the dampers, interacting with plant piping and equipment are amplified by acoustic plant resonance. These resonances are due to the specific piping plant length and boundary conditions that in some operating conditions can lead to pressure pulsation values of up to 10-20 times higher than the allowable limits. Therefore, it is critical to control plant resonances phenomena, through a dedicated acoustical study so to investigate proper recommendations to protect plant operations.
When the Customer plant isometrics are available the pulsation study restarts to minimize plant pressure pulsation and consequently reduce pulsation induced forces acting in the compression system, connected piping, and equipment [3,4]. Given the complexity of the system to be analyzed (4 compressors), the extreme variability of the operating conditions to be checked (single-phase / two-phase, flow regulation, etc.) the traditional plant piping modifications are not an effective solution because they just move the resonance from a condition to another one. The common method of reducing the amplification of plant pressure pulsations is the use of Fixed Hole Orifice (FHO see figure 3) that generates known pressure drops in precise points of the line (usually in a point where the flow pulsation is at maximum) defined by the study. The simplicity of FHO makes them economical to manufacture and easy to install. On the other hand, FHO can be optimized only in a limited range of operating conditions (1 or 2 certified points). In this application the acoustical study has been performed for all the 6 certified conditions (I1-I2-I3 and E1-E2-E3) plus other 8 conditions (point

by: M. Passeri, L. Guerrini – Baker Hughes GE; C. Rossi, M. Mazzoli – SAIPEM; G. Ferrari – NIDEC; S. Melis – Florence University

2- point 15-Ver 1- Ver 15 and point 3 - point 4 - Ver 1 -Ver 3) for a total of 14 cases (see figure 4 and 5). For each of these cases, a +/-10% variation in process conditions has been considered as study tolerance. To be noted that in this case a higher variation in process conditions is not allowed by the Compressor manufacturer.

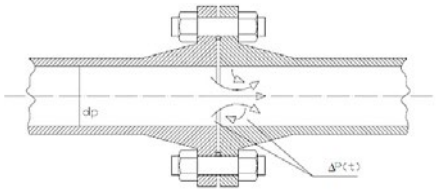

Figure 3: Fixed hole orifice.

They are sized based on the frequencies to be dampened, the pressure levels to be reached, the flow rate, the operating pressure and the gas sound velocity. When there are several and different operating conditions, there is a very large variation in the above parameters, then FHO pressure drop varies consistently and their general efficiency drastically decreases. In gas storage facilities, such as Cornegliano, it is normal to have a wide range of operating conditions (e.g. application requires large compression ratio variations) and consequently the pressure drop generated by a single set of FHO is expected to vary significantly. For this reason, the initially proposed pressure pulsation study solution (see the relevant pressure drop on table 3), to have API 618 pressure pulsations under certified conditions, has the following issues:

- Conditions with high un-necessary pressure drop; (difference up to 42 times)
- Conditions with low-pressure drop resulting in excessive residual pressure pulsations;
- Exceeding of API 618 pressure drop limits in the 6 certified conditions injection (allowed value is 0.5% for 1st stg. and 0.7% for 2nd stg.) and extraction (allowed value is 0.9%) highlighted in red on table 3. Value within the limits are in green;

Table 3: FHO ΔP% variation in the conditions

FHO ΔP% in the certified conditions				
Full load	**1st stg. Suct.**	**1st stg. Disch.**	**2nd stg. Suct.**	**2nd stg. Disch.**
E3	1.5	1.5	1.5	1.5
E1	0.82	0.44	0.85	0.45
E2	1.19	1.09	1.19	1.09
I1	1.25	1.44	1.17	1.09
I2	1.38	1.82	1.48	2.37
I3	1.39	2.81	1.80	2.53
FHO ΔP% variation considering all conditions				
Max	2.13	5.46	2.11	5.37
Min	0.24	**0.13**	0.25	0.14
ratio	9	**42**	8	**38**

Customer clarified that no deviation to API618 pressure drop limit is admitted, for certified conditions, so this solution was not considered.
The second solution investigated was the use of a double set of FHO (depending on the configuration used for Injection or Extraction). But once proposed it was impractical because the system had to be stopped each time (depressurized with relevant atmospheric emissions) to replace the FHO based on the configuration used.
Finally, to achieve the required API 618 pulsation levels and to comply with the pressure drops requirements, a third solution was considered with Dynamic Variable Orifices (DVO) [10,11]. This was possible because the DVO allows the orifice size to be adjusted (by valve opening) as conditions changes for optimal pulsation control and efficiency. In this case, the selected device is a control valve that is regulated by the static pressure drop. The pressure drops in Table 4 are the static ones allowed by API 618. The most part of these pressure drops is generated by the selected DVO in the injection and extraction of certified conditions. The pressure drops in table 4 are inclusive of the minor ones relevant to the fix orifices at the volume bottles nozzles cylinders side connections (variable from 0.05% ÷ 0.1% among the certified cases).
In this connection, it must be noted that also the total flow pressure drop is calculated to verify compliance with the requirements (see section 2.4).

Table 4: ΔP% with DVO in the certified condition

DVO ΔP% in the certified conditions				
Full load	**1st stg. Suct.**	**1st stg. Disch.**	**2nd stg. Suct.**	**2nd stg. Disch.**
E3	0.9	0.9	0.9	0.9
E1	0.9	0.9	0.9	0.9
E2	0.9	0.9	0.9	0.9
I1	0.5	0.5	0.7	0.7
I2	0.5	0.5	0.7	0.7
I3	0.5	0.5	0.7	0.7
DVO ΔP% variation considering all conditions				
Max	0.9	0.9	0.9	0.9
Min	0.5	0.5	0.7	0.7
ratio	1.8	1.8	1.28	1.28

Figure 4 shows the comparison of the pressure drops generated by FHO (red) vs DVO (green) vs API pressure drop limit (blue) in the 3 certified conditions (extraction) in **discharge plant** (single stage) including capacity control conditions.

Figure 5 shows the comparison of the pressure drops generated by FHO (red) vs DVO (green) vs API pressure drop limit (blue) in the 3 certified conditions (Injection) in 2nd stage discharge plant (double stage) including capacity control conditions.

by: M. Passeri, L. Guerrini – Baker Hughes GE; C. Rossi, M. Mazzoli – SAIPEM; G. Ferrari – NIDEC; S. Melis – Florence University

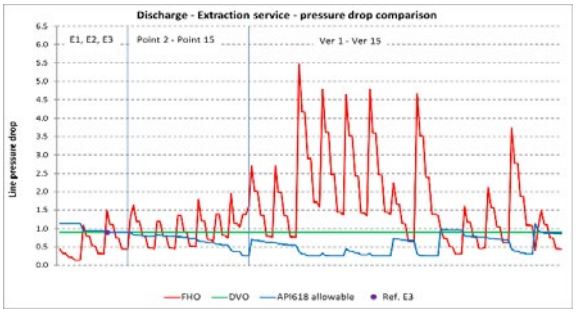

Figure 4: FHO-DVO ΔP% trend Discharge. Extraction

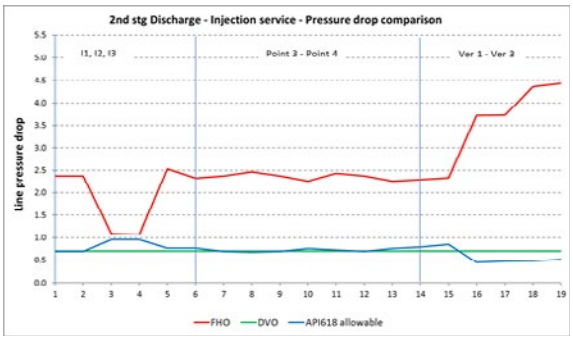

Figure 5: FHO-DVO ΔP% trend Discharge. Injection

The solution selected requires the use of 16 DVO (4 for each compressor) and must ensure a constant pressure drop (see table 4) for all operating conditions. The DVOs are installed in the suction and discharge manifolds of each individual compressor (see Figure 6).

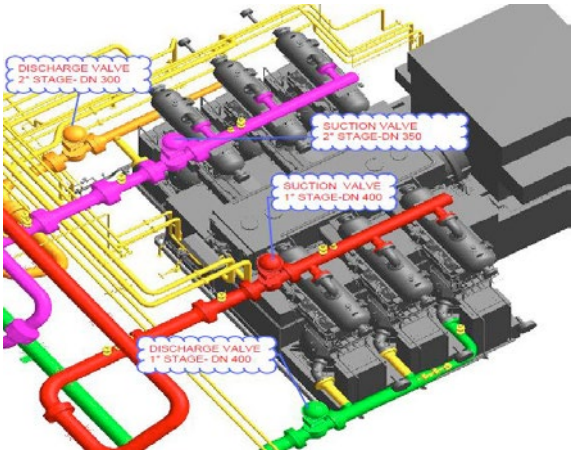

Figure 6: DVO position on suction & discharge

To ensure the expected plant reliability, the selected DVO type is a control valve of the same type as those used for the by-pass line. In this case, the DVO control valve philosophy has only to maintain a fixed pressure drop regardless of the operating condition. Pressure drop is changed only when the plant switches from single-phase to a double-phase configuration (injection and extraction).
Among the possible DVO regulation methodologies, this is considered the simplest and best in terms of plant reliability. The DVO opening is regulated by the pressure difference measurements (upstream and downstream), without considering the compressor setting, by a Control Unit (CU), see figure 7. By these measurements, the pressure drops generated by the valves can be monitored to verify the compliance with the study requirements and in case introduce the necessary adjustment (by a software parameter multiplicator).

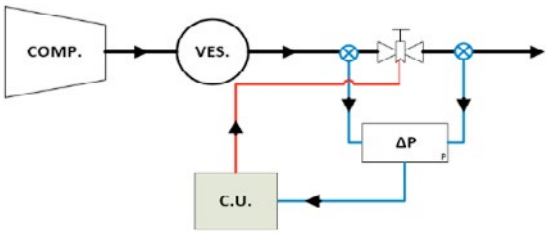

Figure 7: Cornegliano DVO control unit

For similar applications, a future possible solution could be to adjust the DVO pressure drop, using the compressor system controls, to optimize the pressure drop requirement for each operating condition to further minimize the residual pressure pulsations and relevant pulsation induced vibrations. An adjustment of this type requires a more complex control unit, which must be in direct communication with the compressor control unit (C.C.U (see figure 8).

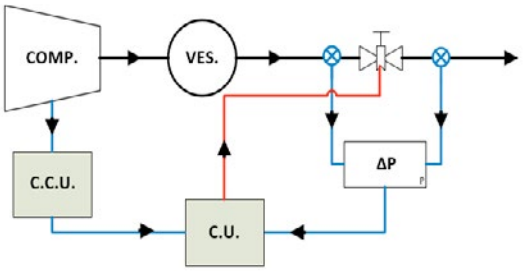

Figure 8: More complex DVO control unit

Of course, the use of a more complex control unit must be duly evaluated considering that plant reliability is a key parameter to be targeted. The more complex software and logic, even if not used, is included in the present application for future developments.

3 Energy saving

Purpose of FHO and DVO devices is the same, both dampen the pressure pulsations to minimize relevant plant pressure pulsation induced forces. Usually, the best compromise between the introduced pressure drops, the residual pressure pulsation levels, and customer requirements can be achieved by FHO.
For Cornegliano, the complexity of the application coupled with the mandatory requirements of the customer, lead to finding satisfactory results only by using DVO. Comparing FHO and DVO solutions, it is easy to understand that they have opposite advantages and disadvantages. The main differences

by: M. Passeri, L. Guerrini – Baker Hughes GE; C. Rossi, M. Mazzoli – SAIPEM; G. Ferrari – NIDEC; S. Melis – Florence University

are that the FHO have an initial lower cost with higher energy consumption while DVO has an initial higher cost with lower energy consumption.
Analyzing the selection of the orifice type from only a cost point of view one might think that the high initial cost of DVO cannot ever be compensated, while in this type of application, one may discover the opposite considering the cost of energy consumption over the years [11]. Table 5 shows the values of the instantaneous power absorbed by a single 6HG/2 compressor with the DVO installed at Cornegliano, the values of power absorbed with the alternative FHO and the saving. The comparison shows that in the 6 certified conditions the DVO further allows for full compliance with the API 618 requirements also needs less energy to operate the compressors in respect to FHO.

Table 5: the instantaneous power of the 6HG/2 compressor

Oper. Cond.	Power DVO [kW]	Power FHO [kW]	Saving [kW]
I1	11 342	11 494	152
I2	12 964	13 576	612
I3	11 307	11 931	624
E1	7 253	7 223	-30
E2	8 247	8 293	46
E3	8 251	8 348	97

3.1 Annual saving using DVO

Once the savings in kW have been calculated (see table 5), the days of operation of the compressors can be evaluated considering that the two energy-intensive operating conditions are the extraction and injection phase and the extraction phase occurs only in the final phase of emptying the reserve. An operating time of approximately 201 days (just over 6 months) can be estimated. Since it is impossible to know exactly the distribution of operating days in various operating conditions, an arbitrary allocation between the certified conditions (i.e. 19 days for E1, E2, E3 and 48 days for I1, I2, I3) has been supposed to evaluate the energy consumption. In 201 working days, through the DVO, approx. 1.650.000 kWh are saved, considering a price for electricity of 0.12 €/kWh an annual saving of 200 k€ (for a single 6HG/2 compressor) is achieved. Assuming an average use of 3 compressors, an approximate annual saving of about 600 k€ is achieved. Based on the pressure drops values (see figures 4 and 5) it is easy to understand that if the compressors operate in alternative conditions the saving is higher than the one calculated for certified conditions. The conclusion is that the initial cost investment for the 16 DVO will most-likely be recovered in less than two years of operation.

4 Pressure pulsation combination

In systems connected to several compressors, the pressure pulsations that propagate on the plant are given by the combination of the effects of the pulsations generated by each individual compressor. In case of parallel compressors running at the same RPM, the max pressure pulsation levels that may occur is the sum of the pulsations generated by each compressor. Considering that the crankshaft phase between the compressors is random, it will change anytime an additional compressor starts, resulting in pulsation levels that may vary between (theoretically) zero and complete single signal sum. The number of cylinders, the number of unloading conditions and the shafting phase among the cylinders of the same compressor affect the sum of pulsation. The common practice to perform the study of parallel compressors is to consider all the compressors working, in the various cases of operations up to the max possible, imposing all compressor crankshaft with the same phase (usually the worst case). Alternatively, another approach to reducing study runs is, to calculate only the single compressor contributes and consider that in the worst case there will be the full sum. In both cases, as the number of active compressors increases, the sum of pressure pulsation applied to the system proportionally increases. Then the calculated values, with parallel operation, often exceed what is allowable as per API618, unless interaction between the compressors is almost eliminated by plant damping/filtering elements. The interaction between the compressors can be reduced by Big Drum or Volumes (located at a specific distance from the single compressor to leverage the Helmholtz frequency filter phenomena), but in the real cases, it is difficult to accommodate these elements unless they are already present for process needs. For this reason, API618 specifies that, with customer agreement, pressure pulsation limits may be exceeded, verifying that the resulting forces applied to the piping result in allowable vibrations levels and allowable cyclic stress. In any case, experiences gained by pulsation studies specialists with thousands of plants studied [3,4, 9], suggest:

- The pressure pulsations value calculated for the single compressor operation must be within API618 limitations;
- The highest calculated sum of pressure pulsation must never exceed the pressure pulsation value calculated for a single compressor multiplied by the square root of the number of the compressors running in parallel.

4.1 Sum of pulsations on the manifold

In Cornegliano, having 4 compressors, each having 6 double effect cylinders, there are 48 different pulsation sources that can be activated or deactivated. Even if, at the suction and at the

by: M. Passeri, L. Guerrini – Baker Hughes GE; C. Rossi, M. Mazzoli – SAIPEM; G. Ferrari – NIDEC; S. Melis – Florence University

discharge of each compressor there are separators that partially dampen the pulsation combination, being that common piping is 32", the relevant worst case calculated pulsation induced forces remain quite high, although strongly reduced by the DVO. This leads to thinking about how to reduce these forces further. Remembering that at each additional compressor start-up, the phase among the compressors (being random) will change inducing a significant change also in the sum of pulsations, the study effort was concentrated on this aspect.
To keep the duration of the study within a reasonable length of time and taking into consideration that for each different phase to be verified, hundreds of runs must be performed, it was decided to first use a purely theoretical approach. This simplified study neglect dampers and plant effect and only connect all working cylinders together to calculate the sum of pulsations. This approach needs the following steps:

- First to confirm that the worst phase case remains the same found with the full acoustical study (i.e. all compressors in phase) previously described (see section 2). This is a fundamental step to validate this simplified approach.

- Then to find the best phase to minimize the sum of pulsations.

After the selection of the best phase by the simplified approach, the full plant acoustic study must be repeated to verify the pulsation induced forces reduction. To perform the theoretical evaluation, it is necessary to identify the key player of the pulsations combination, here below listed:

- The compressor model is a 6HG/2 with 6 double-acting cylinders divided into two balanced opposed banks. Each bank has 3 cylinders at 120° between them. Each compressor taken individually at full load is perfectly balanced having distributed the cylinders every 120°;

- There are several capacity controls that, depending upon the number of active cylinder effects, generate several different harmonic components;

- Normal operation is with 4 compressors operating in parallel, however, also the cases with 2 and 3 compressors must be verified.

The exercise starts with the calculation of theoretical unfiltered pressure pulsation at the suction cylinder flange of a single full loaded 6HG/2 compressor. Figure 9 shows the global results (Peak-Peak 1.3 bar) and the relevant harmonic spectrum.

Figure 10 shows the theoretical sum of pressure pulsation (Peak-Peak 5 bar), assuming all 4 compressors are working with the crankshaft in phase (0°), for the suction manifold of the 4 fully loaded 6HG/2 compressors.

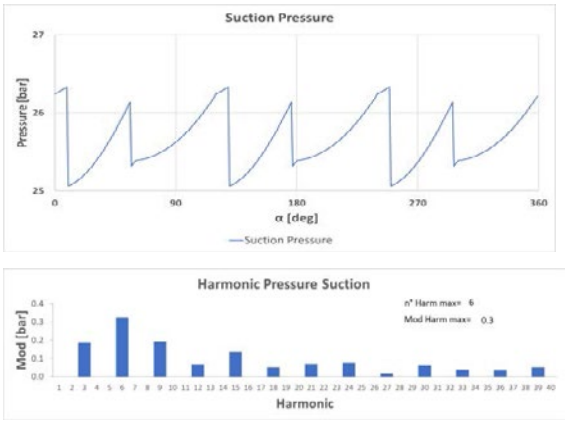

Figure 9: Theoretical suction pressure pulsation for one 6HG/2 compressor at 100% (Cornegliano)

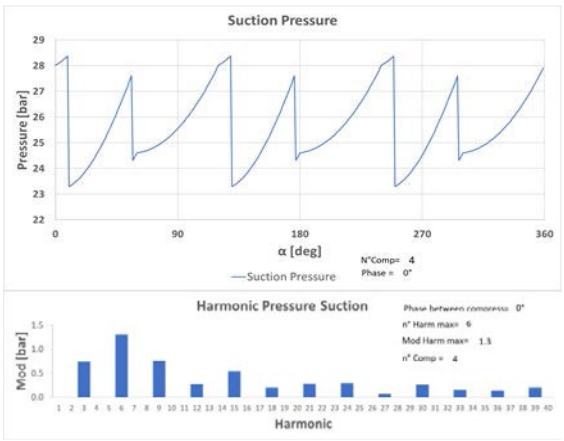

Figure 10: a Theoretical sum of pressure pulsations for 4 fully loaded 6HG/2 at 0° phase (Cornegliano)

Comparing the theoretical pressure pulsation of one compressor (Figure 9) with four compressors at the full load at 0° (Figure 10), it is evident that the Peak to Peak pressure proportionally increases in function of the active compressors (1.3 bar vs 5 bar, 4 times).

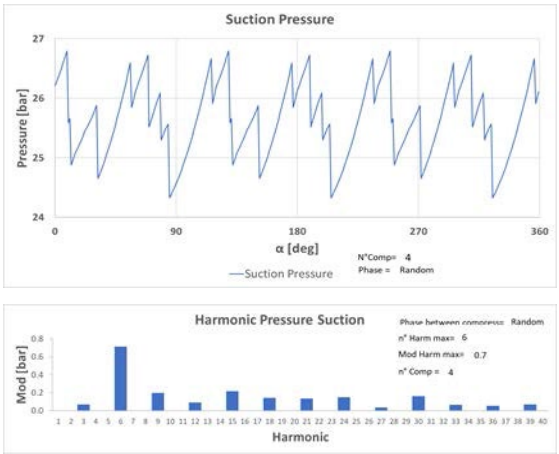

Figure 11: a Theoretical sum of pressure pulsations 4 fully loaded 6HG/2 - random phase (Cornegliano)

Figure 11 shows the sum of pressure pulsations and its harmonic spectrum for 4 full loaded 6HG/2 compressors with a random start. Comparing the results of figure 11 with figure 10, the peak to peak pressure is lower (2.5 bar VS 5 bar). Figure 11 also

by: M. Passeri, L. Guerrini – Baker Hughes GE; C. Rossi, M. Mazzoli – SAIPEM; G. Ferrari – NIDEC; S. Melis – Florence University

evidenced how the harmonic spectrum changes.
Analyzing several cases with various loads, the worst possible theoretical sum of pressure pulsations was discovered (see figure 12 that shows a Peak to Peak of 8,6 bar). This is relevant to 4 compressors working with the crankshaft in phase (0°) at 83% of the load. Also, in this case, the pulsation spectrum is different (note that 1st harmonic main component is detected). To be noted that this worst case is the same case previously detected by the full study (inclusive of the plant) which evidenced the quite high pulsation induced forces on the 32" common piping. This confirms that the simplified approach phase selection can be used.

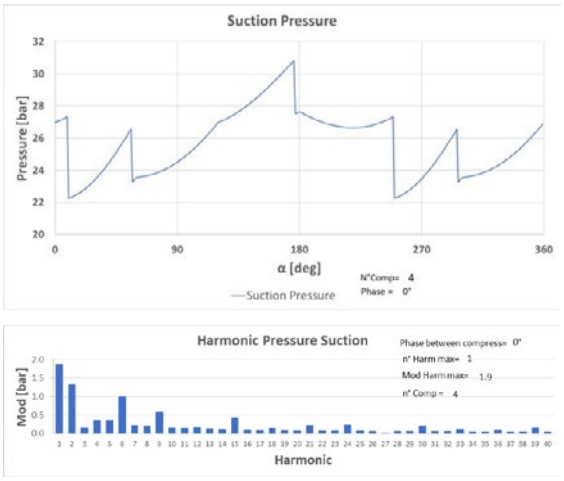

Figure 12: Worst theoretical sum of pressure pulsations for 4 6HG/2 at 83% of the load at 0° phase

All the above theoretical examples of phase among the compressors operating in parallel clearly indicated that the sum of pulsations changes at each startup and capacity control. Using traditional approach of the worst-case sum in this complex application may lead to conservative recommendations on supports and structure requirements. At the same time using a more relaxed approach (e.g. considering only the forces due to a single compressor), the uncertainty due to the random start-up phase may lead to underestimating the real pulsation induced forces. This may lead to underestimating the relevant piping supports requirements resulting in excessive piping vibrations. So, the worst-case pulsation sum remains the only way to properly protect plant operations.
At the same time, the above theoretic examples indicated that adopting a specific phase the pulsation sum may be strongly reduced.
Then another important refined acoustic solution was introduced. This was achieved by an investigation of the best phasing among the compressor shafts to efficiently control the sum of pressure pulsations, considering all possible combination cases of operation, and then finding a way to impose compressors crankshaft phase, eliminating the described random start-up uncertainty.

4.2 Research of best phase among compressors

To find the best phase, the theoretical exercise was repeated with various compressors phase shifting, considering that the case to be optimized is with 4 compressors. In this parallel case, the simplified analysis leads to choosing 90° (see figure 13, with 4 compressors running at 83% of load) as the better phase between the crankshafts of the compressors for all the operating cases.

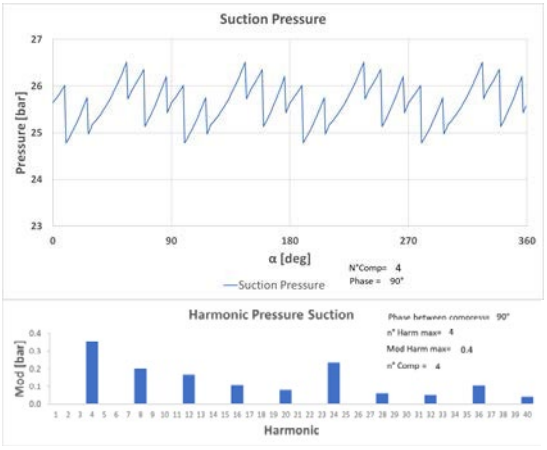

Figure 13: Optimized theoretical sum of pressure pulsations for 4 6HG/2 at 83% of the load at 90° phase

Comparing this with the previous one in the same case (see figure 12) it can be noted that the reduction of the sum of pressure pulsations is significant (1.7 bar peak-to-peak vs 8,6 bar). Significant reductions are obtained also for the case at full load and other capacity control (i.e. 66% and 50%).
The analysis also continues investigating all the other cases with a reduced number of compressors and partial load conditions. This simplified analysis indicated that the 90° phase is the best solution also for the condition with three active compressors.

Theoretically, one could think that the best phasing with three compressors crankshafts is 120°, but considering the total number of cylinders present, the phase between them and the number of active effects, this phase results equal to the condition with 0° phase already identified as worst-case. It should be noted that from the various simulations performed it results that for some specific case the optimal phase was 45°, but under the others cases the 45° phase is worse than 90°. The exercise was repeated for two compressors running and also in this case the best phase was with a 90° phase.
The conclusion of the theoretical exercise, done for all the plant parts, is that the resulting best phase was 90°. Then the full pulsation study restarted, including the full plant piping and equipment using the 90° phase selected by the theoretical exercise.

by: M. Passeri, L. Guerrini – Baker Hughes GE; C. Rossi, M. Mazzoli – SAIPEM; G. Ferrari – NIDEC; S. Melis – Florence University

The studies were performed for the whole plant, all compressor combinations, all the operating conditions and capacity controls (i.e. for each section of plant hundreds of runs have been done again). The study confirmed that the minimum sum of pressure pulsations is achieved using a 90° phase among the crankshaft of the compressors. As an example for the suction plant, in figure 14 (worst case to be considered in case of random start-up) and figure 15 (selected phase with controlled phase) are shown the calculated residual pressure pulsations. In these picture color from orange to red indicated higher pressure pulsations while color from green to blue indicated lower pressure pulsations. Comparing the clouded area of figure 14 with the same clouded area of figure 15 the resulting reduction pressure pulsations in the common piping plant (clouded area) is evident.

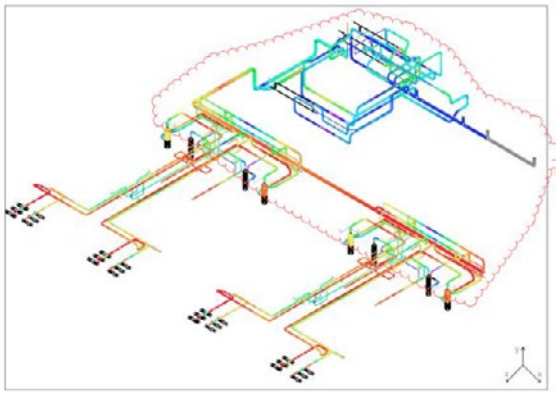

Figure 14: Suction plant pressure pulsations results 4 compressors running - RC motors in phase

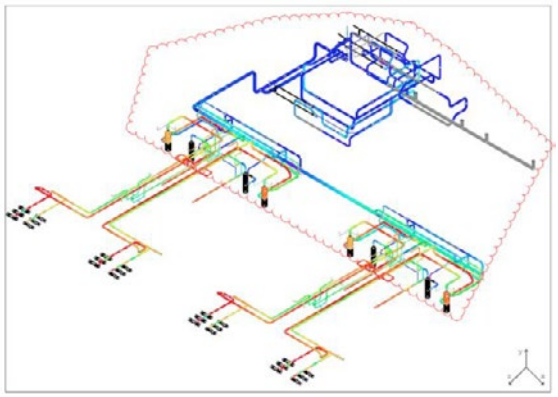

Figure 15: Suction plant pressure pulsations results 4 compressors running - RC motors start every 90°

In figure 16 a summary of the full plant pulsation induced forces calculated for Suction plant is shown, considering the worst-case scenario (red = 0° phase worst case for random start-up) and the best phase scenario (green = 90° phase), detected by the several studies above described. Adopting the 90 ° phase the resulting pulsation induced forces initially calculated with 0° is reduced by approximately 3 times (from approx. 30000 N to 1000 N zero to peak). In the same figure, it can be noted that the main effect is detected in the 32” common piping upstream the compressors (location in which the sum of pressure pulsation takes place).

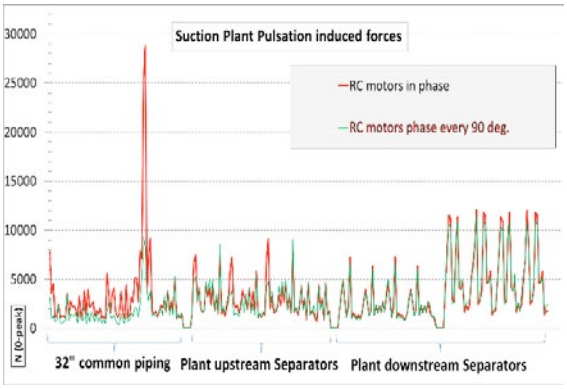

Figure 16: Suction plant pulsation induced forces comparison (Cornegliano)

In figure 17 the same summary of the pulsation induced forces calculated for full plant acoustic study of Discharge plant with 4 compressors is shown.

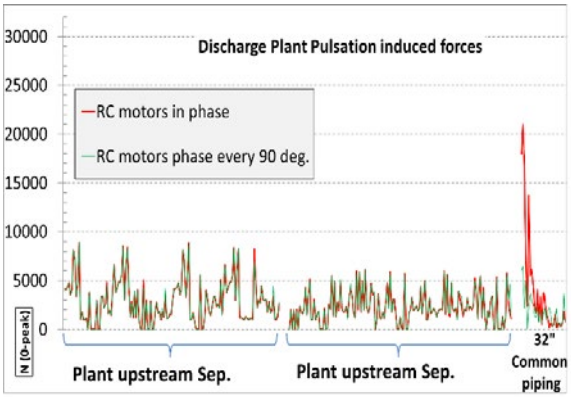

Figure 17: Discharge pulsation induced forces comparison (Cornegliano)

For Suction and Discharge plants, the selected best phase allows for pulsation induced forces reduction in the 32” common piping (i.e. upstream/downstream the separators). In the plant sections between the compressors and the separators, thanks to the separators damping action and the smaller pipe size, the forces were already of acceptable amplitude (i.e. values that can be normally found with a single compressor running) and the effect of the change in phase was limited (i.e. several values were superimposed). It should be noted that if the volume of the separators had been lower, the beneficial effect would have been extended to the whole system. On the contrary, if the volume of the separators had been higher, the beneficial effect would have been nullified. The above is to clarify that, considering that the selection of separator volume only depends from process needs, separator volume increase (to dampen the sum of pulsations) is usually impractical for cost and procurement reasons.

To summarize, using the 90° selected phase between

by: M. Passeri, L. Guerrini – Baker Hughes GE; C. Rossi, M. Mazzoli – SAIPEM; G. Ferrari – NIDEC; S. Melis – Florence University

the crankshaft of the compressors the relatively high pulsation induced forces in the 32" common piping can be reduced. Then it was time to think about how to physically obtain the selected fix phase.

4.3 Qualitative description of the driving motors' synchronization

In a complex system like Cornegliano, a very refined solution was necessary to guarantee a precise and well-defined compressors start-up phase. The mechanism that allows for setting the right phase at startup was made in cooperation with Saipem and Nidec. The project electrical configuration of the main compressor system considers 4 main synchronous motors (15 MW each). To accelerate the motor from 0 to nominal speed, due to the size of the system, the installation of a dedicated starting device was initially provided for. Considering that the motors are synchronous, the presence of the starting device was further evaluated to verify the possibility of synchronizing all running motors not only with the external grid but also with each other with a specified shift. In this way, it is expected that the pressure variation in the common piping could be reduced due to different phase shifting of all compressor crankshafts. The project motors run at 375 rpm being the grid frequency of 50 Hz and having the motors 16 poles. The proposed logic for the phase control considers starting the first motor without any special sequence and starting the next motors synchronizing on the same pole as the already running motors. To know the exact relative position of each shaft, an additional inducting sensor on each motor shaft has been considered. Since there are 16 holes in the motor and compressor shaft flange extensions there is a possibility to choose among them with a possible shift of 22.5°. Finally, the compressor crankshafts have been coupled with motor shafts with specific mechanical shifts (0° for the 1st system, 90° for 2nd one, 180°for 3rd one and 270° for 4th one) based on full plant pulsation study results. The initial evaluation has been confirmed and the logic has been implemented. The plant is under finalization and will be started-up at the end of 2018 (see figure 18).

Figure 18: Plant under construction view

As an additional feature, the same logic allows returning to the standard random start-up for system fine-tuning during plant commissioning.

4.4 Piping Vibrations and Cyclic stress

To complete the design, the reduced pressure pulsations induced forces calculated are introduced automatically as input forces for the plant's final mechanical study. This study is performed by a FEM-program that provides the mechanical natural frequencies, total vibration amplitudes, and relevant stresses, along with the reactions at supports location. Then, the overall forced response of the piping system is calculated using the "modal super-imposition" technique as the sum of the response of each mode to the exciting harmonics, each with its module and phase [5,6].

Finally, the piping maximum alternate stress is calculated using the procedure explained in ASME VIII-2 appendix 5 [2].

The calculated vibrations and cyclic stress are compared with the limits and, if necessary, a combination of additional structural stiffness or additional supporting restraints are recommended to maintain them within the limit.

As example, the max maximum calculated vibration levels in the 32" common Suction piping (see figure 19), after the insertion of the modifications recommended by the study (see figure 20), are at 90% of the allowable level. The relevant max calculated cyclic stress level is 2 N/mm^2 peak-to-peak (allowable 40 N/mm^2 peak-to-peak).

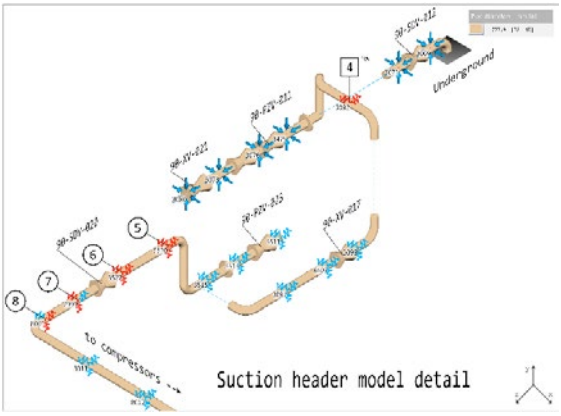

Figure 19: Suction plant, 32" common piping section (one with the max pulsation induced forces)

MODIFIED SUPPORTS												
			BHGE PROPOSED MODIFICATION									
Modification No.	Node BHGE	Supports type	Original Stiffness [kN/mm]			Modified Stiffness [kN/mm]			FORCES TO BE RESTRAINED N (0-PEAK)			Note
			Kx [kN/mm]	Ky [kN/mm]	Kz [kN/mm]	Kx [kN/mm]	Ky [kN/mm]	Kz [kN/mm]	Fx [N]	Fy [N]	Fz [N]	
4	3092					195.00		195.00	5257		1010	NEW
5	3520	SPS-S-1601BA	9.94	5.51	2.02	25.00	30.00	68.00	340	1978	16296	
6	3522	SPS-G-6001E SPS-F-5004A	11.35	34.92	1.03	30.00	34.92	68.00	300	300	16044	
7	7999	SPS-G-6001E	9.36	98.18	1.02	30.00	98.18	68.00	337	2643	15426	
8	8001	SPS-G-6001F	53.05	13.63	22.18	53.05	50.00	68.00	3524	3810	16148	

Figure 20: Suction plant - 32" common piping section - supports recommendations details

by: M. Passeri, L. Guerrini – Baker Hughes GE; C. Rossi, M. Mazzoli – SAIPEM; G. Ferrari – NIDEC; S. Melis – Florence University

The solution found in term of piping restrains and structure stiffness (see figure 20) is also verified for the worst-case phase scenario (random start-up) to be sure that in any case the vibrations, in the common piping, even if higher than the limit, will be significantly below the danger limit and the cyclic stress remain within the limits. The same exercise is performed for the compression system. The relevant model is updated considering compressor and dampers manufacturing drawings and inserting directly connected piping (up to the second support upstream and downstream of the dampeners). Then the forced Mechanical response analysis of the Compressor Mechanical Model [7,8] is repeated using as input the pulsation induced forces resulting from the acoustic study, cylinder gas loads and foundations dynamical loads. The resulting vibration amplitude is compared with the manufacturer vibration limit levels for the cylinder-frame-spacer block. For the dampers and piping, the relevant limits are based on experience and field measurements. The cyclic stress is compared with the limits (API618 cyclic stress limit 180 N/mm2) [1], reduced to consider the stress concentration factors and safety factor. When a preliminary cylinder manifold response is performed, as described at the beginning prior to the compression system manufacturing, this final verification (see figure 21) can only identify minor adjustments to piping support constraints and/or their structures stiffness.

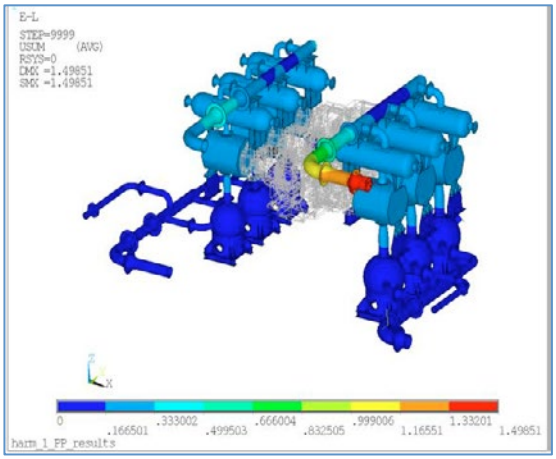

Figure 21: Cylinder Manifold forced response

5 Conclusions

In a complex storage application plant, such as Cornegliano Laudense, the standard acoustical solutions (dampers + FHO) are not sufficient to comply with API 618 pressure drop requirements and to obtain acceptable pressure pulsation induced forces. After several investigations, including a double set of orifices to maintain the pressure drop within reasonable values a refined solution with DVO has been identified. This solution allows for compliance with pressure drop requirements for certified operating conditions. This solution involves an initial investment to buy the necessary valves, but further to give more flexibility to the plant and better compressor performance, it allows for saving energy during operations and recovering the cost in less than 2 years.

Furthermore, considering that the 4 compressors operate in parallel in all the possible combinations in various operating conditions and capacity control, the worst-case sum of pressure pulsation calculated in the 32" common piping, lead to a quite high pulsation induced forces in case of uncontrolled random compressor start-up. For this reason, another refined study acoustic solution was investigated to find, considering the hundreds of possible operating cases, the best phasing between the compressor shafts to efficiently control the pressure pulsation sum and relevant forces. To minimize studies software runtime, the best phase is initially selected by a purely theoretical approach. The effectiveness of the simplified approach selection is then verified by the full plant acoustical study. Results confirm that the pressure pulsations and relevant pulsation induced forces in the common piping can be significantly reduced. Finally, the selected phase is achieved by a system solution that requires a precise start coupling of each compressor electric motor.

In conclusion, the insertion of the DVO coupled with the possibility to select by acoustic study the best start-up phase among compressors allows for energy saving and for obtaining the lowest possible pulsation induced forces on the system. Lower pulsation induced forces to allow the minimization of mechanical piping vibrations/cyclic stress requirements. The plant pulsations and vibrations behavior will be monitored during start-up. With special care to verify the effectiveness of described refined solutions.

Finally, it can be observed that the refined acoustical solutions here described, may also be used in other applications with a wide range of operating conditions or parallel compressor operations, in which the balance between the requirements, the energy consumption, the cost of introduction of the mechanical/electrical devices is positive. The subject matter of the present article is currently under patenting procedure.

6 Acknowledgments

The authors wish to thank BHGE Nuovo Pignone, Saipem, Nidec and IGS for permission to publish the information reported in this paper.

7 Nomenclature

FEM = Finite Element Model
DVO= Dynamic Variable Orifice - (adaptive valve)
FHO = Fix Hole Orifices
OP = Operating pressure
TEG= Tri-Ethylene Glycol

References

[1] API 618 STD 5th ed., December 2007, "Reciprocating Compressor for Petroleum, Chemical and Gas Industry services" American Petroleum Institute.

[2] ASME - Boiler and Pressure Vessel Code, sect. VIII Div. 2 2015, The American Society of Mechanical Engineers

[3] Giacomelli E., Passeri M., Giusti S., Zagli F., Generosi S., 2004, "Modeling of Pressure Pulsations for Reciprocating Compressors and Interaction with Mechanical System", ESDA, Engineering System Design and Analysis, 19-22 July, Manchester, UK, The American Society of Mechanical Engineers.

[4] Giacomelli E., Passeri P. Battagli, M., Euzzor, "Pressure vessels design for reciprocating compressors applied in refinery and petrochemical plants", PVP2005 Pressure Vessel and Piping July 17-21, 2004, Denver, Colorado, USA

[5] Passeri M., Romiti. M., Generosi S., "Dynamic analysis of large intercooler and tubular reactors installed in LDPE plant with a hyper compressor". 5th Conference of the EFRC March 21st / 23th, 2007, Prague

[6] Passeri M., Generosi S., Bagagli R., Carmelo M.: Preliminary piping sizing and pressure pulsation evaluation, Proceedings of ASME PVP 2014 Pressure Vessels & Piping Conference PVP 2014 July 20-24, 2014, Anaheim, California, USA.

[7] Passeri M., Bagagli R., "Cylinder Manifold automation". 10th European forum for Reciprocating Compressors 2016, Düsseldorf - Germany

[8] A. Eijk: Economic benefits of CAD models for compressor manifold vibration analysis according to API 618, 3rd EFRC Conference 27-28 March 2003, Vienna

[9] A. Eijk, J.P.M. Smeulers, A.J. Smalley, L.E. Blodgett: Improvements and extensions to API618 related to Pulsation and mechanical Response Studies, The Recip – state of the art Compressor 4.-5. November 1999, Dresden- Germany

[10] Tetenborg P., Brummer A. "Development of a new adaptive pulsation damping device without external energy supply". 10th European forum for Reciprocating Compressors 2016, Düsseldorf - Germany

[11] Norm shade, Tyler Clark. Jared W. Adair. Evaluation of a dynamic variable orifice for reciprocating compressor control, Gas Machinery Research Council Nashville, Tennessee October 5-8-, 2014.

Mitigation and resolution of piping vibrations of a critical hydrogen make-up reciprocating compressor

by:

Smail Haddadi
TOTAL Refining & Chemicals
Harfleur, France
smail.haddadi@total.com

Jozef Van De Peer
TOTAL Refining & Chemicals
Antwerp, Belgium
jozef.van-de-peer@total.com

André Eijk
TNO, Delft, NL
andre.eijk@tno.nl

11th EFRC CONFERENCE
September 13 – 14, 2018, Madrid

Abstract:
The control of pulsations and vibrations requires rigorous attention from the beginning of the plant design to compressor start-up and operation. A close cooperation between Engineering Contractor, Compressor Manufacturer, Pulsation Study Provider and Operator, is necessary at the different steps of a project.
Pulsation and mechanical response studies performed during engineering in accordance with the API standard 618 are necessary to target pulsations, vibrations and stress levels within acceptable limits. The pulsation and vibration study include different system configurations to cover the planned operation of a new hydrogen make-up compressor in parallel of 3 existing reciprocating compressors.
This paper presents the approach applied during engineering, construction and start-up phase and provides some examples of resolution of piping and instruments vibrations during start-up.
To achieve piping vibrations within an acceptable range, a site check of the piping supports and Small Bore Connections/instrumentation hook-up is recommended to ensure correct match of pulsation and vibration study recommendations and actual plant design. Piping vibration measurement plan was defined before start-up and vibrations are recorded at the first start-up at critical points.
The compressor is released to Operations after a complete survey of compressor and piping vibrations.

by: Smail Haddadi, Jozef Van De Peer – TOTAL; André Eijk – TNO

1 Introduction

1.1. Plant location

TOTAL Antwerp integrated platform is located in the industrial area of Antwerp (see figure 1).

Figure 1: Location of TOTAL Antwerp platform

The platform includes the largest refinery of TOTAL in Europe with a capacity of 338 kilo barrels per day.

In the frame of the OPTARA project, one of the two trains of the existing atmospheric residue desulphurisation unit (ARDS) is modified in a mild hydrocracking unit (MHC) to convert heavy fuel to diesel and ultra-low sulphur heating oil.

Figure 2: Overview TOTAL Antwerp Platform with its refining and petrochemicals units

To fulfil the hydrogen supply to the upgraded ARDS unit and to the MHC unit, a new hydrogen make-up compressor J8151D is included in the project.

1.2. Hydrogen compression set-up

The hydrogen compression unit set-up is shown in figure 3. Three machines are required to fulfil the demand of both process units. The fourth machine will act as a spare. The running and spare compressors will sequentially alternate their duty.

J8151A/B/C are existing compressors, 3 stages with 4 cylinders with an installed power of 5650 kW and a fixed speed of 333 rpm.

The new hydrogen make-up compressor J8151D is a 3 stage, 3 cylinders compressor that boosts the hydrogen pressure from 25 barg to 200 barg.

This compressor is driven by a 6800 kW electric motor and has a fixed speed of 370 rpm.

The duty (flow) of the new machine is comparable with the existing machines.

The three existing compressors have stepped suction valve unloaders (50%, 75% 100%) while the new machine is fitted with step less flow reverse control system from 100%-30%.

The spill back loop is common to the four compressors and is designed for 100% flow of one compressor.

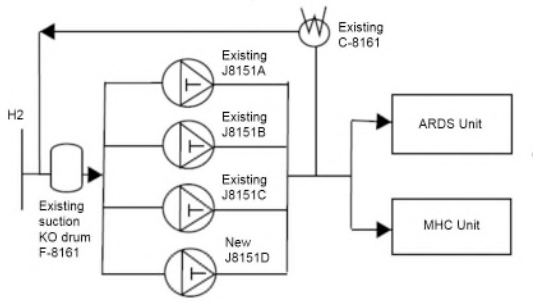

Figure 3: Simplified scheme of ARDS/MHC hydrogen compression

A 3D view (figure 4) shows the layout of the new compressor package.

Figure 4: Layout of the new compressor

2. Engineering phase

2.1. FEED phase

Pulsation and vibration control starts at the FEED phase.

Technical requirements are included in a general specification relevant to reciprocating compressors. This general specification, to be prepared by the End User or the Engineering Contractor, refers to the 5th edition of the API 618[1] "Reciprocating Compressors for Petroleum, Chemical, and Gas Industry Services" and includes clarifications, modifications and additions to the API 618[1].

Furthermore, small bore piping design, piping supports standards and hook-up standards are issued at this stage either by the End User or by the Engineering Contractor.

by: Smail Haddadi, Jozef Van De Peer – TOTAL; André Eijk – TNO

The API Recommended Practice 688[2] "Pulsation and Vibration Control in Positive Displacement Machinery Systems for Petroleum, Petrochemical, and Natural Gas Industry Services" gives valuable guidelines for all involved parties.

An example of small bore piping bracing guideline, as applied for the OPTARA project is given in figure 5.

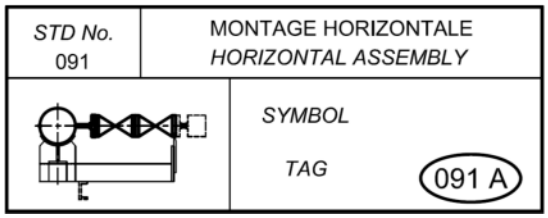

Figure 5: Principle of bracing of small bore piping (double block valves for pressure measurement)

Acceptance criteria for field vibrations measurements should be defined at this stage.

2.2. Detail engineering phase

In accordance with table 6 of the API 618[1], design approach 3 is required for the new hydrogen make-up compressor J8151D.

The End User defines all the predicted operating conditions and the planned parallel operating cases. 15 cases were taken into account for OPTARA compression unit (see table 1).

Case	Gas composition	MW	Compressors			
			J8151A	J8151B	J8151C	J8151D
		(kg/kmol)	load	load	load	Load
1	Hydrogen	2.04	100%	100%	Off	100%
2	Hydrogen	2.04	100%	100%	Off	30%
3	Hydrogen	2.04	50%	50%	Off	30%
4	Hydrogen	2.04	Off	100%	100%	100%
5	Hydrogen	2.04	75%	75%	Off	100%
6	Hydrogen	2.04	100%	Off	100%	72%
7	Nitrogen	28.02	Off	Off	100%	100%
8	Hydrogen	2.04	Off	Off	Off	100%
9	Hydrogen	2.04	Off	Off	Off	66%
10	Hydrogen	2.04	Off	Off	Off	72%
11	Hydrogen	2.04	Off	Off	Off	58%
12	Hydrogen	2.04	Off	Off	Off	44%
13	Hydrogen	2.04	Off	Off	Off	30%
14	Hydrogen	2.04	Blocked	Blocked	Blocked	100%
15	Hydrogen	2.04	blocked	blocked	Blocked	30%

Table 1: Cases included in the acoustic study

Figure M3 of API 618[1] defines the main steps of the studies.

Before the selection of the Compressor Manufacturer, the schedule of the different studies is to be defined to keep a broader range of solutions at the different main steps:

- Pre-study or pulsation dampers check.
- Compressor valves dynamic response analysis.
- Mechanical compressor manifold system analysis (mode shapes, vibration and dynamic stress analysis).
- Pulsation analysis.
- Mechanical response analysis.

During the kick-off meeting, Engineering Contractor, Compressor Manufacturer and End User shall review and confirm the schedule and deliverables of the pulsation and vibration study (input data from Engineering Contractor / End User; reports contents from Compressor Manufacturer / Study Provider).

It is important that the results of the pre-study of the dampers design are shared between Compressor Manufacturer, Pulsation Study Provider, Engineering Contractor and End User at the early stage of the detail engineering to allow an optimisation of the dampers size. Margins, in e.g. the speed of sound should be agreed between the parties to cover the molecular weight variations from specified conditions to ensure that the pulsation and vibrations are also acceptable at these conditions

The existing compressors dampers sizes were also checked and found adequate at the pre-study stage.

The main risks of lack of cooperation between the parties are related to the schedule and reliability:

- Equipment delivery delay in case of late modification of dampers due to under-sizing.
- Equipment start-up delay due to field corrective measures to solve unacceptable vibrations.
- Fatigue failure due to too high cyclic stress levels caused by pulsation-induced shaking forces.

The acoustic simulation shall be initiated as soon as the pertinent input data are available (P&ID arrangement drawings, isometrics, construction drawings of related equipment (vessels, dampers, separators, coolers, etc.), and cylinder gas passages details.

It is beneficial for all the parties that the results of the simulation are shared, and modifications reviewed before a formal issue of the acoustic study report.

A late acoustic study will reduce the possible modification options or will increase the project cost considerably due to rework in the design process

The new compressor J8151D and the existing compressors J8151 A/B/C were included in the study (see Figure 6 for the overall set-up).

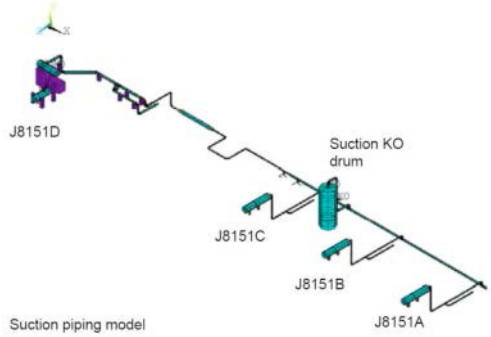

Figure 6: Overview of suction piping model of the 4 compressors

by: Smail Haddadi, Jozef Van De Peer – TOTAL; André Eijk – TNO

Several recommendations were defined to reduce pulsations within acceptable limits. A few piping modifications were required as shown in figure 7. An acoustic separation between the new and existing compressors was necessary to achieve acceptable pulsations in case of parallel operation of the new and existing compressors. This was achieved by increasing the diameter of the main header locally from 6" to 18".

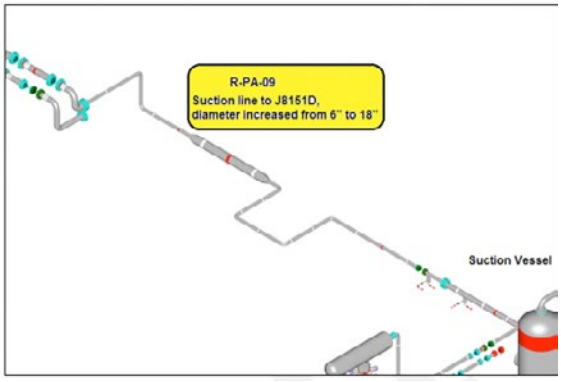

Figure 7: 1st stage suction piping size increase from 6 to 18" to reduce pulsations

Additional modifications were recommended after the completion of mechanical response analysis.

Figure 8 illustrates the mode shape at 15.8 Hz for the location of too high calculated vibration level at the third stage suction elbow. The maximum calculated level was 150 mm/s peak-to-peak (53.4 mm/s rms) and occurs in the crankshaft (X) direction.

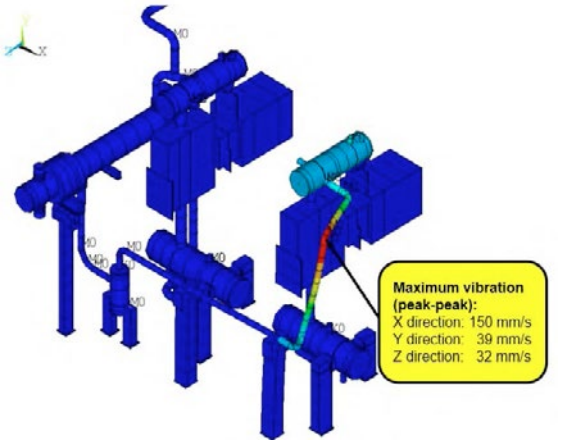

Figure 8: Mode shape at 15.8 Hz

The piping layout is modified as per figure 9, resulting in acceptable vibration levels.

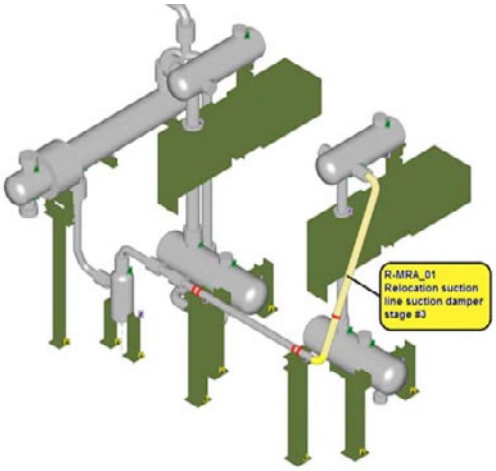

Figure 9: 3rd stage suction piping lay-out modification

Maximum dynamic loads applied at the supports or foundations are included in the mechanical study report. It is recommend to verify, if the fixation of the piping to the mechanical structure and the stiffness of the supporting structures is adequate to restrain the loads.

3. Construction phase

3.1 Site survey

When the construction of the piping around the compressor was close to 90% completion, a site survey was carried out.
The survey was focused on the following aspects:

1. Verification if the pulsation and vibration simulation models (pipe routing, pipe supports, Small Bore Connections, etc.) with assumed boundary conditions were consistent with the as-built piping layout.
2. Verification if the recommendations from the pulsation study (e.g. orifice plates) have been correctly implemented.
3. Verification if the recommendations from the mechanical response study (e.g. additional/changed pipe supports, etc.) have been correctly implemented.
4. General "mechanical" inspection of the compressor and piping system: pipe supports, supporting structures, bracing of Small Bore Connections (SBC's) , etc.

The main outcomes of the survey are:

- Identification of differences between the as-built piping lay-out and the simulation model lay-out.
- Assessment of Small Bore Connections regarding the risk of fatigue failure.
- Practical recommendations for improving the function of the piping supports (e.g. removing gaps between the pipe and pipe supports, etc.).
- Definition of the location of vibration measurement points.

by: Smail Haddadi, Jozef Van De Peer – TOTAL; André Eijk – TNO

For the identified discrepancies between model and as-built situation, the mechanical response of the modified parts was redone .

A challenging task in the mechanical response analysis is to find suitable (stiff) boundary conditions. One of the discrepancies which was found during the field inspection was a support in the suction 1st stage piping. It was shown that this support was mounted on a very slender concrete column which was not known during the mechanical response analysis, see Figure 10.

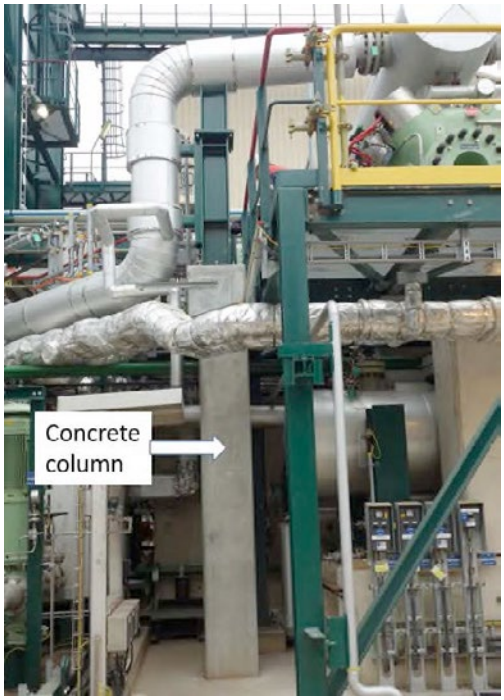

Figure 10 Concrete column

The vibration analysis was redone, and the flexible concrete column was included. Figure 11 shows the mode shape at 24.4 Hz and it is clear that the concrete column on which the pipe support is mounted does not behave like a stiff boundary condition for this frequency.

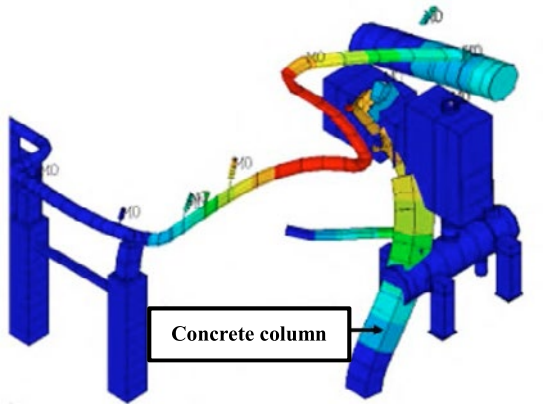

Figure 11: Mode shape at 24.4 Hz of the 1st stage suction piping

Before changing this construction, it was decided to measure the vibrations.

Further on, the results of the review is that vibration and fatigue problems are not expected to occur for other parts of the system caused by pulsation-induced shaking forces.

3.2 Plan for vibration measurements

As a part of the field survey, a plan of compressor and piping vibrations was set-up in preparation of the start-up of the unit. The EFRC guideline[3] is used for the location of points of measurements and for the acceptance criteria. Small Bore Connections (SBC's) vibration measurements are included in the plan. There are in total 90 points of measurements in three axis and for 3 different loads (100%, 70% and 40%).

The vibration velocity levels (in mm/s rms) are normally compared with the levels according to evaluation zone boundary B/C of the 4th edition of the EFRC guidelines[3]. However, TOTAL has used the stricter levels of the A/B zone for this system.

The EFRC guidance levels for vibrations of the compressor parts and the pipe system are shown in Table 2.

Compressor system part	rms. vibration velocity values for horizontal compressors [mm/s]			rms. vibration velocity values for vertical compressors [mm/s]		
	Evaluation zone boundary			Evaluation zone boundary		
	A/B	B/C	C/D	A/B	B/C	C/D
Foundation	2,0	3,0	4,5	2,0	3,0	4,5
Frame (top)	5,3	8,0	12,0	5,3	8,0	12,0
Cylinder (lateral)	8,7	13,0	19,5	10,7	16,0	24,0
Cylinder (rod)	10,7	16,0	24,0	8,7	13,0	19,5
Dampers	12,7	19,0	28,5	12,7	19,0	28,5
Piping	12,7	19,0	28,5	12,7	19,0	28,5

Table 2: EFRC guidance levels for vibrations for compressor parts and pipe system

For SBC's the difference between the highest and lowest vibration velocity level, including the correct phase differences, determines the maximum cyclic stress levels. The guidance values for acceptable overall vibrations are for that reason based on the difference in vibration levels of the main piping and the SBC.

Guidance vibration levels for SBC's based on the difference in vibration levels have been included in the 4th edition of the EFRC Guideline[3]. A summary of the difference in guidance vibration levels are shown in Table 3.

Compressor system part	rms. vibration velocity values [mm/s]		
	Evaluation zone boundary		
	A/B	B/C	C/D
Small bore connection piping	12,7	19,0	28,5

Table 3 : EFRC guidance levels (difference) for Small Bore Connections

A site review at the end of construction phase is a crucial step that can catch any changes that might

by: Smail Haddadi, Jozef Van De Peer – TOTAL; André Eijk – TNO

affect the system dynamic response (vibration and cyclic stress levels) that were not communicated earlier to the Compressor Manufacturer / Study Provider.

4. Start-up phase

4.1 Vibration measurements

At the first start-up, the vibrations levels were measured.

The positive points at the first start-up are:

- Low vibration levels at compressor foundation and compressor frame (see table 4 and figure 12 for measurements locations).
- Low vibration levels at the compressor platform. There was no interaction between platform structure and piping supports except for the 1st and 2nd stages relief valve lines.

Pos	Description	40% load			70% load		
		A	H	V	A	H	V
1	Top frame	3	2	2	3	2	2
2	Bottom frame	3	1	1	2	1	1
3	Foundation	2	1	1	2	<1	1
4	Top frame	3	3	2	3	2	2
5	Bottom frame	2	1	1	2	1	1
6	Foundation	2	1	1	2	<1	1
7	Top frame	3	2	2	3	2	2
8	Bottom frame	3	1	1	2	1	1
9	Foundation	2	1	1	1	1	1
10	Top frame	3	2	2	2	2	2
11	Bottom frame	3	1	1	2	1	1
12	Foundation	2	1	1	1	1	1
13	Top frame	3	2	2	3	2	2
14	Bottom frame	3	2	1	2	1	1
15	Foundation	1	1	<1	1	<1	1
16	Top frame	4	4	2	3	2	2
17	Bottom frame	3	1	1	3	1	1
18	Foundation	2	1	1	2	<1	1

Table 4: Frame and compressor foundation vibration levels (mm/s rms)

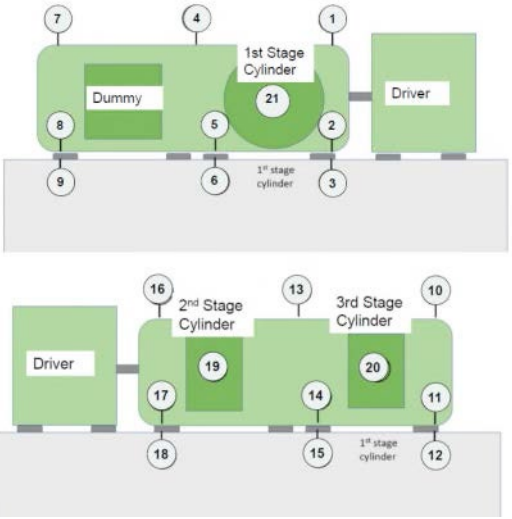

Figure 12: Vibrations measurement locations at compressor frame and foundation

Few points were in excess of A/B and even C/D boundary zone of the EFRC guidelines[3].

Especially the suction 1st stage piping of which a discrepancy between the model and field application was found as described in section 3.1, showed an unacceptable vibration level. The maximum measured vibration level was 32 mm/s rms in the piston rod direction and at 40% load.

Compressor Manufacturer, Engineering Contractor, TNO and TOTAL worked together in a win-win spirit to perform additional modifications to reduce vibrations where necessary.

4.2 Experience based modifications

In a mechanical response analysis, all possible worst-case conditions are investigated to ensure that the system can run safe and reliable for the long-term operation.

From the site survey it was concluded that the boundary condition of the support of the 1st stage suction piping was not stiff enough as assumed in the mechanical response analysis, see section 3.1. It was decided to measure at first the maximum vibration levels before modifying the construction. From the vibration measurements it was indeed shown that a worst-case situation occurred, and unacceptable vibration levels were measured on the 1st stage suction piping. This caused by the fact that the mode shape as shown in Figure 11 at 24.4 Hz was excited.

The final solution to reduce the vibration levels was however easy and could be achieved by an additional beam between the stiff concrete foundation block on which the compressor is mounted and the top of the flexible concrete column. Figure 13 shows the field implementation.

Measurements showed acceptable vibration levels after installation of the additional beam.

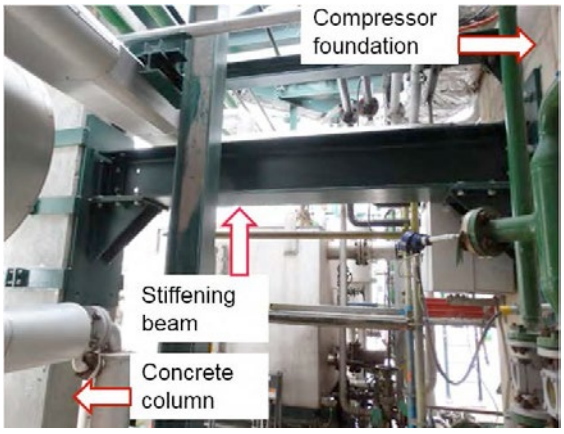

Figure 13: Stiffened concrete column

by: Smail Haddadi, Jozef Van De Peer – TOTAL; André Eijk – TNO

5. Conclusions and recommendations

The OPTARA project illustrates the importance of effective communication and cooperation between all the involved parties in the acoustic and mechanical response studies. This is the key for a successful control of vibrations of compressor and piping systems. This cooperation is necessary during the different phases of the project from FEED phase to unit start-up and hand over to Operations:

- Main milestones are to be agreed between the parties at the early stage of a project.
- A pre-study is necessary at the beginning of detail engineering to validate the dampers size.
- Mechanical system manifold response study and acoustic study shall be launched as soon as the necessary input data are available and results / modifications are to be shared, discussed and agreed upon between the involved parties prior to the issue of the study report.
- Iterations between piping thermal design performed by the engineering Contractor and mechanical response analysis done by the compressor Manufacturer or the Study Provider are generally necessary to control vibrations and stress levels, static pipe stresses and nozzle loads.
- Flexible structures on which pipe supports or other equipment is mounted, shall be included in the simulation models
- Supporting and bracing of Small Bore Connections of piping and vessels (pulsation dampers, separators) shall be investigated thoroughly during the detailed design.
- A site survey, involving the Study Provider, at the end of the construction phase gives the opportunity to verify adherence to study recommendations and to mitigate risk of vibrations or fatigue failure.
- Vibrations assessment of compressor and piping systems is to be performed at the first start-up of the unit at different loads and configurations.
- In case of vibrations above acceptance criteria, inputs, form Engineering Contractor, Compressor Manufacturer and Study Provider can be necessary for the definition of corrective actions or additional studies.

The new compressor J8151D is successfully handed over to Operations in May 2017 with vibration levels well within acceptable levels.

References

[1] API 618, 5th edition “Reciprocating Compressors for Petroleum, Chemical, and Gas Industry Services”.

[2] API RP 688, 1st edition “Pulsation and Vibration Control in Positive Displacement Machinery Systems for Petroleum, Petrochemical, and Natural Gas Industry Services”.

[3] EFRC Guidelines for vibrations in Reciprocating Compressor Systems, 4th edition.

Effects of pipe strain on vibration in reciprocating compressor systems

by:

Ramin Rahnama, MSc, PEng
Principal Engineer
Wood
Glasgow, United Kingdom
ramin.rahnama@woodplc.com

Kelly Eberle, BSc, PEng
Principal Consultant
Wood
Calgary, Canada
kelly.eberle@woodplc.com

Steven Crocker, CET
Senior Analyst
Wood
Houston, United States
steven.crocker@woodplc.com

11th EFRC CONFERENCE
September 13 – 14, 2018, Madrid

Abstract:
Pipe strain and flange misalignment have been shown to lead to higher than normal vibrations in piping systems. This problem seems to be more problematic on reciprocating compressor packages due to the high energy present in these systems, tight spaces between different components (for example suction bottle and scrubber) and piping assembly and installation practices. This paper presents insights into the effects of pipe strain, measures to reduce pipe strain and case studies that show the effect of pipe strain and flange misalignment on piping vibration.

by: Ramin Rahnama, Kelly Eberle, Steven Crocker – WOOD

2. Introduction

Many vibration problems are the result of, or amplified by, pipe strain or flange misalignment. In some cases, the measured vibration amplitudes are double, triple or even higher when under pipe strain, compared to after relieving pipe strain. Pipe strain on the main line can intensify vibrations on small-bore attachments, which can lead to failures.

Although the effect of pipe strain on piping vibration is observed on many packages, particularly with units that are assembled on tight schedules or minimum quality control checks, this topic is rarely discussed at industry events. Howes and Maxwell [1] discussed pipe strain effects on vibrations and presented some examples in 2013. Some industry standards such as API 686 [2] and ASME B31.3 [3] include limits for pipe strain and flange misalignment. However, these limits are mainly set for increasing the reliability of the machinery, rather than reducing vibrations on the piping and attached components.

This paper reviews several case studies. A theory on the reasons for higher vibrations due to excessive pipe strain is discussed. In addition, suggestions are made to reduce pipe strain in reciprocating compressor packages, and future studies are proposed.

3. Definitions and categories

Static deflection of the pipe from its neutral position or zero-stress condition is called pipe strain. By itself, pipe strain may not be sufficient to cause failure. However, when combined with the dynamic stresses from other sources such as unbalanced forces and pulsation-induced forces in reciprocating compressor systems, pipe strain becomes an element critical to the reliability of piping systems.

One of the major contributors of controllable pipe strain is piping misalignment. The root cause of misalignment can be attributed to deficiencies in design, fabrication, assembly and installation practices. Figure 3.1 and 3.2 show examples where pipe strain and flange misalignments were observed on real piping systems.

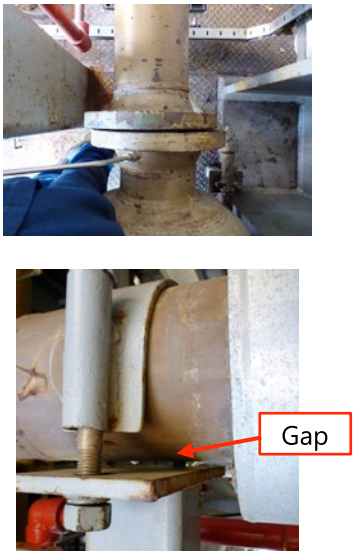

Figure 3.1 – Examples of pipe strain problems in a piping system

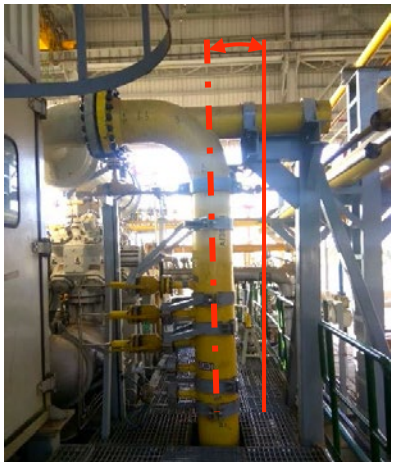

Figure 3.2 – Examples of pipe strain problems in a piping system

Improper support installation can induce pipe strain. Figure 3.3 shows 3 different scenarios where a pipe could be held away from its neutral position resulting in pipe strain.

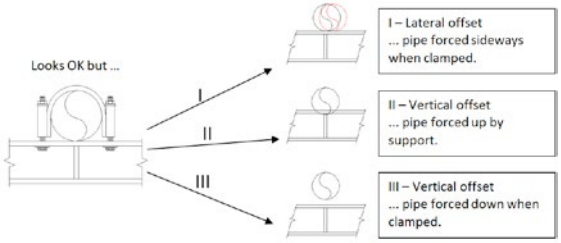

Figure 3.3 – Types of pipe strain

by: Ramin Rahnama, Kelly Eberle, Steven Crocker – WOOD

Two flanges can have one or more types of misalignments:

- Axial offset
- Radial offset
- Angularity (not parallel)

See the excerpt below from API 686 [2] that shows three types of flange misalignment. The paragraph numbers in these plots refer to API 686 text.

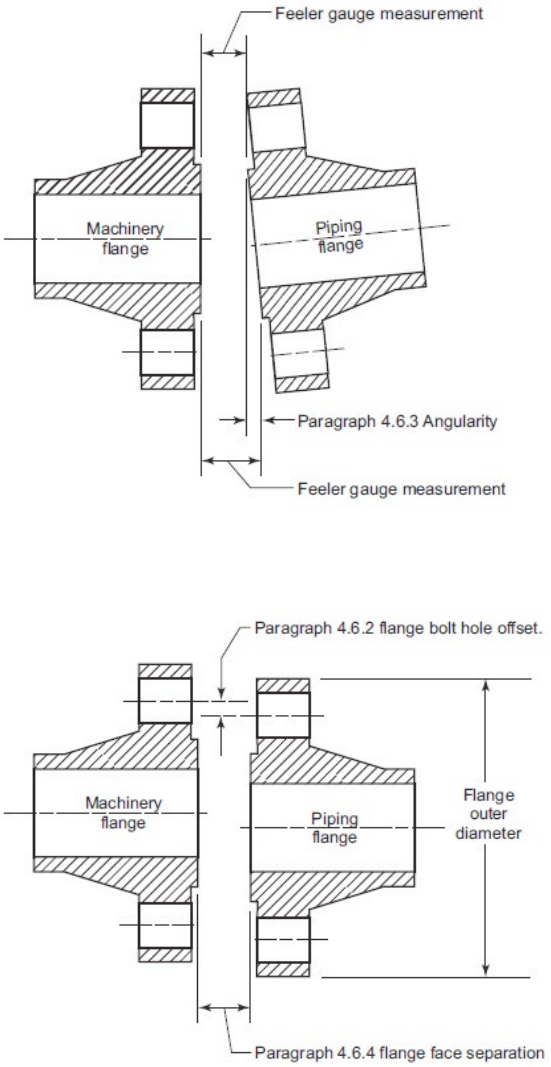

Figure 3.4 – Types of flange misalignment [2]

4. Case study

This case study is about high vibrations on a reciprocating compressor unit. The 4-throw, 3-stage compressor was being driven by a reciprocating engine at 1250 to 1400 RPM. A fleet of 12 nominally identical reciprocating compressors was assembled in a very tight timeline. This was led to many areas with excessive flange misalignment and pipe strain.

Figure 4.1 shows the piping between the suction scrubber and suction pulsation control bottle on the third stage for this compressor.

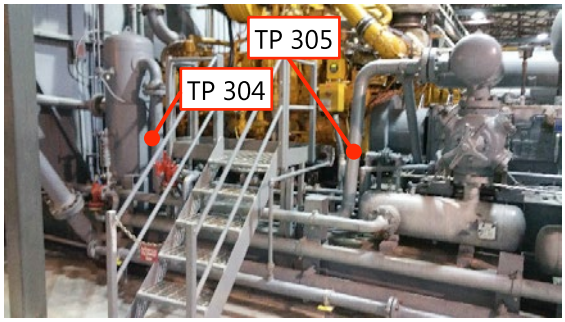

Figure 4.1 –Third stage suction piping

Our analysis showed high vibrations on test points 304 and 305. Signs of the pipe strain and flange misalignment was observed on the piping, and the operators were asked to loosen the clamps. Once the clamps were removed, up to 25 mm displacement was observed on some of the piping. Figure 4.2 shows the gap between the pipe and support once the clamp is loosened. In addition, the pipe was not parallel to the support base. When the clamp was removed fully, as shown in Figure 4.3, signs of forcing the pipe into position were visible on both pipe and flanges. Temporary shims were installed under some of the pipes to assess the effect of pipe strain. Figure 4.4 shows the temporary shims. Flange misalignment was also observed. Figure 4.5 shows a flange mating against a straight edge, that clearly presents the flange misalignment.

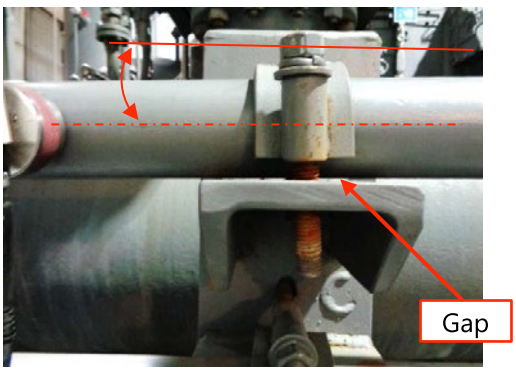

Figure 4.2 –Signs of pipe strain

by: Ramin Rahnama, Kelly Eberle, Steven Crocker – WOOD

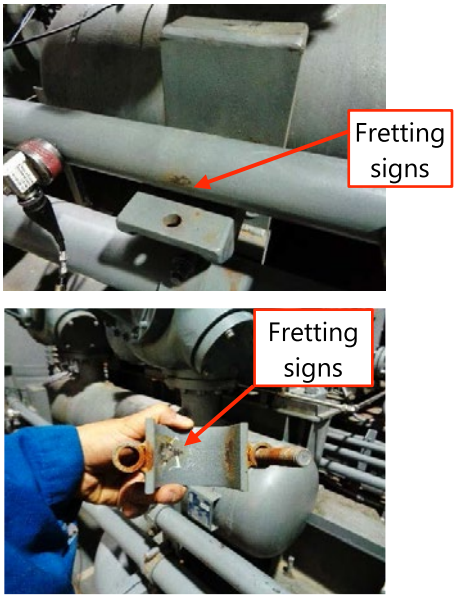

Figure 4.3 – Signs of pipe strain

Figure 4.4 – Temporary shims under the pipe

Figure 4.5 – Flange misalignment

The customer was recommended to remove all clamps and mitigate the pipe strain and flange misalignment, based on the procedure discussed in Section 7. After the pipe strain was mitigated, vibration was measured again. Figure 4.6 to Figure 4.8 show examples of before and after vibration plots. The vibration plots below show peak hold vibration amplitudes when the units were run throughout the speed range. The modifications led to significant vibration reductions. The vibration amplitudes are compared against Wood's (formerly BETA Machinery Analysis) vibration guidelines.

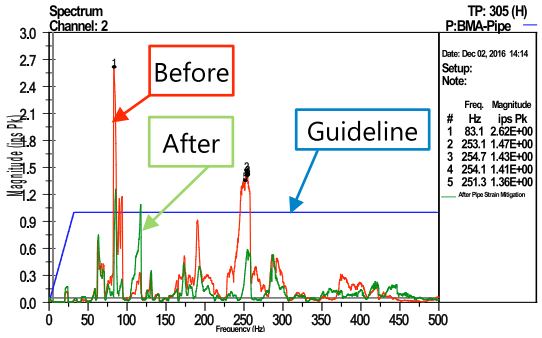

Figure 4.6 – Comparison of before and after pipe strain is mitigated, TP 305, horizontal vibration

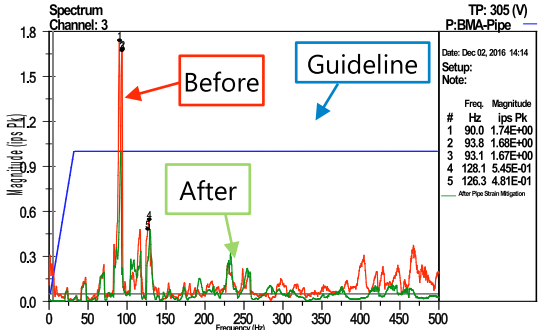

Figure 4.7 – Comparison of before and after pipe strain is mitigated, TP 305, vertical vibration

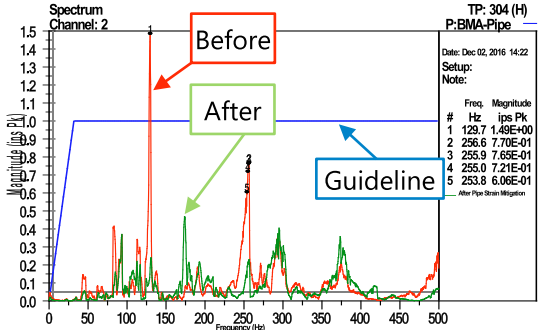

Figure 4.8 – Comparison of before and after pipe strain is mitigated, TP 304, horizontal vibration

by: Ramin Rahnama, Kelly Eberle, Steven Crocker – WOOD

5. Effects and mechanism

The effect of pipe strain, even if vibration does not increase, is a higher static force is imposed on the piping. The static forces from pipe strain increases the static or mean stress that the pipe experiences. The combined stress, which includes both the mean stress and alternating stress, can be represented on a Goodman diagram. The Goodman diagram (Figure 5.1) shows that the allowable amplitude of alternating stress decreases as mean stress increases. Vice versa, the allowed amplitude of alternating stress increases as the mean stress is lower. In Figure 5.1, Y.S. is the abbreviation for yield stress, S_n is the fatigue life at 10^7 cycles, and U.T.S. is the abbreviation for ultimate tensile stress.

Pipe strain increases the static stress in the system. When static stress increases, the allowable dynamic stress, hence the allowable vibration levels, drop.

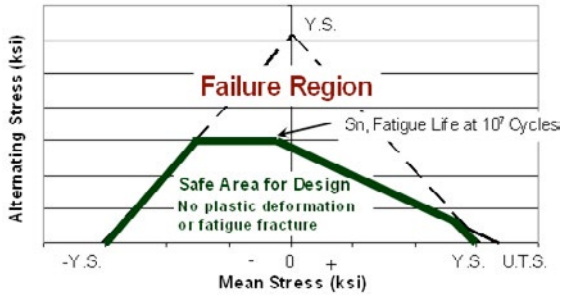

Figure 5.1 – Goodman diagram

As demonstrated by the case study and many other field tests on compressor piping systems, high pipe strain tends to be associated with high vibration. Research into the fundamental mechanisms whereby pipe strain leads to higher vibration levels is required. One proposed theory is that pipe strain will lead to a reduction in damping. Damping results from many different mechanisms in a piping system. One method of damping is energy dissipating as two parts move relative to each other. For example, joints between the pipe, pipe clamps and pipe support will have a small amount of relative motion under normal vibration. If the pipe is under a high static load, the mating surfaces between the pipe, clamp and support are distorted, and the same joints are fully closed. Less relative motion between these components occurs when the piping is subjected to dynamic forces, so there is less energy dissipated and less damping.

Reduced damping will cause increased vibration at the mechanical natural frequency (MNF). Figure 5.2 shows the vibration amplitudes and phase at different damping ratios at different frequencies. ξ represents damping ratio, f is the frequency, f_n represents the mechanical natural frequency.

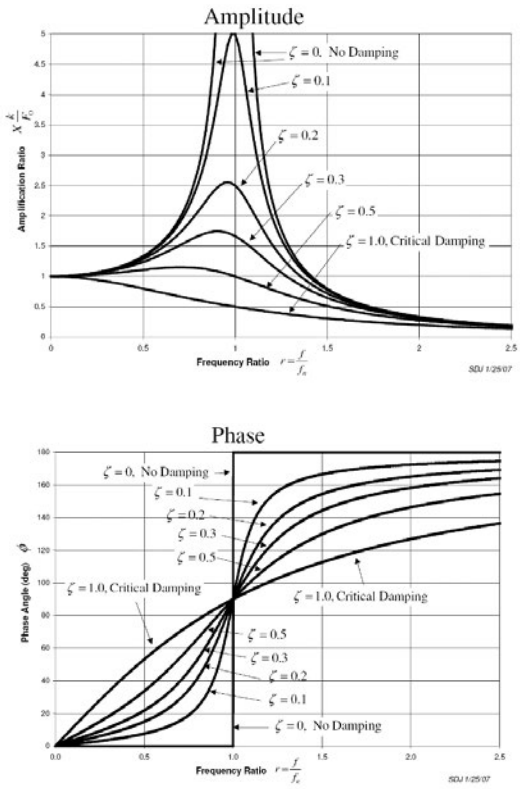

Figure 5.2 – Vibration amplitude and phase at different damping ratios [4]

6. Assembly procedure to avoid pipe strain

Following is the suggested procedure to avoid pipe strain during the assembly. This procedure applies to the assembly process when none of the flanges are tightened and none of the clamps are installed.

1. For each system (first stage suction, first stage discharge etc), start at the compressor cylinder. Installing pulsation control vessels (bottles), especially a bottle that is common to multiple cylinders,

by: Ramin Rahnama, Kelly Eberle, Steven Crocker – WOOD

requires special attention and precision. Start at the first pairs of flanges, for example, the flange set connecting the piping to the suction pulsation volume, and bring the flanges to a neutral position by adjusting the shims and/or modifying the support structure and nearby pipe clamps. The misalignment should be kept within the limits suggested by ASME B31.3 guidelines between each two flange faces.

The information in B31.3 is further described by the Los Alamos National Laboratory (LANL) as shown below [5]. ASME B31.3 doesn't have any guideline on the axial offset of the flanges. In this case, it is recommended to use API 686 guideline of "Gasket flanging must be within ±1.5 mm (1/16 in.) of the gasket spacing" [2].

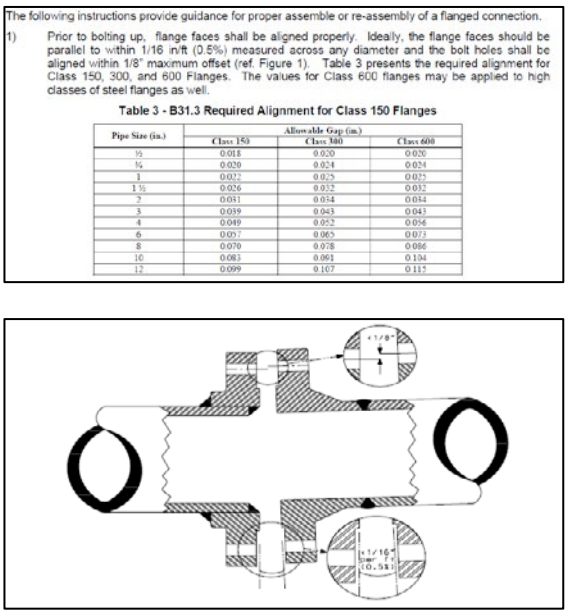

The following instructions provide guidance for proper assemble or re-assembly of a flanged connection.

1) Prior to bolting up, flange faces shall be aligned properly. Ideally, the flange faces should be parallel to within 1/16 in/ft (0.5%) measured across any diameter and the bolt holes shall be aligned within 1/8" maximum offset (ref. Figure 1). Table 3 presents the required alignment for Class 150, 300, and 600 Flanges. The values for Class 600 flanges may be applied to high classes of steel flanges as well.

Table 3 - B31.3 Required Alignment for Class 150 Flanges

Pipe Size (in.)	Allowable Gap (in.)		
	Class 150	Class 300	Class 600
½	0.018	0.020	0.020
¾	0.020	0.024	0.024
1	0.022	0.025	0.025
1 ½	0.026	0.032	0.032
2	0.031	0.034	0.034
3	0.039	0.043	0.043
4	0.049	0.052	0.054
6	0.071	0.065	0.073
8	0.070	0.078	0.086
10	0.083	0.091	0.104
12	0.099	0.107	0.115

Figure 6.1 – LANL notes on ASME B31.3 [5]

Some companies have chosen to use more stringent limits compared to ASME B31.3, especially for the connection between the suction bottles and closely coupled scrubber. This is one of the special applications related to reciprocating compressors which should be investigated further.

2. Once the work on the first pair of flanges is done, move on to the next pairs of flanges (starting from cylinders and working toward skid edge or coolers).
3. For each pipe clamp, place the clamp on the pipe, mark the neutral location of the pipe clamp on the sleeper, remove the clamp and then drill the sleeper. The holes should be drilled ¼" oversize to allow for hot alignment. Avoid clamp designs that require welding the studs or bolts to the sleeper. A welded stud design doesn't allow for potential future corrections. Also, high bending loads can be imposed on the fastener and weld as the pipe goes through thermal cycles. When dealing with extreme temperature, special clamp type should be considered to avoid pipe strain problems due to thermal expansion. The clamp fastener must only be tightened enough so there is no relative vibration between the pipe, clamp and support. Over tightening the fastener limits small movement due to thermal cycles that will reduce pipe strain.
4. For each pipe clamp, make sure one ½ inch thick packing is placed under the pipe to allow for future pipe strain adjustments. The packing can be tack welded in place if needed. The number of shims under the pipe should be limited to three shims.

7. Mitigating pipe strain after assembly

The suggested procedure for assembling the piping system to avoid and minimise the pipe strain is discussed in the previous section. The procedure below explains the suggested procedure for checking for pipe strain on an existing assembled unit.

1. Shut down the unit and perform a thorough visual inspection:
   a) It is recommended to perform a systematic inspection throughout the whole package. For example, start with the compressor cylinders on the first stage suction system and move toward the off-skid edge. Once the inspection of the first stage suction system is done, move to the first stage discharge system.
   b) Loosen all the clamps. Document the movement of the pipe when the clamps are removed.
   c) Inspect the flange alignment for all flanges. Use a straight edge to inspect the lateral alignment of flanges. Use a

by: Ramin Rahnama, Kelly Eberle, Steven Crocker – WOOD

micrometre to make sure the flange faces are parallel.

d) Check if the pipe is pushing on the support by removing the shims, packers, spacers, or liner under the pipe.

2. Correct the pipe strain by adding or removing shims, modifying the pipe supports and structures.
3. If after all modifications have been completed, some pipe strain and flange misalignment are observed, breaking the flanges can be used as the last resort. Make sure to monitor the flange position before and after bolts are loosened.
4. In extreme cases, replacing the pipe spool and/or bottles may be required to remove the pipe strain.
5. The final pipe strain checks must be done after the unit and piping has reached a stable operating temperature. Depending on the system, the ambient temperature, compressor setup, operating temperature, and other factors, the time to reach stable operating temperature may vary. Slight adjustments may be needed in shims and pipe supports when the unit has reached operating temperature. The ideal procedure includes bringing the unit up to temperature, shutting down the unit and then inspecting the line. However, a large-scope inspection may require multiple start-ups and shutdowns. If this is not feasible, the inspection can be done while the unit is operating.
6. Adjust shims and packing to place the pipe at its hot, neutral position.

8. Conclusions

The following conclusions can be made based on the authors' experience with reciprocating compressor piping system vibration.

- Pipe strain has been shown to contribute to significant vibration problems including vibration-induced piping failures.
- The root cause of misalignment can be attributed to deficiencies in design, fabrication, assembly and installation practices. Installation and assembly procedures were identified as the most critical steps of the project to avoid pipe strain.
- By itself, pipe strain may not be sufficient to cause failure, but when combined with the dynamic stress related to reciprocating compressors, pipe strain becomes an element critical to the reliability of piping systems.
- It is believed that increased vibration occurs mainly due to a reduction in damping when pipe strain is present. However, more research is needed to find the exact mechanism that leads to higher vibrations when pipe strain is present.
- Existing standards can provide a minimum required level for preventing excessive pipe strain. However, more stringent criteria may be needed for reciprocating compressor applications. The application of existing standards in cases where multiple flanges are used in near vicinity of each other, or multiple nozzle pulsation control vessels (commonly known as multi-nozzle bottles) may be misleading.
- The existing body of knowledge is not sufficient to draw solid conclusions and develop a guideline. More research is required.

9. Future research

It is recommended to perform additional studies to investigate the effects of pipe strain on vibration. The following studies should be conducted for different configurations such as straight pipe, two nozzle bottles, head and shell nozzles and other piping and vessel configurations common to reciprocating compressor installations:

- Laboratory study on the mechanism that pipe strain leads to higher vibrations. The outcome of this work is development of a set of laboratory measurements that can be used to develop and verify a theory and simulation approach to calculate the effects of pipe strain.

by: Ramin Rahnama, Kelly Eberle, Steven Crocker – WOOD

- Finite element analysis (FEA) to compare the change in static stress due to various levels of flange misalignment and pipe strain, for different pipe size and configurations.
- Finite element analysis to compare the change in vibration and dynamic stress due to various levels of flange misalignment and pipe strain.
- Field measurements of real piping systems to verify the results from the FEA work for assessing static and dynamic effects of pipe strain and flange misalignment.

10. References

[1] B. Howes and Maxwell, Gary, "Piping Misalignment and Vibration Related Fatigue Failures," in Gas Machinery Conference, Albuquerque, New Mexico, 2013.

[2] American Petroleum Institute, API686 - Recommended Practice for Machinery Installation and Installation Design, 2009.

[3] The American Society of Mechanical Engineers, ASME B31.3 - Process Piping, 2014.

[4] "Wikipedia," Wikimedia, [Online]. Available: https://en.wikipedia.org/wiki/Vibration. [Accessed 3 April 2018].

[5] "Los Alamos National Lab," [Online]. Available: http://engstandards.lanl.gov/esm/pressure_safety/Section%20REF-3-R0.pdf. [Accessed 22 Jan 2018].

EXPERIENCE. RELIABILITY. **ARIEL.**

Visit Ariel at Booth #1

www.arielcorp.com

ARIEL

WORLD STANDARD
COMPRESSORS

EUROPEAN FORUM
for RECIPROCATING
COMPRESSORS

TRIBOLOGY AND WEAR

Compressor Lubricants based on Polyglycol

by:

Henrik Heinemann
Technical Service Manager
BASF SE
Ludwigshafen, Germany
Henrik.Heinemann@basf.com

11th EFRC CONFERENCE
September 13 – 14, 2018, Madrid

Abstract:
For various applications, ranging from small air compressor in service stations to big gas compressors in chemical plants, different lubricants have been developed to meet unique requirements in each case. As the market demands higher performance of industrial compressors increase, same came to the field of lubricants to face several challenges. These include reducing downtime, enabling higher pressures and operating temperatures while reducing power consumption and overall costs. Synthetic lubricants have been well accepted to market and helped compressor system reaching its next levels that may not be possible by using mineral oil lubricants. With growing demand, today approximately more than 50% to 75% of compressor lubricants have already switched to synthetic basestocks.
An important group of basestocks for compressor lubricants are Polyglycols (PAGs). PAGs have several advantages such as low solubility to hydrocarbon gases and a cleaning effect to reduce the risk of deposits and varnish. PAG based lubricants are widely available for various type of compressors and gasses ranging from air to specialty gases such as LNG. Along with general information regarding PAG based compressor lubricants, BASF will present a recent field experience with screw and reciprocating compressors for natural gases. With the right design of equipment and understanding of the respective application, the use of PAG based lubricants can be an ideal solution to meet both technical and commercial requirements.

by: Henrik Heinemann – BASF

1 Introduction

Requirements to lubricants have steadily increased to meet the prerequisites of today's high performing industrial compressors.
This includes reducing downtime, enabling higher pressures and temperatures while also reducing power consumption and overall costs.
After the market introduction high performance synthetic lubricants have enabled compressor systems to achieve their goals, which previously had not been possible with current mineral oil lubricants.

2 General Market Overview

While industrial compressors bring higher performance claims to the market, many OEMs now recommend synthetic lubricants to meet their performance claims. According to market studies, approximately more than 50% to 75% compressor lubricants used in the market are already based on synthetic basestocks[1].
Figure 1+2, POE – Polyol-Ester,
PAO – Polyalphaolefin,
PAG – Polyalkylenglycol,
PAO FG – Polyalphaolefin for Food Grad

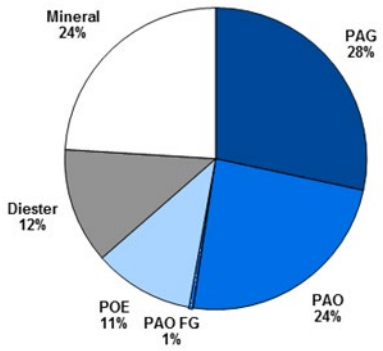

Figure 1: Industrial Air Compressor Lubricants [1]

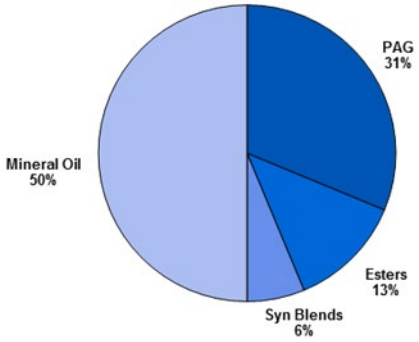

Figure 2: Industrial Oil & Gas Compressor Lubricants[1]

3 Requirements for Compressor Lubricants

The requirements for compressor lubricants are first defined by the compressor design, followed by the application and associated working conditions.
Most commonly used compressor types are screw, vane and turbo compressors (lubricating of bearing and valve, cooling, sealing – low viscosity) and reciprocating compressors (lubricating of bearing, piston, cylinder and valve – higher viscosity).
This also leads to different requirements regarding the performance and formulation of the lubricant. While temperature stability for screw compressors is not a major concern (operating temperature around 80-90°C), the same can be a key selection criterion for reciprocating compressors with temperatures higher than 200°C.
Besides general material compatibility, the compatibility/solubility with gas is an additional challenge. Depending on working condition behaviors like pour point (for low working temperatures), oxidation stability and air release (for air compressors and high oil temperatures), demulsibility (water contamination), corrosion protection and foaming characteristics could be important as well. Specialty additives, e.g. for anti-wear, are typically used for longer service life of compressor components. However, if the compressor system also has gears to be lubricated with the same oil, it is essential to make a reasonable compromise between wear resistance and the risk of residues and deposits when selecting the appropriate lubricant.

All these parameters can also be influenced by the choice of basestock technology.

4 Basestock Technologies for Compressor Lubricants

Depending on the application and its requirements all present basestock technologies have a reason to exist and may legitimately coexist because of their individual suitability for specific purposes.

Following the steadily increasing requirements for lubricants, synthetic based products present a preferable option in most cases.

General attributes of synthetic compressor lubricants are:

- Outstanding oxidation and thermal stability which enable an extended product life time and reduced drain intervals (mineral oil based compressor oils: 1.000 – 2.000 hrs vs. synthetic lubricants with up to 10.000 hrs)
- Low evaporation loss which means lower oil consumption

by: Henrik Heinemann – BASF

- Lower coking tendency which leads to reduced sludge, deposits and varnish and therefore results in lower maintenance costs
- Excellent air release which means higher compressor efficiency and suitability for high pressure application
- High corrosion protection which means longer compressor / equipment lifetime
- Higher lubricity and good viscosity temperature behavior which means higher efficiency and reduced energy cost
- Higher flash point which means improved safety due to higher auto ignition temperature

4.1 Mineral Oils

Mineral oils are the most commonly used basestock technology in the global lubricant industry. The technology is well proven, product costs are lower compared to synthetics and most additives are developed for these basestocks.

Advantages:

- Low lubricant price
- Compatible to most materials (elastomers, paints, metals)
- Good additive solubility and response
- World wide availability
- Sufficient viscosity-temperature behavior (VI 95-100)
- Contaminants and oxidation products are removed out of the compressor with frequent oil changes (typical drain interval in air compressors =1.000 hrs)

Disadvantages:

- Frequent oil changes - meaning longer down time and higher maintenance/labor cost.
- Limited temperature working window
- Poor cooling
- Low temperature and oxidation stability
- Sludge or varnish formation at higher temperature and pressure

Based on latest refinery technologies, new types of mineral oils (called API Group II and Group III) have established in the market. These compressor oils are mainly used in air compressors and show improved oxidation stability which enables longer lubricant life time and a good viscosity-temperature behavior. In some cases, the performance of the products is close to those based on Polyalphaolefin (PAO) and their price is lower. However, solubility of additives and oxidation products is worse compared to standard mineral oils and therefore problems with sludge and deposits can be observed.

4.2 Diester

There are many types of synthetic Esters available in market. Based on their chemical structure and quality, performance can also vary within a wide range. Diesters are mostly used in special applications.

Advantages:

- Wide temperature spectrum with pour points, ranging from -50 to -65°C
- Resistance to carbon formation
- Less evaporation losses
- Low friction coefficient
- Excellent solvency and can remove deposits
- Good temperature stability
- Good biodegradability
- Compatible with mineral oil and most synthetic lubricants as well as with different catalysts

Disadvantages:

- Dissolve paint
- More aggressive toward typical sealing materials
- Low hydrolysis stability
- High price

4.3 Polyol Ester (POE)

Advantages:

- Wide temperature spectrum with pour points spanning -30 to -70°C
- Resistance to carbon formation
- Excellent solvency and can remove deposits
- Excellent temperature stability
- Long service interval
- Good biodegradability
- Compatible with mineral oil and most synthetic lubricants as well with different catalysts

Disadvantages:

- More aggressive toward typical sealing materials

by: Henrik Heinemann – BASF

- Hydrolysis stability in presence of water
- High price

4.4 Polyalphaolefin (PAO)

PAO based lubricants are similar to mineral oils based on hydrocarbon structure. In general, it is the most widely used synthetic basestock for lubricants.

Advantages:

- Very good overall lubricity
- Good thermal stability
- Compatible with most materials and mineral oils
- Good water separation
- Excellent air release
- Good viscosity-temperature behavior (VI 150) with pour points below -40°C
- Longer oil change intervals (typical drain interval in air compressors = 6.000-8.000 hrs)

Disadvantages:

- Limited ability to dissolve additives and oxidized byproducts which could cause deposits and varnish at high temperatures (this can be overcome by adding a small amount of Ester to the formulation)
- Tend to shrink seals
- Poor lubricity
- High price

4.5 Polyalkylene Glycols (PAG)

Lubricant performance and properties of PAGs depend on the structure and monomers used. Thus, a wide range of different types and individual properties exist.

Advantages:

- Less evaporation losses (lower oil consumption)
- Excellent friction coefficient (reduced power consumption)
- Wide working temperature window (VI up to 280)
- High temperature and oxidation stability (higher pressure and working temperature)
- High load carrying capacity (reduced wear)
- Reduced gas solubility especially with hydrocarbon based gases
- Cleaning effect which reduces the risk of deposits and varnish
- Longer oil change intervals (typical drain interval in air compressors = 8.000-10.000 hrs)
- Excellent cooling
- Good biodegradability

Disadvantages:

- Depending on the respective type, the PAG can attract water (condensate separation is typically difficult) (Figure 3)
- Incompatible with some paints, plastics, metals and elastomers as well as mineral oils and PAO
- High price

Figure 3: Water-soluble compressor oil with contamination of 10% to 50% of water

5 Outstanding Advantages of Polyalkylene Glycol based Compressor Oils

An important group of basestocks for compressor lubricants are Polyalkylene Glycols (PAGs).

Generally, the type of compressor determines what lubricants to choose meaning viscosities and type of additives can be different. Also, properties of gas also have an important influence on the selection of the appropriate lubricant due to a gas' solubility

5.1 PAG based Lubricants for Air Compressors

If you are looking for PAG-based compressor lubricants, there are products for air compressors available in the market with life times of more than 10.000 hrs (up to twice the life time compared to conventional synthetic lubricants) and leading wear protection. Beside general advantages, outlined in chapter 4.5, PAG based air compressor oils may prevent varnishing of critical components which reduces the need for frequent in-line filter change and prevents the drain of clogged condensate. These lubricants have a better cooling efficiency, delivered by an ultra-high thermal conductivity value which is about 10% higher than that of PAOs, and enable

by: Henrik Heinemann – BASF

compressors to run more efficiently in high-ambient temperature environments. With a high flash point of 272°C, which is higher than most PAO's, Diesters or other synthetic lubricants, the operational safety will be also enhanced.

5.2 PAG based Lubricants for Gas Compressors

The increasing global demand for gas production, transport and storage especially of hydrocarbon gases like Methane, Ethene, Propane, LPG, Ethylene or Propylene requires increasingly sophisticated equipment. Better efficiency, lower power consumption, increased uptime, reduced maintenance, higher pressure and temperature resistance are some important aspects here. Only PAG-based compressor lubricants, specifically formulated for hydrocarbon and chemical gases where the crankcase and bearings operate in a gas-filled atmosphere, can satisfactorily fulfill these requirements.

Under these operating conditions the gas is readily soluble in mineral oil lubricants, which upon dilution suffer a significant drop in viscosity and lubricant performance. The reduction of viscosity significantly affects the lubricity and wear protection (Figure 4).

The problem can be overcome by using special PAG based compressor lubricants in which the gases are much less soluble. These products are particularly suitable for marine service on vessels carrying specialty liquefied gases. Due to less solubility of many gases PAGs can be used for multi-gas service for a wide range of gases including vinyl chloride and butadiene.
An extended lubricant life enables longer drain intervals and reduced maintenance.

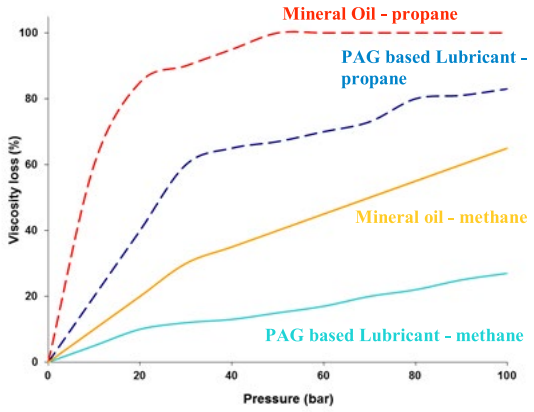

Figure 4: Viscosity loss caused by gas solubility - PAG based compressor oil versus mineral oil

The lubricant does not promote the dimerization of butadiene or generate solid deposits. The cleaning effect of PAG based compressor oils on one hand can clean the system from old sludge caused by using mineral oils. On the other hand, filter life time may be reduced at the first running hours, when changing from mineral oil to PAG based compressor oil (Figure 5).

Figure 5: Heat exchanger before and after changing to PAG based compressor oil

6 Applications for Polyalkylene Glycol Compressor Lubricants

Most common applications for PAG compressor lubricants are screw and reciprocating compressors in the following fields:

- Marine service on vessels carrying specialist liquefied gas cargoes
- Production, storage and transportation of natural gases
- Refineries
- Chemical industry
- Oil field gas re-injection
- Petrochemical industry: GTL (Gas-To-Liquid) production
- Compression of chemical gases prior to reaction
- Refrigeration drying of natural gas
- Compression and production of LPG
- Compression of natural gas for automobile fuel
- "Down hole" re-injection of well gas to aid extraction of crude oil
- Natural gas transportation (pipeline and ship)
- Production of LDPE (Low-Density-Poly-Ethylene) in Hyper-Compressors up to 3.500 bar.

Based on three field experiences we will demonstrate the advantages of PAG based compressor lubricants.

by: Henrik Heinemann – BASF

6.1 Screw Compressor for Natural Gas

The screw compressor is part of the compression equipment for natural gas associated oil exploitation and crude natural gas (Figure 6).

Fig. 6 Equipment for natural gas compression, containing screw compressor (Source: Comoti [2])

- Type of compressor: screw CF 180 GK
- Pressure suction side: 0,7-2 bar
- Temperature suction side: 3-25 °C
- Pressure discharge side: 10-26 bar
- Temperature discharge side: 70-90 °C
- Gas volume: max 35.000 Nm^3/day
- Oil temperature: 60-85°C
- Oil pressure: 6-23 bar
- Oil flow: max 150 l/min
- Oil volume: 370 L

The customer switched from a mineral oil based product to PAO based lubricants three years ago with the aim to increase lubricant life time. The PAO caused problems because natural gases are soluble with PAO as well as mineral oil and the solubility further increased with increasing pressure.

Viscosity loss after a short period of operation is the result of the gas' solubility. This can cause high wear and high temperature in the compressor.

The specific goal was to have a longer oil change interval of 8.000 hrs and better a lubricity.

In close cooperation with the compressor manufacturer (COMOTI) and the customer, a field trail with a PAG based compressor oil was conducted.

After analyzing all materials for compatibility with PAG (only one sealing -PU- needed to be changed) and an intensive flushing procedure, one compressor was changed to special PAG based compressor oil (VG 100).

After more than 8.000 hrs, the oil today is in very good condition. Especially the viscosity is within fresh oil limits compared to the previously used PAO based product which showed a dramatic decrease from 100 to 18 mm^2/s after 3.000 hrs.

Based on these results and experiences, the customer is changing additional compressors to the PAG based compressor oil.

6.2 Reciprocating Compressor for Liquefied Natural Gas (LNG)

The increasing use of natural gas as an energy source has created an increasing demand for storage and transport of LNG. Ocean-going vessels, fueled by LNG, use compressors for various requirements.

Also for this application, the gas solubility of the compressor oil is an important factor. Therefore, some compressor manufacturers prefer lubricants which are non-miscible with hydrocarbon gases.
At typical pressures of 300 bar, the viscosity losses caused by gas solubility when using mineral or PAO based lubricants will have a significant effect on lubricity and wear protection.

An additional challenge is the dissolving of oil in gas at critical temperature/pressure conditions.
Dissolved oil will fall out when gas expands (pressure/temperature drop). At higher pressures, equilibrium of dissolved oil in gas increases with increasing pressure. This effect intensifies when using mineral oil and hydrocarbon base stock with an affinity for natural gas such as PAO because of a high saturation in natural gas.

The only way to solve this and to reduce the high oil carryover from compressor outlets is using a PAG based compressor oil (Figure 7).

An example where this effect plays an important role is the new dual fuel propulsion systems for LNG Carriers (Figure 8). The "Boil-off Gas", which is burned in a gasification unit before, is now used as the fuel of the diesel engine. Therefore, a reciprocating compressor converts the gas (Methane) to a higher pressure. The gas which is not used as fuel can flow back into the cargo tank via the reliquefaction system. This combination increases the delivery volume of cargo, reduces emissions compared to standard fuel and opens the door for alternative propulsion systems.

by: Henrik Heinemann – BASF

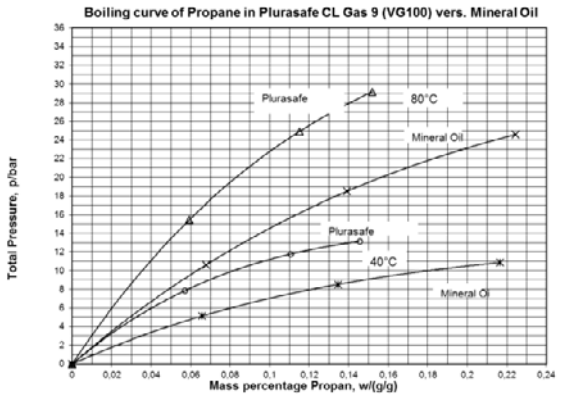

Figure 7: The content of gas within oil is much lower with PAG based lubricant (Plurasafe CL Gas 9) compared to mineral oil

Figure 8: LNG Carrier «Creole Spirit» (Source: Burckhardt Compression)

6.3 Hyper-Compressors for Low-Density-Poly-Ethylene (LDPE)

Finally, LDPE compressor lubricants specifically formulated on Polyalkylene Glycol are used in hyper-compressors with up to 3.500 bar.
PAGs are much less soluble in ethylene than in white oils or polyisobutylene.

That brings two essential advantages:

- Viscosity reduction due to dissolving of ethylene in the lubricant is minimized.
- Lubricant is less likely to be removed or washed from the plunger running zone.

PAG-based compressor lubricants have a superior load carrying and lubricant performance compared to white oils and polyisobutylene. This means:

- Minimized wear on plunger and packing.
- Typical life time figures for packings confirmed by end-users are in the range of 20,000 – 40,000 hrs.

Polyalkylene glycols have relatively flat pressure-viscosity characteristics compared to white oil, polyisobutylene and mixtures thereof. This means:

- They flow more readily in the high-pressure lubricant lines of the compressor
- Are much less likely to solidify in the lines at lower temperatures.

Special additive technologies inhibit the pre-polymerization. In some circumstances LDPE plants using PAG-based Hyper compressor oils have increased maintenance intervals by up to 50%.

7 Conclusion

Close collaborations between OEMs, end-users and lubricant suppliers will be paramount in choosing the most appropriate solution for each individual compressor application. However, whether looking at the traditional compressor applications and new technologies, or discussing about efficiency, costs and environmental requirements - synthetic, and especially Polyglycol-based, compressor lubricants will be the technology of choice to meet and exceed, both, current and future requirements.

References

[1] All figures estimated on information from Ingersoll Rand, Lubes `n` Greases, SCUP Report, Kline&Co

[2] Comoti - Romanian Research & Development Institute for Gas Turbines 2017

New insight into the wear of packing rings: model, calculation, experiment

by:

Andreas Kaufmann and Dr. Tino Lindner-Silwester
Research & Development
HOERBIGER Wien
Vienna, Austria
andreas.kaufmann@hoerbiger.com
tino.lindner-silwester@hoerbiger.com

11th EFRC CONFERENCE
September 13 – 14, 2018, Madrid

Abstract:
The fundamental working principle of sealing elements in the piston-rod sealing system in a reciprocating compressor inevitably leads to wear of the packing rings. While packing rings are designed to maintain their sealing efficiency as far as possible as they wear away, too much wear will ultimately lead to a loss of sealing efficiency.
Due to the paramount importance of ring wear for the reliable, economic, and environmentally sound operation of reciprocating compressors, it has become common to measure wear using tribological test rigs. In such a rig, a defined load presses the specimen against a counterface of known characteristics that moves relative to the specimen. Such wear tests provide valuable insight into the wear resistance of packing ring materials under various tribological conditions. However, it is impossible to extrapolate from the test results to the evolution of packing ring wear in real-world compressors.
To bridge this fundamental gap, this paper presents a model that allows us to calculate how a packing ring wears away under the load created by a prescribed pressure differential. We compare calculation results with experimental data from purpose-designed test rigs.

by: Andreas Kaufmann, Dr. Tino Lindner-Silwester – HOERBIGER

1 Introduction

The piston-rod sealing system is one of the performance-determining components of a reciprocating compressor. The fundamental working principle of such a sealing system inevitably leads to wear of its individual elements (packing rings) and blow-by leakage. As a result, operating reciprocating compressors in an efficient, reliable, and environmentally friendly manner may pose a significant challenge to the packing rings, especially in non-lubricated services.

Even though packing rings are designed to compensate for wear, too much wear will in the end always lead to unacceptably high leakage rates. The extent to which a loss of sealing efficiency can still be regarded as acceptable depends on several factors, such as whether high packing leakage poses a danger to operators, results in uneconomically high gas losses, or causes environmental issues.

Given the predominant role of ring wear in the reliable, efficient, and environmentally sound operation of a piston-rod sealing system, it comes as no surprise that extensive tribological testing has become common in the industry. Such testing ranges from standardized tribotests to runs on fully instrumented compressors. Whereas the former allow for systematic comparisons of different materials in a more or less repeatable manner, the latter provide more insight into how a material can cope with the specific load collective the sealing rings in a real pressure packing face. However, this deeper insight comes at a cost. On the one hand, such compressor runs are typically not only more time-consuming but also more expensive than simple material tests. On the other hand, it is very difficult to keep track of all the variables that may affect the final wear pattern.

This paper presents a simulation-based approach that attempts to bridge the gap between experimental data derived from tribotesting and experience of ring wear in real-world compressors. The model provides genuine insight into how ring wear evolves over time, and the influence of the accompanying stresses, strains, and contact pressures.

2 Problem formulation

The way and the rate at which a packing ring wears away will in general depend on:

- the geometry of the ring,
- the mechanical loads – in essence the gas pressure differential across the ring; special attention has to be paid to the gas pressure distribution across the dynamic sealing surface (i.e. the rod contact surface),
- the contact between the ring, the reciprocating rod and the packing cup face,
- the material behavior, and
- the wear behavior.

This paper considers and compares two well-known packing ring designs: the radial-tangential (RT) ring pair and the balanced cap design (BCD) ring. Figure 1 shows the main inputs to the simulation model in the case of a BCD ring.

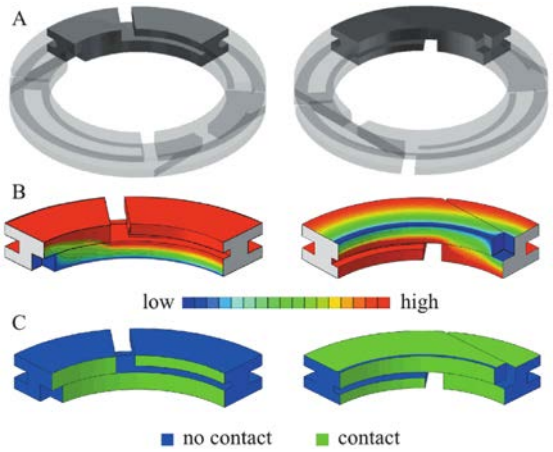

Figure 1: BCD ring simulation-model ingredients. Left column: view from cylinder (high-pressure) side. Right column: view from crank (low-pressure) side. A) BCD geometry: the simulation is based on one quarter of the ring, here shown opaque. B) Gas pressure contours. C) Contact configuration.

2.1 Ring geometry

Packing rings are typically of segmental type to compensate for wear. A well-known example is the RT ring pair where a radially and a tangentially cut ring, each one consisting of three segments, work together to create a single-acting seal. In contrast to this two-ring design, the recently developed BCD ring[1] is a one-ring design that consists in total of four segments. This paper looks at both ring designs. The RT ring pair considered here has a total axial width of 10.1 mm and an outer diameter of 74 mm. The BCD ring is 8 mm in axial width with an outer diameter of 73 mm.

2.2 Gas pressure loading

A pressure packing consists of a series of packing rings, each ring held in a separate “cup”. The way in which the cylinder pressure falls to (in general) ambient pressure across these packing rings, i.e. the cup pressure distribution, depends on the relationship between differential gas pressure and gas leakage for each ring.

Whereas piston rings have a defined leakage gap, packing rings are designed to be gas-tight and have no defined leakage gap. The leakage rate is therefore not necessarily proportional to the differential pressure across the seal. Contrarily, due

to the "self-energizing" working principle where the sealing effect arises from the pressure drop, leakage may even go down when the pressure differential goes up [1,2].

To study the cup pressure distribution we run a straightforward labyrinth-seal simulation for a series of packing rings where leakage does not rise in proportion with the differential pressure. This reveals that the first ring on the high-pressure side typically seals the "dynamic" pressure component, i.e. the difference between the instantaneous cylinder pressure and the suction pressure. The last ring typically takes most of the remaining "static" pressure component. i.e. the difference between the suction and – in general – ambient pressure. This agrees with experimental observations [3]. For what follows, it suggests that we only need to consider the case in which a packing ring wears away under the action of a constant gas pressure differential $\Delta p_G = p_1 - p_2$, where $p_2 = 1$ bar.

Each ring in a packing seals against the piston rod and the face of the packing cup. The gas pressure differential forces the ring against these sealing surfaces, thereby giving rise to a certain contact pressure distribution p_C in those areas. The rate at which material wears away is in general proportional to both the local contact pressure p_C and the speed of the rod, v. Determining how p_C varies along the dynamic sealing surface is therefore of paramount importance.

For the purposes of this analysis the contact pressure is assumed to vary continuously along the nominally flat sealing surfaces. This is despite the fact that in the microscopic view the contact pressure varies tremendously, being nonzero only in localized contact spots and vanishing everywhere else. Although this microscopic variation will be disregarded in the subsequent analysis, the presence of microscopic asperities has an important consequence: it leads to gaps through which gas can leak under the action of a gas pressure differential. On the macroscopic scale the two-dimensional variation of this gas pressure p_G along the sealing surfaces is, to a good approximation, governed by [2]:

$$\nabla^2 p_G^2 = 0 \qquad (1)$$

where ∇ denotes the nabla operator.

2.3 Wear model

We use the simplest possible wear model, the Archard [4] wear equation:

$$\frac{\mathrm{d}w}{\mathrm{d}t} = k p_C v \qquad (2)$$

Here the wear rate $\mathrm{d}w/\mathrm{d}t$ varies linearly with the contact pressure p_C and the relative sliding speed v via a wear coefficient k.

2.4 Material

The rings are made from polytetrafluoroethylene (PTFE) filled with short glass fibers and carbon particles. For the subsequent simulation this material is modeled as an isothermal Hookean body with a Young's modulus E of 1400 MPa and a Poisson's ratio ν of 0.4.

Note that this material grade is typically used for applications that are non-lubricated but not bone-dry. In bone-dry atmospheres this grade wears at a rate that is unacceptable in real-world applications but useful for accelerated wear testing.

3 Numerical implementation

The calculations are performed with the commercial finite-element software package ABAQUS. Additional user-defined subroutines coded in FORTRAN, and PYTHON scripts, are used for the wear calculation.

3.1 Geometry and contact

The packing cup face and the piston rod are modeled as rigid bodies that do not wear away. The rod diameter is 50.8 mm (2") and the packing case bore is 52.8 mm.

We take advantage of the quarter-symmetry of the BCD ring to reduce the size of the model. A new BCD ring has a wear gap of 6 mm between the circumferential ends of the sealing segments. The model therefore includes an artificial rigid stop in the symmetry plane of the cap segment to account for the wear stop. In a new RT ring pair, both the radial and the tangential ring have three wear gaps of 3 mm.

For all rings, the garter spring groove is modeled with a rectangular profile for ease of meshing with C3D8 and C3D6 elements. These linear element types have 8 and 6 nodes respectively. All contacts are frictionless "surface to surface" contacts. As a consequence, special care has to be taken to avoid rotation of the radial and tangential ring segments around the rod. This is done by adding artificial spring elements. The springs, of stiffness 10^4 N/mm, are placed on the outer diameter, acting only in the circumferential direction. To detect any artificial effects on the calculation the springs are distributed non-uniformly (Figure 2).

by: Andreas Kaufmann, Dr. Tino Lindner-Silwester – HOERBIGER

Figure 2: RT ring pair showing positions of the artificial springs that prevent the segments from rotating.

3.2 Loads

During compressor operation the gas pressure differential presses the ring against the cup face and the rod. The effect of the garter spring on the contact pressure p_C is so small that it can be neglected. The loads are applied as surface loads. The gas pressure distribution across the dynamic sealing surface is first determined by solving equation (1) in a sub-calculation and then mapped back into the wear calculation using the user-defined subroutine DLOAD.

3.3 Wear

Archard's wear equation (2) is implemented into the FORTRAN-based user-defined subroutine UMESHMOTION with a mean rod speed $v = 1.19$ m/s and a wear coefficient $k = 7.2 \cdot 10^{-7}$ mm³/(MPa m). The contact pressure, which changes due to wear, is updated every increment. UMESHMOTION allows us to move nodes and thus reduce the element size without giving rise to any stresses or strains. The subroutine runs once in every increment to calculate the local displacement representing the wear of each node.

Moving only the nodes that are in contact with the rod limits the total computable wear to an element's linear dimension. To overcome this limitation we use a "wear box". Within the wear box an arbitrary number of nodes within the body of the ring move in proportion to the wear of the contact nodes (Figure 3). A detailed discussion of the wear box can be found in [5].

The wear during a single stroke is so small that it does not have to be resolved on this timescale – instead, the mean rod speed is used.

Wear takes place in a direction normal to the contact surface. The wear algorithm also takes into account whether a node is placed on a corner or an edge. These nodes will create geometrical incompatibility problems if they do not move within the adjacent surfaces; Rezaei et al.[6] gives more details.

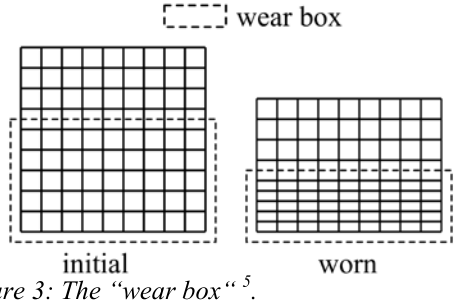

Figure 3: The "wear box" [5].

3.4 Calculation scheme

The packing ring is loaded after setting up the model, i.e. defining the model geometry, an appropriate mesh, the material parameters, the gas loads (p_1 and p_2), and the contact pairs. The gas pressure distribution over the dynamic sealing surface is calculated in a sub-calculation using the dynamic sealing surface geometry of the loaded structure. After mapping this gas pressure distribution back to the ring's dynamic sealing surface, the equilibrium state is solved for and the wear calculation starts in incremental steps. After several wear increments the wear calculation stops and the submodel updates the gas pressure distribution in the dynamic sealing surface of the worn packing ring configuration. This scheme is repeated until the defined wear time is reached (Figure 4).

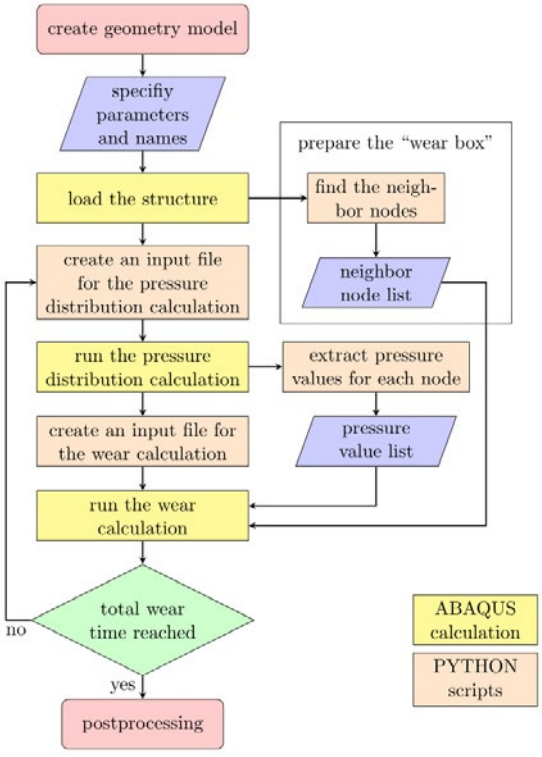

Figure 4: Calculation scheme.

by: Andreas Kaufmann, Dr. Tino Lindner-Silwester – HOERBIGER

3.5 Verification of numerical algorithm

The wear-simulation algorithm was verified by applying it to a simplified configuration for which an analytical solution can be obtained [5].

4 Simulation results

The evolution of wear and frictional force with wear time is calculated for an RT ring pair and a BCD ring.

4.1 Frictional force

The frictional force between rod and ring has to be overcome during operation of the compressor, manifesting itself in higher power consumption and frictional heating of the packing rings and the rod. Depending on the amount of frictional heat released and the efficiency with which it is transferred away, the rod and the rings may reach temperatures that significantly reduce the lifetime of the packing rings.

The dry sliding friction between ring and rod is calculated by assuming it to be of Coulomb type with a constant coefficient of sliding friction. However, in the simulation all contacts are modeled as frictionless. The local contact pressure p_C as calculated from the frictionless model is therefore converted into a local shear stress via the coefficient of sliding friction. Integrating the shear stress over the dynamic sealing surface yields the frictional force.

Figure 5 shows how this calculated value (in the rings' virgin states) varies with applied gas pressure differential for a BCD ring and an RT ring pair for a coefficient of sliding friction $\mu = 0.19$ (as experimentally determined, cf. section 5.1.1). The BCD ring shows a 39% lower value than the RT ring pair.

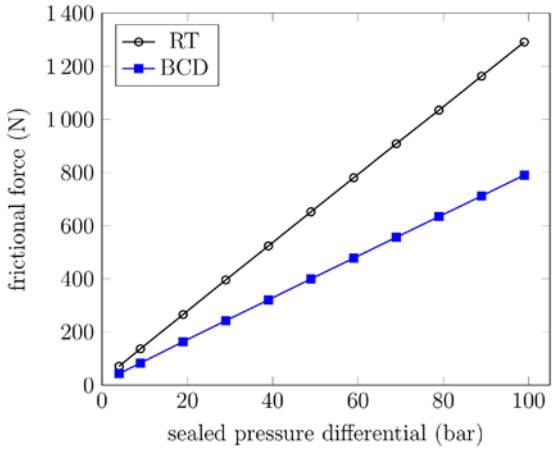

Figure 5: Variation of calculated frictional force with sealed pressure differential for an RT ring pair and a BCD ring, assuming a coefficient of sliding friction of 0.19.

With both the local wear rate and the local frictional shear stress being proportional to the local contact pressure, the frictional force may be regarded as a proxy for the total wear rate. Its value will in general vary with time due to the loss of ring material, even when the coefficient of sliding friction does not change. (The latter assumption disregards any bedding-in phase during which the formation of a transfer film results in a different tribology.)

Figure 6 shows the variation in frictional force due to wear for an RT ring pair and a BCD ring at a gas pressure differential $\Delta p_G = 30$ bar. At first, the frictional force falls at roughly the same rate for the RT and the BCD rings until the tangential ring segments of the RT ring pair start to touch one another. The individual wear gaps of the tangential ring do not close at exactly the same time because of the non-uniform distribution of the artificial springs. The first wear gap closes after 8.7 days, the second after 10.4 days, and the last after 10.9 days (A, B, and C, respectively, in Figure 6). After about 16 days the wear rate for the tangential ring reaches a low and steady value. This happens when the wear gaps in the tangential ring have fully closed, transforming it essentially into a solid (uncut) ring in which bending stresses significantly reduce the contact pressure.

The BCD's wear gaps close after 31.8 days. The BCD ring has a total wear-gap length of 12 mm, whereas the two RT rings have only 9 mm each. Nevertheless, it takes the BCD ring nearly three times longer to reach its wear stop. Note that reaching the wear stop oftentimes leads to higher ring leakages in real-world applications.

Figure 7 and Figure 8 show how the contact pressure varies over the dynamic sealing surface for an RT ring and a BCD ring after one day and ten days.

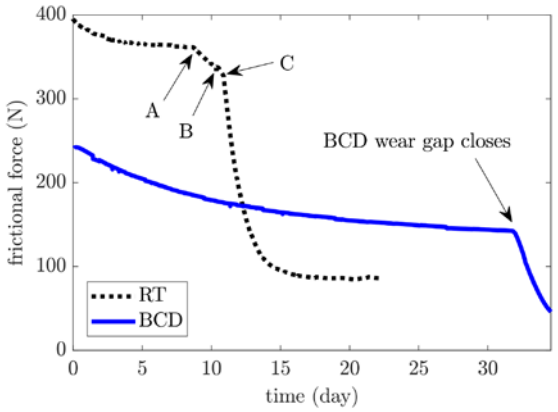

Figure 6: Variation of calculated frictional force with wear time for an RT ring pair and a BCD ring. The wear gaps of the tangential ring do not close simultaneously but one after the other (A, B and C) due to the non-uniform positioning of the artificial springs built into the model.

by: Andreas Kaufmann, Dr. Tino Lindner-Silwester – HOERBIGER

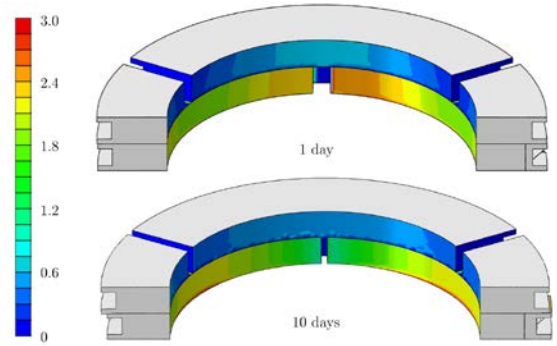

Figure 7: Contact pressure distribution for RT ring pair after 1 and 10 days.

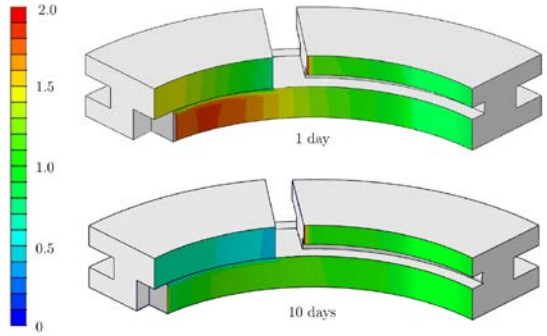

Figure 8: Contact pressure distribution for BCD ring after 1 and 10 days.

4.2 Wear

4.2.1 Worn configuration

Figure 9 and Figure 10 depict the virgin and worn states of an RT ring pair and a BCD ring. It takes the RT ring pair 10.9 days to reach the wear stop of its tangential ring, at which point the BCD still has 3.5 mm of wear gap left. For the BCD an additional worn configuration is shown at 34.5 days, when the wear gap is fully closed.

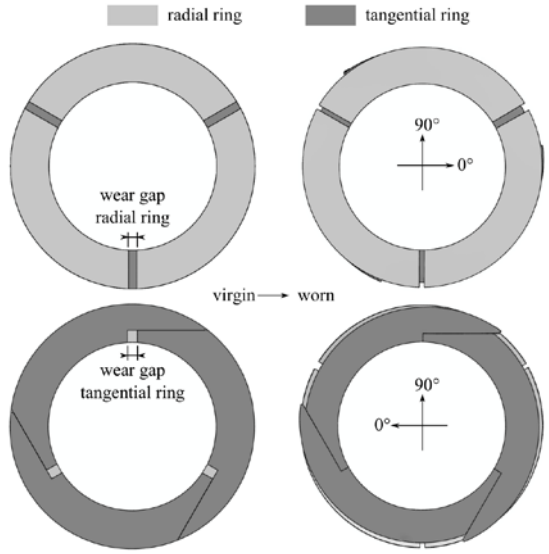

Figure 9: RT ring pair in virgin (left) and worn (right) states after 10.9 days of wear time. Viewing direction: from head to crank end (top) and from crank to head end (bottom).

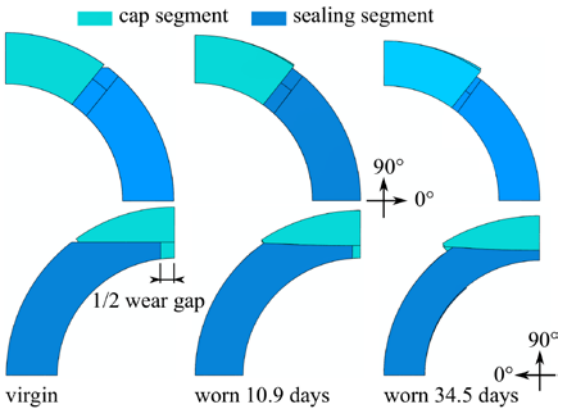

Figure 10: Quarter of BCD ring in virgin condition (left), after 10.9 days (middle), and after 34.5 days of wear time (right). Viewing direction: from head to crank end, high-pressure side (top) and from crank to head end, ambient-pressure side (bottom).

4.2.2 Wear pattern

To give a better picture of how the loss of material varies along the dynamic sealing surface, in what follows we show the accumulated wear in the deformed state. For the difference between accumulated wear in the deformed and undeformed states refer to [5].

Figure 11 shows the wear patterns of both ring designs after 10.9 days. The tangential ring segments wear in a way that is decidedly non-uniform in the circumferential direction. The wear is also asymmetric: for instance, maximum wear of the tangential ring occurs not at 30° but at 23° (Table 1). In accordance with field experience, the tangential ring wears much faster than the radial ring.

The BCD ring also wears non-uniformly, but the wear is symmetrical. The highest wear on the sealing segments occurs near their ends, in the circumferential direction, where they are loaded by the cap segment. The wear in the middle of the sealing segment (0° in Figure 11) is approximately half of that. The cap segments wear less since they are supported by the sealing segments, while the mean gas pressure over their dynamic sealing surfaces is higher (Figure 1).

Table 1 shows the circumferential position at which the components of the BCD ring wear fastest (see Figure 9 for the coordinate system). For the radial and tangential rings the table shows the first maximum in the positive circumferential direction.

by: Andreas Kaufmann, Dr. Tino Lindner-Silwester – HOERBIGER

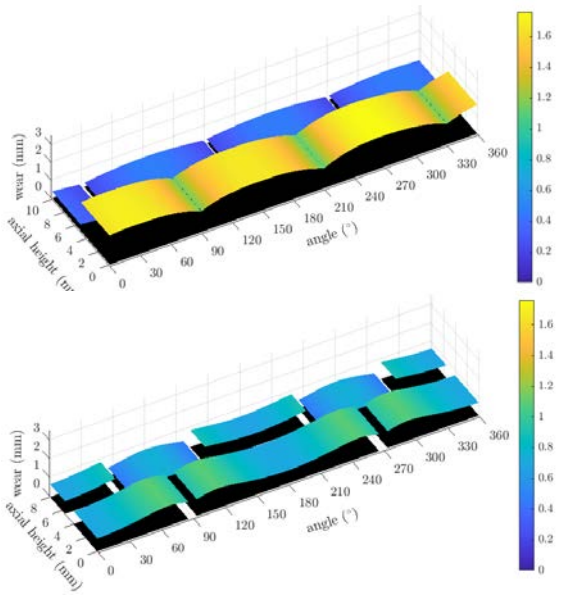

Figure 11: Wear pattern of the RT ring pair (top) and the BCD ring (bottom) after 10.9 days of wear-time.

Table 1: Position of the wear maximum for each ring segment after 10.9 days.

ring segment	position (°)	wear (mm)
radial	89	0.481
tangential	23	1.72
cap	90	0.750
sealing	64	1.09

4.2.3 Wear volume

The total wear volume of the BCD ring after 10.9 days is 42 % lower than the total wear volume of the RT ring pair. This matches well with the difference in the calculated frictional forces (39%, Figure 5) and shows the correlation between frictional force and loss of material.

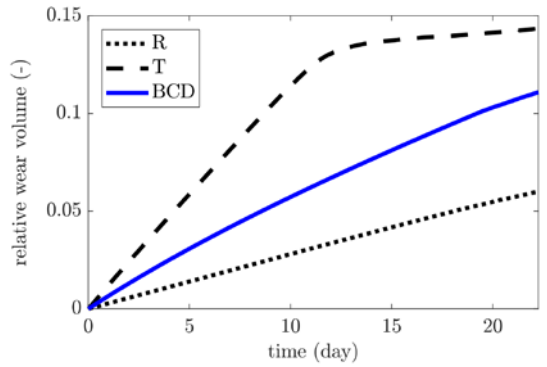

Figure 12: Relative wear volumes of radial ring (R), tangential ring (T), and BCD ring.

Simulation allows us to track how the wear volume changes over time. Figure 12 shows the wear volume relative to the rings' initial volumes. When the wear gaps of the tangential ring close (10.9 days) the structure becomes stiffer. This results in a drop in the contact pressure (Figure 6) and hence the wear rate.

5 Comparison of simulation results with experimental data

5.1 Frictional force

A purpose-designed test rig was used to determine the coefficient of friction between ring and rod and to measure the frictional force exerted by a pressure-loaded packing ring. The test rig comprised a rod and a pressurized packing consisting of a T-cup and flanges. Both were mounted on a standard tensile testing machine so that the rod could be moved vertically through the packing while monitoring the pull-off force required to move the rod at constant speed.

The rod (Ø 50.8 mm) was made from 1.4021 steel, coated with tungsten carbide (TC/Co/Cr, 86/10/4), finished to a roughness of $R_a = 0.3 \pm 0.05$ µm so as to comply with industry standards. The packing was mounted on three pillars allowing the rod to travel a stroke of more than 250 mm. The test setup was located in a climate-controlled (20°C) laboratory. Data for each measurement of frictional force was recorded over at least 10 strokes (5 up and 5 down) and averaged over all the strokes, excluding data points measured within 10 mm of the end of the stroke.

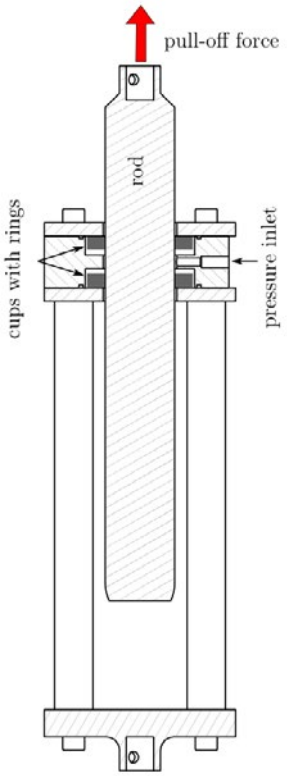

Figure 13: Test rig for determining the coefficient of sliding friction and the frictional force of a packing ring.

by: Andreas Kaufmann, Dr. Tino Lindner-Silwester – HOERBIGER

5.1.1 Coefficient of sliding friction

To determine the coefficient of sliding friction between the PTFE compound and the tungsten carbide coated rod a specially designed 20-piece ring was used. For such a multi-segment ring, the contact force at the inner diameter of each segment depends only on the load applied by the garter spring and not on the stiffness of the material. Thanks to this simple relationship the coefficient of sliding friction can be easily derived from the value of the measured pull-off force and the rod's weight.

Figure 14: 20-piece ring mounted on the rod of the friction test device.

Ring and rod were carefully cleaned with ethanol to remove any grease, oil or other contamination before each test. The ring segments were spaced equally around the rod and fixed by garter springs of known stiffness (Figure 14). The ring was placed in one of the packing cups, the rod moved at a prescribed speed, and the rod's pull-off force measured with a 500 N load cell.

The coefficient of sliding friction was found to be 0.190 for the PTFE compound sliding against a tungsten-carbide coated rod with a relative speed of 500 mm/min.

5.1.2 Frictional force of BCD ring

The frictional force of the BCD ring was measured by placing two such rings into the T-cup. To measure the frictional force created by the tension in the garter spring, the first test was run with no gas pressure applied. Subsequent tests were done over a range of applied pressures, each test measuring the frictional force averaged over several strokes. The frictional force was found to vary linearly with the applied gas pressure differential. Figure 15 shows the results and confirms their excellent agreement with the simulation results. This proves the validity of the assumptions underlying the simulation model.

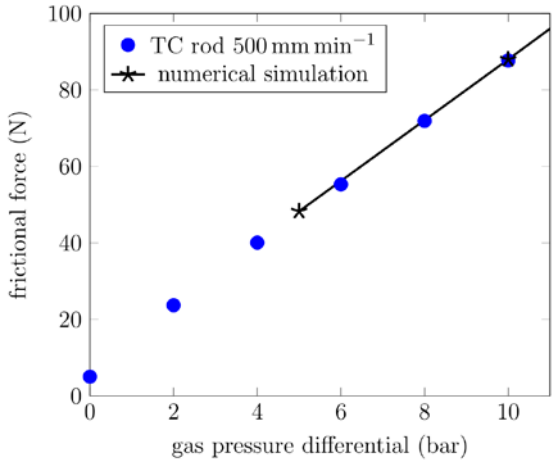

Figure 15: Variation of frictional force with gas pressure differential for a BCD ring, showing both experimental data and simulation results.

5.2 Wear

5.2.1 Determination of wear coefficient

The wear coefficient k (Equation 2) was determined using a linear reciprocating pin-on-flat test rig. The metallic counterface was a plate of 1.4021 grade steel, 4 mm thick, coated with tungsten carbide and finished to a mean roughness of $R_a = 0.3 \pm 0.05\mu m$ with a cross cut.

The steel plate moved through a stroke of 50 mm at a frequency of 10 Hz, giving a mean relative sliding speed of 1 m/s. The contact pressure was 1 MPa, and the temperature was 80 °C. The measured wear coefficient was $7.2 \cdot 10^{-7}$ mm³/(MPa m).

5.2.2 Wear on packing ring tester

Ring wear was created using a specially-designed packing test rig (Figure 16), and measured via precise 3D scanning.

The rod in the test rig is 50.8 mm (2") in diameter and has a stroke of 98 mm. It is coated with tungsten carbide (TC/Co/Cr, 86/10/4). The rod is hollow, allowing compressed air to be blown inside through a lance to provide cooling. Two BCD rings are held in a water-cooled T-cup surrounded by two flanges.

The cup pressure and the total ring leakage were measured by a pressure sensor and a mass flow meter, respectively. The temperature of the packing case was measured at four positions using type K thermocouples. The rod surface temperature was measured by a pyrometer looking through a quartz window in the sealing chamber.

Before and after each wear run, the precise dimensions of the rings were recorded by a 3D coordinate measurement machine. Figure 17 shows the resulting wear pattern for a BCD ring sealing bone-dry nitrogen at 29.8 bar for 359 h (15 days) with a mean rod speed of 1.19 m/s.

by: Andreas Kaufmann, Dr. Tino Lindner-Silwester – HOERBIGER

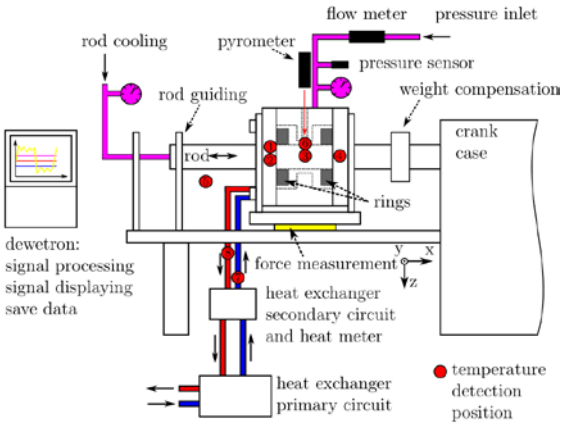

Figure 16: Schematic representation of the wear test rig.

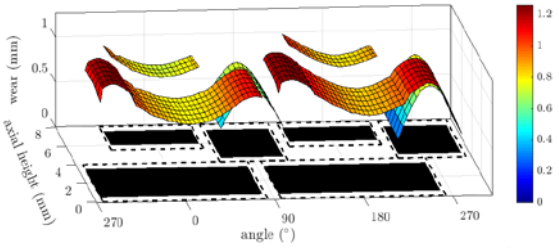

Figure 17: Wear depth measurements (mm) for a BCD ring after 359 h runtime.

The black rectangles in Figure 17 indicate the area over which measurements were taken, while the dashed lines show the total contact areas. Table 2 shows the volumes of material lost from each section of the BCD ring, extrapolated from the measured areas to the total contact area.

Table 2: Measured wear volumes for a BCD ring after 359 h runtime.

	total wear volume (mm^3)
Sealing segment 0°	368
Cap segment 90°	80
Sealing segment 180°	398
Cap segment 270°	76
Full BCD ring	921

These measurements are in good agreement with the simulation results – 92 mm^3 for the cap segment, 466 mm^3 for the sealing segment – corresponding to a wear time of 15 days.

Since the wear pattern does not change appreciably along the axial direction (Figure 11 and Figure 17), we can compare simulation results and measurements at two defined axial positions, as shown in the top part of Figure 18: Position A, 6.44 mm and Position B, 2.08 mm from the cup face, respectively.

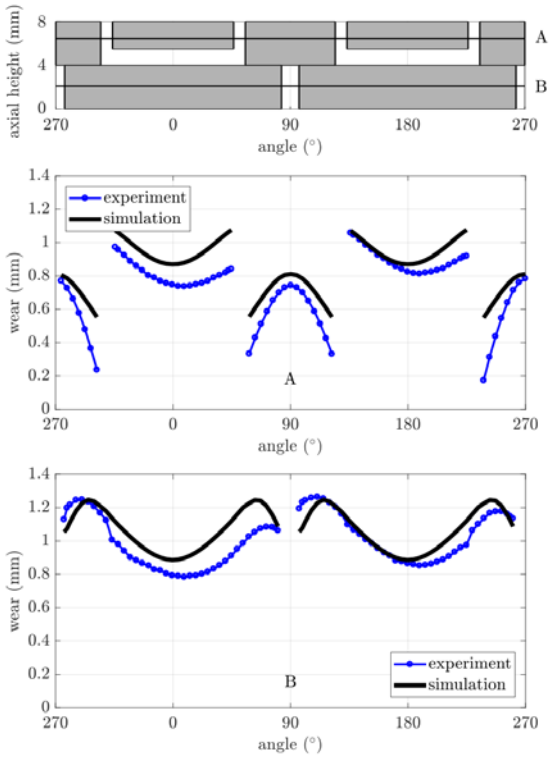

Figure 18: Calculated and measured wear for a BCD ring. Top: Ring sealing surface showing axial locations A and B at which the comparisons are made. Middle: Position A, representing the cap section of the BCD ring. Bottom: Position B, representing the sealing segment section of the ring.

The very good agreement between calculated and measured results confirms the predictive power of the simulation model.

6 Conclusions

This paper presents a simulation model for the wear of packing rings in reciprocating compressors that bridges the gap between standard laboratory wear tests and real-world applications.

There is excellent agreement between measurement and simulation for the sliding frictional force between the packing ring and the piston rod. This confirms correct modeling of the load experienced by a packing ring at a given gas pressure differential.

The current simulation uses the simplest possible wear model – Archard's wear equation – and the simplest possible material model – a Hookean, isothermal body. It nonetheless yields a wear pattern that is in good qualitative agreement with experiments, and in good quantitative agreement too when we use a wear coefficient derived from standard tribotesting.

The simulation model sheds light on how the wear of a packing ring evolves with time, and allows us to keep track of all the other quantities of interest, including contact pressures, frictional forces, stresses and strains.

The simulation technique is flexible enough to allow more elaborate wear and material models to be added in the future.

References

[1] Lindner-Silwester, T., and Hold, C., (2010), "The BCD Packing Ring – A New High Performance Design," Seventh Conference of the European Forum for Reciprocating Compressors (EFRC), Florence, Italy, Oct. 20–22, 112–119.

[2] Lindner-Silwester, T., (2007), "Advances in Fundamental Understanding of the Dynamic Sealing Action in Packing Systems," Fifth Conference of the European Forum for Reciprocating Compressors (EFRC), Prague, Czech Republic, Mar. 21–23, 40–50.

[3] Feistel, N., (2001), "Beitrag zum Betriebsverhalten trocken laufender Dichtsysteme zur Abdichtung der Arbeitsräume von Kreuzkopfkompressoren," Ph.D. thesis, Technische Fakultät der Universität Erlangen, Nürnberg, Erlangen.

[4] Archard, J. F., (1953), "Contact and Rubbing of Flat Surfaces," J. Appl. Phys., Vol. 24(8), 981–988

[5] Kaufmann, A., Lindner-Silwester, T., Antretter, T., (2018), „Modeling Dry Wear of Piston Rod Sealing Elements of Reciprocating Compressors Considering Gas Pressure Drop Across the Dynamic Sealing Surface," ASME J. of Tribology, Vol. 140(4), 042201, 1-7, doi:10.1115/1.4038863

[6] Rezaei, A., van Paepegem, W., de Baets, P., Ost, W., and Degrieck, J., (2012), "Adaptive Finite Element Simulation of Wear Evolution in Radial Sliding Bearings," Wear, Vol. 296(1–2), 660–671.

EXCITE

THE HOERBIGER PIONEER CLASS

XperLUBE

Getting lubrication right

Delegate important tasks to the expert.

HOERBIGER developed XperLUBE to boost the performance and cost efficiency of your compressors. At all times. Under any conditions.

www.xperlube.hoerbiger.com

CHALLENGE
YOUR
HORIZON

HOERBIGER
because performance counts

New concept lubrication system application on a HP reciprocating compressor

by:

Marco Sacco
CST S.r.l.
Package Engineering Leader
Florence, Italy
marco.sacco@cstfirenze.com

Pamela Tani
CST S.r.l.
Maintenance Consultancy Engineer
Florence, Italy
pamela.tani@cstfirenze.com

Massimo Maffeis
SIAD MI S.p.A.
Global Service Technical Director
Bergamo, Italy
massimo_maffeis@siad.eu

Alessio Scialpi
Eni Refinery
Reliability Leader
Taranto, Italy
alessio.scialpi@eni.com

11th EFRC CONFERENCE
September 13 – 14, 2018, Madrid

Abstract:
Among the most widespread lubrication systems on the market two types are most commonly used, the “pump to point” and “divider block” types, but further solutions can be developed according to the specific application and customized to fit the user’s requirements.
This paper describes the solution applied to a critical application: retrofitting of the cylinder lubrication system of five hydrogen make-up reciprocating compressors operating in the ENI Refinery in Taranto. The criticality of the application was due to the high discharge pressure of the final stage of the compressors (~200 bar-a) and the requirement to provide a fully redundant oil distribution system, retaining the existing lubricator as a stand-by system as well as in automatic combined operation with the new one. The applied solution included flow and pressure instruments installed at strategic points of the system and management of the various signals to allow automatic switchover to the stand-by pump or to the old lubrication system, in case of major problems. The few unexpected situations that occurred at the startup of the compressors are also examined, as well as the subsequent investigations that were performed using the supplied instrumentation, and the applied improvements that were the result of the lessons learned. The experience showed how the presence of a redundant system and of adequate monitoring and diagnostics makes it possible to achieve high safety levels, high availability and optimized maintenance.

by: Marco Sacco, Pamela Tani – CST; Massimo Maffeis – SIAD; Alessio Scialpi – ENI Refinery

1 Introduction

Cylinder and packing lubrication system is one of the most critical item for the correct operation and reliability of a lubricated reciprocating compressor. What should be avoided is the poor lubrication and the consequent premature wear of piston rings and wear bands but, although maintaining proper lubrication is essential, it is not always technically simple and the injected oil quantity is very often higher than necessary, with side effects on process gas contamination, machine performance and operating costs. The two most commonly used lubrication systems currently on the market are [1]:

- the “pump to point” system,
- the “divider block” system,

each of which has pros and cons.

The pump to point mechanism consists of a lubricator system with a pump unit for every injection point; each pump has its own pressure rating and size, and a dedicated rocker arm system with a screw for adjusting the stroke. The oil delivery is adjusted individually and manually and can therefore be approximate (often resulting in over-lubrication) requiring technical time of setup and continuous inspection by the operator. Moreover, usually the only way to check and adjust the oil drip is by a sight glass, the reliability of which often proves to be a critical point in the system.

In the divider block (or divider valve) system, the lubricant is pumped into a single input of the "divider" and is spread volumetrically into a certain number of outputs through the progressive movement of the pistons in the elements arranged in sequence (see Figure 1) [2]:

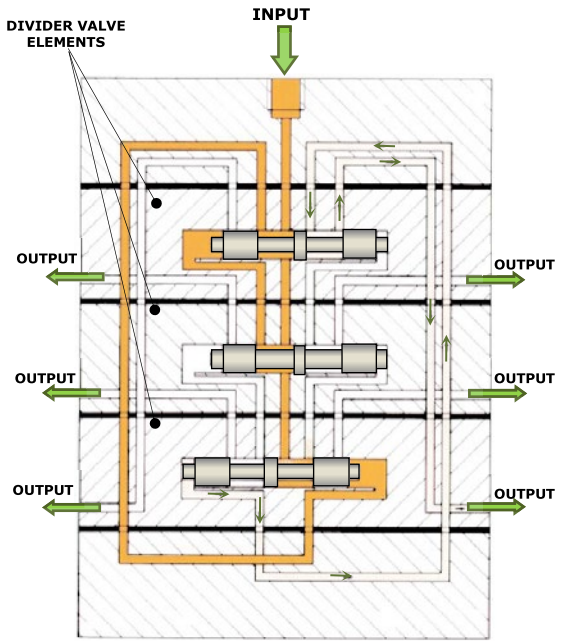

Figure 1: Divider valve section schematic

Each primary divider block outlet may lead to a secondary divider, usually one for cylinder and, from here, the oil flow is split again into smaller rates and sent to all the points on the compressor to be lubricated. The oil delivery is still adjusted by the pump, so this system does not allow any adjustment of the lubricant flow to the individual points either to the individual cylinders, unless the replacement of one or more elements respectively in a secondary or primary divider valve. As a matter of fact, the precision of the divider valve is entrusted to the dimensional tolerance with which each block is made and reliability cannot be guaranteed without an adequate control and maintenance of the quality of the oil and a system of properly designed alarms and trips. Moreover, obstruction of only one of the lubrication points can cause the whole system to shut down, also causing the machine to stop.

This paper describes the realization of a completely customized lubrication system aimed at overcoming the drawbacks of the two existing basic mechanisms. The adopted solution guarantees the intrinsic accuracy of the divider valves, dispensing with the approximate and inadequate adjustment of the drip rates; it also avoids the possibility of a compressor trip in the event of any critical issue, thanks to the provision of an optimized instrumentation and control system and of a redundant oil distribution arrangement, both perfectly manageable, even remotely.

The high pressure present on the last stage brought to light a further criticality of the divider block system; nonetheless, the intended instrumental equipment allowed the issue to be resolved, creating a lesson learned which must not be neglected in the future and emphasizing the importance of redundancy, of the proper instrumentation and of the monitoring system for the success of the project.

2 Project scenario

This paper concerns the installation and testing of a new lubrication system which was required for five hydrogen make-up three-stage reciprocating compressors, operating in the ENI Refinery in Taranto.

The existing reciprocating compressors were equipped with old pump-to-point systems, which were starting to present recurrent problems, mainly due to malfunctioning sight glasses: these elements were periodically and randomly losing their vacuum, with the result that the related pump units were not able to draw the oil from the tank; therefore the relevant injection points did not receive any oil, making the compressor run partially dry. Each time operators had to manually manage and force the relevant pump unit to try and restore the operating function. Finally, the end user decided to solve the problem with a definitive solution, substituting the existing lubrication system.

by: Marco Sacco, Pamela Tani – CST; Massimo Maffeis – SIAD; Alessio Scialpi – ENI Refinery

Besides solving the sight glasses issue, the new system was also required to assure continuity of lubrication and reliability, avoiding any unexpected shutdowns of the running compressor.

3 The new lubrication system in detail

3.1 Basic principle overview

The new cylinder lubrication system is based on a combination of the old pump to point conception, having more than one pump unit that allows us to adjust and optimize the oil flow to the single cylinder, and the divider block system, that has the capability of splitting the lubricating oil into precise fractions.

The oil pump is equipped with three pump units (see Figure 2), one for each cylinder of the compressor that needs to be lubricated.

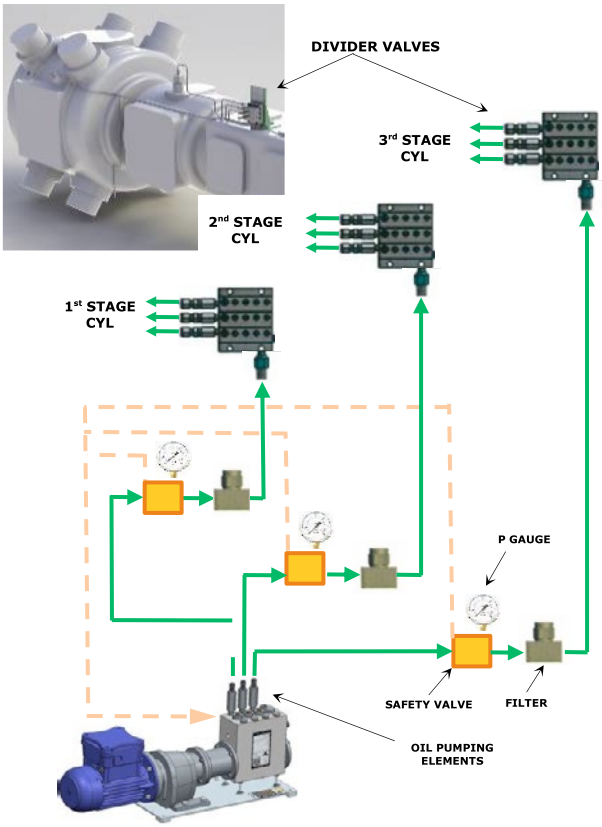

Figure 2: New lubrication system principle schematic

Each pump element is connected to a divider valve that splits the incoming flow into fractions and each of them is injected into the relevant injection point.

In some applications the outlet flow of a single pump is too high of a single cylinder therefore an additional line is provided to release the exceeding flow.

An accessory assembly, consisting essentially of a 10µm filter, a pressure gauge and a pressure relief valve, located between each pump element and the related divider block, protects the divider block from any impurities in the oil.

The hydraulic pump is a piston type and, according to the particular requirements of the application, it is designed for a relatively high operating pressure (550bar). It is suitable for a wide range of viscosity oils (10 cSt ÷ 460 cSt at 40°C) and it has high reliability, requiring minimal maintenance.

3.2 Functional mechanical description

The new lubrication unit, installed on an independent rack near the compressor (Figure 3), is composed of the following main items:

- Oil tank;
- 2 hydraulic pumps: one in operation and one on stand-by; each driven by an electric motor and fed by a line from the oil tank. The feed line of each pump is equipped with a 150µm filter, to prevent solid particles from entering the pump and compromising the proper functioning;
- accessory assemblies: one downstream of each pump unit; they are clamped over the tank and each equipped with a filter (10µm cartridge rating) and a pressure gauge / transmitter;
- local control panel, with main warning lamps and start/stop commands, installed on the rack;
- divider blocks, downstream of each accessory assembly and clamped on the compressor; each block is equipped with an overpressure visual indicator on every outlet, a visual flow indicator and a flow transmitter.

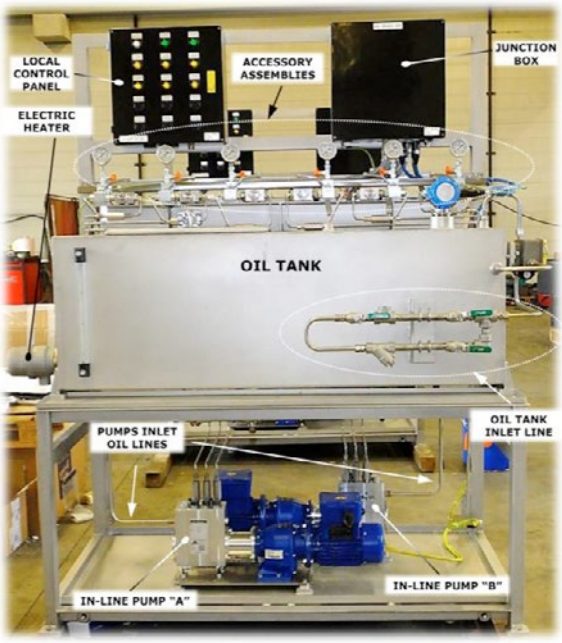

Figure 3: New divider valves lubrication rack

The compressor is equipped with three divider valves, one for each cylinder, that work at the pressure value corresponding to the stage. Each valve has as many outputs as the injection points of that stage.

by: Marco Sacco, Pamela Tani – CST; Massimo Maffeis – SIAD; Alessio Scialpi – ENI Refinery

When the pressure difference between the output lines of the same divider valve exceeds a certain value (typical prescription is DP > 70bar [3]), it is advisable to install a balance valve on the lower pressure lines in order to balance all output pressures and to ensure accurate dispensing of the lubricant volume. In this case recycle lines were provided on both 2nd and 3rd stage divider valves and, being the relevant outlet lines at rather high pressure (120bar-g and 215bar-g respectively), balancing valves were necessary on the tank "recycling" lines with a set value according to the differential pressure to be faced.

3.3 Instrumentation and control logic

The system is provided with the following instrumentation:

- Electric heater, with a thermostat, on the oil tank, with high temperature alarm and heater exclusion;
- Level switch on the oil tank, with permissive signals to the pumps to start, low level alarm and heater switch off;
- Pressure transmitters with high and very high alarms upstream of the filter on the accessory assembly to indicate the obstruction of the filter when it needs to be replaced. In case the measured pressure is lower than the expected, the running pump automatically switches to the stand-by one.
- PSV upstream of each 10µm filter with a set value slightly higher than the average pressure of the line to be protected; it deviates the flow towards the oil tank. The safety valve opens in the event of overpressure or blockage of the divider block: in this case, after a period of time (5 minutes) the pumps are switched over. If the problem persists the pumps switch again and if it still does not work, the new lubricator switches off while the pump to point lubricator starts working.
- A pop-up indicator is provided on each element outlet of the divider block in the event of overpressure: if a divider block piston stops, arresting the whole valve, a visual indicator signals that the line needs to be reset.
- A proximity switch with a low flow alarm is provided on the divider block; if flow is very low, the running pump automatically switches to the stand-by one. If the problem persists even with the other pump, the pumps switch again and if it still does not work, the lubricator goes off while the pump to point lubricator starts working.

In the event that both pumps are not allowed to run, the existing lubricator is put in service.

The system supplied provides for the presence of two reciprocally redundant divider block type systems, plus the original pump to point system ready to go into operation if the first two have problems; this solution ensures delivery of lubricant at every injection point, ensuring complete reliability of the entire system and the machine (see Figure 4)

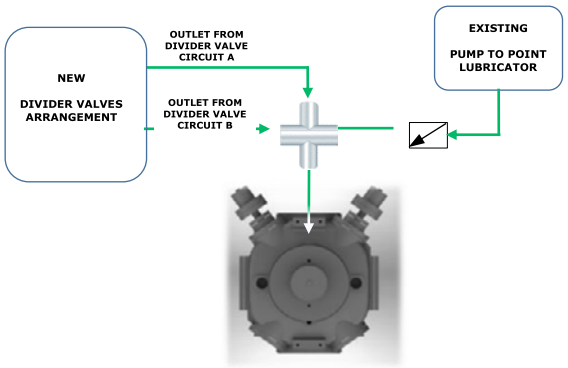

Figure 4: Lubrication supply redundancy

4 Start up

The first control units to start operating were those on the A, D and E machines, while machines B and C were to start only at a later time.

The commissioning and setting up of the lubrication system and the instrumentation was rather quick and did not present any particular problems. The control units had already been tested in the workshop by means of the pressure test, but what represented the unknown was the software part that was to integrate the system only during installation in the field. The software configuration took its time, but proved to be successful for the management of the signals and the logic.

4.1 Issues

An unexpected situation occurred at the start-up of the compressors: blockage of the high pressure line (3rd stage) of the new lubricator.

At the first start-up step, corresponding to a counter-pressure of 20 bar-g at each injection point, there was a blockage of a 1st stage divider (on one machine) and of a 2nd stage divider (on another machine) but it was immediate to realize that the cause was located in the check valves of the injection quills installed on the cylinders, which were obstructed. Once the injection quills had been replaced the system started working but, when the running conditions were reached, the 3rd stage divider blocks always appeared as if they were obstructed.

The same situation occurred on intial startup of all three compressors A, D, and E, therefore it was believed to be due not to a random malfunction of a divider block or an accessory but to the design of the high pressure line.

The hypothesis by which the problem was due to a high differential pressure between the injection lines downstream of the divider valve was soon deleted, since this phenomenon cannot cause complete blockage of the divider but only affect the quantity of

by: Marco Sacco, Pamela Tani – CST; Massimo Maffeis – SIAD; Alessio Scialpi – ENI Refinery

injected oil due to a leakage of lubricant inside the divider valve, from the high to low pressure points [4].

The cause of this issue was investigated using, at first, a series of pressure gauges installed at the oil injection points, and it was verified that the counter pressure values had been evaluated correctly, therefore the cause of the issue had to be found elsewhere.

At this point a test bench was set up for the 3rd stage divider block to replicate the same behaviour that occurred in the field and better evaluate the phenomenon.

5 Testing

5.1 Bench preparation

The test bench (see Figure 5) was used to simulate the third stage behavior providing a counter-pressure of 100bar on all the injection points. In particular, the test conditions were the following:

Cylinder injection point: **100**bar

Cylinder packing injection point I: **100**bar

Cylinder packing injection point II: **100**bar

Balancing valve set setpoint **80**bar

Oil viscosity: ISO VG **32** and ISO VG **150**

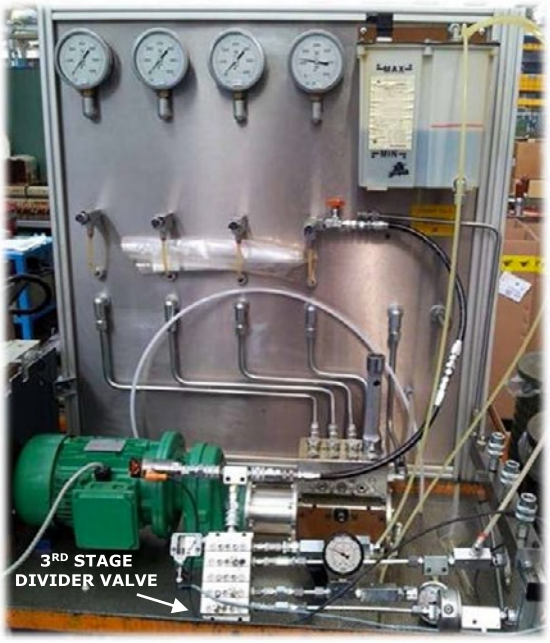

Figure 5: Test bench

The same problem that occurred in the field was experienced after about 3 minutes of operation, applying the above conditions and using both types of oil reported above.

The registered pressure trend was the same as that registered by the DCS in Taranto, shown in following Figure 6.

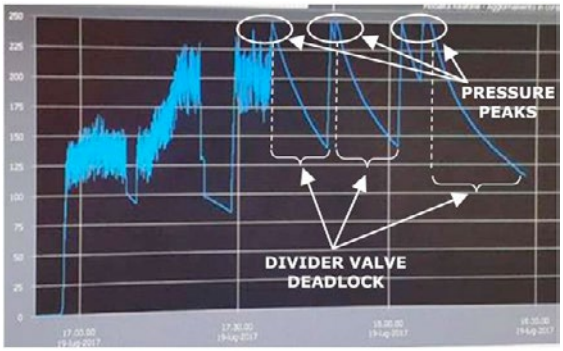

Figure 6: DCS pressure trend registration

The anomaly manifested by the pressure trend consisted in a divider block stall and a subsequent pressure increase, beyond the expected operating values, reaching 250/270 bar. Actually, the divider block ran at first for a few minutes until it reached the expected values of 130/150 bar and then stopped and restarted cyclically; subsequently, on reaching pressures above 250/270 bar, the divider block stalled and it was necessary to reset the inlet pressure and restart the pump to restart the system.

Since the test facility replicated the same issues experienced in the field, an accurate investigation and measurement campaign made it possible to understand the causes of the recurring issue and to implement the corrective actions listed below.

5.2 Testing and solution of the first issue: divider block stall

The divider block is normally supplied with a single check valve at each outlet but, in this case, a double check valve had been required by the customer due to the high pressure. However, instead of having a double check valve, two valves were arranged in series (see Figure 7).

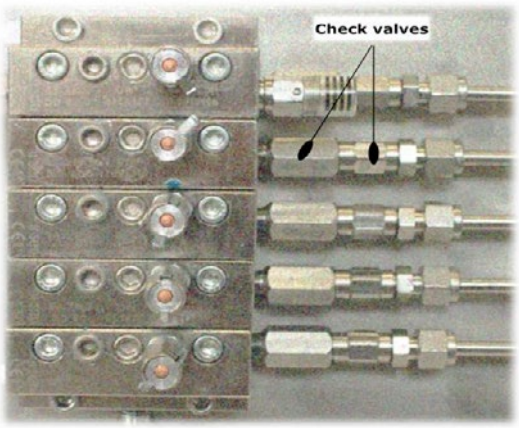

Figure 7: Divider output check valves

Before carrying out the tests, as a first step, it was decided to fit only a single check valve at each outlet on the test bench assembly, in order to reduce the variables to be examined.

by: Marco Sacco, Pamela Tani – CST; Massimo Maffeis – SIAD; Alessio Scialpi – ENI Refinery

The new series of tests and a careful analysis of the phenomenon revealed that the particular arrangement of the divider valve elements, combined with low flow rates (3÷4 cycles per minute) and a back pressure of 100 bar, caused the systematic fail of the 0.04 cm^3 element, that integrated the Namur sensor. To confirm this, at higher flow rates (~25 cycles per minute) the problem did not occur.

It is to be considered that the pistons in a divider valve normally have different diameters, being sized according to the quantity of oil to be dispensed at each lubrication point. The Namur is a 2-wire proximity sensor that transmits a signal every time the divider valve has completed a lubrication cycle, therefore it is used to measure the quantity of injected oil to monitor the condition of the divider valve. From a functional perspective, the Namur can be mounted on any divider valve piston and the position is normally determined by ease of assembly and minimum overall dimensions.

The displacement of the piston generated by the passage of the lubricant inside the block is detected by a proximity sensor through a dipstick with a very thin diameter. Moreover, the piston of the element on which the Namur is mounted has a particular shape, the dipstick being an integral part of the piston.

The explanation of the stall issue is related to the dimensions of the internal pistons used in the divider block element and the Namur sensor. The internal piston of the 0.04 cm^3 element has a 3mm diameter and the shaft connected to the Namur sensor has a 1.6mm diameter (see Figure 8) with the result that the surface on which the oil pressure acts is a ring given by the difference between the piston diameter and the dipstick diameter; at low flow rates the piston needed a much higher pressure in order to be moved with the same translation force, because of the small section differences.

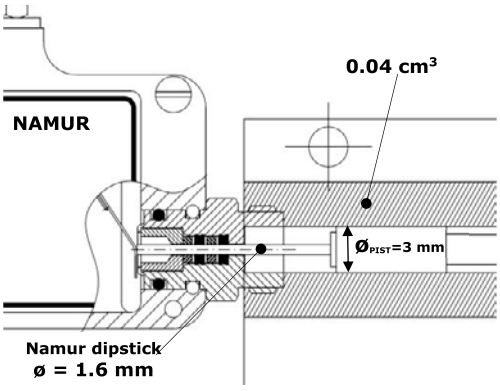

Figure 8: Namur to 0.04 cm^3 element connection detail

The force acting on the circular area was not sufficient to move the piston, which remained blocked despite the pressure rising, until the divider block was blocked: this explains the very high pressures read by the field pressure sensors.

By modifying the position of the Namur sensor (see Figure 9) and moving it to the 0.16 cm^3 block (taking advantage of the divider block modularity) which had an internal diameter of 5mm, the phenomenon no longer occurred and the operating pressures drastically reduced to values congruent with expected values: the new measured values were, in fact, between 130 and 150 bar (100 bar counter-pressure + 20 bar divider block pressure drop + 10/15 bar of pressure drop on the check valves).

5.3 Testing and solution of the second issue: pressure peaks

Once the first problem was solved, the additional check valves were installed on the test bench divider block (Figure 9), to exactly replicate the configuration of the divider blocks present in the field.

The test bench was finally left in operation for a few hours, and the stall phenomenon no longer appeared.

Nevertheless, pressure peaks of around 190 bar were noted over time.

It was found that with the installation of two identical check valves of the original type with the same masses and opening pressures, the pressure peaks no longer occurred.

Actually, the check valves added at a later time required a different (greater) opening force but, although the overall losses remained negligible since the operating pressure was high, the interaction between the different stiffnesses and the particular combination of the low flow rate and the high pressure impeded the lubricant flow, occasionally increasing the upstream pressure.

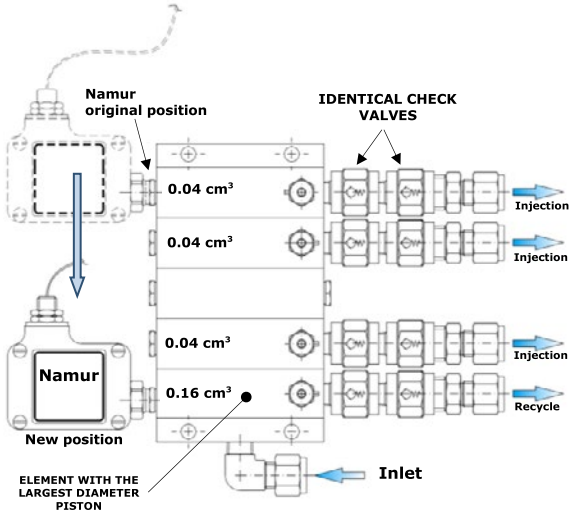

Figure 9: Divider block final configuration

by: Marco Sacco, Pamela Tani – CST; Massimo Maffeis – SIAD; Alessio Scialpi – ENI Refinery

Finally, the test bench was left in operation for 8 hours, monitoring and recording the pressure values and the Namur sensor signal.

None of the above phenomena occurred again, therefore the divider valve was considered to be operating correctly and reliably and the systems installed in the field were modified accordingly.

After units A, D and E, also those mounted on the last two machines B and C were rearranged in the same way and, to date, all five compressors and lubrication units have been running for more than six months and none of the above mentioned phenomena has recurred, to the complete satisfaction of the customer.

6 Lesson learned

Although progressive systems are now widely applied, there are still some critical applications, like the one mentioned in this paper, that can present problems and issues on system start-up for which there is no apparent immediate solution.

The experience that was gained using a test bench has taught that the two following actions are necessary to avoid inconvenient stalling of the divider valve and undesired pressure irregularities:

- installation of the position sensor on the larger diameter element;
- if two check valves are installed on each divider outlet, it should be ensured that they are identical and have the same opening force; if possible, use one double type check valve.

For accessibility and maintainability, the Namur sensor is generally applied in line with the piston at the opposite side to the inlet oil on the divider valve, but experience shows that it is appropriate to revise this philosophy, taking into consideration the dimensions of the element on which it is applied.

The reported case suggests that both the above two counter-measures should always be adopted, even under normal pressure conditions and with greater oil flowrates.

7 Conclusion

Basically, the progressive system technology is quite simple, therefore making it suitable for a large amount of applications. In this case, the equipment redundancy, the provision of an adequate instrumentation and control system and the combination with the existing PTP lubrication unit, made the system perfectly versatile, functionally valid and reliable, suitable even for the strict regulations generally applied in refinery and petrochemical sectors.

Nevertheless, when new solutions are needed due to the criticality of the application, unforeseen issues can still arise: in the case described above particular operating conditions, such as the high operating pressures and the low lubricant flow rates required, revealed intrinsic problems of the system that do not emerge in the majority of applications. Nonetheless, the presence of a measurement and monitoring system has also been a very useful tool for the evaluation and detection of unexpected problems and made it possible to identify the nature of the possible causes, finally leading to the solution.

Moreover, the redundancy of the system, not only applied to each single piece of equipment but also to the whole architecture, allowed the customer to continue production even during the testing. In fact, adopting a particular tubing and check valve arrangement enabled lubrication to be remotely switched from the old PTP to the new progressive system. The switch-over is also performed automatically in the event of malfunctioning of one of the systems.

With the modifications that were carried out, the system can be considered completely reliable and the proposed solution could represent a valid and innovative update to be evaluated both for newly developed lubrication systems and for existing lubricated compressors which have been running for a long time and which have the old pump to point type of lubrication or other poor lubrication system, in order to improve the lubrication performance and also the reliability of the machine as a whole.

References

[1] Hanlon, Paul C., Compressor Handbook, Chapter 18.10 “Compressor Lubrication”, McGraw-Hill, 2001.

[2] SKF Lubrication Solutions, Progressive Metering Devices: “Modular Feeders for Grease and Oil”, *www.SKF.com* 11.04.2018;

[3] Dropsa Lubrication Systems, Lubrificazione per Compressori, “La lubrificazione precisa e costante ad alte pressioni e bassa portata”, DropsA S.p.A., *www.dropsa.com*, 11.04.2018

[4] *CPI Lube Prod Guide US-4 12*: “Divider blocks and pump to point systems”, www.c-p-i.com, 11.04.2018

Promoter

European Forum for Reciprocating Compressors e. V.
c/o Technische Universität Dresden
01062 Dresden, GERMANY
Telefon: +49 (351) 463-32815
Fax: +49 (351) 463-37247
E-Mail: contact@recip.org
www.recip.org

EFRC Board

René Peters (Chairman)
Gunther Machu
Matthias Tanner

Editor

Herbert Steinrück
TU WIEN
Institute of Fluid Mechanics and Heat Transfer

Conference Committee

Christian Prinz, HOERBIGER (Chairman)
Martina Frenz, NEUMAN & ESSER
Michèle Infanger, BURCKHARDT Compression
Leonard van Lier, TNO
Anja Parnigoni, HOERBIGER
Maja Schütz, EFRC

Adversory Board

Herbert Steinrück, TU WIEN (Chairman)
Roland Aigner, BURCKHARDT Compression
Jean-Christoph Courcol, TOTAL Refining & Chemicals
Peter Duineveld, HOERBIGER
André Eijk, TNO
Jeroen van Koperen, SHELL
Marc Langela, STASSKOL
Massimo Maffeis, SIAD
Christian Prinz, HOERBIGER
Andrea Raggi, COZZANI
Luzi Valär, BURCKHARDT Compression
Cyril Wentzel, WENTZEL Dynamics

Layout

sanja.at e.U., Sanja Kaltenbrunner-Jelic, A-1160 Wien

Druck

Druck.at, A-2544 Leobersdorf

ISBN 978-3-00-060551-2

WWW.RECIP.ORG